Investigation of the Augmin complex, the template dependent microtubule nucleator, in *Drosophila melanogaster*

Submitted by Jack Wei-Chu Chen to the University of Exeter

as a thesis for the degree of

Doctor of Philosophy in Biological Sciences

In August 2014

I certify that all material in this thesis which is not my own work has been identified and that no material has previously been submitted and approved for the award of a degree by this or any other University.

Signature: …………………………………………………..

Acknowledgements

I am very grateful for the support and guidance of many people, without which, this PhD would not have been possible. First and foremost, I must thank my supervisor Dr. James Wakefield for his cultivating and nurturing of my innate curiosity, for enlightening me to a unique way of understanding and visualising science. His guidance has helped me to become a much more effective thinker, and to be more aware of the larger picture.

I would like to thank my fellow lab members, past and present. They have truly made my PhD experience an enjoyable one.

I would also like to thank my family for their care and belief in me. They have been the pillars of support in my life, and I would not have come this far without them.

Lastly, I would like to thank my girlfriend Dr. Amy Barker. She has painstakingly refined my science to have greater finesse. She has taught me to be a more effective writer, and presenter. She has always been there to support and guide me throughout my PhD.

Both James and Amy were instrumental for developing me into the scientist that I am today. While James built on my natural self, Amy polished it. In the years I have known them, they have helped me grow into the person I am today, and I am forever grateful for them to have come into my life.

Abstract

In order for life to continue, proper segregation of genetic materials by the process of mitosis is essential. Mitosis is facilitated by a bipolar spindle, usually composed of a symmetrical array of microtubules (MTs). MTs consist of Tubulin polymers, and are generated *in vivo* with the aid of nucleators. The most predominant nucleator is the γ-Tubulin Ring Complex (γ-TuRC). During mitosis, multiple pathways contribute to proper spindle formation, including centrosome-dependent, kinetochore-dependent, and a recently discovered pathway in which new MTs are nucleated from the sides of existing MTs. This last pathway relies on the Augmin complex, a template-dependent MT nucleator which recruits γ-TuRC to the spindle. Mitotic cells lacking Augmin have weak spindles due to a lower density of MTs and in human cells, Augmin reduction also causes centrosome fragmentation. To date, very little is known about the functional properties of Augmin. I have purified individual Augmin subunits and examined their properties *in vitro*. I show that the Augmin subunits Dgt4 and Wac are responsible for interaction with MTs and that Dgt6, Dgt3 and Dgt5 interact with the γ-TuRC subunit Dgp71WD. I have also shown that Wac protects MTs from destabilisation. Interestingly, the Augmin complex promotes MT assembly in the absence of γ-TuRC, suggesting a novel function for Augmin. I have also successfully purified intact Augmin complex. With this, I determined some of the relationships between Augmin subunits and generated a model of how Augmin might recruit γ-TuRC to MTs. Lastly, I have determined that at least one subunit, Wac, plays a role in MT organisation beyond mitosis. This work significantly improves our understanding of the Augmin complex and provides an excellent complement of tools for further investigation.

Table of Abbreviations

MTs   Microtubules

GTP   Guanosine-5'-triphosphate

EM   Electron Microscopy

TEM   Transmission electron microscopy

GMPCPP   Guanosine-5'-[(α,β)-methyleno]triphosphate

CLASP   Cytoplasmic Linker Asssociated Protein

EB1   End-Binding protein 1

MAPs   Microtubule Associated Proteins

DNA   Deoxyribonucleic acid

cDNA   complementary DNA

RNA   Ribonucleic acid

RNAi   RNA interference

k-fibres   Kinetochore-fibres

SAC   Spindle assembly checkpoint

APC/C   Anaphase Promoting Complex/ Cyclosome

CDC20   Cell-division cycle protein 20

Scc1   Sister chromatid cohesion protein 1

CDK1   Cyclin dependent kinase 1

PP2A   Protein phosphatase 2

γ-TuSC   γ-Tubulin Small Complex

γ-TuRC   γ-Tubulin Ring Complex

MTOCs   Microtubule organisation centres

aMTOCs   acentrosomal microtubule organisation centres

PCM   Pericentriolar material

Cnn   Centrosomin

Spd2   Spindle defective 2

Asl   Asterless

Ran   Ras related nuclear protein

RCC1   Regulator of Chromosome Condensation 1

SAF   Spindle assembly factor

TPX2   Targeting Protein for XKlp2

HURP   Hepatoma Up-Regulated Protein

Dgt   Dim γ-Tubulin

Msd   Mitotic spindle density

GCP-WD/ NEDD	Neural precursor cell expressed, developmentally down-regulated 1
HAUS	Human Augmin subunit
RZZ	Rod-Zw10-Zwilch
DTACC	*Drosophila* Transforming acidic coiled-coil protein
Msps	mini spindles
NuMA	Nuclear Mitotic Apparatus
EMS	ethyl methanesulfonate
FLP-FRT	Flippase-Flippase Recognition Target
Didum	Dilute class unconventional myosin
HEPES	4-(2-hydroxyethyl)-1-piperazineethanesulfonic acid
PIPES	piperazine-N,N′-bis(2-ethanesulfonic acid)
PBS	Phosphate buffered saline
GST	Glutathione S-transferase
SDS-PAGE	Sodium dodecyl sulphate polyacrylamide gel electrophoresis
LC-MS/MS	Liquid chromatography– tandem mass spectrometry
CLMS	Crosslinking mass spectrometry
TFA	Trifluoroacetic acid

SCX	Strong cation exchange
PCR	Polymerase chain reaction
RT-PCR	Reverse transcription PCR
E. coli	Escherichia coli
MBP	Maltose binding protein
PVDF	Polyvinylidene fluoride
EGTA	ethylene glycol tetraacetic acid
EDTA	Ethylenediaminetetraacetic acid
TEV	Tobacco Etch Virus
TAP	Tandem affinity purification
Wac	wee Augmin
GFP	Green fluorescent protein
TMT^{TM}	Tandom mass tag
QC	Quality control
Mud	Mushroom body defect
Stai	Stathmin
FDR	False discovery rate

Table of Contents

1. Introduction

1.1. A Brief history of mitosis and microtubules

In the mid 17 century, Robert Hooke examined various organisms under the microscope. One of which was a section of cork, which he observed to be composed of hollow box units which he called cells (Gabriel and Fogel, 1955). Hooke also saw similar structures in vegetables, and although not observed at the time, Hooke hypothesised the existence of channels that facilitate nutrient passage between the cells (Gabriel and Fogel, 1955). The idea that all life on Earth is made of these cells was not conceived until 1838 by Matthias Jakob Schleiden and 1839 by Theodor Schwann, from their observations of plant and animal cells (Wagner, 1999). Although it was theorised that all life is formed of communities of cells, it was not until Rudolf Virchow first stated that all cells must come from pre-existing cells (Sapp, 1994; Wilson, 1911) that it became accepted that the key to all biological questions can be reduced to the cell (Sapp, 1994). In order for life to continue, these cells need to divide. As early as the 1840s, scientists made observations on these cell division events, although the details of the process were a topic of heated debate. Some believed the nucleus arose exogenously, some believed the nucleus arose through division, while others believed the nucleus disappeared completely, and was replaced by two nuclei (Baker, 1955). It was not until 1882, when Walter Flemming made detailed observations of thread-like structures during cell division and coined the term mitosis from the Greek word for thread (Mitchison and Salmon, 2001), that it was generally accepted that nuclei

arose from pre-existing nuclei and that chromosomes were segregated by spindles (Wilson, 1911).

1.2. Mitosis and the mitotic spindle

In order for a cell to properly segregate its genetic material - its chromosomes - into two equal complements, a robust apparatus with a plane of symmetry is necessary. Eukaryotes have adapted to use a structure termed the mitotic spindle (or bipolar spindle) to achieve this. This bipolar spindle is composed of two symmetrical arrays of spindle fibres, consisting of microtubules (MTs). These MT fibres coordinately align the sister chromatid pairs, such that upon dissolution of the link between the pairs each sister chromatid can be correspondingly segregated to opposite sides of the cell. The spindle fibres do this by interacting with specialised proteinaceous structures on the chromosomes, termed kinetochores, and exerting force on the sister chromatid pairs through their polymerisation and depolymerisation (See Section 1.2.2). Mitosis can be open, during which the nuclear envelope breaks down, or closed, during which the nuclear envelope remains intact throughout the process and the MT fibres are generated within the nucleus. Higher eukaryotes such as animals and plants generally adopt the open mitosis system, whereas lower eukaryotes such as yeast and fungi generally adopt the closed mitosis system (Güttinger et al., 2009). It is also possible to have a third, intermediate system called semi-closed mitosis, which is used by, for example, *Drosophila* syncytial division in the early stages of embryo development. During these semi-closed mitoses, the nuclear envelope never completely disassembles, but instead becomes porous at the polar regions to allow an influx of Tubulin

(Güttinger et al., 2009; Kiseleva et al., 2001). Regardless of the type of mitosis, a bipolar spindle is always generated at the onset of eukaryotic cell division.

Although details of the molecular architecture of the spindle would not be elucidated until many decades after its initial discovery, the process of mitosis was observed and categorised into distinct phases (Wilson, 1911). These are: prophase: the preparatory step; metaphase: the initial step; anaphase: the step in which nuclear material is separated; and telophase: the step in which the cell body is divided. Although defined as separate steps, these phases were initially characterised as a set of processes without distinct boundaries (Wilson, 1911). It is now currently accepted that mitosis can be categorised into 6 stages: prophase, prometaphase, metaphase, anaphase, telophase, and cytokinesis (Fig. 1.1).

1.2.1. Tubulin and Microtubules

Although mitotic spindles were observed in the late 19th century, the spindle fibres were seen only in fixed and stained conditions. This gave rise to the idea that the spindle was structureless, and the threads seen had no biological importance. It was not until 1953, with the advancement of polarised light microscopy, that the mitotic spindle was clearly observed in live cells (Inoué, 1953).

Around the same time, direct evidence that Colchicine affects these fibres, now termed Microtubules (MTs), was also observed (Inoué, 1952). Through the use of electron microscopy (EM), cytoplasmic MTs were determined to be consisted of 13 protofilaments (Ledbetter and Porter, 1964). Similarly, the A-tubule of the flagellar microtubule doublet also consist of 13 protofilaments, although the B-tubule consist
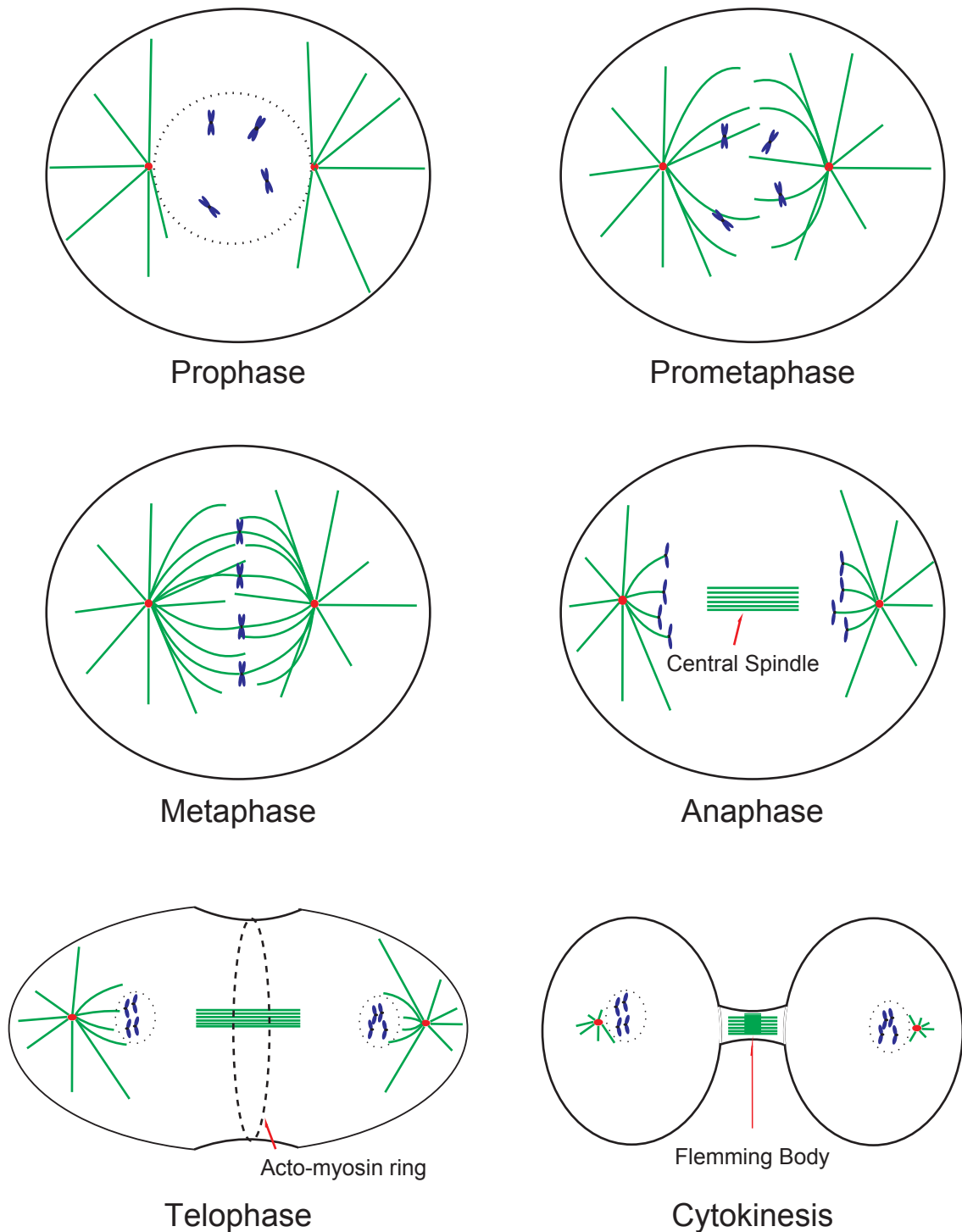
Figure 1.1- Stages of mitosis.
There are 6 stages during mitosis:
Prophase: chromosomes condense in preparaion for mitosis.
Prometaphase: the nuclear envelope breaks down and astral MTs grow.
Metaphase: chromosomes align and MTs attach to kinetochores.
Anaphase: chromosome segregation occurs with sister chromatids moving towards opposite poles and central spindle formation begins.
Telophase: the acto-myosin ring begins to contract and the nuclear envelope is reformed.
Cytokinesis: the Flemming body is formed and acto-myosin ring constriction continues until daughter cells are pinched off from each other.

of 10 protofilaments (Vaughan et al., 2006). However, it was not until 1965 that the mode of action of Colchicine at the protein level was determined, with the observation that at 0.1 µM Colchicine, synthesis of DNA, RNA, or protein was not affected but spindle formation ceased (Taylor, 1965). It was also determined that Colchicine was unlikely to be acting on an enzyme, since the rate of Colchicine binding was proportional to the concentration (Taylor, 1965). Further studies found that Colchicine bound to tissue sources that exhibited high levels of MTs, the common denominator between mitotic cells, cilia and flagella, and neurons, which led to the discovery that Tubulin was the constituent of MTs (Borisy and Taylor, 1967). The name Tubulin was not coined by the discoverers (who found the name jarring), but later by Mohri (Mohri, 1968).

During further investigation of Tubulin, it was found to have a molecular weight of approximately 110kDa under native conditions, but under denaturing conditions this molecular weight was reduced to approximately 55kDa (Shelanski, 1968; Weisenberg et al., 1968b) indicating that Tubulin must exist in a dimer. Studies of Tubulin Guanosine-5'-triphosphate (GTP) binding dynamics revealed that GTP hydrolysis only occurs within one of the two protein subunits within the dimer, and therefore it was theorised at the time that the dimer was composed of non-identical subunits with the unhydrolysed GTP embedded between them (Weisenberg et al., 1968b). The subunits were later determined to have different amino-acid compositions, as well as slight differences in electrophoretic mobility (Bryan and Wilson, 1971; Stephens, 1970). These subunits became known as α and β Tubulin.

From EM examination of plant root tip sections, MTs were found to be composed of hollow tubes (Ledbetter, 1963). The structure of these 25nm wide MTs (Kline-

Smith and Walczak, 2004) was later discerned by observing the outer doublet MTs in flagella by EM and computer modelling of the results (Amos and Klug, 1974). Although it was known that MTs consisted of protofilaments of αβ-Tubulin dimers, this computer modelling was able to determine that most MTs were made of 13 protofilaments. By comparing the diffraction patterns of MTs to α or β Tubulin, it was determined the MT lattice was composed of staggered α and β subunits spanning 8nm for each dimer (Fig. 1.2), and that the longitudinal interactions are more substantial than the lateral interactions (Amos and Klug, 1974). However, these lateral interactions between Tubulin dimers play an important role in MT formation, since Tubulin dimers can form sheets from single MT protofilament, which eventually seals itself to form a cylindrical tube due to the natural curvature formed by the lateral interactions (Erickson, 1974). The Tubulin dimer exhibits a natural polarity, and when incorporated into MTs, the α subunit faces the minus end, whereas the β subunit faces the plus end (Fig. 1.2) (Nogales et al., 1999). MT polymerisation occurs at both ends, but the plus-end exhibits faster dynamics of polymerisation/depolymerisation than the minus-end.

Various other Tubulin has since been discovered. γ-Tubulin was identified as a suppressor of a β-Tubulin, and has since been shown to be very important in MT nucleation. Details of γ-Tubulin are discussed in Chapter 1.4.1. δ-Tubulin was discovered to be an important protein in forming the C-Tubule in the basal bodies of *Chlamydomonas* (Dutcher and Trabuco, 1998). η-Tubulin was identified to be important for basal body duplication (Ruiz et al., 1987; Ruiz et al., 2000). ε-Tubulin was discovered independently in mammalian cells, and with bioinformatics approaches (McKean et al., 2001), and have been implicated in MT maintenance
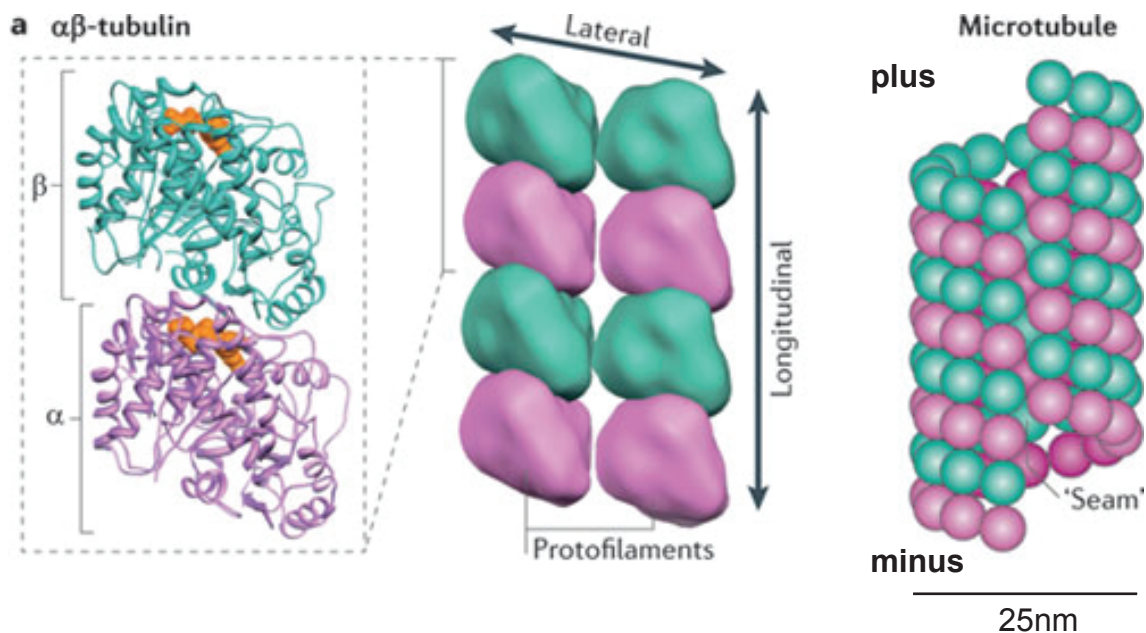
Figure 1.2- Structure of a Microtubule.
Microtubules are formed of dimers of α- and β-Tubulin, each of which can bind GTP (orange). Heterodimers can interact longitudinally to form protofilaments, or laterally. Lateral interactions have a natural curvature such that a 'sheet' of protofilaments will naturally curve into a hollow tube of ~25nm in diameter. Microtubule polarity is determined by the polarity of the Tubulin heterodimers in the protofilaments, with α-Tubulin facing the minus end and β-Tubulin facing the plus end.
Figure adapted from Kollman et al (2011).

in the basal bodies, and transition zone formation (Dutcher et al., 2002; Goodenough and StClair, 1975). ζ-Tubulin has been identified in *T. brucei* and *Leishmania major*, and localises to the basal body (McKean et al., 2001), but specific function has not been elucidated. For the purpose of this thesis, only α, β, and γ-Tubulin will be focused on.

1.2.2. Microtubule dynamics

During the characterisation of MTs, it was found that certain conditions - such as increased GTP concentration - promote MT growth, while others - such as Colchicine treatment, low Tubulin concentration, and cold temperature - promote MT destabilisation and depolymerisation (Borisy et al., 1975; Borisy and Taylor, 1967; Olmsted et al., 1974). However, the behaviour of MTs *in vitro* did not reflect the dynamic nature of *in vivo* MTs. That is, MTs *in vivo* are seen to actively grow and shrink, and to make sudden transitions between these states. The switch from MT growth to MT shrinkage is termed catastrophe, and the reverse is termed rescue (Fig. 1.3). MTs naturally undergo the switch between catastrophe and rescue, exhibiting dynamic instability (Mitchison and Kirschner, 1984). This dynamic instability was first described by Mitchison and Kirschner in 1984, who observed that MTs nucleated by centrosomes below steady-state conditions had both growing MTs as well as shrinking MTs, whereas MTs in *in vitro* conditions rarely undergo catastrophe or rescue (Mitchison and Kirschner, 1984). However, the stability of the MTs was drastically reduced when the MTs were sheared (Mitchison and Kirschner, 1984). The presence of GTP promotes MT growth (Mitchison and Kirschner, 1984), and since Tubulin has an inherent GTPase
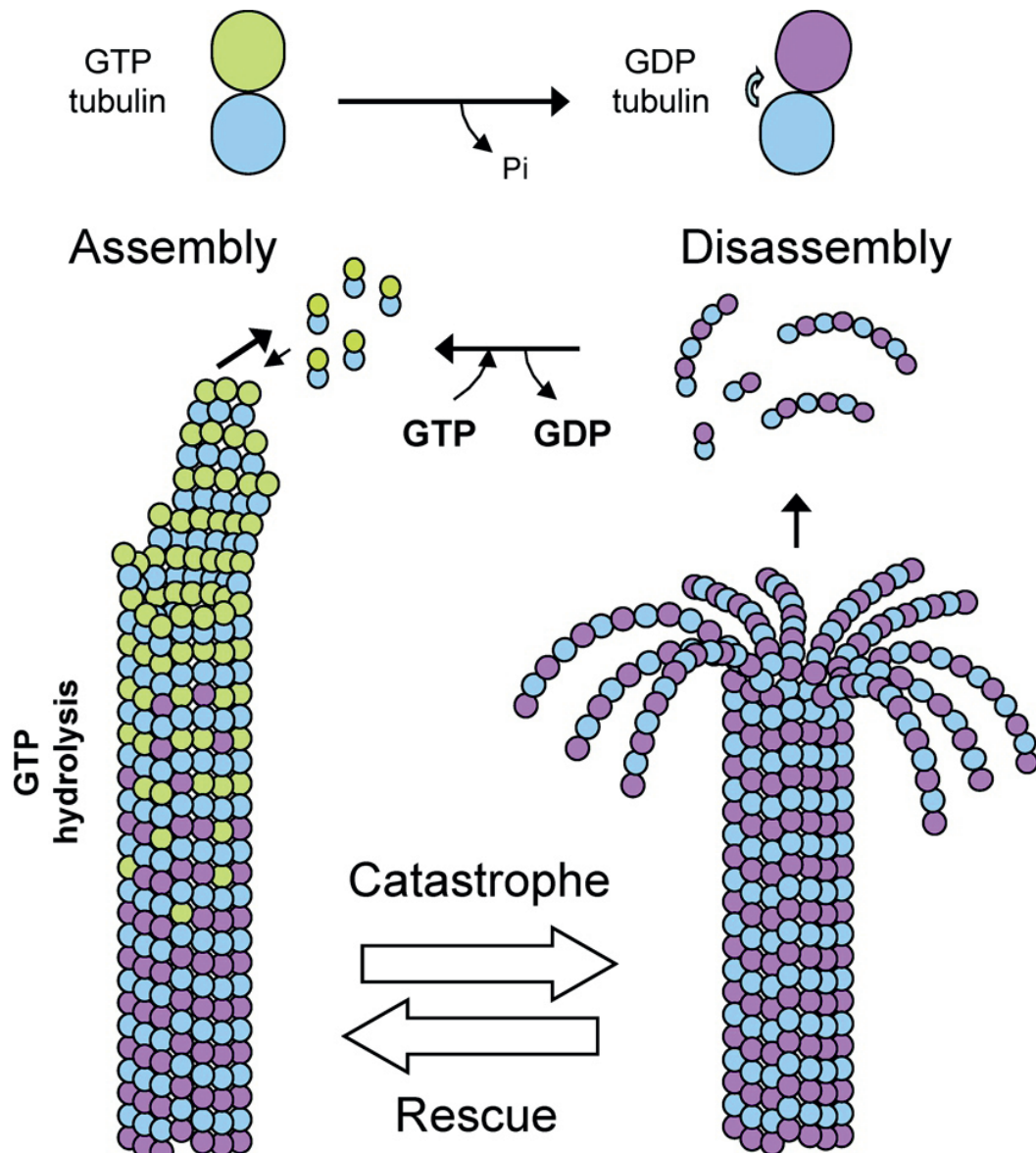
Figure 1.3- GTP is required for MT nucleation and stabilisation.

Tubulin dimers adopts a straight configuration which promotes MT assembly when GTP is bound to the β subunit. When GTP is hrdrolysed to GDP, the tubulin dimer adopts a bent configuration which promotes MT disassembly. The conversion from assembly to disassembly is termed catastrophe, and the reverse is termed rescue.

Figure taken from Bassam & Chang (2011)

activity (Borisy et al., 1975; Olmsted et al., 1974), it was believed that as Tubulin was incorporated into MTs the chance of GTP hydrolysis increases in proportion to time (Mitchison and Kirschner, 1984). Thus, the MT lattice would mostly consist of GDP-Tubulin, resulting in an inherent instability, whereas the MT tip is consisted of a stable GTP-cap (Mitchison and Kirschner, 1984). The existence of a GTP-cap which stabilises MTs is supported by the fact that the rate of MT depolymerisation is faster than polymerisation by a factor of 2-3 order of magnitude (Mitchison and Kirschner, 1984), and sheared MTs – which lose this cap - are more likely to undergo depolymerisation. It was also theorised that the MT shrinking phase was due to the loss of the GTP-cap (Mitchison and Kirschner, 1984).

Since this conceptualisation of the mechanisms behind MT dynamic instability, the molecular basis of dynamic instability is now quite well understood. Both α and β subunits are able to bind GTP and have intrinsic GTPase activity (Nogales et al., 1998). However, the GTP bound to the α subunit is trapped between the Tubulin dimer interface, and thus is never hydrolysed (Hamel and Lin, 1990; Mejillano et al., 1990). When GTP is bound to the β subunit, the Tubulin dimer adopts a "straight" conformation allowing easy polymerisation (Kollman et al., 2011; Mitchison and Kirschner, 1984). After this GTP is hydrolysed, the Tubulin dimer undergoes a conformational change, and becomes "kinked". When Tubulin dimers are incorporated into MTs, the GTP bound to the β-Tubulin will be hydrolysed (Carlier and Pantaloni, 1981; O'Brien and Erickson, 1989; Stewart et al., 1990) Using crystal structure-based sequence alignment, the molecular mechanism of GTP hydrolysis by Tubulin has been shown to be similar to the GTPase FtsZ (Ma et al., 1996), a bacterial protein that forms a filamentous ring at the site of bacterial cell

division (Ma et al., 1996). It has since been confirmed by many studies that the existence of the GTP-Tubulin cap promotes growth through supplementation of GTP (Caplow et al., 1989; Caplow and Shanks, 1996; Drechsel and Kirschner, 1994; Melki et al., 1990; Stewart et al., 1990; Voter et al., 1991; Walker et al., 1991). MT catastrophe occurs when the GTP cap of a MT is lost, and the Tubulin dimer adopts a curved configuration unfavourable for polymerisation (Desai and Mitchison, 1997; Mandelkow et al., 1991). As a result of this change, the MT protofilaments peel away from their lateral bonds (Fig. 1.3). This is consistent with the observation that MTs made of Tubulin containingGuanosine-5'-[(α,β)-methyleno]triphosphate (GMPCPP), a slowly hydrolysable GTP analogue, do not exhibit dynamic instability (Caplow et al., 1994; Hyman et al., 1992). Cryo EM on growing and shrinking MTs has shown that growing MTs generally have blunt ends while shrinking MTs generally have frayed ends, supporting this model (Mandelkow et al., 1991). However, cryo EM analysis of growing MTs in *Schizosccharomyces pombe* revealed mostly flared ends, suggesting *in vivo* MT assembly may occur differently under various cellular conditions (Hoog et al., 2011). To add further complexity to *in vivo*, patches of GTP-Tubulin are placed by Cytoplasmic Linker Asssociated Protein (CLASP) along the lattice of MTs (Al-Bassam et al., 2010). As MTs undergo catastrophe, their depolymerisation becomes halted by these GTP-Tubulin islands since their conformation favours polymerisation (Dimitrov et al., 2008). These islands then function as a new GTP cap, from which MT rescue then occurs (Dimitrov et al., 2008).

1.2.3. MT Associated Proteins (MAPs)

MAPs are a class of proteins whose function and localisation are dependent on MTs. The very first MAP identified was Dynein, identified as an ATP-dependent protein responsible for ciliary movement (Gibbons, 1963; Gibbons and Rowe, 1965). However, the role of Dynein as a molecular motor capable of traveling along the lattice of MTs was not elucidated until many years later, since the composition of MTs were not characterised at the time. Upon discovery of Tubulin, it was noted that of all the tissues examined, brain tissue contained highest levels of the protein (Borisy and Taylor, 1967; Weisenberg et al., 1968a). Due to the high availability, crude MT sedimentation procedure was then developed to isolate large quantity of Tubulin from brain tissue (Weisenberg et al., 1968a), and these Tubulin was able to repolymerise into MTs (Weisenberg, 1972). Due to the availability of brain tissue, and an estabilished protocol of generating MTs, this led to the first characterisation of MAPs being from brains (Borisy et al., 1975; Keates and Hall, 1975). These high molecular weight MAPs co-sedimented with MTs, and this association was lost under cold MT depolymerisation (Borisy et al., 1975; Keates and Hall, 1975). The high affinity of these high molecular weight MAPs was demonstrated by their ability to co-precipitate with MTs even after multiple rounds of polymerisation/ depolymerisation cycles (Borisy et al., 1975; Keates and Hall, 1975). These MAPs and were noted for their ability to aid assembly of Tubulin into MTs (Borisy et al., 1975; Keates and Hall, 1975). Further studies showed that by adding MAPs purified from brain tissue to MTs *in vitro*, MT catastrophe events can be decreased and rescue increased, hinting the importance of MAPs on MT dynamic regulation (Murphy et al., 1977; Pryer et al., 1992). Later MAP studies eventually expanded to include liver (Collins and Vallee, 1989), and testes (Collins and Vallee, 1989).

MAPs can be classified as enzymatically active MAPs, MT motors, or structural MAPs (Mandelkow and Mandelkow, 1995) (Fig. 1.4). Kinases such as Aurora B of the Chromosome Passenger Complex fall under the category of enzymatically active mitotic MAPs. They generally function to increase affinity of other MAPs such as Augmin to MTs during mitosis, which will be discussed in section 1.5.

Dynein and Kinesins fall under the category of MT motors. Dynein, as mentioned before, was discovered as the protein responsible for causing ciliary movement (Gibbons, 1963; Gibbons and Rowe, 1965). Dynein is the larger of the two types, and is a minus-end directed MT motor (Raaijmakers and Medema, 2014). During mitosis, Dynein functions to separate centrosomes in prometaphase, and upon spindle formation, functions to focus the spindle poles where MT minus-ends are concentrated (Raaijmakers and Medema, 2014). Kinesins are smaller in size, and with a few exceptions, are generally plus-end directed MT motors. They were originally identified as a protein responsible for transporting organelles, as well as moving MTs in the axons of squid (Vale et al., 1985). During mitosis, kinesins aid spindle formation by sliding MTs in an anti-parallel manner, driving MTs towards opposite ends of the bipolar spindle (Tanenbaum and Medema, 2010). Together, Dynein and Kinesins act together during mitosis, and promote spindle self-assembly (Karsenti and Vernos, 2001; Loughlin et al., 2010; Ma et al., 2010; Tournebize et al., 2000; Vernos and Karsenti, 1996).

The final category are structural MAPs which regulate the structure of MTs by means of nucleation, stabilisation, or destabilisation, and can either preferentially localise to plus or minus ends of MTs, or localise to the MT lattice. Although Tubulin naturally are able to assemble into MTs *in vitro*, the concentration *in vivo*
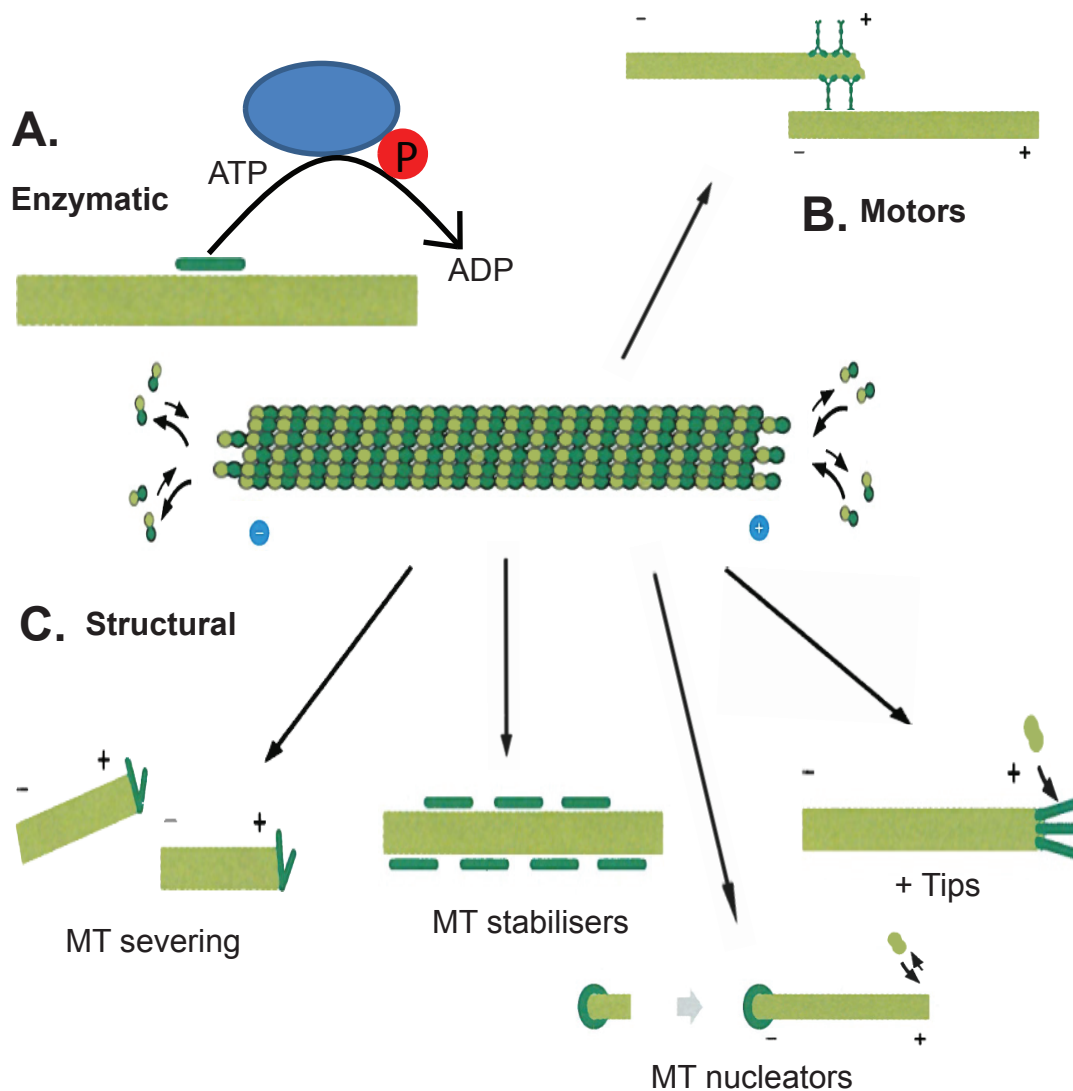
Figure 1.4- Classification of MAPs.

MAPs can be classified into enzymes (A), motors (B), or structural (C). During mitosis, kinases are the best characterised enzymatic MAPs, where they control the affinity of other MAPs to MTs. Motors are involved in MT sliding, and by extention, play an important role in spindle self-assembly. Structural MAPs are the most diverse group, consisting of MT severing, MT stabilising, MT nucleating, and plus-end binding proteins. Together, these MAPs regulate the dynamic instability of MTs during mitosis.

Figure adapted from Molecular Biology of the Cell, 5th edition.

are too low for spontaneous polymerisation to take place. Structural MAPs, more specifically MT nucleators and stabilisers are important since they may reduce the critical concentration for MT polymerisation to occur (Maccioni and Cambiazo, 1995), and are important to regulate MT dynamic instability during mitosis. γ-Tubulin complexes are the predominant MT nucleators, and are discussed more in detail in Chapter 1.4.1. Patronin specifically recognises MT minus end, and protects MT from depolymerisation (Goodwin and Vale, 2010). Doublecortin, which binds to the valleys found between the MT protofilaments and acts as additional scaffold for the MTs (Moores et al., 2004). In addition, the mechanism of Doublecortin promotes the assembly of MTs composed of 13 protofilaments (Fourniol et al., 2010). Plus-tip proteins such as End Binding 1 (EB1) binds to the plus end of MTs by recognising the GTP-cap and promote MT growth by enhancing lateral contacts (Maurer et al., 2012), while XMAP215 enhances Tubulin dimer addition (Cassimeris et al., 2001).

In order for a cell to maintain MT dynamic instability, destabilisers are also needed. Althoughg Katanin severs MTs along the lattice (McNally and Vale, 1993; Vale, 1991), it is localised to centrosomes (McNally et al., 1996; McNally and Vale, 1993), where it facilitates minus-end directed MT disassembly. This process of MT disassembly is important in separating chromosomes at anaphase, as well as destabilising the MT network at the G2/M transition.

It is important to note that MAPs may fall into more than one classification. For an instance, although the Kin 1 Kinesin family Kinesin 8 (Klp3) traverse on MTs towards the plus-end, and Kinesin 13 (MCAK) traverse towards both the plus-end and the minus-end, they also affects MT structure by promoting MT destabilisation

(Desai et al., 1999; Gardner et al., 2011; Hunter et al., 2003; Oguchi et al., 2011; Roostalu and Surrey, 2013; Walczak, 2006). Although Doublecortin acts as a MT stabiliser, it has a secondary effect of promoting MT nucleation (Moores et al., 2004). Although all categories of MAPs are important in mitosis, my thesis has predominantly focused on structural MAPs.

The importance of MAPs in regulating MT dynamics is clear, and mitosis is a process which heavily involves MT dynamic regulation. However, it was not until 1989 did the first major study in identifying mitotic MAPs occur. MAPs were purified by MT cosedimentation from early *Drosophila* embryos which cycles through S phase and M phase, and antibodies were raised against the proteins after separation by polyacrylamide gel electrophoresis (Kellogg et al., 1989). Of the 24 antibodies generated, 20 identified a protein which localised to MT structures. Subsequently, the antibodies were used in a screen against a cDNA expression library, and the positive hits were cloned (Kellogg and Alberts, 1992). This approach was inefficient, and MAPs that were not solubilised during the initial elution would not be detected. With the advancement of technology in the fields of mass spectrometry, bioinformatics, RNA interference, and with the availability of the full sequence of the *Drosophila* genome (Adams et al., 2000), it has been possible to vastly improve the number of MAPs identified, including work in our own laboratory which identified 270 MAPs, 83 of which were previously uncharacterised (Hughes et al., 2008). This suggests that there are currently large numbers of MAPs about which we know very little, and that a great deal of work still needs to be done before we have a full picture of the complement and function of MAPs in whole cells.

1.3. The co-ordinated process of mitosis

Although mitosis has been categorised into distinct phases (Fig 1.1), it is important to note that the process orchestrates co-ordinated, dynamic changes to all the elements and structures within a cell, and that the phases of mitosis flow into one another (Wilson, 1911). Nonetheless, the semantic distinctions between phases make it easier to compare cell types and organisms when considering the main elements of mitosis - the chromosomes and the mitotic spindle.

During prophase, chromosomes condense in preparation for segregation (Wilson, 1911). Interphase MTs also depolymerise to make way for the bipolar spindle to be constructed. In addition, centrosomes migrate away from each other, and many highly dynamic MTs begin to be nucleated from them. During open mitosis, the onset of prometaphase is marked by nuclear envelope breakdown. At this point, the bipolar spindle forms, with MTs sorted in relation to one another by MT motor proteins, which also functions to bundle MTs (Gatlin and Bloom, 2010). Mitotic MTs are especially dynamic (Inoué and Sato, 1967), increasing the likelihood that a MT will associate with one of the kinetochores found on chromatin (Tanaka, 2013). Although kinetochores can attach MTs laterally, all attachments are eventually processed to be end-binding (Tanaka, 2013). Each kinetochore will bind multiple MTs, and these MTs are bundled to form Kinetochore fibres (k-fibres) (Meunier and Vernos, 2012). As the chromosomes become amphitelically attached to MTs, they are subjected to force from opposing k-fibres (Matos et al., 2009). An equalisation of this force results in the alignment of a sister chromatid pair approximately halfway between the poles of the k-fibres. As all the chromosomes begin to

congress in this way, they form what is known as the equatorial, or metaphase, plate.

Metaphase itself is defined as the point at which all the sister chromatid pairs have aligned at the equatorial plate (Wilson, 1911). At this point, there is a time delay prior to the initiation of chromosome segregation. It is crucial that the cell does not initiate segregation in the presence of a chromosome that has yet to align at the equatorial plates as, in doing so, that sister chromatid pair would be segregated to a single pole (Musacchio and Salmon, 2007), thus leading to aneuploidy and chromosomal instability. Cells therefore have a spindle assembly checkpoint (SAC), which at the onset of mitosis, is turned on. SAC halts entry into anaphase until all the chromosomes are aligned by kinetochore-MT interactions (Musacchio and Salmon, 2007). The SAC is satisfied and turned off when MTs are properly attached to, and tension is exerted on the kinetochore (Musacchio, 2011; Nicklas and Koch, 1969). Although the details of how the SAC senses tention is currently not well understood (Musacchio, 2011).

Prior to full alignment, the SAC functions by negatively regulating CDC20 (Hwang et al., 1998), the co-factor for the ubiquitin ligase Anaphase Promoting Complex/ Cyclosome (APC/C). When the final chromosome reaches alignment, this inhibition on CDC20 is relieved and the APC/C is activated (Hwang et al., 1998; Peters, 2006). The active APC/C is targeted to specific protein substrates with distinct but overlapping timing, priming them for proteolytic degradation by the proteasome (Musacchio and Salmon, 2007). One of these targets is Securin, the inhibitor of Separase, degradation of which leads to activation of Separase (Uhlmann et al., 1999). Separase is a protease which cleaves the Scc1 subunit of Cohesin, a

complex which maintains concatenation between sister chromatid pairs (Hauf et al., 2001; Schöckel et al., 2011; Uhlmann et al., 1999). The result of Separase activation is therefore cleavage of the "glue" holding sister chromatids together, a pre-requisite for their segregation to opposite poles (Hauf et al., 2001; Uhlmann et al., 1999; Uhlmann et al., 2000). Shortly after initiation of Securin degradation, the APC/C is targeted to CyclinB (Hauf et al., 2001), the regulatory co-factor of the master mitotic kinase CDK1 (Fisher et al., 2012). Degradation of Cyclin B leads to inactivation of CDK1 (Jeong and Yang, 2013), and the many substrates of CDK1 begin to be dephosphorylated by mitotic phosphatases such as PP2A (Jeong and Yang, 2013; Musacchio and Salmon, 2007). At this point, the cell can be said to have exited mitosis and, by default, chromosome segregation (anaphase) will occur.

Anaphase is therefore marked by the separation of the sister chromatids and their movement towards the spindle poles. Not only does the sister chromatid cohesion need to be removed, but also the kinetochore-MT bundles linking the chromosomes to the poles need to depolymerise. In yeast, this process is facilitated by the Dam1 ring complex (Salmon, 2005), which couples the depolymerising MTs while attaching to the kinetochore through its association with NDC80 (Fig 1.5) (Joglekar et al., 2010). As the MT depolymerises, the Dam1 ring complex is pushed backwards away from the fraying plus-end, which provides the energy to efficiently transport the daughter chromosomes to the poles (Westermann et al., 2006). Although higher eukaryotes do not possess the Dam1 ring complex, cryo-EM has suggested that NDC80 acts in a similar mechanism without the need for the Dam1 ring (Tooley and Stukenberg, 2011).
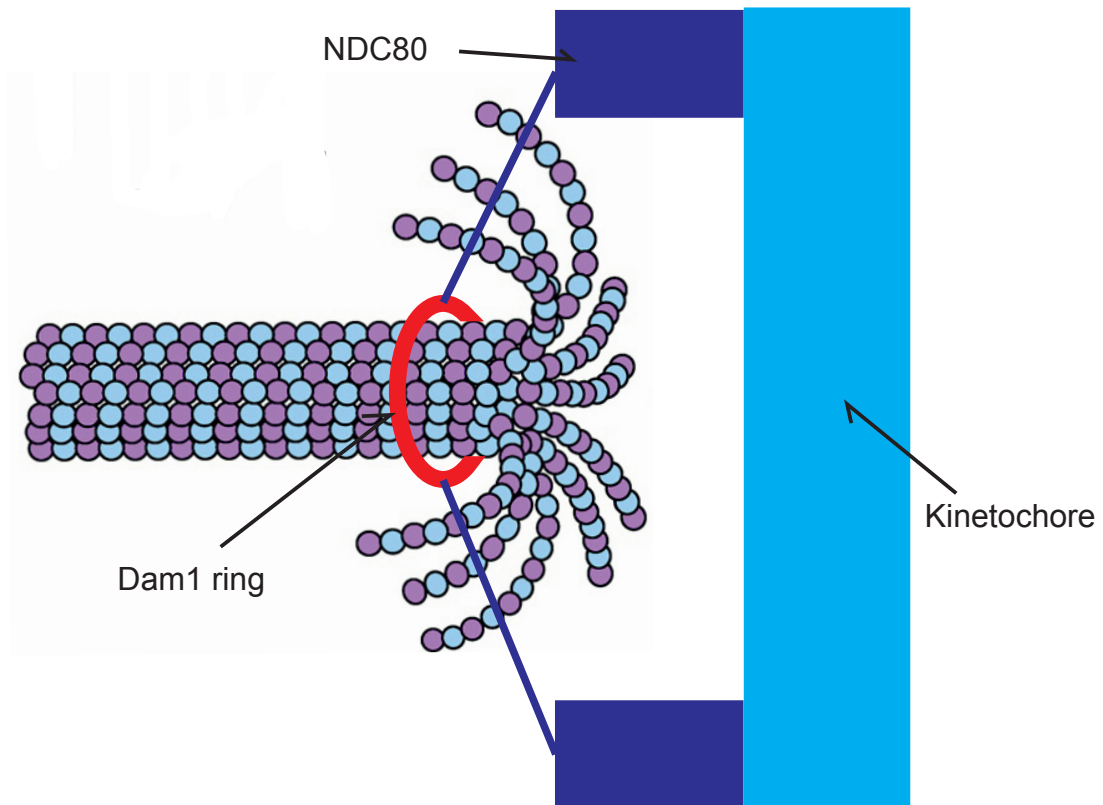
Figure 1.5- The Dam1 ring complex captures the energy from destabilising MTs.

The Dam1 ring complex is an essential component of kinetochore in yeast and forms a ring around the destabilising MT which processively moves along the MT as the end depolymerises while tethering the MT to the kinetochore via interaction with the kinetochore protein NDC80. This tethering allows efficient transport of daughter chromosomes along MTs to the spindle poles during anaphase.

At the onset of anaphase, MTs are actively depolymerised at the plus-end (Zhang et al., 2007). Due to the resemblance to the video game, the mechanism is termed Pacman (Zhang et al., 2007). MT depolymerisation also occurs at the minus-end, reeling in the chromosomes, in a process termed Flux (Sharp and Rogers, 2004). The combined MT depolymerisation processes of Pacman and Flux are predominantly facilitated by the enzymes Katanin, Spastin, and Fidgetin (Zhang et al., 2007).

Simultaneously to chromosome segregation, additional MTs are generated, moved to the centre of the cell, and bundled, between the separating DNA (Douglas and Mishima, 2010). These MTs form the central spindle and resolve into an anti-parallel MT bundle (Douglas and Mishima, 2010) which accumulates proteins such as the kinases Aurora B at its centre (Crane et al., 2004). In many cells, the central spindle functions during late anaphase and telophase to activate the downstream targets necessary for formation and stability of the cortical acto-myosin ring at the midzone cortex (Weiss, 2012), facilitating cleavage furrow ingression.

Telophase begins as daughter chromosomes reach the spindle pole regions, and spindle elongation has completed (Wilson, 1911). At this point, the cleavage furrow continues to ingress, forming a transient structure called the midbody or Flemming body (White and Glotzer, 2012). In addition, the chromosomes begin decondensation, and the nuclear envelope begins to reform around them (Wilson, 1911).

This series of co-ordinated but incredibly complex events results in the completion of mitosis.

1.4. MT nucleation

αβ Tubulin dimers are able to polymerise spontaneously in vitro at high concentrations (Mitchison and Kirschner, 1984; Tran et al., 1997). However, in the cell the process of MT nucleation is facilitated by MT nucleating proteins. Such nucleation events probably result in the formation of very short but stable MT seeds which additional αβ dimers can bind to. Thus the rate limiting step - the formation of a 13 protofilament structure - can be overcome. By localising and activating these nucleating factors at specific places and times, the cell can orchestrate the sites of MT nucleation.

1.4.1. γ-Tubulin

γ-Tubulin is a distinct member of the Tubulin superfamily (Ludueña, 2013) and is almost essential for MT nucleation in eukaryotic cells. It was first identified in *Aspergillus* as a suppressor of a β-Tubulin mutant, sharing homology to α and β-Tubulin (Oakley and Oakley, 1989). Soon after, γ-Tubulin was identified in animals, plants, fungi, and diatoms, where it localises to centrosomes (Stearns et al., 1991). Much of what we now know regarding the way in which γ-Tubulin nucleates MTs has come from *in vitro* biochemical work using both *Xenopus* and *Drosophila* extracts. Purification by immunoprecipitation and peptide elution yielded a complex that, upon examination by electron microscopy, had the appearance of ring structures resembling washers (Zheng et al., 1995). This γ-TuRC binds to the minus-end of MTs, blocking minus-end growth, and also lowers the critical concentration of Tubulin dimer for MT polymerisation (Zheng et al., 1995). Similar ring structures were later identified by immuno-EM and shown to consist of multiple

units of γ-Tubulin in each ring (Moritz et al., 1995). Initial examination of γ-Tubulin by sucrose gradient fractionation however identified two separate complexes: γ-Tubulin Small Complex (γ-TuSC) with an apparent molecular weight of 280kDa, and γ-Tubulin Ring Complex (γ-TuRC) with an apparent molecular weight of 2000kDa (Oegema et al., 1999). Both species of γ-Tubulin complexes are able to nucleate MTs (Oegema et al., 1999).

Later experiments demonstrated that the γ-TuRC caps the minus end of MT and not only prevent growth but also protects the minus end from depolymerisation (Wiese and Zheng, 2000). Immuno-EM demonstrated that the γ-Tubulin subunit decorates the very end of the MT and does not extend into the MT (Keating and Borisy, 2000), while structural reconstruction from electron tomography revealed that the γ-TuRC adopts an asymmetric cap configuration consisting of γ-TuRC bound to the ends of each protofilament (Fig. 1.6A) (Moritz et al., 2000; Wiese and Zheng, 2000). γ-TuRC was later shown to have 13-fold symmetry (Kollman et al., 2011). The structure of the γ-TuRC cap at the minus end combined with this 13-fold symmetry has led to the current model, in which γ-TuRC nucleates MTs by acting as a template (Evans et al., 1985; Wiese and Zheng, 2000). In this model, γ-TuRC provides an initial helix at the minus-end and setting up the 13 protofilament configuration through the γ-Tubulin interaction with the α-Tubulin of the Tubulin heterodimer (Fig. 1.6B). Further supporting the γ-TuRC template model is that MTs polymerised spontaneously *in vitro* in the absence of γ-TuRC usually have 14 protofilaments, whereas MTs polymerised *in vivo* or in the presence of cell extracts generally consist of 13 protofilaments with a 'seam' (Fig. 1.2) (Evans et al., 1985).
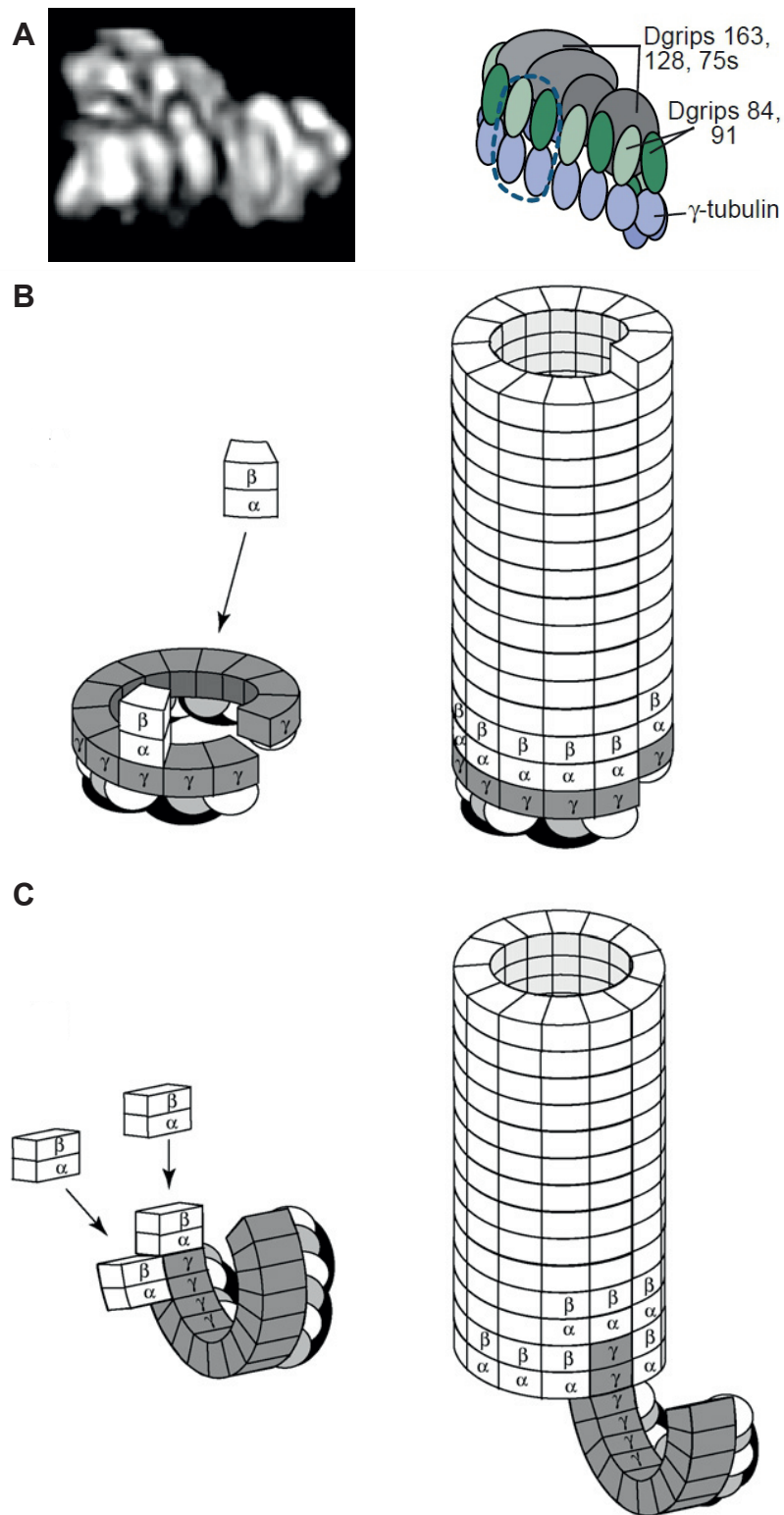
Figure 1.6- The two models of MT nucleation by γ-TuRC.
(A) Electron-microscopic tomography shows that γ-TuRC adopt a cap-like structure at the minus-end of MTs. (B,C) Currently, there are two models on how γ-TuRC nucleate MTs. In the template model (B), γ-TuRC provides the initial 13-fold helix, and the α-Tubulin subunit interacts with the γ-Tubulin subunit to promote nucleation. In the protofilament model (C), γ-Tubulin at the end of the curved ring provides an interface for nucleation by interacting laterally with both the α and β subunits.
Figure 3A is taken from Moritz et. al. (2000). Figures 3B and C are taken from Raynaud-Messina & Merdes (2007).

However, there exists an alternative protofilament model where γ-TuRC provides a single protofilament that interacts with the Tubulin dimers through lateral contact, forming a second protofilament (Fig. 1.6C) (Raynaud-Messina and Merdes, 2007). This version has been proposed due to some inconsistencies of the observed data with the template model. For example, in the template model, γ-Tubulin would only interact with the α-Tubulin subunit exposed at the MT minus end. However γ-Tubulin can, and does, interact directly with β-Tubulin (Erickson and Stoffler, 1996). Further, although immuno-EM and tomography show that γ-Tubulin only decorates the minus end and does not extend into MTs (Keating and Borisy, 2000), such observations do not rule out γ-TuRC nucleating MTs via a very short protofilament. Since monomers of γ-Tubulin have nucleating capability (Leguy et al., 2000) as well as capping MT minus ends, γ-Tubulin protofilaments do not need to be long for MT nucleation to occur (Erickson and Stoffler, 1996). In addition, the smaller γ-TuSC, consists only of two γ-Tubulin subunits (Oegema et al., 1999) yet can also nucleate MTs (Oegema et al., 1999), demonstrating that a template is dispensable for MT nucleation. Finally, in early MT nucleation events *in vitro*, Tubulin dimers arrange into sheets before coming together to form a tube, demonstrating the natural behaviour of Tubulin to be nucleated from protofilaments as opposed to from a template.

1.4.2. MTOCs and the localisation of γ-Tubulin

Centrosomes are animal cell organelles composed of two MT-based centrioles, serving as the predominant microtubule organisation centre (MTOC) of the cell. Each centriole is composed of 9 MT blades surrounding a central cartwheel

(Azimzadeh and Marshall, 2010; Paintrand et al., 1992). Surrounding the centrosomes is an electron-dense cloud, termed the pericentriolar material (PCM). This PCM contains hundreds of proteins, including many MAPs and the MT nucleating γ-TuRC complex (Giansanti et al., 2008; Moritz et al., 1995; Zhang et al., 2007). As such, the amount of PCM at the centrosome is, in many cases, directly proportional to the MT nucleating capacity of the centrosome (Khodjakov and Rieder, 1999; Piehl et al., 2004). Not surprisingly, PCM recruitment by centrosomes increases as cells enter mitosis (Woodruff et al., 2014), concomitant with the increased number of highly dynamic MTs that are generated here (Piehl et al., 2004). Much of our understanding of PCM recruitment comes from mutational studies in *Drosophila*. It has been shown that the core centriolar protein Spd2 is required for recruitment of Centrosomin (Cnn) which in turn recruits γ-TuRC to centrosomes (Dix and Raff, 2007). Interestingly, Cnn recruits γ-TuRC by direct interaction with γ-Tubulin (Zhang and Megraw, 2007), and cells lacking γ-TuRC subunits still recruit γ-Tubulin to the centrosomes (Reschen et al., 2012; Vérollet et al., 2006). This process of γ-Tubulin recruitment by Spd2 and Cnn is facilitated by the Asterless (Asl) protein (Dix and Raff, 2007; Giansanti et al., 2008), and in the absence of both Spd2 and Asl, PCM recruitment is completely abolished (Dix and Raff, 2007; Giansanti et al., 2008).

1.4.3. MT nucleation during mitosis

In early observations of mitotic spindles, MTs were seen to arise from the centrosomes, from which they extend until they come into contact with the kinetochore (Mitchison, 1986). Since the kinetochores only make up a small area

of the chromosome, the likelihood of a growing MTs making contact with this region is low. With the observations that MTs are highly dynamic during mitosis, it was proposed that the rapid growth and shrinkage of MTs increases the chances of MT-kinetochore contact, and that upon contact, the kinetochore caps and stabilises the MTs (Mitchison, 1986). This search and capture model prevailed for several decades. However more recently, mathematical modelling has demonstrated that bipolar, mature spindle formation occurs more quickly than would be theoretically possible if this search and capture mechanism was the only one in play (Mitchison, 1986).

Indeed, although centrosomes have historically been viewed as the predominant MTOCs, they are ultimately dispensable for mitosis. A number of lines of evidence point to this conclusion. Not only are centrosomes absent in plant cells (Masoud et al., 2013) and in many animal meiotic cells (Homer, 2013), but somatic animal cells lacking centrosomes are usually able to complete mitosis (Basto et al., 2006; Mahoney et al., 2006; Stevens et al., 2007), although they often have mitotic defects. The *Drosophila* cell line 1182 lacks centrosomes, but can be maintained in cell culture (Debec and Abbadie, 1989). A functional bipolar spindle still forms when centrosomes are removed from cells via laser ablation microsurgery (Khodjakov et al., 2000). *Drosophila* carrying a mutation in *sas4*, which encodes a core inner centriole protein, have defects in centrosome duplication (Basto et al., 2006; Stevens et al., 2007), and centrioles and centrosomes are completely absent. However, flies lacking such functional centrosomes are sterile but develop fully into adulthood, dying shortly after eclosing (Basto et al., 2006). Both sterility and death are due to an absolute requirement for the centrosome in cilia/flagella formation,

and death of *sas4* mutants is due to mechanosensory defects as a consequence of failure to form cilia on sensory neurons (Basto et al., 2006). These studies imply that the classical model, in which centrosomes form the predominant MTOC, and the idea that MTs solely emanate from centrosomes is incorrect. In fact, kinetochores from purified chromosomes can nucleate MTs (Mitchison and Kirschner, 1985). Since kinetochores have the ability to bind Tubulin directly, it is believed that nucleation of the mitotic spindle occurs in part from the interaction between kinetochore-bound Tubulin, and free-floating Tubulin (Mitchison and Kirschner, 1985).

However, additional mechanisms also contribute to spindle formation (Fig. 1.7). A bipolar spindle can assemble around beads coated with DNA which lacks centromeric sequences (Heald et al., 1996), indicating that chromatin plays an important role in building the bipolar spindle independent of kinetochores. Subsequent studies showed that the small GTPase, Ras Related Nuclear Protein (Ran), regulates this process (Kalab et al., 1999; Wilde and Zheng, 1999). During mitosis, Regulator of Chromosome Condensation 1 (RCC1), a guanine nucleotide exchange factor associated with chromatin, converts inactive Ran-GDP into active Ran-GTP (Carazo-Salas et al., 1999; Ohba et al., 1999). As Ran is present throughout the cytosol, this activation generates a gradient of Ran activity, with high concentrations around the mitotic chromatin and low concentrations towards the cell cortex (Clarke and Zhang, 2008). Active Ran-GTP causes the release of a set of MAPs termed spindle assembly factors (SAFs) (Clarke and Zhang, 2008; Fu et al., 2007). SAFs are normally kept inhibited by association with Importin proteins

Centrosome Driven

Augmin Driven

Kinetochore and Chromatin Driven

Other Mechanisms

All Pathways Combined
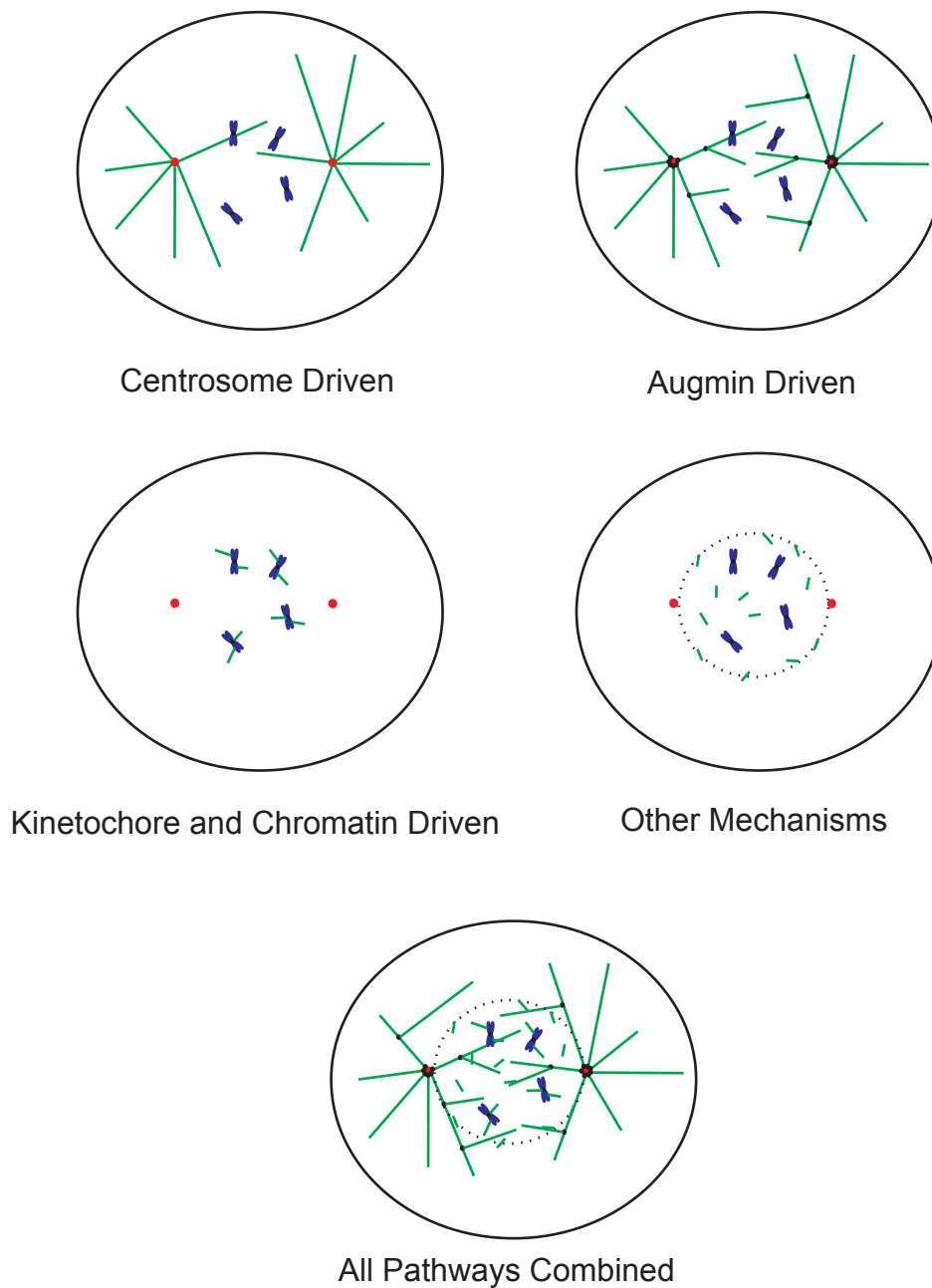
Figure 1.7- The mitotic spindle is built by various pathways.
There are various factors that contribute to building the bipolar spindle. Centrosomes have been historically viewed as the predominant MTOCs, but Augmin, Chromatin, and other mechanisms also contribute to MT nucleation and organisation. Upon perturbation of one pathway, other pathways become up-regulated, which demonstrates the robustness of the system.
Figure adapted from Duncan and Wakefield, 2011

which, outside of mitosis, ensure that SAFs are kept in the nucleus (Clarke and Zhang, 2008; Fu et al., 2007). Examples of SAFs are Targeting Protein for XKlp2 (TPX2) and Hepatoma Up-Regulated Protein (HURP), both of which can facilitate MT nucleation and/or stabilisation (Clarke and Zhang, 2008; Fu et al., 2007).

A third pathway which contributes to mitotic spindle nucleation is termed MT-templated (or MT-dependent) MT nucleation, and has been observed in a variety of organisms. Although the molecular basis of this phenomenon has only recently been described (Uehara et al., 2009; Wu et al., 2008), it is clear that, at least in some organisms, the MTs it generates constitute the majority of spindle MTs during meiosis (Colombié et al., 2013). This pathway is dependent upon a protein complex termed Augmin (Goshima et al., 2008).

In addition to centrosomal, chromosomal, and Augmin mediated MT nucleation, there are other cellular components that may be involved in building the mitotic spindle (Fig. 1.7). During open mitosis, the nuclear envelope breaks down, but remnants may still remain (Duncan and Wakefield, 2011); since the nuclear envelope may nucleate MTs through the interaction of nuclear pore proteins with γ-Tubulin complexes, these remnants may provide additional MT nucleation (Duncan and Wakefield, 2011). The Golgi has been characterised as an important MT nucleator during interphase (Chabin-Brion et al., 2001; Rivero et al., 2009) and recent evidence suggests it may be an additional MTOC during prophase, anaphase, and telophase, but not prometaphase or metaphase (Maia et al., 2013). Even the cytoplasm itself can nucleate MTs (Bajer and Molè-Bajer, 1986), which may self-assemble (Brunet et al., 1998). The spindle matrix remains perhaps the most controversial component of spindle assembly (Heinrichs, 2006), but proteins

from this region such as Skeletor (Walker et al., 2000), Megator (Qi et al., 2004), Chromator (Rath et al., 2004), and East (Qi et al., 2005) localise ahead of growing spindle MTs during mitosis, seemingly guiding them, and may also aid in MT organisation.

1.5. The Augmin complex

γ-Tubulin was originally thought to localise exclusively to centrosomes and MT minus ends (Joshi, 1993; Stearns et al., 1991; Zheng et al., 1991). As described in Section 1.3.1, γ-Tubulin is capable of acting as a MT nucleator as a monomer (Leguy et al., 2000), as γ-TuRC (Keating and Borisy, 2000; Moritz et al., 2000; Oegema et al., 1999; Zheng et al., 1995), or as γ-TuSC (Oegema et al., 1999). However, both fluorescence microscopy and electron microscopy studies have consistently reported a distinct localisation of γ-Tubulin to the mitotic spindle itself (Lajoie-Mazenc et al., 1994). However, the significance of this spindle-associated γ-Tubulin was overlooked and it was only in 2005 that it was demonstrated that this population of γ-Tubulin, found on pre-existing spindle MTs, was functional and capable of generating additional spindle MTs (Murata et al., 2005).

Around this time, in an attempt to identify those proteins with an essential role in mitotic spindle assembly, two *tour de force* studies using the model organism *Drosophila melanogaster* were performed (Goshima et al., 2007; Hughes et al., 2008). A genome-wide RNAi screen identified ~200 genes important in spindle assembly. RNAi of 6 of these proteins reduced γ-Tubulin staining at the spindle, and therefore these 6 were termed Dim Gamma Tubulin (Dgt) proteins 1-6 (Goshima et al., 2007). RNAi against Dgt1 reduced γ-Tubulin staining both within

the spindle and at centrosomes, whereas RNAi against Dgt2-6 only reduced γ-Tubulin staining within the spindle (Goshima et al., 2007). Co-immunoprecipitation and sucrose sedimentation subsequently confirmed that Dgt2-Dgt6 interacts with each other and likely to form a complex which was termed Augmin (Goshima et al., 2008). The size of this complex was larger than the sum of the 5 subunits however, suggesting that additional subunits were present (Goshima et al., 2008).

Concomitantly, a biochemical study was published which identified ~250 novel mitotic MAPs and their interactions in *Drosophila* embryos using MT co-sedimentation, mass spectrometry, RNAi, and bioinformatics (Hughes et al., 2008). Five of these MAPs exhibited low spindle density after RNAi, and were named mitotic spindle density (msd) 1-5 (Hughes et al., 2008). Msd2, Msd3 and Msd4, and two other proteins characterised in this study were found to be identical to Dgt proteins.

Subsequently, Msd1 was shown to co-purify with the Dgt proteins and therefore to be an additional subunit of the Augmin complex. Similarly, another protein identified as having a severe mitotic defect, CG13879 (Hughes et al., 2008), was identified as belonging to the complex and was termed Wac (Meireles et al., 2009). Mass spectrometry analysis of Dgt2 immunoprecipitates from S2 cells also identified Msd1, Wac and Msd5 (Uehara et al., 2009). Taken together, this indicates that the Augmin complex actually comprises 8 proteins whose nomenclature is slightly confusing (see Table 1.1). The Augmin complex has since been shown to be present in many eukaryotic organisms, including humans, Xenopus and higher plants (Hotta et al., 2012; Lawo et al., 2009; Petry et al., 2011;

Uehara et al., 2009). The names of the human homologues is also given in Table 1.1.

1.5.1. The molecular basis of Augmin function

RNAi studies in S2 cells revealed that removal of any single Augmin subunit, with the exception of Dgt4, results in the reduction of the protein levels of all other subunits, likely due to the destabilisation of the complex (Goshima et al., 2008; Meireles et al., 2009). In addition, reduction or removal of any Augmin subunits results in the reduction of γ-Tubulin localisation to the spindle, as well as reduced spindle density (Goshima et al., 2008; Hughes et al., 2008; Meireles et al., 2009; Wainman et al., 2009). Combined with the evidence that all Augmin subunits localise to the mitotic spindle (Goshima et al., 2008; Hughes et al., 2008; Lawo et al., 2009; Meireles et al., 2009; Wainman et al., 2009), and EB1 tracks originating within the spindle are reduced in cells lacking subunits of the complex (Wainman et al., 2009), the current model suggests that Augmin acts as a MT-dependent MT nucleator by recruiting γ-TuRC to the spindle. Augmin is not responsible for targeting γ-TuRC to the centrosomes, since centrosomal γ-Tubulin localisation is unaffected in cells lacking Augmin (Goshima et al., 2008; Hughes et al., 2008; Meireles et al., 2009; Wainman et al., 2009).

In humans, the molecular interactions linking γ-TuRC and Augmin occur between the γ-TuRC subunit GCP-WD/NEDD1 (termed Dgp71WD in *Drosophila*), and the C-terminus of HAUS6 (termed Dgt6 in *Drosophila*) (Uehara et al., 2009; Zhu et al., 2008; Zhu et al., 2009). During mitosis, CDK1 phosphorylates GCP-WD on residues S460 and T550, promoting association of GCP-WD with another kinase,

Homo sapiens	Molecular Weight		Drosophila melanogaster	Molecular Weight
HAUS1/ CCDC5	32 kDa		**Msd5**/ Dgt7	28.5 kDa
HAUS2/ CEP27	27 kDa		**Msd1**/ Dgt9	15.7 kDa
HAUS3/ C4ORF15	70 kDa		Dgt3	65.8 kDa
HAUS4/ C14ORF94	42 kDa		**Wac**/ Dgt8	19.1 or 17.5 kDa
HAUS5/ KIAA0841	72 kDa		Msd2/ **Dgt5**	78.0 kDa
HAUS6/ FAM29A	109 kDa		Msd4/ **Dgt6**	72.8 kDa
HAUS7/ UCHL5IP	41 kDa		Dgt2	25.8 kDa
HAUS8/ HICE1	45 kDa		Msd3/ **Dgt4**	21.4 kDa

Table 1.1- The names and molecular weights of Augmin subunits in *Homo sapiens* and their homologues in *Drosophila melanogaster*. Where multiple names are given, the most common (and the one used throughout this thesis) is marked in bold.

Plk1 (Johmura et al., 2011). Although the interaction between GCP-WD and HAUS6 does not appear to be through direct Plk1-mediated phosphorylation, the interaction in turn promotes phosphorylation of HAUS8, the human Dgt4 homologue, on 17 different residues (Johmura et al., 2011). This phosphorylation, particularly on residues S129, T130, S131, S133, S143, and S151, affects the ability of HAUS8 to bind to MTs and increases the interaction between Augmin and MTs (Johmura et al., 2011). Conversely, Aurora A has also been shown to phosphorylate HAUS8, but at the Ser/Thr 17-21 cluster, which inhibits the interaction between HAUS8 and MTs, and this phosphorylation is important for bipolar spindle establishment (Tsai et al., 2011). It can therefore be said that the Augmin complex relies heavily on mitotic kinases to both increase and decrease its MT binding function during mitosis, although the precise details are clearly complex.

Although the suggestion that Augmin and γ-TuRC act together to generate branching MTs is compelling, until very recently the evidence was mainly circumstantial. Recently however, Augmin has been demonstrated to use pre-existing MT as a directional template, and MT branching has been directly visualised *in vitro* using fluorescence based microscopy in *Xenopus* embryo extracts (Petry et al., 2013). This study showed that Ran-GTP stimulates branching MT generation, and that immunodepletion of either Augmin or TPX2 (the main downstream effector of Ran-GTP in *Xenopus*), resulted in a specific loss of MT branching. Interestingly, although immunodepletion of γ-Tubulin greatly attenuated branched MT formation, after a delay branched MTs still formed (Petry et al., 2013). Electron tomography confirmed that Augmin-dependent MT branches are

directional, allowing newly generated MTs within the spindle to maintain spindle polarity (Kamasaki et al., 2013) .

In addition to generating branched MTs, the Augmin complex may also be involved in kinetochore driven MT nucleation. In *Drosophila*, the Rod-Zw10-Zwilch (RZZ) complex localises to the kinetochore prior to metaphase, and at metaphase, this complex streams towards the spindle pole in a Dynein-dependent manner. *Drosophila* S2 cells in which Dgt6 expression has been reduced via RNAi do not show correct streaming of a component of this complex, Zeste White-10 (ZW10) (Bucciarelli et al., 2009), suggesting that there are defects in k-fibre structure. Furthermore, MTs did not regrow from chromosomes following temperature-mediated depolymerisation in Dgt6 RNAi-treated cells (Bucciarelli et al., 2009), strengthening the idea that Augmin plays a role in kinetochore-mediated MT nucleation. The Augmin subunit Dgt6 interacts with kinetochore proteins NDC80 and Cenp-meta as well as the D-TACC/ Msps complex in S2 cells (Bucciarelli et al., 2009), and a second subunit Dgt4 also interacts with NDC80 (Wu et al., 2009). Therefore, it has been postulated that Augmin might bind k-fibres, and facilitate their interaction with NDC80 (Bucciarelli et al., 2009).

1.5.2. Conservation of Augmin structure and function

The importance of Augmin has been characterised in humans (Lawo et al., 2009; Uehara et al., 2009), *Arabidopsis thalania* (thale cress) (Ho et al., 2011; Hotta et al., 2012; Nakaoka et al., 2012), *Danio rerio* (zebrafish) (Du et al., 2011), and *Xenopus laevis* (African clawed frog) (Petry et al., 2011). In all studies so far disruption of the Augmin complex results in disruption of γ-TuRC localisation to the spindle MTs, but

there are some notable differences in Augmin function between human, *Drosophila*, and plant. In humans, depletion of any single Augmin subunit by RNAi causes centrosome fragmentation in a Nuclear Mitotic Apparatus (NuMA) dependent manner (Lawo et al., 2009; Leber et al., 2010), but this fragmentation phenotype is not observed in *Drosophila* - either in cell lines, or in the organism itself (Goshima et al., 2008; Meireles et al., 2009; Wainman et al., 2009). In plants, the Augmin complex appears to be essential, since homozygous seeds are unable to be generated from heterozygous mutants in any Augmin subunit (Hotta et al., 2012). This is unsurprising, since plants lack centrosomes and thus the importance of MT-templated MT generation would be greater. There is also evidence that the Augmin complex may function to replace centrosomes, which may contribute to its importance in plants. Acentrosomal spindles generated by incubating *Xenopus* embryo extracts with DNA-coated beads have indicated that Augmin is important for focusing spindle poles (Colombié et al., 2013; Petry et al., 2011), while in the *Drosophila* meiotic spindle, which as in many organisms forms without centrosomes, Augmin localises to the spindle poles and is required for chromosome congregation (Colombié et al., 2013). This is in contrast to *Drosophila* mitosis where Augmin localises along the MTs of the spindle. This further suggests that Augmin functions to replace centrosomes in meiosis.

In all four organisms in which Augmin has been characterised, the complex appears to have 8 subunits (Du et al., 2011; Ho et al., 2011; Hotta et al., 2012; Lawo et al., 2009; Nakaoka et al., 2012; Petry et al., 2011; Uehara et al., 2009). However, subunits are poorly conserved between organisms at the amino acid level. For example, there are clear human homologues of *Drosophila* Dgt3-6

(Duncan and Wakefield, 2011), but Msd1, Msd5, Dgt2 and Wac do not share significant primary sequence homology to their proposed human homologues HAUS2, HAUS1, HAUS7, and HAUS4 (Duncan and Wakefield, 2011). However, *de novo* tertiary structural predictions do suggest significant structural similarity between HAUS2 and Msd1, HAUS4 and Wac and HAUS1 and Msd5 (Duncan and Wakefield, 2011). In plants, where the Augmin subunits are termed Aug1-Aug8 (Hotta et al., 2012), Aug8 behaves differently to the other seven subunits, as it localises specifically to the plus-end of MTs (Cao et al., 2010). It is therefore currently difficult, particularly given the recent discovery of this complex, to compare the functional conservation of this protein complex between organisms. Even in *Drosophila*, in which the Augmin complex has perhaps been best studied, our understanding of its exact composition and function is limited. The only current known protein-protein interactions within the complex are Wac with Dgt2 (Meireles et al., 2009), and Dgt4 with Dgt6 (Uehara et al., 2009). The only two subunits with a characterised function are Dgt4, which associates with MTs (Wu et al., 2008), and Dgt6, which associates with γ-TuRC (Uehara et al., 2009; Zhu et al., 2008), though thus far both of these interactions have only been shown in humans. The main aims of this Thesis was therefore to further our understanding of the molecular relationships between *Drosophila* Augmin subunits, and between Augmin, MTs and the γ-TuRC.

1.6. Drosophila melanogaster as a model organism

William Earnest Castle first had the idea to use *Drosophila melanogaster* as a model organism in the early 1900s due to the ease and relative cheapness of

maintaining the organism. However, Castle found it difficult to make valid conclusions due to the variation of growth stages between individuals, and abandoned the idea (Stephenson and Metcalfe, 2013). However, Thomas Hunt Morgan saw the potential of *Drosophila* and continued to use it in his research. During his research career, Morgan noticed a male fly with white eyes, contrary to the wild-type phenotype of red eyes. By breeding the white-eyed fly with his red-eyed sisters, 1237 red-eyed progeny of both genders and 3 white-eyed male progeny were recovered (first filial generation, F1). These progeny were interbred and produced more male white-eyed flies, but no female white-eyed flies (second filial generation, F2). The F1 white-eyed male flies were crossed with females of the F2 progeny, and this cross produced both male and female white-eyed flies (Morgan, 1910). This demonstration of sex-linked inheritance eventually won him a Nobel Prize.

Hermann Joseph Muller, a student of Morgan's, later discovered that X-rays could be used to cause heritable mutations, chromosome translocations, inversions, and fragmentations, in a dose-dependent manner (Muller, 1927). This discovery also won Muller a Nobel Prize. In addition to X-rays, a powerful chemical mutagen ethyl methanesulfonate (EMS) was also widely used for studying gene function. The ability of such mutagens to induce chromosome rearrangements was later used to create artificial chromosomes that resisted recombination during female meiosis (Venken and Bellen, 2014). These artificial chromosomes are called balancers, carry a homozygous lethal allele, and allow sterile or lethal mutants to be kept as a stable heterozygous stock (Venken and Bellen, 2014).

Using *Drosophila* as a model organism provides the advantage of examining the function of a gene in a whole organism as well as on the cellular level, allowing a more comprehensive and contextual picture of gene function to be built. Since the *Drosophila* genome has been fully sequenced (Adams et al., 2000) and there are excellent publically-available repositories for various genetic tools and mutant lines, the ease of studying fly genetics has also tremendously improved. In addition, inducible site-directed recombination using the Flippase-Flippase Recognition Target (FLP-FRT) system allows recombination to take place only in specific tissues, allowing the study of mutations that normally lead to early lethality (Chou and Perrimon, 1996).

In terms of cell division, *Drosophila* is an excellent organism for studying mitosis since it is relatively easy to examine both symmetric and asymmetric cell divisions. The Drosophila early embryo also represents an excellent tool for the studies of the mitotic spindle, since the early embryo undergoes syncytial divisions in which the cytoplasm is shared, and only the nuclei divide (Foe and Alberts, 1983). There are several advantages to using this system. Firstly, mitoses in this early embryo are well-characterised and defined. A specific number of divisions occurs prior to cellularisation, with 7 rounds of mitosis (cycles) at the central region of the embryo proceeding post-fertilisation (Foe and Alberts, 1983). At cycle 8 to 9, the nuclei migrate from the centre of the embryo towards the cortex (Foe and Alberts, 1983). Cycles 10-13 therefore occur as a monolayer close to the embryo cortex, making these cycles easy to observe with conventional fluorescence microscopy techniques (Foe and Alberts, 1983). These cycles also occur within a short span of time, typically between 9 and 21 minutes per cycle. Secondly, as these mitotic

cycles occur within a shared cytoplasm, proteomic manipulation can be easily achieved throughout the embryo by injection of, for example, interfering antibodies, or dominant negative proteins. Thirdly, prior to the midblastula transition at mitosis cycle 14, all proteins necessary for cell division are provided by the mother (Tadros and Lipshitz, 2009), and the embryo itself is transcriptionally and translationally silent. Lastly, *Drosophila* embryos are an exceptional source of protein, since large quantities of tissue can easily be obtained for biochemical study.

Drosophila egg chambers are another useful tool in the study of MT nucleation, organisation, and maintenance outside of mitosis. The oocyte, nurse cells, and follicle cells undergo different differentiation events, all of which require functional MTs (Cooley and Theurkauf, 1994). In the egg chamber, a set process of incomplete cell divisions results in the production of a single oocyte connected by cytoplasmic bridges to a defined number of nurse cells. These nurse cells provide maternal mRNAs and proteins to the oocyte, which are transported through these cytoplasmic bridges to the oocyte by MT dependent motors (discussed in Chapter 6). As such, the egg chamber represents an excellent system to examine the functionality of MTs.

1.7. Aims of the project and summary of findings

As discussed in Section 1.4.3, the Augmin complex is potentially vital to the process of mitosis. However, while the function remains the same, conservation of all 8 subunits across the organisms in which it has been identified is low, and some subunits have only been identified using predicted structural homology. Thus far, the exact composition of the complex (in terms of numbers of each subunit), the

precise dynamics and relationships between the individual subunits and of the complex as a whole, and the binding capacity of each subunit to MTs or to γ-TuRC have not been fully determined.

Drosophila provides a variety of convenient systems to study MT dynamics and function in both interphase and mitotic cells. Therefore, using *Drosophila* as a model system, the aims of the work presented here were:

(i)   To determine the biochemical properties of the Augmin complex and its relationship to MTs.

(ii)   To find additional proteins recruited by Augmin to pre-existing MTs.

(iii)   To determine the molecular relationships between the Augmin subunits.

(iv)   To determine whether the Augmin complex plays a role outside of mitosis, using the polarised MT network in the *Drosophila* oocyte as an example.

I have purified individual subunits of the Augmin complex and examined their properties *in vitro*. While it has been shown previously that Augmin binds both MTs (via HAUS8/Dgt4) and γ-TuRC (via HAUS6/Dgt6), these studies have only been done in human cell lines. Using biochemical assays, I show here that the subunits Dgt4 and Wac are responsible for interaction with MTs and that the C-terminus of Dgt6 and the combined N-termini of Dgt3 and Dgt5 interact with the γ-TuRC subunit Dgp71WD. I have also identified Wac as a subunit that protects MTs from destabilisation. This provides that the first proof in *Drosophila* that the Augmin complex binds both MTs and γ-TuRC, and characterises the importance of additional subunits not previously known to contribute to these interactions. Interestingly, I also found evidence that the Augmin complex is able to promote MT

assembly in the absence of γ-TuRC, suggesting a novel function for Augmin independent of the major MT nucleating complex.

I also characterise the first successful purification of the intact Augmin complex, an essential step in determining its biochemical and functional composition. Using this purified complex, I have begun to determine the molecular relationship between the Augmin subunits and have generated a model of how Augmin might function to recruit γ-TuRC to the sides of existing MTs. In conjunction with this, I show that the complex binds specifically to the MT lattice. Lastly, I have determined that at least one subunit, Wac, plays a role in MT organisation outside of mitosis.

Together, the work presented here significantly improves our understanding of the Augmin complex and also provides an excellent complement of tools for further investigation.

2. Materials and Methods

Unless otherwise stated, all chemicals are from Sigma-Aldrich, or Malford Laboratories Limited.

2.1. *Drosophila* Husbandry

2.1.1. General *Drosophila* maintenance

Drosophila stocks were maintained at 18^oC or 22^oC for general maintenance, or at 25^oC for crosses and amplification in *Drosophila* culture medium - 1kg yeast, 800g glucose (Fisher), 500g flour, 110g agar, 60mL propionic acid, 40mL 10% nipigen in 10L H_2O. Stocks were maintained in 25 x 95mm vials, and amplified in 6oz bottles. Fly sorting was done under CO2 aesthesis.

2.1.2. Drosophila stocks

The *Drosophila* line W^{1118}, obtained from the Bloomington Stock Center and donated by Michael Ashburner, was used as the wild-type unless otherwise stated. When making transgenic Drosophila lines, plasmids were sent to BestGene Inc. for transgenic lines to be generated from *Drosophila* embryos with the W^{1118} genetic background. All pUAS fly lines were driven by maternal-α-Tubulin VP16-Gal4 (mat-α-T-Gal4), donated by Andrea Brand to the Bloomington Stock Center.

Augmin lines: Three pUAS-based GFP-tagged Augmin subunits fly stocks were made previously in the Wakefield laboratory. The pUAS-Msd1-GFP;mat-α-T-Gal4 line has been previously described (Wainman et al., 2009). The pUAS-Dgt5-GFP

on chromosome 3 as well as the pUAS-Dgt6-GFP on chromosome 2 lines were maintained without an expression driver. The pUAS-HAUS4-GFP was created by the process described in Section 3.2.1 and the initial fly stock generated by BestGene, and several transformants were obtained, only one of which was used in the work presented here. The Augmin null *Drosophila* line *wacΔ12* was generated previously in collaboration with Prof. Hiro Ohkura (Meireles et al., 2009).

Lines used for visualising Tubulin: The *Drosophila* line pUbi-Tubulin-GFP on chromosome X which expresses Tubulin-GFP ubiquitously, were kind gifts from Prof. Jordan Raff. The *Drosophila* lines EB1-GFP (Liang et al., 2009) and γ-Tubulin-GFP (γ-Tubulin37C-GFP on chromosome X expressed under ndc promoter) were a kind gift from Prof. Sharyn Endow (Hallen et al., 2008).

Other lines: The *Drosophila* line *oskar* mRNA-MS2*MCP-GFP on chromosome 2 was used to visualise *oskar* mRNA transport in the oocyte, and was a kind gift from Dr. Tse-Bin Chou. The pUAS-Didum-GFP line was a kind gift from Dr. Sonia Lopez de Quinto (Cardiff University) (Krauss et al., 2009). The *Drosophila* line carrying the *cnn*[HK21] mutant allele was obtained from Bloomington Stock Center. The *Drosophila* line carrying the *cnn*[mfs7] allele was a kind gift from Prof. Jordan Raff.

2.1.3. Embryo collection

Adult Drosophila were trapped in a collection chamber, and acclimatized to yeast paste on apple juice agar (25g agar, 300ml apple juice, 700ml H2O) for 24 hours. Flies were allowed to lay embryos on fresh apple juice agar plate with yeast paste for 4 hours. The embryos were dechorionated with bleach for 2 minutes. The

bleach containing embryos were decanted into a filtration unit. Dechorionated embryos were washed with generous amounts of H2O 0.05% Triton X-100. The embryos were placed into eppendorf tubes, weighed, flash-frozen in liquid nitrogen, and stored at -80 $^{\circ}$C.

2.2. Molecular Biology and Biochemistry

2.2.1. Making Human cDNA

Human oral epithelial tissue was obtained by rinsing the oral cavity with tap water containing table salt (Tesco). The resulting water was collected in 50 ml falcon tubes, and centrifuged at 5000 g 10 minutes. Total RNA was extracted with the SV Total RNA Isolation System (Promega). cDNA was generated with Revertaid First Strand cDNA Synthesis Kit (Thermo Scientific) with poly-T primer.

2.2.2. Polymerase Chain Reaction (PCR)

Amplification was carried out in T3 Thermocycler (Biometra). Phusion polymerase (Finnzymes) was used HF buffer with $MgCl_2$ adjusted to 3mM. Amplification program consist of initial denaturing stage of 30 seconds at 98°C, followed by 34 cycles of denaturation (10 seconds at 98°C), annealing (30 seconds at 61.5°C), and elongation (30 seconds 72°C). A final elongation step of 5 minutes 72°C was carried out after the completion of 34 cycles.

2.2.3. Gateway^{TM} cloning of HAUS4

HAUS4 ORFs were amplified from human cDNA using primers flanking the start codon and the termination codon. Kozac consensus sequence (**in bold**) was added to the 5' end prior to the start codon to improve translation efficiency. Termination codon was replaced by a lysine codon (***in bold italics***) for C-terminal tagging.

CACCATGGCATCCGGGGATTTCTGCT Forward primer

AAAACGGTAGACCTTGCTGAACTCCT Reverse primer

After amplification, the insert DNA was cloned into the pENTR™ vector using Directional TOPO® Cloning Kit (Life Technologies). After sequence confirmation of the presence of HAUS4 insert was without mutations, the HAUS4 insert was recombined into the pPWG destination vector (Drosophila Genomics Resource Center, Indiana, donated by Dr. Terence Murphy) by Gateway® LR Clonase™ II Enzyme Mix.

2.2.4. Transformation of *E. coli*

E. coil was incubated with plasmid for 30 minutes on ice, placed in a 42 °C water bath for 45 seconds, then placed back on ice for 2 minutes. 250 µl S.O.C. medium was added to the bacteria, and incubated at 37 °C with shaking. 50 µl of the culture is plated on LB agar plates with Kanamycin (Sigma) for pENTR (Life Technologies) constructs, and Ampicillin (Sigma) for all other constructs.

2.2.5. Plasmid DNA preparation

E. coli transformed with plasmids were grown overnight at 37 ^{o}C. The bacteria culture was harvested by centrifugation at 6800 g for 2 minutes, and subjected to a modified alkaline lysis plasmid prep protocol, in accordance to instructions from the manufacturers (Qiagen, Fermentas).

2.2.6. Restriction digest and agarose gel electrophoresis

Restriction digestion was carried out by incubating plasmid with EcoRV (New England Biolabs) at 37°C for 1 hour. The digests were resolved on 1% agarose (Fisher), in TBE buffer (89mM Tris, 89mM Boric acid, 2mM Ethylenediamine-tetraacetic acid) with 100 volts for 30 minutes.

2.2.7. Making *Drosophila* embryo high speed supernatant

Frozen *Drosophila* embryos were placed in a glass homogenizer. Two volumes of BRB80 (1mM MgCl$_2$, 1mM ethylene glycol tetraacetic acid (EGTA), 80mM piperazine-N,N′-bis(2-ethanesulfonic acid) (PIPES)) containing 10% glycerol, and cOmplete Mini protease inhibitor (Roche), and PhosSTOP phosphatase inhibitor (Roche) was added to the embryos before homogenization. The mixture was centrifuged at 13,000g for 10 minutes at 4^{0}C. The middle phase was taken, and subjected to centrifugation at 100,000g for 30 minutes at 4^{0}C. The middle phase of the high speed centrifugation was taken, and subjected to another centrifugation at 100,000g for 10 minutes at 4^{0}C. The middle phase is kept for downstream application.

2.2.8. GFP-Trap immunoprecipitation

Batches of 0-3 hr old embryos laid by cages of 1-10 day-old flies were dechorionated, weighed, flash frozen in N_2 (l) and stored at -80°C. Frozen embryos were homogenized in 2 volumes of C buffer (50mM HEPES [pH 7.4], 50mM KCl, 1mM MgCl$_2$, 1mM EGTA, 0.1% IGEPAL CA-630, protease inhibitors [Roche]). Extract was clarified through centrifugation at 13,000 g for 10 min, 100,000 g for 30 min, and 100,000 g for a further 10 min. Clarified extract was incubated with 50 µl GFP-TRAP-A beads (Chromotek) overnight at 4^{0}C. GFP-TRAP-A beads were washed 3 times with ice-cold C buffer. For Augmin samples was subsequently used for crosslinking, an additional wash step of 3 times with ice-cold C buffer without IGEPAL CA-630 was done.

2.2.9. GST co-sedimentation assay

GST and GST-Dgp71WD, immobilized individually on Glutathione Agarose resin, were washed 3 times with PBS containing 150 mM imidazole, and 0.1% IGEPAL CA-630. Approximately 20 µg of His-tagged proteins were incubated with 10 µl of resin for 2 hrs at 4 ^{o}C with agitation. After incubation, resins were washed 3 times with PBS containing 150mM imidazole, and 0.1% IGEPAL CA-630 and re-suspended in 30 µl of protein sample buffer for SDS-PAGE/Western Blotting analysis.

2.2.10. Microtubule co-sedimentation assay using *Drosophila* embryos

Guanosine-5'-triphosphate (GTP) (Sigma) was added to *Drosophila* high speed supernatant to a final concentration of 1mM. Paclitaxel (Sigma) was added to a final concentration of 50mM. The *Drosophila* high speed supernatant was incubated at 25°C for 30 minutes, and layered onto two-volumes of BRB80+40% glycerol. The samples were centrifuged at 100,000g for 30 minutes at 4°C to pellet the microtubules. The supernatant was removed by aspiration, and the top surface of the sucrose cushion was washed twice with BRB80. The remaining sucrose cushion was then removed by aspiration, and the pellet washed once with BRB80.

2.2.11. Mass spectrometry sample preparation for crosslink mass spectrometry

2.5% of total beads were analyzed by LC-MS/MS to estimate sample quality and digestion efficiency. This Augmin aliquot was re-suspended in 50 µl of 50 mM ammonium bicarbonate. Trypsin was added with a final concentration of 20 ng/µl. Digestion was incubated at 37°C with shaking. After an overnight digestion, supernatant (containing peptides) was collected and acetified to pH 3 with 0.1% Trifluoroacetic acid (TFA). Peptides were subsequently desalted using C18-StageTips (McKean et al., 2001) for mass spectrometric analysis.

The remaining (97.5%) purified Augmin was resuspended in 200 µl C buffer and cross-linked using 400 µg of bis[sulfosuccinimidyl] suberate (BS3) (i.e. 1:5 protein to cross-linker ratio (g/g)). The cross-linking reaction was incubated on ice for 2 hours with periodic agitation. After removal of supernatant, the beads were

incubated with 200 µl of 50 mM ammonium bicarbonate for 30 mins on ice with periodic agitation. 3 µg trypsin was added and digestion left to occur at 37 °C with shaking overnight. After digestion, peptide mixture (in supernatant) was collected and fractionated using SCX-StageTips (McKean et al., 2001) with a small variation to the protocol previously described for linear peptides (Goodenough and StClair, 1975). In short, the peptide mixture was acetified with 2.5% acetic acid to pH3 and was loaded on a SCX-Stage-Tip. The bound peptides were eluted in four steps with buffers (10% v/v ACN, 0.5% v/v acetic acid) containing 50 mM, 100 mM, 200 mM and 500 mM ammonium acetate into four fractions. Cross-linked peptides were expected to be in the three fractions that were eluted with higher ammonium acetate concentrations. Peptides in these three fractions were desalted using C18-StageTips (McKean et al., 2001) prior to mass spectrometric analysis.

2.2.12.   Microtubule co-sedimentation assay using purified proteins

Tubulin (Cytoskeleton Inc.) was resuspended in BRB80 containing 10% glycerol, and 1mM GTP at 5mg/ml concentration. Microtubules were polymerized at 37^0C for 45 minutes. Paclitaxel (Sigma) was added to the plus-taxol sample to a concentration of 50µM. The same amount of Tubulin resuspension buffer was added to the minus-taxol sample. Microtubules are then incubated at 37^0C for 30 minutes. Bacterially expressed and purified proteins were centrifuged at 100,000g for 30 minutes to precipitate non-soluble protein. The proteins were incubated with microtubules at a 1:1 tubulin:protein molar ratio at 37^0C for 15 minutes, then placed on ice for 15 minutes. Samples were spun through 150µl ice cold 40% glycerol

cushion at 100,000g for 45 minutes. Supernatant was collected from the top phase. The glycerol cushion was washed 3 times with 50µl BRB80, each time removing 50µl of the remaining cushion. The pellets were resuspended in BRB80 with the same volume as the supernatant.

2.2.13.   Mass spectrometry

Mass spectrometry analysis of crosslinked peptides was done on LTQ-Orbitrap Velos (Thermo Fisher Scientific), and crosslinked peptides were identified by Dr. Angel Chen (Rappsilber Laboratory, Wellcome Institute for Cell Biology, University of Edinburgh) with an in-house program. Mass spectrometry analysis for all other samples were done by University of Bristol Proteomics Facility. For the quantitative mass spectrometry, two-tailed T-Test was perfomed with Excel (Microsoft).

2.2.14.   Protein expression and purification

pGEX-Dgp71WD was a gift from Professor Jordan Raff (University of Oxford, UK). pQE80-His-GFP was obtained from Dr. Steven Porter (University of Exeter, UK), pMal-Wac from Professor Hiro Ohkura (Meireles et al., 2009), and pMal-c2x/DEST from Jason Carlyon (Huang et al., 2010).   pRSETA-Dgt3^N, pRSETA-Dgt5^N, and pRSETA-Dgt6^C were created using the GeneArt service (Life Technologies). pRSETA-Dgt3^N constituted aa 1-350 of Dgt3-PA, pRSETA-Dgt5^N constituted aa 1-450 of Dgt5-PA and pRSETA-Dgt6^C constituted aa 298-654 of Dgt6-PA. pMal-Dgt4 was created by amplifying the full length Dgt4-PA cDNA by PCR with appropriate

terminal restriction enzyme sites, cloning first into pGEM-T, and subsequently into pMal-c2x via standard procedures.

All plasmids were transformed into BL21 (DE3) cells (genotype: fhuA2 [lon] ompT gal (λ DE3) [dcm] ΔhsdS λ DE3 = λ sBamHIo ΔEcoRI-B int::(lacI::PlacUV5::T7 gene1) i21 Δnin5) and grown in LB medium at 37 ^{o}C to an OD_{600} of between 0.4-0.6 before induction with 0.1mM IPTG. pGEX-Dgp71WD and pQE80-His-GFP were induced at 18 ^{o}C overnight, pRSETA-Dgt3^{N}, pRSETA-Dgt5^{N}, and pRSETA-Dgt6^{C} were induced at 4 ^{o}C overnight, while pMal-c2x, pMal-Wac and pMal-Dgt4 were induced at 22 ^{o}C for 4 hours. Cells were pelleted at 6800 g and stored at -80°C until required.

Bacteria expressing GST-Dgp71WD were incubated in Buffer A (PBS adjusted to 900 mM NaCl, 0.5% IGEPAL CA-630, 0.2 mg/ml lysozyme, 1mM PMSF) for 1 hr with rotation at 4 ^{0}C, sonicated with 6 x 10 seconds bursts and centrifuged at 10,000 g for 10 min at 4 ^{0}C to pellet cell debris. The supernatant was incubated with Glutathione Agarose beads (Sigma, UK) overnight at 4 ^{o}C with rotation and washed twice with 10 volumes of Buffer A and once with PBS, ready for use in the GST-pull down assay (see following section). Bacteria expressing His-tagged Dgt3^{N}, Dgt5^{N}, Dgt6^{C} were incubated in Buffer B (PBS adjusted to 500 mM NaCl, 0.5% IGEPAL CA-630, 10 mM imidazole, 0.2 mg/ml lysozyme, 1 mM PMSF) for 1 hr with rotation at 4 ^{o}C, sonicated with 6 x 10 seconds bursts and centrifuged at 10,000 g for 10 min at 4 ^{o}C to pellet cell debris. The supernatant was incubated with HisPur Cobalt resin (Pierce, USA) for 2 hr with rotation at 4 ^{o}C, before being loaded into a standard 1ml column (Pierce, USA), washed with at least 20 volumes of Buffer B and eluted with PBS containing 150 mM imidazole, and 0.1% IGEPAL

CA-630. His-tagged GFP was purified as above, except using Buffer D (PBS adjusted to 500 mM NaCl, 25 mM imidazole) and Ni-Sepharose Fast Flow resin (GE, UK). His-tagged proteins were concentrated using an Amicon Ultra column (30kDa cut-off) and buffer exchanged into Buffer A, for immediate use in the GST-pull down assay. Soluble MBP, and MBP-tagged Wac or Dgt4 were purified as for GST-Dgp71WD except for incubation with Amylose resin (NEB, UK) instead of Glutathione Agarose and a final wash into BRB-80 containing 10% glycerol, for use in the MT co-sedimentation assay.

2.2.15. Sodium dodecyl sulphate polyacrylamide gel electrophoresis (SDS-PAGE)

Proteins were separated by 1-dimensional electrophoresis using the Bio-Rad MiniProtean II system. 1.0mm thick gels were prepared such that the resolving gel consisted of 10% (v/v) 29:1 acrylamide/bis-acrylamide, 375mM Tris-Cl pH 8.8, 0.1% (v/v) SDS, 0.1% (v/v) ammonium persulphate and 0.0006% (v/v) N,N,N',N'-tetramethylethylenediamine, and the stacking gel consisted of 4% 29:1 acrylamide/bisacrylamide, 125mM Tris-Cl pH 6.8, 0.1% SDS, 0.1% ammonium persulphate and 0.001% N,N,N',N'-tetramethylethylenediamine. Gels were run under a constant current at 30mA per gel in 25mM Tris, 250mM glycine and 0.1% SDS. Page Ruler or Page Ruler Plus (Thermo Scientific) were used to indicate apparent molecular weights. Protein samples were boiled with SDS gel-loading buffer to a final concentration of 2% (w/v) SDS, 0.1% (w/v) bromophenol blue, 10% (w/v) glycerol, 100mM dithiothreitol (DTT).

2.2.16. Western Blot

Polyacrylamide gels were transferred onto either PVDF or nitrocellulose membrane using Mini Trans-Blot® cell immersed in ice. Transfer was done in transfer buffer (25mM Tris, 192mM glycine, 10% methanol) at 150mA 1 hour for 1 gel, or 200mA 1 hour 30 minutes for 2 gels. Membranes were blocked with 5% milk (Tesco) in 0.1% PBST for 1 h room temperature. Membranes were probed with primary antibody at 4^0C overnight, and then washed 3 times 10 minutes with 0.1% PBST. HRP-conjugated secondary antibody was used at 1:10,000 for 1 h room temperature. Membranes were washed again 3 times 10 minutes with 0.1% PBST. Proteins were detected with ECL Western Blotting Substrate (Pierce).

Primary antibodies were used as follows:

Mouse anti-GFP (Roche) was used at 1:1000. Mouse anti-α-Tubulin clone DM1A was used at 1:10,000. Rabbit anti-Dgt6 (a kind gift from Prof. Maurizio Gatti) was used at 1:1000. Mouse anti-His-Tag antibody clone 27E8 (Cell Signaling Technology, USA) was used at 1:1000. Anti-MBP mouse monoclonal antibody (NEB, UK) was used at 1:10,000. Rabbit anti-GST (GE Healthcare) was used at 1:1000.

2.2.17. Gel-filtration chromatography

Gel-filtration chromatography was performed on Superose 6 10/300 GL with ÄKTAprimeplus liquid chromatography system (GE Healthcare). Flow rate was adjusted to 0.5ml/ minute. The system was calibrated with proteins of known molecular mass - carbonic anhydrase (29kDa), albumin (66kDa), alcohol

dehydrogenase (150kDa), β amylase (200kDa), and apoferritin (443kDa) - by Dr. Ewa Bielska.

2.3. Cell Biology

2.3.1. Immunofluorescence of *Drosophila* ovaries using anti-Tubulin

Flies were fed fresh yeast 2 days prior to dissection. Female flies were held by forceps, incision was made and ovaries were removed with a 25G needle. The ovaries were teased apart with a tungsten wire superglued to a 25G needle. Female flies were dissected in Robb's Medium (100mM HEPES, 55mM potassium acetate, 40mM sodium acetate, 100mM sucrose, 10mM glucose, 1.2mM magnesium chloride, 1mM calcium chloride) under 10 minutes. Ovaries are fixed in oocyte fixation buffer (100mM cacodylic acid, 100mM sucrose, 40mM potassium acetate, 10mM sodium acetate, 10mM EGTA) 8% formaldehyde for 20 minutes. Supernatant was removed, and ovaries were washed twice with PBS 0.1% Triton X-100. Ovaries were then incubated with PBS 1% Triton X-100 for 1 hour. Ovaries were then blocked in PBS 1% Triton X-100 0.5% BSA 1 hour at room temperature. Ovaries were then incubated with 1:100 FITC conjugated mouse anti-tubulin DM1A clone in PBS 0.3% Triton X-100 0.5% BSA overnight room temperature.

2.3.2. Immunofluorescence of *Drosophila* ovaries (non-tubulin)

Flies were fed fresh yeast 2 days prior to dissection. Fly dissection was done the same way as for microtubule staining. Female flies were dissected in PBS under

30 minutes. Ovaries were fixed in 200µl 2% formaldehyde in PBS, 600µl heptanes, 1µl NP40 for 10 minutes. Fixed ovaries were rinsed 3 times with PBS 0.2% Tween-20. The ovaries were then washed 3 times 5 minutes with PBS 0.2% Tween-20. Ovaries were incubated 1 hour PBS 0.2% Tween-20 1% Triton X-100. Blocking was done with PBS 0.2% Tween-20 1% BSA 1 hour at room temperature. Ovaries were incubated in primary antibody overnight at 4^0C. After primary antibody incubation, the ovaries were washed 3 times 20 minutes with PBS 0.2% Tween-20 at room temperature. Washed ovaries were subjected to secondary antibody for 1 hour at room temperature, and then washed 3 times 30 minutes in PBS 0.2% Tween-20.

Rabbit anti-Oskar (a kind gift from Dr. Tse-Bin Chou) was used at 1:400. Mouse monoclonal anti-Gurken (Queenan et al., 1999) was used at 1:50. Rhodamine-labeled Phalloidin (Sigma) was used at 1:1000. Rabbit anti-Cnn was used at 1:150. Rabbit anti-Dgt6 (a kind gift from Prof. Maurizio Gatti) was used at 1:150.

2.3.3. Microinjection

MBP-Dgt4 was buffer-exchanged with injection buffer (100mM HEPES pH 7.4, and 50mM Kcl) and concentrated with 30 kDa size-exclusion column (Amicon). The protein sample was centrifuged at 100 000g for 10 minutes at 4^oC to precipitate non-soluble proteins. Embryos were injected using Eppendorf Inject Man NI 2 and Femtotips II needles (Eppendorf).

2.3.4. Live microscopy for syncytial mitosis

Drosophila adults were kept in collection chambers at 25°C and allowed to lay embryos on apple juice agar plates for 1 hour, after which the plates were taken off and aged for an additional 30 minutes. The embryos were manually dechorionated by gentle rolling on double-sided tape. Heptane-glue was prepared by adding heptane to double-sided tape in a 50mL Centrifuge tube (Fisher). Amounts of heptane and double-sided tape were adjusted until the heptane-glue was slightly viscous. Heptane-glue was applied to a coverslip, and dechorionated embryos were transferred onto the coverslip. A 1:1 ratio of Halocarbon oil 27 and 700 was applied on the embryo to prevent desiccation. Imaging was performed on a Visitron Systems Olympus IX81 microscope with a CSO-X1 spinning disk using a UPlanS APO 1.3 NA (Olympus) 60× objective.

2.3.5. Confocal microscopy

Confocal microscopy was performed with Zeiss LSM 510 Meta Confocal Microscope with 40x DIC oil objective. Images were acquired with the frame size of 1024 x 1024 pixils. Data depth was set to 16 bits, and scans were performed unidirectional. Scan average was performed per line, with mean averaging of 4 scans. Imaging was performed on Zeiss LSM image browser.

2.3.6. Electron microscopy

Electron microscopy samples were mounted on formvar coated grids prepared by Peter Splatt (University of Exeter). Samples were stained with 0.5% uranyl acetate. Excess stain was removed with Whatman filter paper, and the formvar coated grids were washed 3x with BRB80. Wash buffer was removed by Watman filter paper.

Formvar coated grids were air dried before electron microscopic examination. Samples were also sent to and examined by electron microscopy by Dr. Carolyn Moores (Birkbeck University).

3. The Augmin complex binds to the microtubule lattice, and promotes microtubule assembly.

3.1. Preface

Work presented in this chapter was contributed to by a technician, Lucy Green, who developed a method for purifying protein complexes from Drosophila embryos and contributed purified protein for experiments in **3.2.6** and carried out initial experiments for Figure 7 (D, E).

3.2. Introduction

The γ-Tubulin Ring Complex (γ-TuRC) is important for mitotic spindle bipolarity. Composed of multiple copies of the γ-Tubulin Small Complex (γ-TuSC) components γ-Tubulin, Dgrip84 and Dgrip 91, as well as γ-TuRC specific components Dgrip75, Dgrip128, Dgrip163, and Dgp-WD, the γ-TuRC complex acts by providing a template upon which αβ-Tubulin dimers can attach, substantially increasing the efficiency of a MT nucleation event (Fava et al., 1999; Gunawardane, 2000; Gunawardane et al., 2003; Moritz et al., 2000; Vogt et al., 2006). In most animal cells, γ-TuRC is recruited to centrosomes prior to mitosis. Centrosomes then migrate to opposite poles of the cell, and become the major MT nucleating site within the cell, ensuring mitotic spindle bipolarity. However, a bipolar spindle can be formed in the absence of centrosomes, even in cells which would normally possess them (Giansanti et al., 2008; Khodjakov et al., 2000; Mahoney et al., 2006). Indeed, centrosomes are dispensable for the development of Drosophila (Basto et al., 2006; Stevens et al., 2007). In the absence of centrosomes, cells

possess alternative ways to localise and concentrate the γ-TuRC complex, and are described to be acentrosomal MT organisation centres (aMTOCs). aMTOCs have been observed in a variety of cells undergoing cell division (Colombié et al., 2013; Debec and Abbadie, 1989; Homer, 2013; Mahoney et al., 2006).

Augmin is a hetero-octomeric protein complex, identified independently both genetically in a genome-wide RNAi screen and biochemically via MT-MAP co-sedimentation/mass spectrometry (Goshima et al., 2007; Hughes et al., 2008). Studies have shown that removal of any single Augmin subunit by either RNAi or mutation results in long bipolar spindles with low MT density. This phenotype corresponds with the specific loss of a population of γ-TuRC normally found on the mitotic spindle itself, without affecting centrosomal γ-TuRC, as well as removal of anastral γ-Tubulin localisation (Fourniol et al., 2010; Goshima et al., 2008; Lawo et al., 2009; Loughlin et al., 2010; Meireles et al., 2009; Wainman et al., 2009). Studies of the human Augmin complex have found the hDgt4 subunit interacts with MTs (Wu et al., 2008), while the hDgt6 subunit has been shown to interact with the NEDD1 (Uehara et al., 2009; Zhu et al., 2008), the human homologue of the Drosophila Dgp71WD (a subunit of γ-TuRC). It has been theorised that Augmin recruits γ-TuRC to pre-existing MTs of the mitotic spindle, facilitating MT-templated MT nucleation (Goshima et al., 2007; Goshima et al., 2008; Hughes et al., 2008; Johmura et al., 2011; Lawo et al., 2009; Meireles et al., 2009; Wainman et al., 2009; Zhu et al., 2008).

The Augmin complex has been identified in many multicellular organisms across the Plantae and Opisthokont supergroups (Goshima et al., 2007; Ho et al., 2011; Hotta et al., 2012; Lawo et al., 2009). However, the conservation of Augmin

subunits across these supergroups is complicated. While human and *Drosophila* Augmin both have 8 subunits, only 4 have good sequence homology (Duncan and Wakefield, 2011). Using *de novo* tertiary structure prediction, Msd1, Msd5, and Wac have been postulated to share structural homology with HAUS2, HAUS1, and HAUS4 respectively (Duncan and Wakefield, 2011). As a consequence, the remaining subunit, Dgt2, has been suggested to be the functional homologue of HAUS7 (Duncan and Wakefield, 2011).

Although Augmin is clearly important in generating MTs in plants, humans and *Drosophila*, very little is known about its molecular function. To date, while it has been shown that Augmin nucleates MTs in a γ-TuRC dependent manner (Kamasaki et al., 2013; Petry et al., 2013), there is no direct evidence that Augmin recruits γ-TuRC to facilitate nucleation from pre-existing MTs. Since the Augmin complex was only recently discovered, very little about its structural and biochemical properties have been elucidated, including how it affects MT dynamics or if it has a preferential MT binding location. Reconstitution of functional Augmin would pave the way for a detailed exploration of the function of this protein complex. For example, *in vitro* MT localisation, nucleation, stabilisation and cross-linking experiments could determine the nature of the interactions between Augmin and MTs, while electron microscopy of the purified complex could provide structural information regarding the way in which Augmin binds to MTs. Such an approach has been used to investigate the role of the γ-TuRC itself (Moritz et al., 1995; Zheng et al., 1995).

Attempts to reconstitute Augmin through expression of each subunit in bacteria have been undertaken (Lawo, 2013). However, many subunits are insoluble during

bacterial expression and only limited success has been achieved in obtaining soluble intact complex through denaturing-refolding procedure (Lawo, 2013). Baculovirus expression systems have also been explored but produce limited yields (Lawo, 2013), which hinders the ability for purified Augmin to be visualised on MTs. Thus, an alternative method of purifying Augmin may be required to produce intact complex in sufficient quantities for successful *in vitro* functional investigations.

In this chapter, I describe two routes taken to further investigate Augmin function. Firstly, to test the hypothesis that HAUS4 is the human homologue of *Drosophila* Wac, I generated a transgenic fly line carrying HAUS4-GFP and examined the localisation to determine if HAUS4 and Wac are homologues. Secondly, I developed an affinity purification technique to purify endogenous Augmin complex from *Drosophila* embryos.

The tandem affinity purification (TAP) tag has been described as the gold standard in purifying protein complexes from cells (Forler et al., 2003). The TAP tag consists of two immunoglobulin-binding domains from Protein A, a Tobacco Etch Virus (TEV) protease cleavage site, and a calmodulin-binding peptide. Protein complexes are incubated with IgG beads which bind the immunoglobulin binding domain, and are released by TEV protease. A second round of purification is done by incubating the resulting protein with Calmodulin beads, and eluted with EGTA. This two-step purification allows protein complexes to be obtained at a high purity.

TAP was not explored as an option for Augmin purification because a simple immunoprecipitation/ elution have previously been used successfully to purify the γ-TuRC (Oegema et al., 1999; Zheng et al., 1995). In addition, expression of Msd1-

GFP rescues the Msd1^{ex51} mutation (Wainman et al., 2009), demonstrating that the GFP tag does not interfere with Augmin function, and Msd1-GFP is incorporated into the Augmin complex. I therefore utilised a *Drosophila* line expressing Msd1-GFP and commercially available anti-GFP antibodies to isolate Augmin via immuno-precipitation, prior to competitive elution. Here, I demonstrate that this one-step technique can be used to purify all eight subunits of Augmin, and that this soluble Augmin has the ability to bind to MTs in vitro.

3.3. Results

3.3.1. Production of a Drosophila line expressing the human homologue of Wac, HAUS4.

Although both *Drosophila* and human Augmin complex consist of 8 subunits, only 4 have good sequence homology (Duncan and Wakefield, 2011). However, *Drosophila* Msd1 and Wac have predicted structural homology to HAUS2 and HAUS4 in humans respectively (Duncan and Wakefield, 2011). To test the hypothesis that HAUS4 is the human homologue of Wac, I generated a transgenic construct designed to express GFP-tagged human HAUS4 in *Drosophila* embryos.

There are currently 2 known isoforms of HAUS4 in the NCBI non-redundant human database – isoform 1 (NP_001159741.1) and isoform 2 (NP_001159742.1). Both isoforms consist of the same start and termination sequences, with isoform 2 missing amino acids 110-125 (Fig. 3.1A), making isoform 1 the longer isoform. Primers were designed to flank the start codon and the end of the HAUS4 sequence, with a Kozac consensus sequence at the 5' end, and the nucleotides

AAA to replace the termination sequence, in accordance with the Gateway^{TM} TOPO cloning protocol (Fig. 3.1B). Total human RNA was extracted from cheek cells and cDNA was made by RT-PCR using poly-T primer to reverse-transcribe the mRNA population. PCR was performed to amplify HAUS4 ORF, and multiple bands of around 1kb were present by agarose gel electrophoresis, corresponding to the expected sizes of the HAUS4 coding region of 1341bp (isoform1) and 1198bp (isoform2), and possible uncharacterised isoforms (Fig. 3.1C). These bands were gel-purified together, and cloned into the pENTR Gateway entry vector. 13 clones were screened by restriction digest, revealing a single clone with an approximately 3.5 kb product corresponding to the expected size of the wac ORF when integrated into the vector (colony 3, Fig. 3.1D). Sequencing of this clone confirmed the presence of full-length HAUS4 isoform 1, the longest characterised isoform corresponding to the human sequence (NP_001159741.1) (not shown). A subsequent recombination reaction was performed to exchange the insert into the pPWG vector (Obtained from Drosophila Genomics Resource Center, donated by T. Murphy, unpublished) in order to generate the corresponding destination vector (pPWG-HAUS4). Purified pPWG-HAUS4 was sent to BestGene Inc. for transformation into *Drosophila*.

Transgenic flies carrying pPWG-HAUS4 will express the transgene in a tissue specific manner, once crossed to flies expressing GAL4 under the control of a suitable promoter. To express HAUS4-GFP, homozygote pPWG-HAUS4 transformants were crossed to the standard lab stock expressing GAL4 under the maternal α-Tubulin promoter (Mat-α-T-GAL4 flies), which drives expression in early *Drosophila* embryos.

A CLUSTAL 2.1 multiple sequence alignment

```
HAUS4-iso1    MASGDFCSPGEGMEILQQVCSKQLPPCNLSKEDLLQNPYFSKLLLNLSQHVDESGLSLTL 60
HAUS4-iso2    MASGDFCSPGEGMEILQQVCSKQLPPCNLSKEDLLQNPYFSKLLLNLSQHVDESGLSLTL 60
              ***********************************************************

HAUS4-iso1    AKEQAQAWKEVRLHKTTWLRSEILHRVIQELLVDYYVKIQDTNVTSEDKKFHETLEQRLL 120
HAUS4-iso2    AKEQAQAWKEVRLHKTTWLRSEILHRVIQELLVDYYVKIQDTNVTSEDK----------- 109
              ************************************************

HAUS4-iso1    VTELMRLLGPSQEREIPPLLGLEKADLLELMPLSEDFVWMRARLQQEVEEQLKKKCFTLL 180
HAUS4-iso2    --------------------------------KDFVWMRARLQQEVEEQLKKKCFTLL 135
                                              :*************************

HAUS4-iso1    CYYDPNSDADSETVKAAKVWKLAEVLVGEQQQCQDAKSQQKEQMLLLEKKSAAYSQVLLR 240
HAUS4-iso2    CYYDPNSDADSETVKAAKVWKLAEVLVGEQQQCQDAKSQQKEQMLLLEKKSAAYSQVLLR 195
              ***********************************************************

HAUS4-iso1    CLTLLQRLLQEHRLKTQSELDRINAQYLEVKCGAMILKLRMEELKILSDTYTVEKVEVHR 300
HAUS4-iso2    CLTLLQRLLQEHRLKTQSELDRINAQYLEVKCGAMILKLRMEELKILSDTYTVEKVEVHR 255
              ***********************************************************

HAUS4-iso1    LIRDRLEGAIHLQEQDMENSRQVLNSYEVLGEEFDRLVKEYTVLKQATENKRWALQEFSK 360
HAUS4-iso2    LIRDRLEGAIHLQEQDMENSRQVLNSYEVLGEEFDRLVKEYTVLKQATENKRWALQEFSK 315
              ***********************************************************

HAUS4-iso1    VYR 363
HAUS4-iso2    VYR 318
              ***
```

B Forward primer

CACCATGGCATCCGGGGGATTTCTGCT

-----TCAA**ATG**GCATCCGGGGGATTTCTGCT--

--AGGAGTTCAGCAAGGTCTACCGTTGA------

HAUS4 mRNA

TCCTCAAGTCGTTCCAGATGGCA**AAA**

Reverse primer
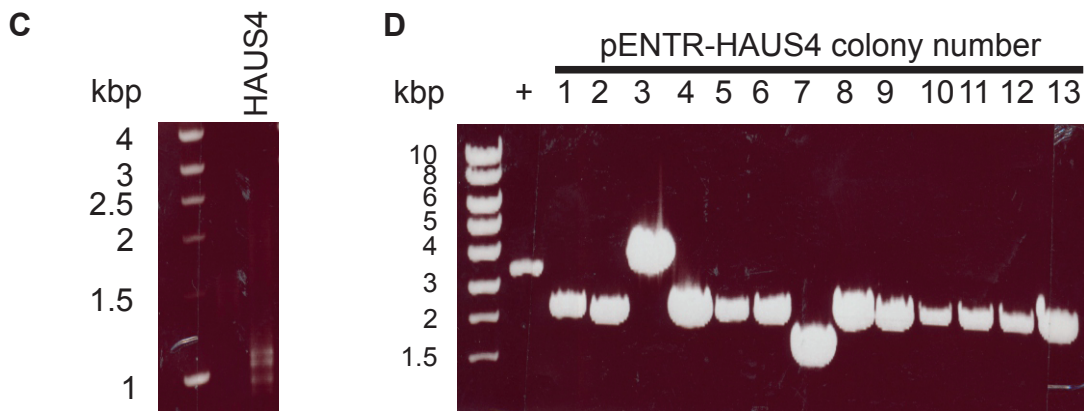
Figure 3.1- Cloning of human HAUS4 into *Drosophila melanogaster*.

(A) Alignment of human HAUS4 predicted isoforms. Both isoforms have the same start and end sequences, with HAUS4 isoform 2 lacking amino acids 110-125. (B) Primer design for HAUS4. For simplicity, HAUS4 mRNA is represented with dashed lines other than the beginning and end of the ORF. A Kozak consensus sequence (red) was added before the start codon (orange) and the termination sequence was changed to AAA (blue) in order to make a C-terminal fusion protein. (C) PCR using the HAUS4-specific primers shown in B, using human cDNA as a template. Predicted sizes of HAUS4 isoforms 1 and 2 are 1341 and 1198bp respectively. The third band may represent an additional unknown isoform not present in the NCBI database. (D) Bacterial colonies transformed with pENTR-HAUS4 were screened by restriction digest to linearise the vector. A single positive clone, colony 3, was found with the expected band size of 3.5kb.

3.3.2. HAUS4-GFP in Drosophila does not have the same localization as Augmin

Transgenic flies carrying pPWG-HAUS4 will express the transgene in a tissue specific manner, once crossed to flies expressing GAL4 under the control of a suitable promoter. To express HAUS4-GFP in early embryos, homozygote pPWG-HAUS4 transformants were crossed to the standard lab stock expressing GAL4 under the maternal α-Tubulin promoter (Mat-α-T-GAL4 flies). The localisation of HAUS4-GFP was examined in early embryos of Mat-α-T-GAL4 flies.

In *Drosophila* early embryos, Augmin subunits show a dynamic, but consistent, localisation pattern. During interphase, Msd1-GFP localises to MTs but is excluded from the nucleus. Upon entry into mitosis, Msd1-GFP accumulates on the growing bipolar spindle and remains on spindle MTs throughout metaphase, anaphase and telophase (Wainman et al., 2009). Wac has the same localisation (Meireles et al., 2009), as do other GFP-tagged Augmin subunits (Wakefield laboratory, unpublished). In contrast, although HAUS4-GFP was similarly excluded from the nucleus prior to nuclear envelope breakdown, it did not localize to MTs during interphase. Following nuclear envelope breakdown, HAUS4, although predominantly remaining cytoplasmic, weakly associated with the spindle from prometaphase to metaphase. This localisation was lost as nuclei progressed towards anaphase and telophase (Fig. 3.2, Movie 3.1 found in electronic appendix in folder Chapter 3).

When HAUS4 is expressed in *Drosophila* embryos, it appears to be associated with the mitotic spindle. However, the lack of MT localisation during interphase and the loss of HAUS4 from the spindle during progression of mitosis suggests that
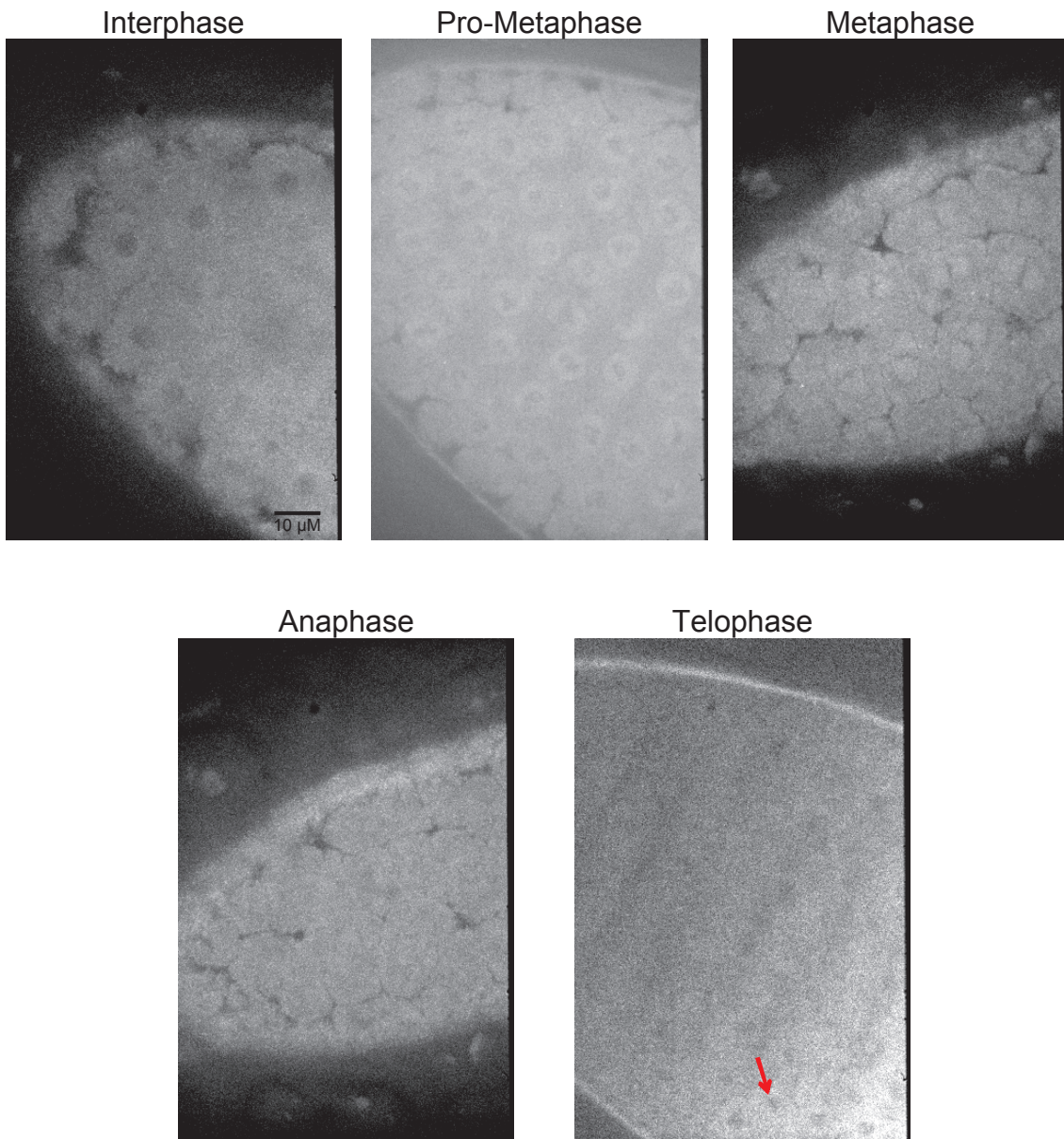
Figure 3.2- HAUS4 localises to the mitotic spindle.

Localisation of HAUS4-GFP in Drosophila early embryos. HAUS4 is excluded from the nucleus during interphase, and localises to the spindle during pro-metaphase, and metaphase. As the cell transitions to anaphase, localisation disappears. Telophase is marked by the onset of nuclear reformation in a proportion of the area in the embryo (red arrow). Scale bar applies to all images.

HAUS4 may not act as a functional homologue of Wac in *Drosophila*. Further investigation of HAUS4 in mutant lines may be necessary to confirm this.

3.3.3. The Augmin complex cannot be purified using bacterially expressed MBP-Wac

Purification of functional Augmin is necessary for a thorough investigation of the *in vitro* properties of the complex and would lead to a much greater understanding of function. A DNA construct for bacterial expression of MBP-Wac has been previously constructed; using this construct, I investigated whether the Augmin complex could be purified. The construct (a kind gift from Prof. H. Ohkura) was transformed into BL21 *Escherichia coli*, protein expression induced with Isopropyl β-D-1-thiogalactopyranoside (IPTG). Cells were lysed and MBP-Wac was immobilized on amylose resin. This resin was then incubated with Msd1-GFP embryo extracts, so that other Augmin subunits could bind to the immobilised MBP-Wac. After extensive washing, the proteins present on the beads were eluted with 10mM maltose, and the eluent centrifuged through a size-exclusion column to separate any proteins of less than 100kD from those of greater size. As Augmin has an approximate combined molecular weight of ~340kD, any intact Augmin complex would be present in the retained fraction. Samples from all stages of this purification process were subjected to SDS-PAGE and Western blotting with anti-GFP (to detect Msd1-GFP) and anti-Dgt6 (Fig. 3.3). A band of approximately 40 kDa, which corresponds to Msd1-GFP, was detected by anti-GFP in all samples except the beads after maltose elution, demonstrating that Msd1-GFP can be effectively purified using immobilised MBP-Wac and that elution completely
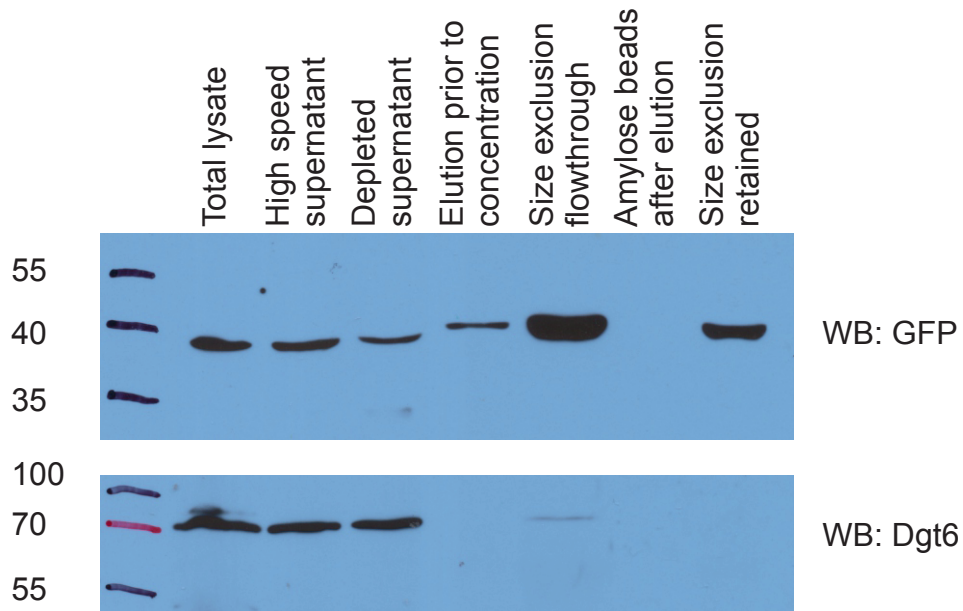
Figure 3.3- Augmin subunits can interact with MBP-Wac, but the whole complex cannot be purified.

MBP-Wac was immobilised on amylose resin, incubated with the supernatant (lane 2) Msd1-GFP Drosophila embryo extracts (lane 1), washed extensively, and the supernatant removed (lane 3). Protein was eluted using 10mM maltose (lane 4) and depleted beads retained (lane 6). Eluate was subjected to size exclusion to separate proteins greater than 100kDa (lane 7) from those less than (lane 5). A promienent band of 40KDa was detected by anti-GFP in all lanes except in beads post-elution, indicating that Msd1-GFP is purified and is present in eluate both as a single protein (<100kDa) and as part of a larger complex (>100kDa). A 70kDa band is detected by anti-Dgt6 in total lysate, supernatant, depleted supernatant (indicating a large quantity of protein failed to bind to MBP-Wac) and in flowthrough of of the 100kDa size exclusion column. No band was detected by anti-Dgt6 in the retained fraction after size exclusion. Thus, although at least 2 Augmin subunits were purified with MBP-Wac, Dgt6 does not appear to be present in a larger complex and thus the whole Augmin complex cannot be purified by this method.

dissociates the protein from the beads. However, more Msd1-GFP was present in the flow-through from the size-exclusion column (<100kDa) than in the retained fraction (>100kDa), indicating that the intensity of the in the flow-through lane was greater than that present in the retained fraction (Fig. 3.3). This suggests that the majority of eluted Msd1-GFP is not part of a complex. An antibody against Dgt6 detected a band of approximately 70 kDa, close to the expected size of Dgt6, in the flow-through of the 100 kDa size-exclusion column, but no Dgt6 was present in the retained fraction (Fig. 3.3). As such, the Msd1-GFP-containing complex retained after size exclusion does not contain Dgt6 and therefore is not a full Augmin complex. It should also be noted that levels of Dgt6 was not notably reduced in the depleted supernatant, implying MBP-Wac is not efficient at pulling down Augmin subunits from embryo extracts. As such, I conclude that although MBP-Wac can purify Msd1-GFP from embryo extracts, it cannot be used to effectively purify soluble Augmin complex.

3.3.4. The Augmin complex cannot be eluted from GFP-TRAP-A with excess His-GFP

Although an Msd1-GFP-containing complex can be purified using a bacterially-expressed MBP-Wac, the resulting complex lacks Dgt6 and therefore is not a full Augmin complex. I therefore examined alternative methods to purify Augmin from Drosophila embryos. I took an affinity purification approach, using Msd1-GFP-expressing embryos to attempt to purify the full Augmin complex. Initial attempts used GFP-Trap-A beads (Chromotek), which are composed of an anti-GFP nanobody (a single chain antibody generated in camelids) covalently coupled to

Protein A Agarose beads (Rothbauer et al., 2008). 0-4hr embryos were lysed and centrifuged at high speed to pellet insoluble debris. The supernatants were incubated with GFP-Trap-A beads overnight, prior to extensive washing. Protein was eluted from beads using highly concentrated GFP protein. Initial Western blot analysis of GFP-Trap-A beads after incubation and washing shows Msd1-GFP running at the expected size of 40 kDa (Fig. 3.4A).

To examine whether immuno-precipitation of Msd1-GFP co-precipitated other Augmin subunits, samples were subjected to western blotting using an antibody recognising Dgt6 (Bucciarelli et al., 2009). Two bands of 70 kDa, and 55 kDa were detected in the GFP-Trap-A beads lane (Fig. 3.4A). The highest molecular weight band corresponds to the expected size of full length Dgt6 (72.8 kDa).

To determine other components which were co-immunoprecipitated with Msd1-GFP, bead fractions were subjected to LC-MS/MS. A list of interacting proteins was produced (Table3.1) using a standard in-lab procedure. This procedure consists of:

(i)   comparing the list of identified proteins to a "false positive" list of Drosophila embryo proteins known to bind to GFP-TRAP-A beads, generated from 3 independent GFP-TRAP-A-based experiments using GFP-fusion proteins expressed in embryos that failed to pull-down the bait protein.

(ii)   removal of any false positive that was not >4 time enriched in the affinity purification.

(iii)   removal of any protein with a Mascot score of below 50.

(iv)   removal of any protein identified on the basis of a single-peptide hits.
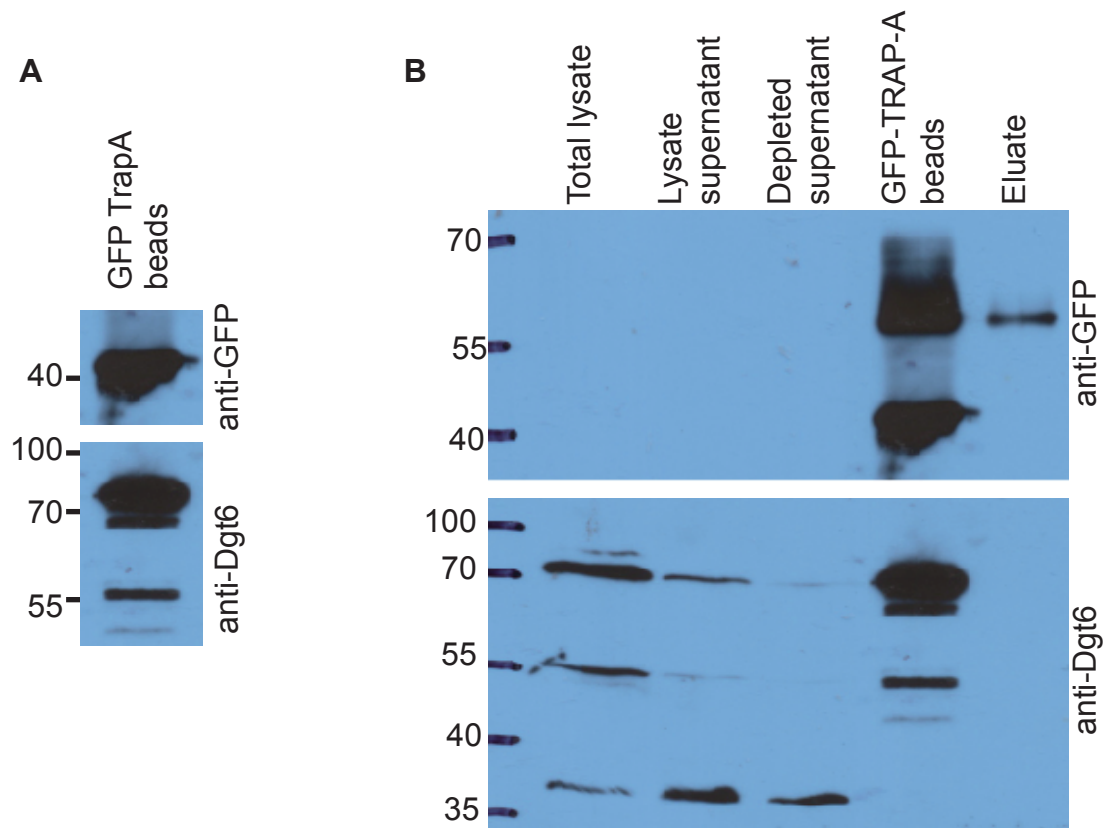
Figure 3.4- Msd1-GFP and Dgt6 can be purified by GFP-Trap but cannot be eluted with His-GFP

(A) Lysates of early embryos were incubated with GFP-TRAP-A beads and subjected to extensive washing. A Western blot against the beads was performed with anti-GFP or anti-Dgt6. Anti-GFP detected a band of 40kDa, which is the predicted size of Msd1-GFP. Anti-Dgt6 detected three bands, of which the highest (~70kDa) corresponds to the molecular weight of Dgt6 (72.8kDa). (B) GFP-TRAP-A beads were used to immunoprecipitate Msd1 and its interactors from early Drosophila embryos. Total lysate (lane 1) was centrifuged to remove insoluble debris and the resulting supernatant (lane 2) incubated with GFP-TRAP-A beads (lane 4). After incubation, the depleted supernatant (lane 3) was discarded and beads washed extensively before competitive elution with concentrated His-GFP. The eluate was blotted with anti-GFP and anti-Dgt6. Anti-GFP detects Msd1-GFP at 40kDa only in the GFP-TRAP beads and not in total lysate or supernatant - the concentration is likely to be below the detectable limit in these fractions. A second band of 55kDa is present in GFP-TRAP beads and in eluate and is likely to correspond to dimerised GFP from the competitive elution. Anti-Dgt6 detects three bands, of ~70, 55 and 37kDa, in total lysate and supernatant fractions and also on GFP-TRAP-A beads. The band corresponding to Dgt6 (70kDa) is substantially concentrated by GFP-TRAP though a small amount of unbound protein can be detected in the depleted supernatant after incubation with beads (lane 3). Neither Msd1-GFP nor Dgt6 is detected in the eluate, nor in the depleted supernatant, suggesting that both remain bound to GFP-TRAP beads and were not eluted by competition with His-GFP.

Protein Name	Coverage	# Peptide	Score
DGT6	75.38	56	1517.32
DGT5	72.85	57	1178.49
DGT3	77.88	51	1152.25
MSD5	75.10	18	797.94
DGT2	85.71	29	720.16
MSD1	70.29	14	718.75
WAC	88.96	17	370.96
DGT4	61.70	15	337.77
MSPS	29.27	47	284.72
BETATUB97EF	18.82	11	272.13
BSG25D	37.54	27	198.30
BSG25D	36.72	27	196.43
CP1	44.87	15	141.69
NIPPED-A	10.24	29	132.51
CMET	17.61	32	128.10
UBI-P5E	64.23	5	101.73
DNAPOL-EPSILON	9.88	16	93.40
HYD	9.64	19	93.33
TOR	8.62	17	93.08
UBA1	18.25	14	91.14
TACC	15.58	13	89.50
CG2118	23.50	14	88.84
CUP	16.74	13	87.09
CG8036	31.72	14	81.51
DIDUM	14.96	17	81.36
CG9795	26.61	13	78.49
L(1)G0334	38.60	11	70.55
SPN-A	35.12	9	67.86
LOK	23.75	9	67.72
TORSIN	37.35	11	66.97
CG12512	26.48	12	65.32
LDS	14.70	12	65.00
SLAM	16.28	11	64.10
CG31739	13.77	11	62.53
MUD	9.68	10	54.82
JAR	10.30	10	53.99
CG10399	46.44	10	52.18
CG3532	11.19	11	51.92
CG11092	20.17	11	51.18

Table 1- Proteins identified by mass spectrometry from Msd1-GFP immunoprecipitation. A cut-off score of 50, and a filter list of non-specific proteins was applied. The top 8 hits as ranked by MASCOT score are the 8 Augmin subunits (**in bold**).

The top 8 proteins as ranked by MASCOT score were the 8 Augmin subunits. As such, it is possible to immunoprecipitate the complete Augmin using a GFP-TRAP approach from Msd1-GFP.

Having verified that the GFP-TRAP immuno-precipitation approach successfully isolates all 8 Augmin subunits, I next attempted to elute intact Augmin from GFP-TRAP-A beads using competitive elution by bacterially expressed and purified His-tagged GFP. An excess of His-GFP (282µg) was incubated with beads for 2 hours at 4°C. Both the GFP-Trap-A beads and the eluent were green after elution, indicating the beads were saturated with GFP. The supernatant, which would be expected to contain displaced Augmin, was subjected to Western blotting (Fig. 3.4B). Two bands of approximately 55kDa and 40kDa were detected using an anti-GFP antibody in the GFP-TRAP-A bead sample post elution with His-GFP, corresponding to His-GFP dimer (predicted MW 56kDa) and full-length Msd1-GFP (predicted MW 40kDa). Although no bands were detected in the total lysate or high speed supernatant as would be expected for Msd1-GFP embryo extracts, the most likely explanation is that the concentration of Msd1-GFP in lysates and supernatants was below the detection limit of the Western Blot. Although a band corresponding to dimerised GFP was present in the 50kD cut-off fraction, full-length Msd1-GFP was not detected.

Three bands of approximately 70, 55, and 37 kDa were detected with anti-Dgt6 antibodies in the centrifuged lysate. The highest molecular weight band corresponds to the expected size of full length Dgt6 (72.8 kDa). The bands corresponding to 70 and 55 kDa were reduced in the depleted supernantant, and enriched in the GFP-Trap-A beads, but no Dgt6 could be detected in the eluent.

These results indicate that neither Msd1 nor Dgt6 was eluted from the GFP-TRAP beads even with an excess of His-GFP. Longer incubation times at higher concentrations of His-GFP were undertaken, however in all cases the fraction of GFP-Msd1 competed off the GFP-TRAP-A beads was very low. I therefore conclude that this competition assay is not an effective way to displace Augmin from GFP-TRAP-A beads. However, it is still possible to use the purified Augmin complex, bound to the GFP-TRAP beads, in further assays.

3.3.5. The Augmin complex can bind unpolymerized Tubulin

Components of the Augmin complex have been shown to bind MTs (Goshima et al., 2008; Hughes et al., 2008; Meireles et al., 2009; Wainman et al., 2009) and are required to nucleate branched MTs (Petry et al., 2013). However, whether Augmin is capable of binding free Tubulin dimer has not been investigated. Msd1-GFP-purified Augmin complex bound to GFP-TRAP-A beads were incubated with purified Tubulin at $4^{o}C$ to prevent MT polymerisation, extensively washed and centrifuged to separate beads from soluble protein supernatants, which were subjected to SDS PAGE and Western blotting. GFP-Trap-A beads incubated with extract from embryos expressing Histone-GFP were used as a control. If the protein complex bound to the GFP-Trap beads binds to Tubulin dimer, then Tubulin should be detectable with the GFP-Trap beads. Histone-GFP and Msd1-GFP were detectable in the respective pellets by anti-GFP (Fig. 3.5). Tubulin was clearly detectable by anti-Tubulin in the input, and the unbound fraction after incubation for Histone-GFP and Msd1-GFP. In contrast to the Histone-GFP beads, a Tubulin

signal was also seen in the Msd1-GFP beads (Fig. 3.5) suggesting that Tubulin can associate with the Augmin complex.

3.3.6. The Augmin complex can be eluted from anti-GFP IgG

Since a GFP-Trap approach is capable of binding all 8 subunits of the Augmin complex, it remains a valid approach for purification of an intact complex for biochemical assays. I theorised that the Augmin complex was not properly eluted from GFP-Trap-A (see Fig. 3.4) because the nanobodies had too high an affinity to the GFP tag. I therefore investigated whether a GFP antibody with a lower affinity for GFP could be used to purify Augmin and disrupted using excess His-GFP.

The anti-GFP IgG from Roche has been used to detect Msd1-GFP in Western blots, demonstrating its ability to bind the GFP antigen. I therefore generated Protein-A beads covalently coupled to the Roche anti-GFP antibody and incubated these with Msd1-GFP embryo extract. After extensive washing, the beads were incubated with an excess of His-GFP (256µg) and the resultant supernatant and beads analysed. Western Blot analysis with anti-GFP antibody showed the presence of Msd1-GFP in the input (high speed supernatant) extracts, as expected (Fig. 3.6A). Although most of the Msd1-GFP remained on the anti-GFP IgG beads, after incubation with His-GFP, some Msd1-GFP was released. Encouragingly, this eluent also showed a band of 72kDa when probed with anti-Dgt6 antibody, indicating that Dgt6 is co-purified and co-eluted with Msd1-GFP (Fig. 3.6A).

The above methodology results in the potential purification of soluble Augmin, in the presence of His-GFP. To remove the His-GFP and to further characterise the
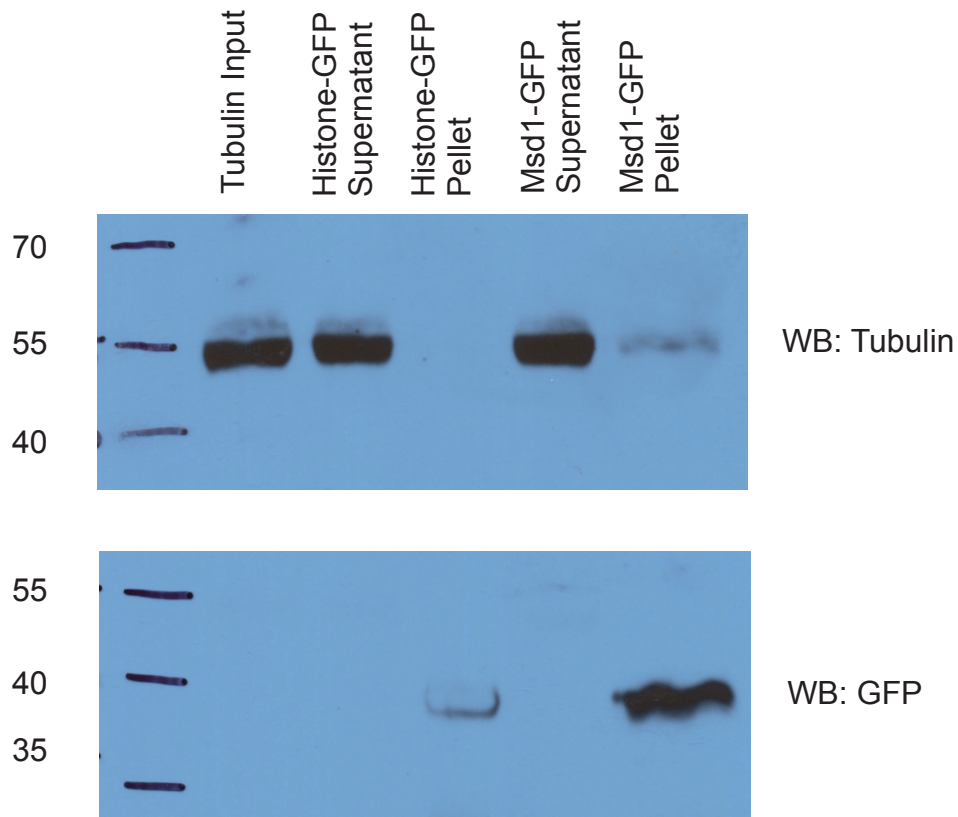
Figure 3.5- Augmin binds unpolymerised Tubulin

Tubulin pulldown was performed at 4°C, where MT polymerisation does not take place, using either His-GFP or Msd1-GFP supernatant bound to GFP-TRAP-A beads. The sample was centrifuged to pellet beads and any bound tubulin. A band of approximately 40kDa was detected in both Histone-GFP (expected size 43kDa) and Msd1-GFP (expected size 40kDa) pellets, showing that protein remained bound to beads and was pelleted correctly. A 55kDa Tubulin band was detected in input, supernatants from both samples, and also in the Msd1-GFP pellet, indicating that Tubulin was bound by Msd1-GFP beads. Since this Tubulin band was detected in Msd1-GFP but not Histone-GFP, it is likely that Augmin can bind unpolymerised Tubulin.

eluent, gel-filtration chromatography was undertaken. Three main peaks could be seen from the chromatography (Fig. 3.6B). Calibration of the column using standards identified an initial peak beyond the range of the standards, and thus, it is not possible to accurately estimate its size. It is likely that this peak corresponds to aggregated proteins, or very large protein complexes. Encouragingly, a middle peak of eluted protein corresponded to approximately 400 kDa, which is close to the expected size of the sum of all Augmin subunits and GFP. A final peak of low molecular weight proteins is likely a combination of free-floating Msd1-GFP, GFP dimers, and GFP monomers.

To confirm the presence of Augmin subunits in the ~400kD gel filtration peak, the fractions were precipitated using 10% TCA and subjected to SDS PAGE and western blotting. Unfortunately, neither anti-GFP nor anti-Dgt6 antibodies generated signals on the blots in any fraction. It is therefore likely that the amount of purified Msd1-GFP/Dgt6/Augmin following gel filtration is below the detection limit of the reagents used. Although this means that the amount of purified Augmin complex following gel filtration is too low to be of use in biochemical assays, the presence of both GFP-Msd1 and Dgt6 in the eluent from anti-GFP IgG purification and the presence of a gel filtration peak at approximately the correct molecular weight of Augmin indicate that anti-GFP IgG is indeed a viable method of purifying intact Augmin complex.
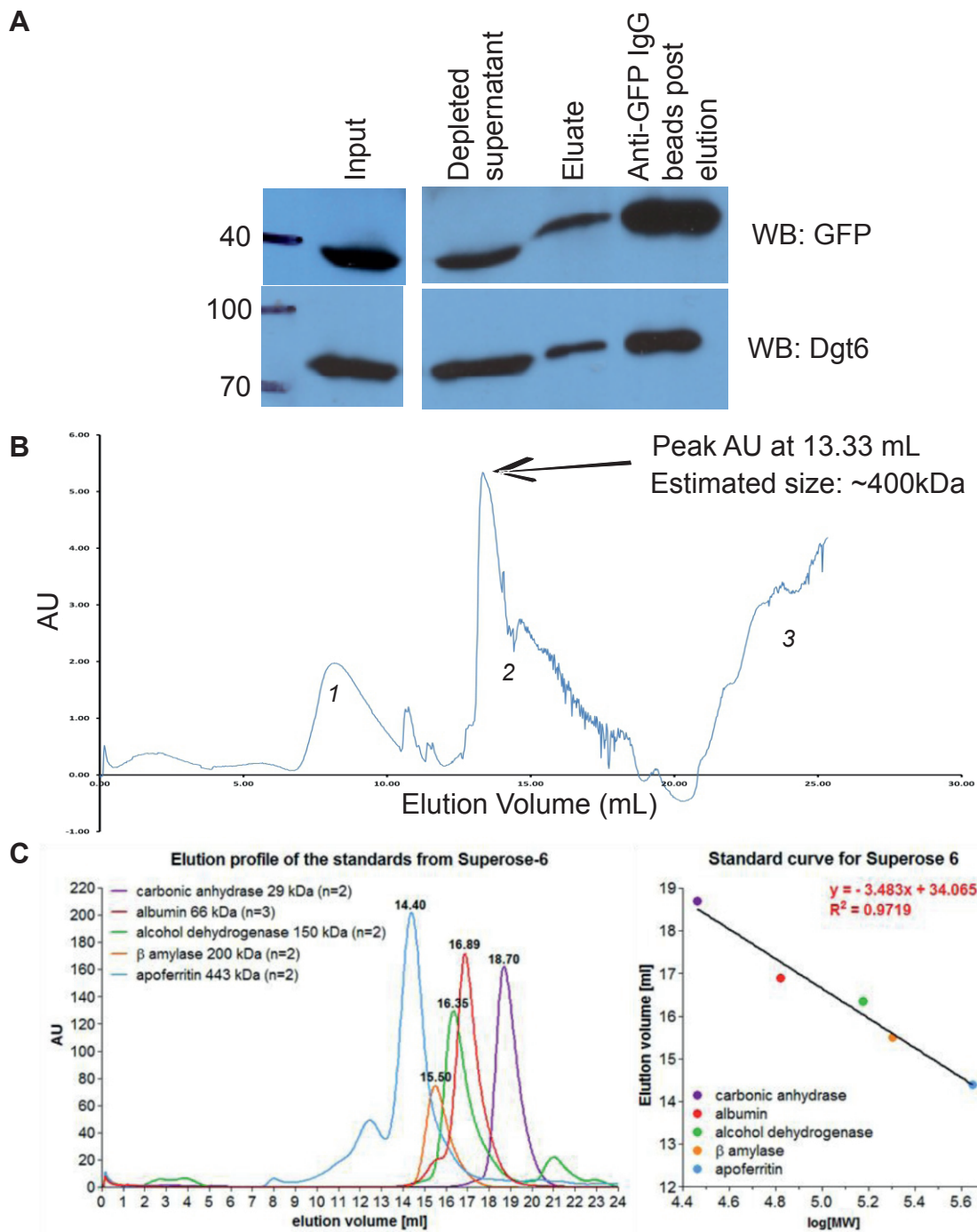
Figure 3.6- Soluble Augmin complex can be purified by competitive elution from anti-GFP IgG beads using His-GFP

(A) Msd1-GFP embryo extract (lane 1) was incubated with protein-A beads covalently bound with anti-GFP IgG. After incubation, the depleted supernatant (lane 2) was removed, beads washed and protein eluted using an excess of His-GFP. All samples plus the eluate (lane 4) and the beads post-elution (lane 5) were examined by Western blotting. Full-length Msd1-GFP (40kDa) and Dgt6 (72.8kDa) can be detected in the eluate, indicating at least these 2 Augmin subunits can be purified by competitive elution. (B) Gel filtration chromatography of eluate showing 3 distinct populations (italics). Populations 1 & 3 are beyond the range of the standards (C) and therefore beyond the resolution of the gel filtration unit. Population 2 (black arrow) has a peak at 13.33mL, corresponding to ~400kDa. (C) A standard elution profile graph and standard curve (constructed by Dr Ewa Bielska) for the gel filtration chromotography.

3.3.7. Purified, soluble Augmin appears to recruit ring-like structures to MTs, and is able to promote MT generation in vitro

To date, there is no physical structural information on Augmin. Therefore, I decided to use purified Augmin complex eluted from anti-GFP IgG beads for preliminary investigations into Augmin structure. Since electron microscopy has been used to determine the structure of protein complexes, such as γ-TuRC (Moritz et al., 1995; Oegema et al., 1999; Zheng et al., 1995), I used negative staining-based electron microscopy to examine the purified Augmin complex (Fig. 3.7). MTs were generated from purified Tubulin in vitro, stabilised with taxol, and incubated with either His-GFP (as a negative control) or with purified Augmin complex. Samples were then transferred to formvar-coated grids, stained with uranyl acetate, and examined by transmission electron microscopy.

There were no discernible structures present on MTs with incubated with GFP alone. MTs incubated with purified Augmin complex showed clusters of density along the MTs (Fig. 3.7B, red arrow). In addition, clear ring-like structures of approximately 50nm in diameter were observed to be along the lattice of the MTs (Fig. 3.7B, purple arrow).

Since GFP-TrapA beads were able to affinity-purify all Augmin subunits, and presumably the Augmin complex itself, Augmin on GFP-TrapA beads were incubated with MTs, and examined by EM in collaboration with Dr. Carolyn Moores (Birkbeck University, London). With this sample, Augmin showed long chains of protein along the MTs (Fig. 3.7C, red arrow). Taken together, these results show that the Augmin complex binds to the lattice of MTs.
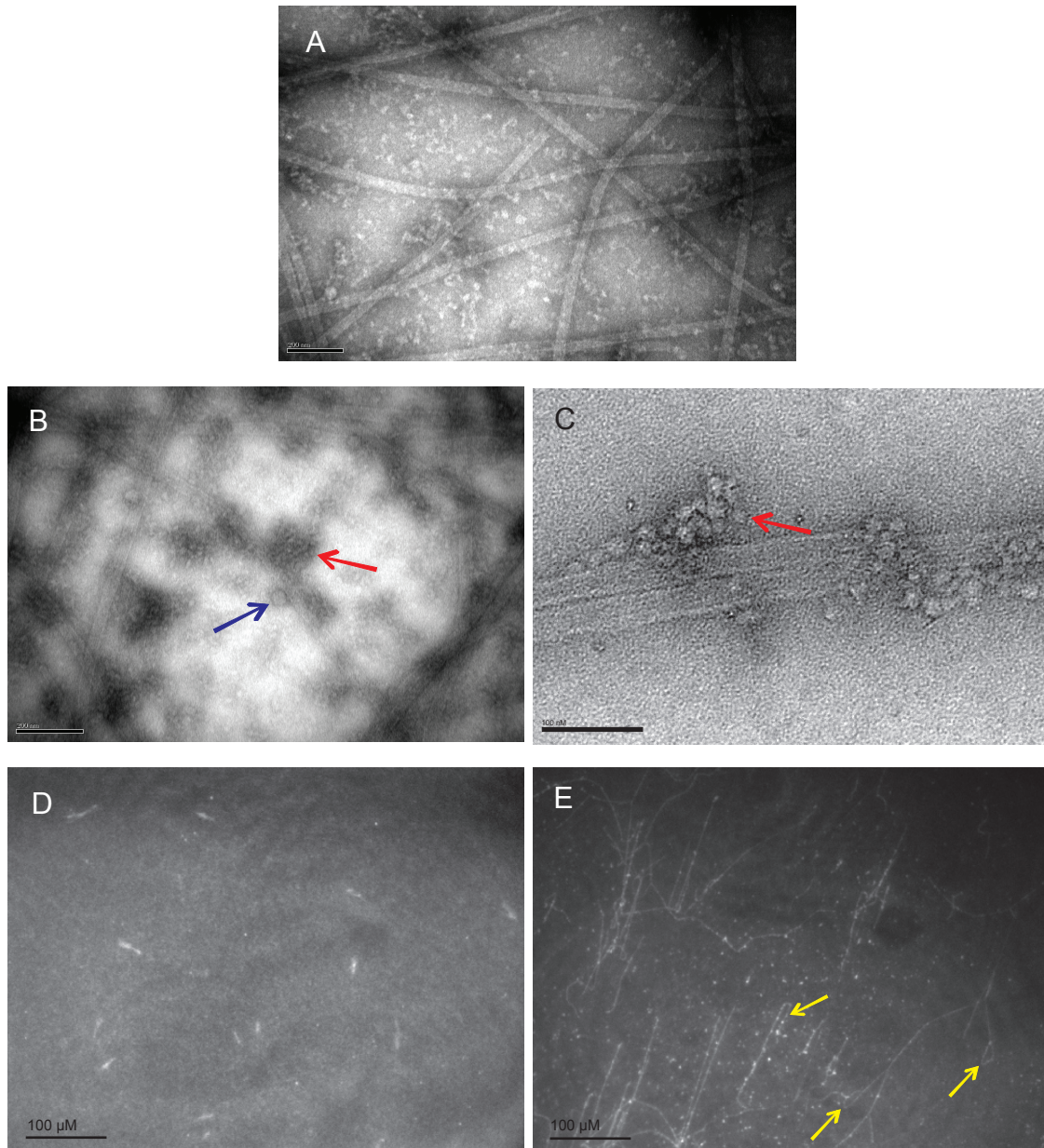
Figure 3.7- Augmin multimerises, and promotes MT growth and/or stabilisation.

(A-C) Transmission electron microscopy of negatively-stained MTs incubated with either His-GFP (A) or purified Augmin complex (B, C). (A) MTs incubated with His-GFP revealed long tubular structures, which are MTs, and general background staining. (B,C) MTs mixed with purified Augmin complex revealed additional ring structures of ~50nm in diameter (purple arrows) and clusters of mass decorated along the MT sides (red arrows). (D, E) MT growth assay in the presence of His-GFP (D) or purified Augmin complex (E). In the presence of His-GFP, few short MTs could be detected, in contrast to incubation with Augmin, where long parallel MTs could be seen. Hook structures were often observed at the end of MTs (yellow arrows). These results inducate Augmin forms multimers and binds the lattice of MTs to promote formation of stablisation.

More recently, we successfully developed a new method of isolating intact, soluble protein complexes from tissue expressing GFP-fusions. The majority of this work was carried out by Lucy Green and as such is not presented here. This technique yields 95% pure soluble Augmin subunits at 1-5ng/ul with no γ-TuRC subunits (data not shown). As a complimentary *in vitro* assay, we decided to assess whether purified Augmin has MT nucleation/stabilisation abilities. By incubating Tubulin with either His-GFP or purified Augmin under conditions in which MTs might be generated, we would expect to see more MT formation if Augmin has these abilities. To test this, in conjunction with Lucy Green, purified GFP or Augmin was added to a mixture of X-Rhodamine-Tubulin and unlabelled Tubulin in the presence of GTP and incubated at 37°C for 5 minutes. Samples were rapidly fixed in 1% glutaraldehydeglutaraldehyde before mounting on coverslips for observation using TIRF microscopy. In the presence of purified GFP, only the occasional short MT was visible throughout the coverslip. In stark contrast, coverslips containing Augmin-GFP showed many long MTs. Interestingly, these MTs were often arranged in parallel (Fig. 3.7E), and hook structures could often be seen at the ends of MTs (Fig. 3.7E, white arrows). Taken together, these results strongly suggest a role for Augmin in binding and stabilising and/or nucleating MTs.

3.4. Discussion

3.4.1. HAUS4 localises to the mitotic spindle when expressed in Drosophila embryos

Bioinformatic-based *de novo* tertiary structural software has suggested that HAUS4 may be the functional homologue of the *Drosophila* Augmin subunit, Wac (Duncan and Wakefield, 2011). To test this, I generated a fly line expressing HAUS4-GFP. The intention was to not only investigate the localisation of HAUS4-GFP in embryos, but to use this fly line to biochemically test MT co-sedimentation and to attempt to rescue the female sterility associated with a null *wac* mutant (Ferretti et al., 2010). In embryos prior to cellularisation, Wac localises to MTs throughout both interphase and mitosis. Encouragingly, I have shown that although *Drosophila* embryos expressing HAUS4-GFP do not localise to MTs during S phase, the protein does weakly associate with the mitotic spindle during mitosis (Fig 3.2). However, the localisation of HAUS4-GFP was not identical to that of Msd1-GFP throughout the cell cycle, suggesting that this protein is not incorporated into *Drosophila* Augmin, but is able to bind MTs on its own during mitosis. HAUS4 being double the size of Wac, may simply be too large to be able to replace Wac. Furthermore, it is possible GFP may interfere with the function if a functional domain was at the C-terminus of HAUS4. Until further experiments can be completed, it is therefore not clear what the relevance of the mitotic spindle staining is, in relation to Augmin. Even if this is the case, the failure of HAUS4 to be incorporated into *Drosophila* Augmin does not necessarily mean Wac and HAUS4 are not homologues. Further studies, such as examining the ability of HAUS4 to complement embryos lacking Wac, would elucidate whether HAUS4 can be functionally incorporated into Augmin.

3.4.2. Intact functional Augmin can be purified from Drosophila embryos expressing Msd1-GFP

Purification of the intact Augmin complex in sufficient quantity for biochemical and cellular assays is an essential step in determining its function. Initial attempts to purify the Augmin complex by co-purification with bacterially expressed MBP-Wac was unsuccessful, although at least 2 subunits were able to be purified (Fig 3.3). The total molecular weight of Augmin is ~340kD and MBP-Wac, Msd1-GFP, and Dgt6 combined is above 100kDa and Msd1-GFP appeared to be present in a complex of >100kDa. However, Dgt6 was unable to be retained from a 100kDa size exclusion column indicating that it was not present in any complex purified by this method. One possibility is that the interacting proteins are folded in a way which minimizes its size. Another possibility is that the *in vitro* interactions between MBP-Wac, and some other Augmin subunits (particularly Dgt6, since much of the protein did not appear to bind to the immobilised MBP-Wac) are weak, and that stable interactions between Augmin subunits are dependent on other factors such as post-translational modifications, or chaperones.

A second technique was to attempt to obtain soluble Augmin through incubating GFP-TRAP-A with extracts from embryos expressing Msd1-GFP followed by competitive elution with His-GFP. This technique was partially successful, as while the complex bound to beads it could not be eluted (Fig 3.4). Mass Spectrometry results (Table 3.1) confirm that all Augmin subunits could be pulled down using this technique, at least one subunit, Dgt6, could not be eluted from the GFP-TRAP-A beads by competition with bacterially expressed His-GFP (Fig 3.4). It is likely that GFP-TRAP nanobody has such a high affinity to GFP that once bound, elution is

very difficult. This is likely, since competitive elution of the avidin-biotin interaction is very challenging due to its high dissociation constant (Erickson and Stoffler, 1996; Green, 1975; Rösli et al., 2008; Rybak et al., 2004).

Subsequently, since IgG has a lower affinity for antigens than nanobodies, I amended my GFP-TRAP approach and investigated purification of Augmin with anti-GFP IgG followed by competitive elution. Western Blot confirmed the presence of Msd1-GFP and Dgt6 in the eluent from beads covalently bound with anti-GFP IgG (Fig. 3.6A). Gel-filtration chromatography (Fig. 3.6B, C) yielded 3 main peaks; one of high molecular weight (likely representing protein aggregates or very large protein complex), one around 400kDa, and one that is low molecular weight. The expected size of the Augmin complex containing Msd1 with a GFP tag is 354 kDa, which could therefore correspond to the peak around 400 kDa. However, although Msd1-GFP and Dgt6 were present in the eluent loaded on to the gel filtration column (Fig 3.6A), Western blot analysis of fractions failed to recognise the presence of either protein in any fraction (data not shown). This is most likely due to the low concentrations of protein following the gel filtration step. However, it is apparent from the gel-filtration analysis and the Western blotting of the eluate prior to gel filtration that the Augmin complex appears to be purified by this method.

The source of tissue for the purification was embryos expressing GFP-Msd1 under the control of the Mat-α-T-GAL4 system. It is therefore highly likely that GFP-Msd1 is not limiting Augmin complex formation in these embryos. The low molecular weight fraction present in the gel filtration probably corresponds to forms of Msd1-GFP in the absence of other Augmin subunits, indicating that Msd1-GFP is present as two populations in these embryos- one in a complex with Augmin and another of

excess Msd1-GFP as a single unbound protein. It is unclear what the high molecular weight peak present in the gel filtration might contain. γ-TuRC is approximately 2MDa, and has been reported to be recruited to pre-existing MTs by Augmin. It is therefore possible that the high molecular weight fraction is composed of Augmin in association with the γ-TuRC. In support of this, EM using anti-GFP IgG-purified Augmin, prior to gel filtration, revealed ring structures of around 50 nm- the reported size of γ-TuRC (Oegema et al., 1999). However, Western blotting analysis of this purified Augmin with anti- γ-Tubulin antibodies (data not shown) did not reveal a corresponding band. This is possibly due to only low levels of γ-TuRC in the sample but, as such, it is difficult to make firm conclusions regarding either the composition of the eluent or the relevance of the 50 nm rings, in relation to γ-TuRC.

The competitive elution method of purifying Augmin was discontinued towards the end of this project, since we developed a photo-cleaving method of protein complex purification. This new method yielded Augmin at 95% purity based on mass spectrometry analysis. Augmin complex purified in this way was able to bind MTs in a MT co-sedimentation assay (data not shown), suggesting it represents functional Augmin. This method of purification has the added benefit of only purifying Augmin without other associated complexes such as γ-TuRC, and provides an important tool with which to investigate the function of Augmin.

3.4.3. The role of Augmin in generating branching MTs

Despite the continued efforts of at least three leading international research groups (Prof. Ronald Vale, Dr. Laurence Pelletier, Prof. Tarun Kapoor), to date there has

been no published study which has purifyied intact, functional Augmin. However, very recently the laboratories of Professor Mitchison and Professor Vale demonstrated the phenomenon of branched MT nucleation in *Xenopus* extracts (Petry et al., 2013). Through the use of immuno-depletion, this study also showed that Augmin was essential for generating these branched MTs. These results strengthen the current hypothesis that Augmin recruits γ-TuRC to pre-existing MTs, where it nucleates branched MTs. However, Xenopus extracts contain all the other proteins involved in regulating MT dynamics and organisation, and no add-back experiments were performed as controls as reconstitution of intact Augmin complex has not yet been successful. As such, while the evidence provided by this study is strong, the precise role of Augmin still remains to be demonstrated fully.

The Petry study also showed that *Xenopus* embryo extract depleted of γ-Tubulin still formed branched MTs, albeit slowly and only in rare cases (Petry et al., 2013). It is therefore possible that the Augmin complex may be involved in branched MT formation independently of γ-TuRC. During Actin filament polymerisation, the Arp2/3 complex it binds to the sides of pre-existing actin filaments, where it is able nucleate new filaments from these regions, producing branched F-Actin (Stevenson et al., 2002). The complex bears structural similarity to Actin monomer, thus acting as a docking site and template for further polymerisation to take place. My results show that the Augmin complex can bind unpolymerised Tubulin (Fig 3.5), and that it binds to the sides of polymerised MTs (Fig 3.7). Thus, it is possible Augmin may function similarly to Arp2/3 and nucleates branched MTs from the sides of existing MTs through its ability to bind unpolymerised Tubulin.

In support of a scenario where Augmin can affect MT generation independent of the γ-TuRC, I have shown that purified Augmin with no γ-TuRC is able to lower the critical concentration of MT formation *in vitro* (Fig 3.7D, E). Interestingly, the MTs that are generated are long, and many have "hooked" ends of variable length. One explanation for these hooks is that multimeric, clustered Augmin complexes, such as those observed via EM (Fig 3.7C, D), are able to cause MT bending and anchoring in an end-specific manner.

The purification of intact, soluble Augmin from Msd1-GFP embryos is an exciting and potentially ground-breaking advance. Repeated experiments, both EM and in vitro, should allow us to studythe functionality of Augmin in relation to MTs in more detail. Moreover, purification of the γ-TuRC using a similar methodology has recently been demonstrated in our laboratory. By combining both purified γ-TuRC and Augmin in the presence of stable MTs and additional fluorescently labelled tubulin we may, finally, be able to observe MT-templated MT nucleation by the Augmin complex *in vitro*.

4. Comparative mass spectrometry of microtubule associated proteins regulated by the Augmin complex

4.1. Introduction

Microtubule Associated Proteins (MAPs) are the essential regulators of the dynamic properties of MTs, and their localisation to specific subsets of MTs allows the cell to regulate sites of MT nucleation, growth and stability. For example, the EB1 recognises the plus ends of MTs and functions by increasing MT protofilament lateral associations (Maurer et al., 2012), while the localisation of Centrosomin (Cnn) to the pericentriolar material (PCM) through its interaction with DSpd2 and Asl, recruits γ-TuRC and γ-TuSC to the centrosome making it the dominant site of MT nucleation (Giansanti et al., 2008). The hetero-octomeric Augmin complex has been shown to initiate the formation of new MTs by localising γ-TuRC to pre-existing mitotic spindle MTs (Duncan and Wakefield, 2011; Petry et al., 2013). However, in Chapter 3, I showed that purified Augmin complex promoted MT growth in the absence of γ-TuRC in an *in vitro* assay, suggesting the MAP complex Augmin may directly affect MT properties. In addition, recent work from our laboratory has shown that upon Augmin depletion, astral MTs nucleated by the centrosome increase their dynamic properties, growing and shrinking more quickly than in control cells (Hayward et al., 2014). The change in MT dynamics may alter the way MAPs interact with MTs. Another possible way Augmin may affect affinity of MAPs to MTs is by direct recruitment. Augmin, a mitotic MAP, has been described recruit γ-TuRC to the spindle (Zhu et al., 2008), as well as being important for localisation of NDC80, Msps, and Cenp meta (Bucciarelli et al., 2009).

However to date, besides γ-TuRC, very little studies have been done on the role of Augmin on other MAPs.

One of the most comprehensive approaches to identifying MAPs is through immunodepletion, which has been used in published studies on the role of Augmin in building the mitotic spindle in *Xenopus* embryo extracts (Petry et al., 2013; Petry et al., 2011; Uehara et al., 2009). These studies determined that Augmin plays an important role in both chromatin mediated MT nucleation and spindle mediated MT nucleation (Petry et al., 2011), as well as an additional role in generating branching MTs, increasing the MT density of the spindle (Petry et al., 2013).

It was through MT cosedimentation and mass spectrometry that Augmin subunits were first identified (Hughes et al., 2008). Using the same technique as the Hughes study, in this assay, tissue extracts are centrifuged at high speed to remove debris and organelles, before the addition of GTP to stimulate polymerisation and Taxol to stabilise MTs. Further centrifugation of the polymerised extract through a dense glycerol cushion results in the co-sedimentation of the MTs and associated MAPs, without sedimentation of other soluble proteins. The components present in this sample can then be identified via mass spectrometry. Theoretically, the same purification technique can be used to identify the changes in quantities of individual MAPs able to bind MTs following a variety of perturbations. Traditionally, stable isotope labeling by amino acids in cell culture (SILAC) has been used to quantitatively compare proteomic changes under different conditions. Indeed, SILAC has been used to identify the difference in MAP population between interphase and mitotic cells (Syred et al., 2013). However, this method is difficult to

implement for *Drosophila* embryos, since the quantity of labeled isotope ingested by flies is difficult to control.

Fortunately, Tandem Mass Tags (TMT^TM)-based mass spectrometry offers an alternative approach (Thompson et al., 2003). TMTs^TM are isobaric chemical tags, meaning each set has the same structure and mass, and have been designed so that the same peptide labelled with different tags migrates into the mass spectrometer at the same rate. TMT tags consist of a mass reporter region coupled to a peptide, as well as a sensitisation group. The mass reporter region consists of varying number of heavy isotopes from tag to tag, which allows for identification of an individual peptide from a sample, and allows for quantitative comparison across different samples. The sensitisation group contains the appropriate number of heavy isotopes such that each tag has equal mass. During tandem MS/MS, the sensitisation group is lost, leaving only the mass reporter and the peptide to be analysed (Thompson et al., 2003). TMT-based approaches have been successfully used to identify biomarkers for rheumatoid arthritis (Cheng et al., 2014), and to probe for differential protein expression and phosphorylation status of cancer stem cells (Nilsson et al., 2010).

In Chapter 3, I used an affinity purification technique based on GFP-TRAP-A to purify all 8 Augmin subunits from *Drosophila* embryos expressing Msd1-GFP. However, this purification technique can also be used to deplete the Augmin complex from embryo extracts. Here, I use these Augmin-depleted extracts to undertake multiple MT co-sedimentation assays and TMT^TM-based quantitative mass spectrometry in order to identify possible MAPs whose affinity to MTs is altered upon Augmin depletion.
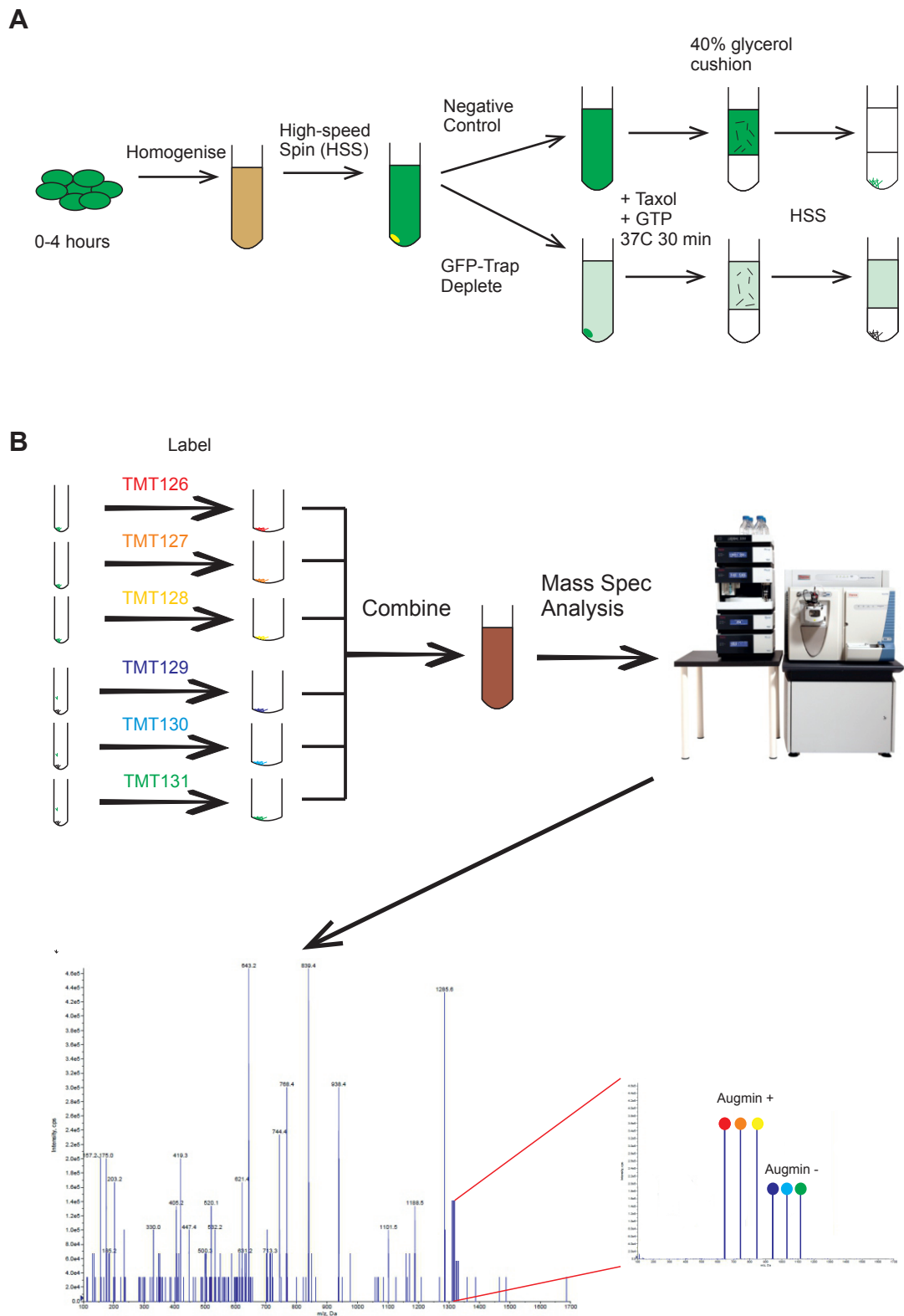
Figure 4.1- Schematic of the experimental procedure for TMT mass spectrometry.

Msd1-GFP embryo extracts were prepared and either depleted of Augmin by incubating extracts with GFP-TrapA beads or left as control extracts, after which a MT co-sedimentation assay was performed (A). 3 control samples and 3 Augmin depleted samples were mass-tagged with Tandem Mass Tags™ (TMTsixplex) before mass spectrometry analysis (B).

4.2. Results:

4.2.1. TMT mass spectrometry identifies Didum and Mud as MAPs that are depleted in Augmin-depleted embryo extract

In the previous chapter, I showed that the Augmin complex appears able to directly affect MT properties in the absence of γ-TuRC. Perturbation of the Augmin complex also induces MT dynamic changes *in vivo* (Hayward et al., 2014). Since MTs of different properties may affect MAP association (Moores et al., 2004), it is important to identify which MAPs, if any, are affected by Augmin. Therefore, I undertook a TMT-based mass spectrometry approach to identify quantitative changes in the MAPs bound to MTs in control and Augmin-depleted Drosophila embryo extracts. A summary of the protocol used is given below, and also shown in Fig 4.1.

In order to determine the quantitative change, MAP pellets from Augmin-depleted extracts were compared with control MAP pellets. *Drosophila* embryos expressing Msd1-GFP were homogenised, incubated with GFP-TRAP-A beads, and analysed by mass spectrometry. The top 8 hits when ranked by MASCOT score were the 8 Augmin subunits indicating that the Augmin complex was immunoprecipitated (Chapter 3, Table 3.1). Triplicate MT co-sedimentation assays were performed on these extracts, and on Msd1-GFP-expressing embryos not incubated with GFP-TRAP-A beads as the control sample.

The total protein content of each sample was quantitated using the Bradford assay and Tubulin quantitated by Western blot, and sample quantity normalised to Tubulin. Each of the MT-MAP pellets produced by co-sedimentation assay were treated with Trypsin and incubated independently with the six Mass Tag labels by

the Bristol University Proteomics Facility. TMT[TM]-126, TMT[TM]-127, and TMT[TM]-128 were used to label the three control samples while TMT[TM]-129, TMT[TM]-130, and TMT[TM]-131 were used to label the Augmin depleted samples. Protein identities were assigned to each peptide to obtain a list of MAPs identified in each of the six samples. In order to compare the relative abundance of each protein in each sample the mass spectrometry intensities were presented as a ratio to the one of the control samples (i.e. the 126 mass tag data for each protein were set as 1). These normalised datasets of proteins were then subjected to two-tailed pairwise T-tests in order to identify those proteins statistically significantly increased or decreased in the Augmin-depleted MAP pellets. After removal of single peptide hits, and of proteins with a Mascot score of less than 50, 33 proteins were significantly decreased (Table 4.1). Of these 33 proteins, 21 were ribosomal, and none were Augmin subunits. I have shown previously that incubation with GFP-TRAP-A beads depletes at least Msd1-GFP and Dgt6 from GFP-TRAP-A beads (Chapter 3, Fig. 3.4) indicating that the absence of Augmin subunits among those proteins significantly increased or decreased is not a consequence of failing to reduce the level of Augmin subunits from extracts. Therefore, I concluded that the failure to measure significant depletion of Augmin in the proteomics was due to either errors in the analysis, or that the reduction in Augmin concentration was below the level of statistical significance.

In an attempt to recover more useful data from the experiment, a manual analysis was undertaken, comparing the fold-difference between each control and each treatment (control 1 to sample 1, 2, 3, control 2 to sample 1, 2, 3 etc). This analysis revealed that there was a great deal of variability in the success of Augmin

Protein list before standardisation	p-value
RanGAP	0.00155
Df31	0.00252
RpL12	0.00676
RpS13	0.00965
RpL22	0.01905
RpL10Ab	0.02033
Cyp1	0.02206
CG9776	0.02440
RpL30	0.02494
mute	0.02634
RpL6	0.03148
RpL3	0.03196
RpS20	0.03298
RpL11	0.03363
RpLP0	0.03421
Rack1	0.03451
RpL35	0.03468
CG8184	0.03543
RpL13	0.03660
sta	0.03666
RpS28b	0.03721
CG7182	0.03725
RpS4	0.03777

CG12512	0.03922
RpL7	0.03972
RpS3A	0.04055
RpLP1	0.04067
RpL21	0.04356
vig2	0.04499
RpL13A	0.04578
RpS15Aa	0.04739
Ef1alpha48D	0.04798

Table 4.1- List of proteins that are significantly lower in the Augmin depleted sample, determined by t-test statistic, with a decision rule of $p < 0.05$. Most of the samples which showed a significant difference were ribosomal proteins (highlighted in blue), while none of the Augmin subunits were significantly decreased.

depletion between samples. Based on this result, I excluded 2 samples in which Augmin did not appear to have been significantly depleted when compared to controls. The remaining sample had reduced levels of all 8 Augmin subunits in comparison to each of the control samples, with the best comparison being to control sample 1, which resulted in all 8 Augmin subunits within the top 9 most significantly different proteins (Table 4.2). From that list, Didum was chosen for further study based on the following criteria:

(i) it was within the Top 25 proteins with the highest changed in abundance,

(ii) it was the highest ranking protein outside of the Augmin subunits to have a previously described role in regulating MTs (Espreafico et al., 1998; Wu et al., 1998),

(iii) it has been identified as directly interacting with the Augmin subunit Dgt4 in yeast-2-hybrid assays (Giot et al., 2003),

(iv) The human homologue of Didum, Myosin V, localises to the centrosome as well as the spindle during mitosis (Espreafico et al., 1998; Wu et al., 1998).

4.2.2. Didum weakly localises to MTs during mitosis

The *Drosophila* protein Didum is the homologue of human Myosin V, a molecular motor that typically travels on actin filaments. During mitosis, however, human Myosin V localises to the mitotic spindle (Espreafico et al., 1998; Wu et al., 1998). Given that Didum has been previously shown to interact with at least 1 Augmin subunit (Giot et al., 2003), and since the Augmin complex also localises to the

Control 1 / Augmin 1
Ccs
dgt4
dgt6
wac
dgt5
msd5
dgt2
msd1
dgt3
ome
CG9603
CG13449
Vha100-1
CG14476
lqfR
Xe7
GCC185
CG11619
RpS30
didum
CG10237
CG9795
mRpS31
Rif1

CG5525
Dcp-1
Trxr-1
Rab14
kz
CG17202
mud
Sym
Tcp-1eta
Rab10
CG5664
ArfGAP1
G9a
CG7246
vir
jar
Dbp80
gw
DNA-ligI
CG11779
CG14651
fs(1)Ya
cnn
Cct1
CG16734

ro

Table 4.2- List of top 50 proteins based on TMT ratios after normalising to Tubulin, with Augmin subunits highlighted in yellow. The ratio between Augmin sample 1 and control sample 1 had all Augmin subunits within the top 9 ratios, indicating it is a good dataset to work with. Didum, which has been shown to interact with Dgt4 via yeast 2-hybrid (highlighted in red) was the number 20 hit in the dataset (Giot et al 2003)

spindle during mitosis, it is possible that Didum interacts with Augmin during mitosis. To elucidate potential functions of Didum in mitosis and its possible relationship to Augmin, I obtained a fly line carrying a Didum-GFP transgene under the control of the bipartite UAS-GAL system (a kind gift from Dr. Sonia Lopez de Quinto, Cardiff University). In order to more easily determine the stages of mitosis and as a marker for the mitotic spindle, a *Drosophila* line expressing Tubulin-RFP under the control of a maternal-alpha-Tubulin VP Gal4 driver was generated by recombination (Fig. 4.2). The Didum-GFP fly line was then crossed with this Tubulin-RFP mat-α-T-Gal4 line (Fig. 4.2) to produce flies which expresses both Didum-GFP and Tubulin-RFP in early embryos.

Early embryos from this fly line were observed by live fluorescence microscopy to identify the localisation of Didum. During interphase, Didum-GFP was found to be excluded from the nucleus, and speckled patterns in the cytosol could be seen. As nuclear envelope breakdown occurs, Didum-GFP could be seen to weakly localise near the chromatin. The speckled pattern could be seen surrounding each mitotic unit, perhaps reflecting the formation of the cortical actin caps that form at this stage (Cao et al., 2010). As the cell progresses towards anaphase, the chromatin localisation of Didum-GFP becomes less pronounced. The speckled pattern surrounding each mitotic unit, however, was still observed. As embryos progress to telophase, the speckled pattern mostly disappears and by the point of nuclear envelope reformation, Didum-GFP once again becomes excluded from the nucleus (Fig. 4.3).
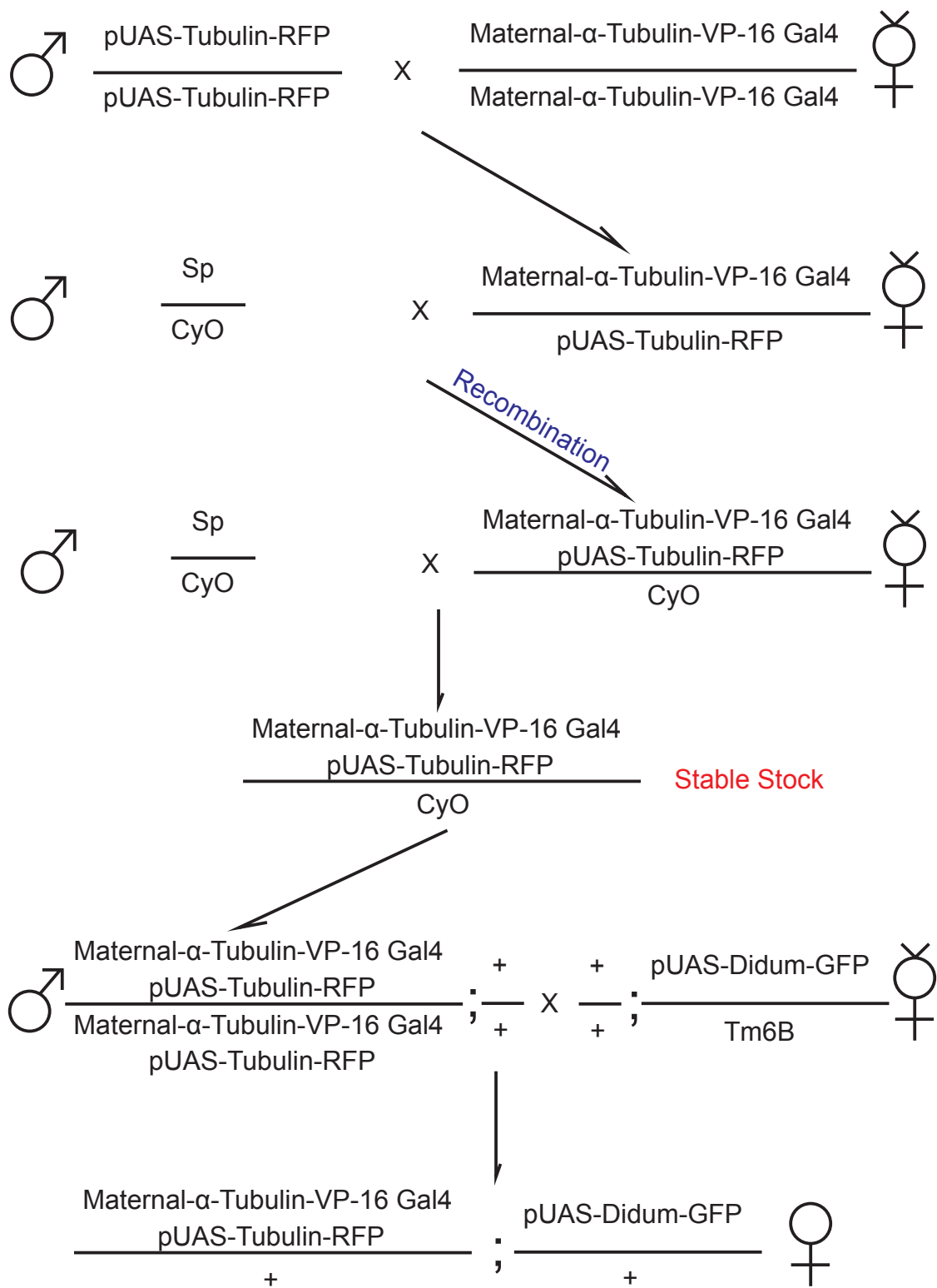
Figure 4.2 - *Drosophila* crosses for creating embryos expressing Tubulin-RFP and Didum-GFP

A UAS-driven Tubulin-RFP Drosophila line was crossed with a line containing maternal-α-Tubulin-VP-16-Gal4, and recombined on the second chromosome to create a stable fly line (marked in red) that expresses Tubulin-RFP in early embryos. This stable line is then crossed with a UAS-driven Didum-GFP line to create a new fly line expressing both Tubulin-RFP and Didum-GFP in early embryos.
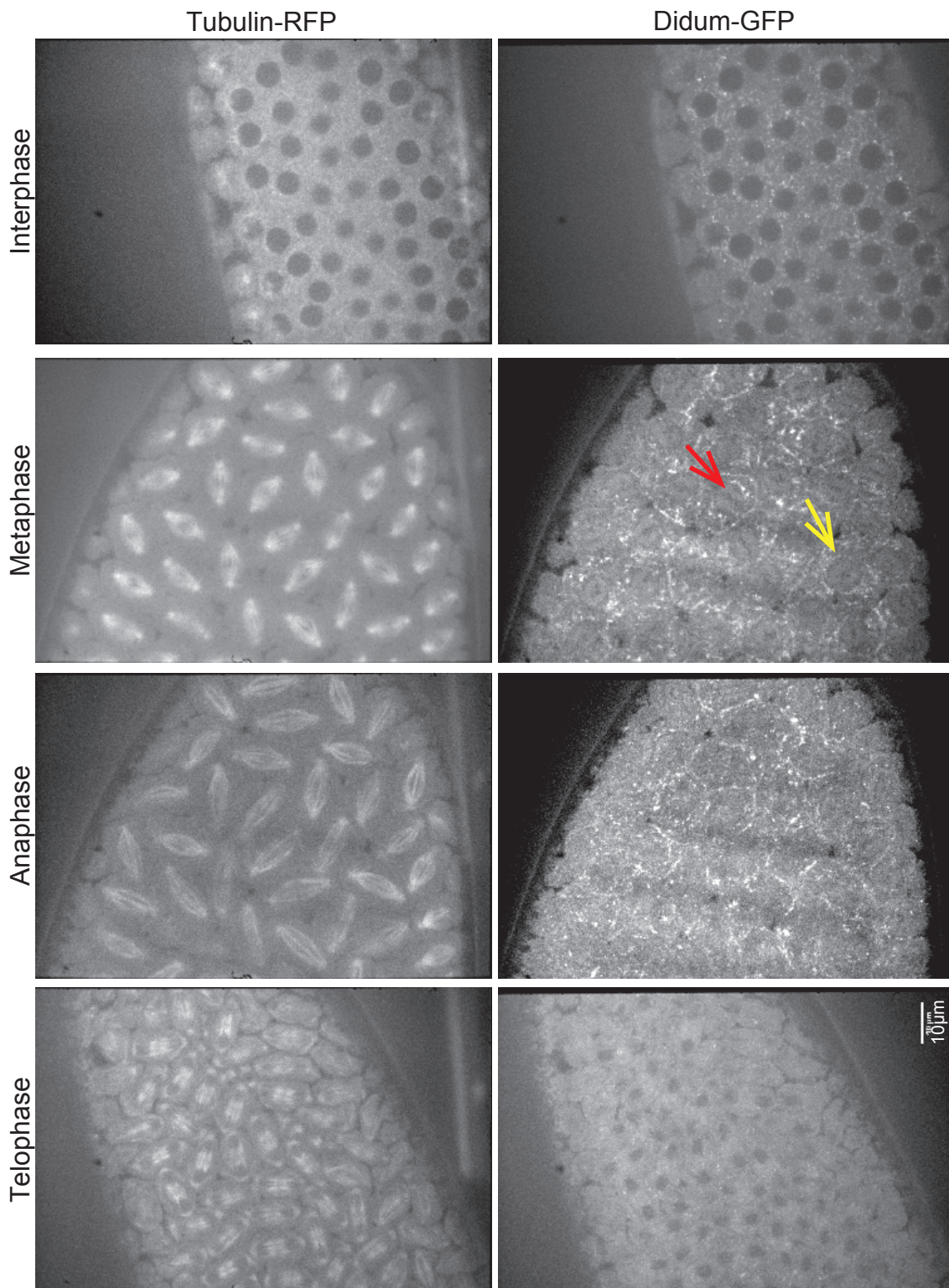
Figure 4.3- Didum-GFP weakly associates with spindle MTs during metaphase

Early embryos expressing Didum-GFP and Tubulin-RFP were observed by fluoresence microscopy. During interphase, Didum is excluded from the nucleus, and forms punctate foci. At metaphase, Didum weakly localises to the mitotic spindle, particularly around chromatin (red arrow). Punctate foci becomes more pronounced, and surround each mitotic spindle (yellow arrow). At the onset of anaphase, both the spindle localisation and punctate foci becomes less pronounced, and disappear almost completely at the onset of telophase.

4.2.3. Didum-GFP can be immunoprecipitated by GFP-TRAP-A

Although *Drosophila* Didum does not have the same localisation as Augmin, it has previously been identified as interacting with Augmin in a yeast two-hybrid system, and therefore it was prudent to examine whether this interaction occurs *in vivo*. In order to do this, I first needed to purify Didum-GFP from embryo extracts. To prevent the possibility of Tubulin-RFP affecting the results, embryos expressing both RFP-Tubulin and Didum-GFP were not used for immunoprecipitation. Heterozygous Didum-GFP flies were mated with homozygous flies carrying the maternal-α-Tubulin VP16 Gal4 driver, resulting in 50% of the F1 progeny carrying both genes, and thus, only 50% of the collected embryos expressed Didum-GFP (Fig. 4.4A). A Western Blot was performed to assess the quantity and quality of Didum-GFP in these embryo extracts (Fig. 4.4B). A prominent band at 250 kDa, and a less prominent band above 250 kDa were present in the input and bound to the GFP-TRAP-A beads. Although those two bands were present in the depleted supernatant, the intensity is reduced, suggesting that the majority of Didum-GFP is indeed bound by the GFP-TRAP beads. The expected size of Didum-GFP is 235 kDa, so it is very likely the band at 250 kDa is the full-length protein. Since Didum is the *Drosophila* homologue of human myosin V, and human myosin V has been characterised as a dimer (Mehta et al., 1999), the high molecular band is likely to be undenatured dimerised Didum-GFP.

4.2.4. Mass spectrometry yielded high score for Didum-GFP

In order to identify proteins which interact with Didum-GFP, the contents of the immunoprecipitated Didum-GFP embryo extract was analysed by mass
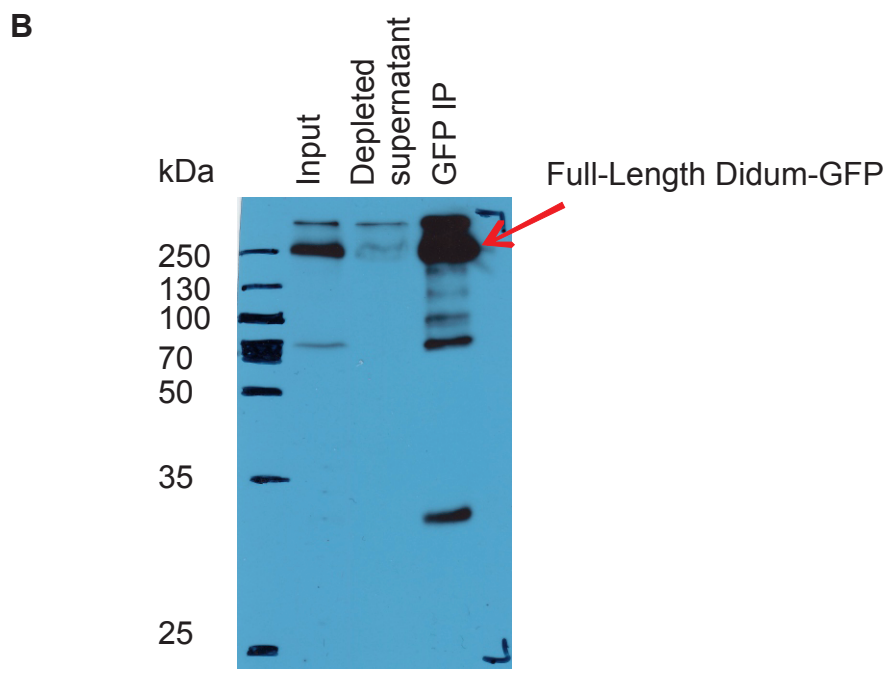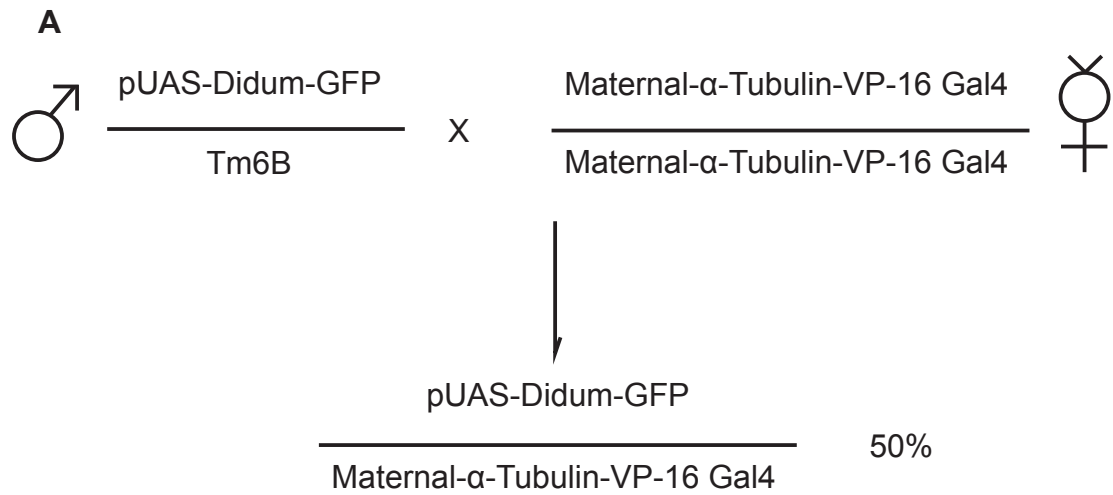
Figure 4.4- Full-length Didum-GFP can be immunoprecipitated from embryo extract.

(A) To generate embryos that expressed Didum-GFP, the pUAS-Didum-GFP line was crossed with the Maternal-α-Tubulin-VP-16 Gal4 driver. Since pUAS-Didum-GFP flies are not homozygous, only 50% of the progeny carry the required alleles. (B) Didum-GFP embryo extracts (input, lane 1) were incubated with GFP-TRAP- beads (lane 3) and depleted supernatant removed (lane 2). A Western Blot of this immunoprecipitation revealed a prominent band at 250 kDa corresponding to full-length Didum-GFP (estimated size 235kDa, red arrow). There is also a lighter band above the 250kDa position, which may correspond to Didum-GFP dimers that were not fully denatured during SDS-PAGE.

spectrometry. As expected, the top protein identified by mass spectrometry was Didum, with a Mascot score of 10786.14 and percentage coverage of >80%. Using the standard in-lab procedure of filtering against a list of negative proteins (as described in Chapter 3, Section 3.4), a list of proteins interacting with Didum was produced (Table 4.3). The resulting list consisted of 23 Didum-interacting proteins as well as Didum itself. Of these proteins, 9 were known to associate with Actin, and 4 had mitotic roles. No Augmin subunits were identified, and the only protein that had a known association with Augmin was CenP-Meta, also known as Cmet (Table 4.3, in bold) (Bucciarelli et al., 2009), which was identified with a Mascot score of 59.61. Given these results, and the localisation of Didum-GFP seen in Section 4.2.2, it is therefore likely that either Didum is not a *bona fide* Augmin interacting protein in the early embryo, or that the interaction is transient and cannot be confirmed either through co-localisation or biochemical means. No further analysis of Didum function in the embryo was therefore undertaken.

4.2.5. Re-analysis of the Augmin QC-MAP data suggests Mud association with MTs may be Augmin dependent

As Didum was the best candidate from the initial TMT^{TM}-based mass spectrometry analysis that it did not appear to interact with Augmin indicated that there may have been flaws in the original analysis. In particular, upon re-examination, it was apparent that Tubulin levels differed noticeably between samples, suggesting that the initial normalisation of samples to Tubulin levels as quantified using the Bradford assay and by Tubulin Western blot was insufficient. Therefore, Augmin-depleted QC-MAP datasets were normalised to the total score of Tubulin within

Protein Name	Coverage	# Peptides	Mascot Score
Didum	80.44	187	10786.14
CG10254	39.20	50	655.39
HERC2	18.40	59	277.25
unc-45	43.61	36	245.75
CG32164	35.13	26	239.06
MyoII (Zipper)	23.90	32	180.70
CG17514	19.01	37	149.10
MLC-c	54.42	10	145.31
Coro	33.14	12	126.60
APC7	25.53	12	115.42
CG4119	20.94	13	100.06
CG2107	36.13	16	93.20
Blue	11.24	12	89.90
Cup	27.66	17	84.02
Rod	9.72	14	78.78
DNApol-epsilon	9.30	14	67.51
CG14309	17.18	12	66.41
Slbp	48.91	8	66.16
Nipped-B	8.74	13	62.54
Myo-VI (jar)	11.65	10	61.08
Cmet	8.11	12	59.61
CG8036	25.86	10	58.24
Diablo	28.39	11	57.53
eIF2-gamma	34.69	11	56.92

Table 4.3- List of proteins identified by mass spectrometry from Didum-GFP immunoprecipitation. A cut-off score of 50, and a filter list of non-specific proteins was applied. Although no Augmin subunits were identified, Cmet, an Augmin interacter (**in bold**), was identified.

each sample, since he absolute quantity of MAPs is likely to depend on the quantity of MTs and therefore on the absolute quantity of Tubulin. As before, these normalised datasets were subjected to two-tailed pairwise T-tests and single peptide hits and proteins with Mascot scores of less than 50 were removed. Following this analysis, 7 of the 8 Augmin subunits were found to be significantly different in quantity between control and Augmin-depleted samples (Table 4.4, yellow), suggesting that this new method of analysis accurately reflects the depletion of Augmin from the experimental samples. 16 proteins were significantly different in the final analysis, all of which were significantly decreased. There were no proteins that significantly increased in quantity after Augmin depletion. Encouragingly, of these 16 proteins, two were components of gamma-TuRC - Grip84 and Grip163 (Table 4.4, green). Of the remaining significant proteins, Mud has been characterised to be important for MT organisation during mitosis (Capalbo et al., 2011). Another protein, Stai, the *Drosophila* homologue of the human protein Stathmin, is a tubulin-dimer sequestering protein which has roles in regulating MT dynamics in both interphase and mitotic cells (Ozon et al., 2002). Additional experiments will need to be undertaken to test the hypothesis that either Stai or Mud have a functional relationship with Augmin in the early embryo.

Protein list after standardisation	p-value
wac	0.00120
CG9915	0.00148
dgt4	0.00231
Sbf	0.01100
CG5815	0.01145
SMC1	0.01223
dgt2	0.01259
msd1	0.01383
Grip84	0.01623
Grip163	0.01735
GCC185	0.01855
Sam-S	0.01962
msd5	0.01976
dgt6	0.03088
wal	0.03472
raptor	0.03575
mud	0.03600
rad50	0.03765
stai	0.03798
simj	0.04627
CG8290	0.04650
CG4169	0.04721

Table 4.4- List of proteins that are significantly different in the Augmin depleted sample, determined by two-tailed pairwise T-tests, with a decision rule of p<0.05 after standardisation against total Tubulin levels. 6 of the 8 Augmin subunits (highlighted in yellow), and two γ-TuRC subunits (highlighted in green) were identified as significantly decreased. Mud and Stathmin (highlighted in red) were the only proteins previously characterised as playing an clear role in mitosis.

4.3. Discussion

4.3.1. Quantitative Comparative MAP proteomics as a tool for investigating cellular function and response to perturbation

By labelling proteins with different mass tags, TMT-based mass spectrometry offers a means to examine quantitative changes in proteomes in samples under different conditions. Here, I have used this technique to examine changes in MAP association with MTs in *Drosophila* embryos depleted of Augmin. Initial analysis yielded highly variable results, both within the experiment itself and also when compared to another TMT based mass spectrometry study done within our laboratory comparing cycling and mitotically arrested early *Drosophila* embryos. Such variable results suggest there were errors in initial quantification of MAP pellets and that the methods used to normalise samples against one another prior to tagging and mass spectrometry were insufficiently sensitive. However, this error was remedied when samples were normalised against Tubulin, and significant decreases in protein level could be seen in Augmin-depleted samples for 7 Augmin subunits as well as 2 γ-TuRC subunits, as compared to controls. This data indicates that normalisation to Tubulin is in important step in MAP quantity standardisation.

Although there was a significant decrease of 7 of the 8 Augmin subunits in the MAP pellets after the new analysis, all 8 subunits were still detected in the Augmin depleted samples. Thus, immunodepletion by GFP-Trap is not complete. As I showed in Chapter 3, Msd1-GFP in genetically-modified flies appears to be present in 2 populations, one of which is in a complex and the other of which is as unbound Msd1-GFP; as such, not all Msd1-GFP protein is incorporated into Augmin, and is

is likely that a proportion of Augmin contains endogenous Msd1. Thus, effects of total Augmin depletion on the association of MAPs with MTs remains to be elucidated.

The MTs used for this experiment were artificially generated by incubating embryo extracts with GTP (to promote MT polymerisation) and taxol (to stabilise the resulting MTs). However, since Taxol artificially stabilises MTs, and shifts the MT dynamic towards growth, the presence of taxol preferentially results in MTs consisting of 14 protofilaments as opposed to the predominantly 13 protofilament MTs that occur *in vivo.* It has been shown that these artificially-generated MTs have different properties and therefore MAP binding to MTs is affected. Further, I have shown that Augmin itself has direct effects on MT properties *in vitro* (Fig. 3.7) and we have not yet characterised the properties of these Augmin-generated MTs. Therefore, while the results presented in this chapter represent an important advance in our understanding of Augmins effects on other MAPs, it is important to consider that there may be differences between the results shown here and the in vivo effects on MAPs, due to the artificial nature of the protocol. It is also important to examine this quantitative MAP proteomics data in conjunction with the GFP-IP data set.

It has been recently shown that mitotic pathways may be up-regulated when one pathway is perturbed (Hayward et al., 2014). By using immunodepleted extracts, there is no way in an extract that this compensation can occur and thus, the results of this experiment cannot be due to changes in alternate mitotic pathways. It would therefore be interesting to compare the results of this experiment with a similar experiment in which embryos from the Augmin mutants wacΔ12 or msd1[ex51] are

used, which will allow us to determine which MAPS are directly affected by Augmin and compare this with the complement of MAPs which are affected by compensatory pathways during Augmin loss.

4.3.2. Analysis of Didum as a mitotic MAP with a relationship to Augmin

The initial QC-MAP proteomic analysis identified Didum as a MAP that appears to change its affinity to MTs depending on the presence/absence of Augmin. Didum has been previously characterised to associate with MTs (Espreafico et al., 1998; Wu et al., 1998), and has been implicated in mitosis (Espreafico et al., 1998; Wu et al., 1998). In addition, the human homologue of Didum, Myosin V, localises to the mitotic spindle (Espreafico et al., 1998; Wu et al., 1998). A yeast 2-hybrid analysis previously identified Didum to interact with Dgt4, an Augmin subunit (Giot et al., 2003). Furthermore, Augmin immunoprecipitation has identified Didum as a significant hit under mass spectrometry, which further suggests that Augmin interacts with Didum (Chapter 3 Table 3.1). This combined available evidence therefore suggested that Augmin and Didum have a relationship and, since both localise to the mitotic spindle and play roles in mitosis, that this relationship may be particularly important during mitosis. Thus Didum was chosen as a candidate from the QC-MAP proteomics to undertake further work on.

Live microscopy of Didum-GFP, however, showed a difference in localisation compared to the previously published results of human MyoV localisation (Fig. 4.3) (Espreafico et al., 1998; Wu et al., 1998). In human cells, MyoV localises to the mitotic spindle and the centrosomes. During *Drosophila* syncytial mitosis, I found

that Didum localises around chromatin, and in punctae around the cortical actin cap area in metaphase. However, it is excluded from the centrosomes and does not appear to localise to MTs. The dynamic localisation of Didum around the chromatin was only present during mitosis, and not interphase, suggesting that the MAP properties of Didum are cell-cycle controlled. To date, the implication and biological role of the mitotic spindle localisation of Myosin-V has yet to be elucidated, but it is possible Myosin-V has a moonlighting function, and may regulate MTs in some way during mitosis.

Although Didum was identified by mass spectrometry from the Augmin immunoprecipitation, mass spectrometry of Didum-GFP embryo extracts failed to identify any Augmin subunits, and Didum-GFP showed a different localisation to Augmin, suggesting that Didum does not interact with the Augmin complex under the conditions studied. CenP-Meta (a protein which has been shown to associate with Augmin (Bucciarelli et al., 2009) was identified from the Didum immunoprecipitation, indicating that Didum and Augmin may interact via this protein. However, the Mascot score for CenP-Meta was low and is close to the cut-off used for our experiments, meaning any interaction between CenP-Meta and Didum is unlikely to be strong or that CenP-Meta is a false positive. No other proteins identified as Didum-interacting had been characterised to associate with Augmin, suggesting Didum and Augmin have no indirect functional relationship. However, It is important to note than the Didum-GFP fly line overexpresses Didum in addition to endogenous Didum, and therefore there may be artefacts due to this overexpression. It is also important to consider that the GFP tag added to the Didum protein in this system may interfere with binding of Didum to certain

interactors and therefore some interactions may not be identified. It is very difficult to prove a negative, thus definitively ruling out any interaction between Didum and Augmin will be complicated. The fact that *Drosophila* Didum has different characteristics to its human homologue suggests any mitotic role of Didum is likely to be *Drosophila* specific and differ from the role of human Myosin V. Since I am using *Drosophila* as a model organism to investigate mitosis, to pursue the project would defeat the purpose of model organisms.

Overall, although initial analysis identified Didum as a target while follow-up experiments suggests otherwise, TMT^{TM} based mass spectrometry remain to have potential. By normalising the mass spectrometry results against Tubulin, variation in sample loading can be minimised. After normalisation, Mud and Stai has been identified as proteins significantly decreased, and offer exciting targets for future studies.

5. Structural constraints within the Augmin complex, as revealed by Cross-linking/ Mass spectrometry: implications for templated microtubule nucleation

5.1. Introduction

Since its discovery in *Drosophila* (Goshima et al., 2007; Goshima et al., 2008; Hughes et al., 2008), the hetero-octomeric Augmin complex has radically changed our understanding of microtubule (MT) generation during mitosis. Augmin amplifies MT number during mitosis and in its absence, the density of MTs within the mitotic spindle is dramatically reduced such that chromosome alignment and mitotic progression is perturbed (Hayward et al., 2014; Ho et al., 2011; Hotta et al., 2012; Lawo et al., 2009; Meireles et al., 2009; Nakaoka et al., 2012; Petry et al., 2011; Uehara et al., 2009; Wainman et al., 2009). Human Augmin subunits associate with the MT nucleating complex γ-TuRC (Teixidó-Travesa et al., 2010; Zhu et al., 2008) and removal of Augmin through RNAi, mutation, or immunodepletion, removes the fraction of γ-TuRC normally present within the spindle without affecting centrosomal levels (Goshima et al., 2007; Goshima et al., 2008; Hughes et al., 2008). The current model is therefore that Augmin acts as a molecular linker between an existing MT and a γ-TuRC, allowing the nucleation of new MTs from the walls of pre-existing ones (Uehara et al., 2009). Such Augmin-dependent branched MT nucleation has recently been observed (Petry et al., 2013). However, little is known of the molecular and structural basis of Augmin function. X-ray crystallography is the traditional method of determining the structure of a protein, or a protein complex, although success is often dependent on having high

concentration and high purity of the protein in question. Obtaining soluble Augmin of sufficient purity and concentration for X-ray crystallography has not been possible (see Chapter 3), which has been the major hindrance in determining any structural data for Augmin.

Another approach to elucidate protein arrangement within a complex is with crosslink mass spectrometry (CLMS) (Fig. 5.1). Using chemical crosslinks to determine protein-protein interaction has been used for approximately 40 years (Clegg and Hayes, 1974), and the robustness of the approach has been confirmed with crystallographic data (Boal et al., 2006; Chen et al., 2010; Denison and Kodadek, 2004; Rappsilber, 2011). CLMS has also been successfully used to examine interactions between MAPs and MTs (Gupta et al., 2010). Combined with the potential of using the distance restraint of the crosslinker for improved modeling (Back et al., 2003), crosslinking proteomics is the ideal approach to investigate the structure of Augmin.

By using CLMS in collaboration with the research group of Professor Juri Rappsilber (University of Edinburgh), I have produced a predictive map of structural restrictions within the Augmin complex. Using both structural bioinformatics (in collaboration with the research group of Professor Charlotte Deane, University of Oxford) and in vitro biochemistry, I have tested these predictions. My results strongly support the orientation of Augmin subunits with one another as determined by CLMS, and their structural relationship to both MTs and the γ-TuRC. This data therefore greatly improves our current understanding on the molecular function of Augmin.
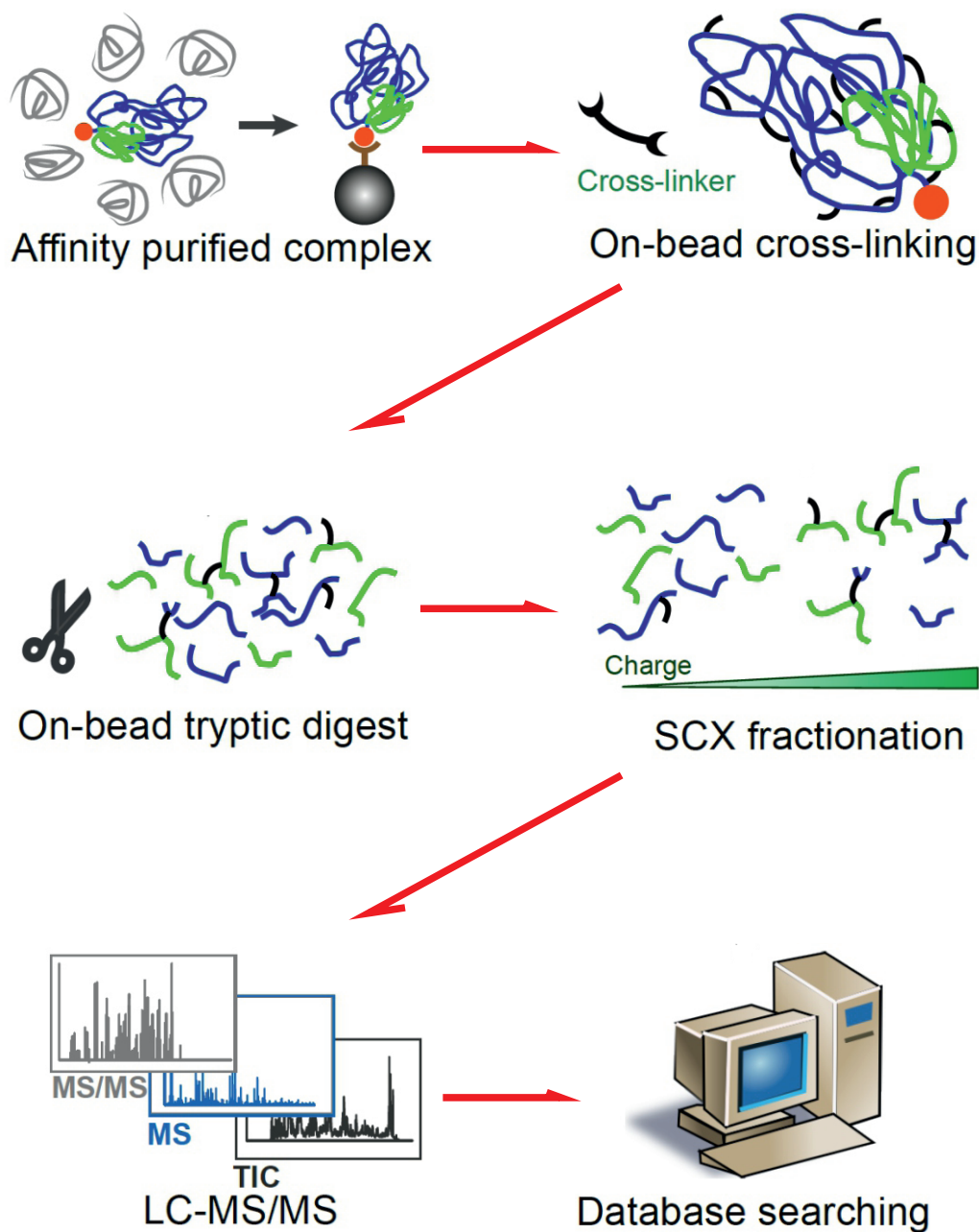
Figure 5.1- Schematic of the experimental procedure for crosslinking mass spectrometry.

The Augmin complex was purified from Msd1-GFP-expressing embryos using GFP-TrapA beads (as per Chapter 3, Section 3.3.4), and crosslinked on the beads with bis[sulfosuccinimidyl] suberate (BS3). After tryptic digest, crosslinked peptides were enriched by Strong Cation eXchange (SCX) fractionation. These enriched samples were examined by mass spectrometry, and the mass spectra searched against the Flybase database to identify the resulting peptides.

5.2. Results

5.2.1. Crosslink mass spectrometry determines the arrangement of the Augmin subunits within the complex

I have previously demonstrated GFP-Trap-A beads can immobilise Augmin from 0-4 hour old *Drosophila* embryos expressing Msd1-GFP (Chapter 3, Section 3.4). It is therefore possible to use this immobilised Augmin complex for CLMS, in collaboration with Dr Angel Chen (Rappsilber Laboratory, Wellcome Institute for Cell Biology, University of Edinburgh). Mass spectrometry of approximately 2.5% of immunoprecipitated Msd1-GFP revealed all 8 Augmin subunits as the top hits (Table 5.1). The abundance of all Augmin subunits with the exception of Msd1 was about equal (Fig. 5.2A). The protein abundance of Msd1 was approximately 3 times that of all other Augmin subunits. The remaining sample (97.5%) was crosslinked with bis[sulfosuccinimidyl] suberate (BS3), which has a theoretical crosslinking limit of 25Å, and was analysed by mass spectrometry. By using 1% false discovery rate (FDR) constraints, 29 intra-protein crosslinks, and 25 inter-protein crosslinks were identified (Appendix Table 2). The search for crosslinked peptides was refined by using the Target Decoy database method, with a 5% FDR constraint. The refined search method revealed 77 intra-protein linkages and 59 inter-protein linkages within the 8 subunits of the Augmin complex (Appendix Table 3). The number of cross-links observed between the subunits of Augmin suggests that there are two sets of core interactions within the complex (Fig. 5.2B): one comprised of Dgt6, Msd5 and Msd1, and another between the C-termini of Dgt5, Wac, Dgt2, Dgt3. The remaining subunit, Dgt4 showed only a single, weak predicted interaction, suggesting it lies on the outside of Augmin and may be

Protein Name	Sequence Coverage	Mascot Score	PAI
Msd1	80.4	1033	5.6
Dgt2	83.5	499	2.4
Dgt5	70.5	1639	2.1
Wac	84	498	2.0
Msd5	79.4	1104	2.0
Dgt6	82.1	1576	1.9
Dgt4	55.9	572	1.8
Dgt3	64.1	1378	1.8
Hsc70-4	80.5	1394	1.6
betaTub56D	78.3	1313	1.5
l(1)G0156	63.6	719	1.5
PyK	74	1106	1.3
Tcp-1zeta	65.5	733	1.3
Yp3	74.5	554	1.2
Cctgamma	77.2	965	1.1
T-cp1	67.3	895	1.1
Hsp27	75.6	244	1.1
alphaTub84D	58.9	681	1.1
Yp2	73.1	763	1.0
Ef1alpha48D	48.4	371	1.0
alphaTub67C	50.4	946	1.0

Table 5.1- Mass spectrometry of immunoprecipitated Augmin complex before crosslinking ranked by protein abundance index (PAI). All Augmin subunits were identified as the most abundant protein species (red), indicating the immunoprecipitation was successful.
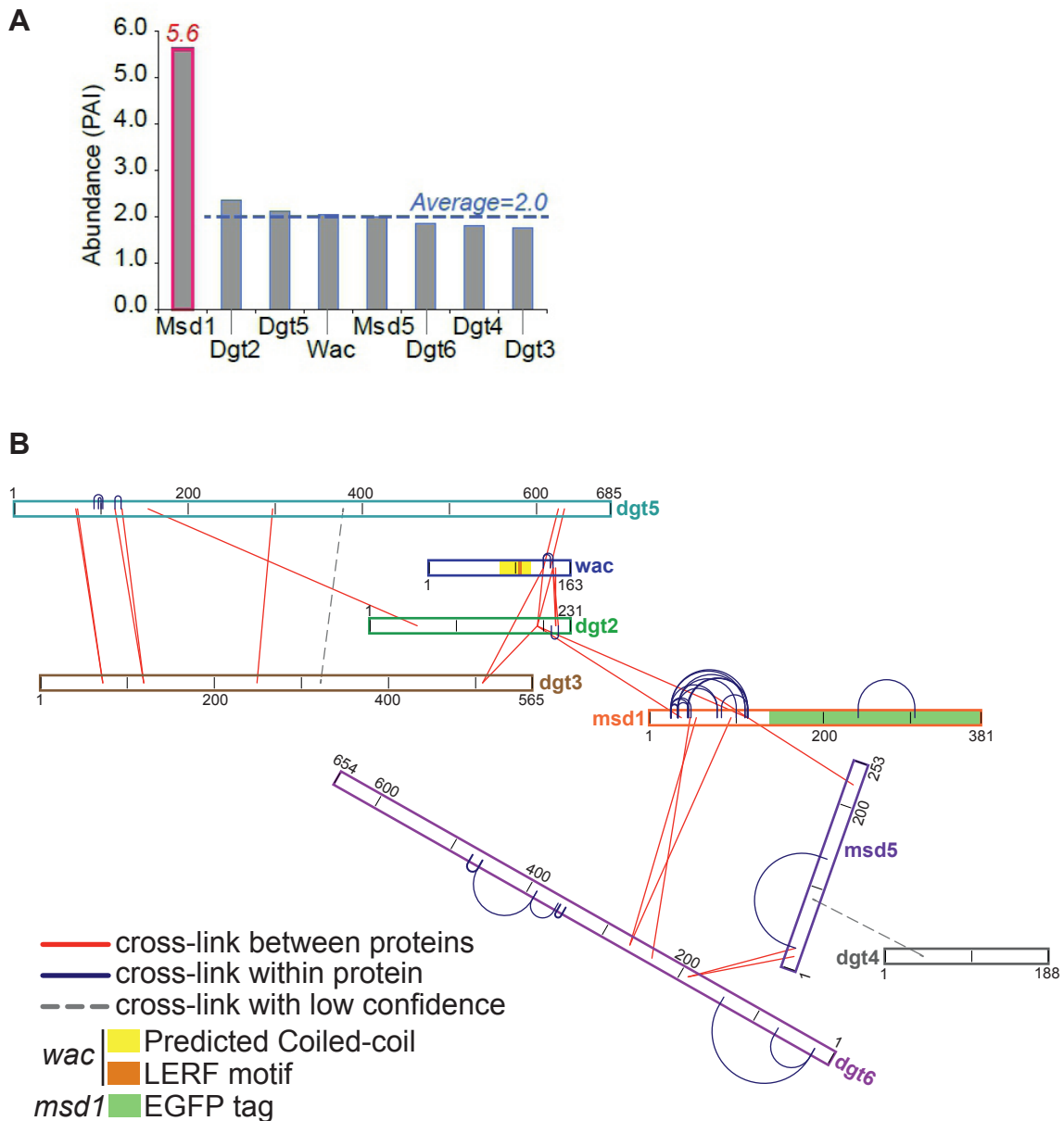
Figure 5.2- Construction of a topological map of the Augmin complex by crosslink mass spectrometry.

(A) Graph of relative abundance of Augmin subunits in the sample prior to crosslinking. Mass spectrometry reveals a 1:1 Protein Abundance Index (PAI) ratio for all subunits except Msd1, which was present at ~3 times as much.
(B) Crosslinking map of the Augmin complex (generated by Angel Chen, University of Edinburgh). Database search with 1% FDR yielded 29 intraprotein linkages and 25 inter-protein linkages, all of which are shown in this cartoon. All proteins are shown to scale. All protein subunits have multiple inter-protein linkages except Dgt4, suggesting it may be more weakly connected to the Augmin complex.

moreweakly connected (Fig. 5.2B). Although using Target Decoy and 5% FDR method yielded a more comprehensive list of crosslinked peptides, subsequent experiments were designed with the data obtained from 1% FDR search constraint due to the apparent greater stringency.

5.2.2. The Augmin subunits Wac and Dgt4 directly bind MTs

Only 1 inter-protein crosslinked peptide was detected for Dgt4, which suggests that Dgt4 may lie at the edge of the Augmin complex. Human Dgt4 (hDgt4) has been shown to directly associate with MTs, and although *Drosophila* Dgt4 lacks the N-terminal MT binding domain found in hDgt4, I hypothesised that *Drosophila* Dgt4 retains MT binding capacity. Most of the inter-protein crosslinks identified in the subunit Wac were near the C-terminal LEFR motif which mediates binding to Dgt2, leaving the N-terminus of Wac free for protein-protein interaction, suggesting that Wac may be an additional MT binding subunit. Msd1 is an Augmin subunit with several inter-protein crosslinks to multiple of the other Augmin subunits, and thus is unlikely to have interfaces for additional protein interactions.

In order to test the MT binding properties of these subunits, I obtained a series of bacterial expression constructs, using Maltose Binding Protein (MBP) as an N-terminal tag. MBP, MBP-Msd1, and MBP-Dgt4 were already available and MBP-Wac was a kind gift from Professor Hiro Ohkura (University of Edinburgh). Proteins were purified from *E. coli* and used in *in vitro* MT co-sedimentation assays. After MTs are generated in the presence of Taxol (to stabilise MTs and protect them from cold depolymerisation), or absence of Taxol, purified proteins (MBP, MBP-Dgt4, MBP-Msd1, and MBP-Wac) were incubated with the MTs. The samples were

placed on ice so that the MTs without Taxol may depolymerise, and the MTs with Taxol are unaffected. The samples were centrifuged through a 40% glycerol cushion, in order to pellet MTs and associated proteins. Western blot analysis of these experiments (Fig 5.3) demonstrated that MBP and MBP-tagged proteins were detected in the supernatant of both the -Taxol and the +Taxol samples, however, MBP was not detected in the pellet of either sample, indicating that MBP alone does not interact with MTs. Very little MBP-Dgt4 was found in the pellet in the absence of Taxol whereas there was a clear increase in the presence of Taxol, indicating that MBP-Dgt4 binds MTs in this assay. Similarly, a clear increase of MBP-Wac in the pellet in the presence of Taxol was detected, though there was also some (though much less) MBP-Wac detected in the -Taxol pellet (Fig. 5.3, red arrow). Interestingly, incubation of MTs with MBP-Wac in the absence of other Augmin subunits resulted in a proportion of MTs remaining after depolymerisation even in the absence of Taxol, suggesting that MBP-Wac has a direct effect of MT stabilisation. The results for MBP-Msd1 was inconclusive, since there was a high amount of MBP-Msd1 present in the absence of Taxol, and only a minimal increase in MBP-Msd1 in the presence of Taxol pellet (Fig. 5.3). It is important to note that after a high speed centrifigation of purified MBP-Msd1, a clear glassy pellet is always present, similar to that seen when pelleting MTs, which could suggest Msd1 naturally oligomerises.

To further investigate the putative interaction between MBP-Dgt4 and MTs, in collaboration with Dr. Carolyn Moores (Birbeck University, London), purified MBP-Dgt4 was incubated with pre-polymerised MTs and examined by negative staining and transmission electron microscopy (TEM). At 1mg/ml, MBP-Dgt4 particles could
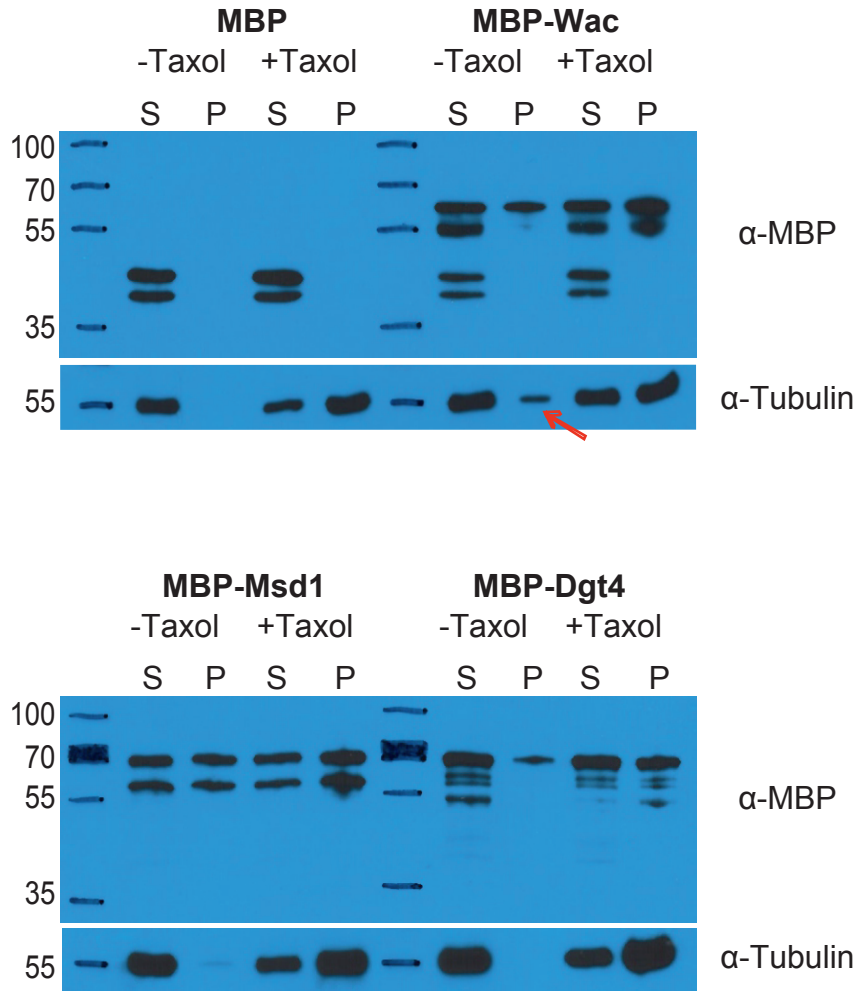
Figure 5.3- In vitro interactions between Augmin subunits and MTs.

In vitro MT co-sedimentation assays with MBP alone, MBP-Wac, MBP-Msd1, and MBP-Dgt4. MTs were generated in vivo, incubated with purified proteins, cold-shocked to depolymerise unstabilised MTs, and MTs (plus bound proteins) pelleted. Experiments were carried out in the presence and absence of Taxol (+/-Taxol) to prevent MT depolymerisation during cold treatment. All proteins (MBP, MBP-Wac, MBP-Msd1 and MBP-Dgt4) were detected in unbound supernatant (S), while only the 3 Augmin subunits were present in MT pellets (P), indicating that the MBP tag alone does not bind MTs. The quantity of Augmin subunits found in the MT pellet (P) is increased in the presence of Taxol, showing that they bind MTs. MBP-Wac consistently resulted in a proportion of Tubulin pellet, even in the absence of Taxol, suggesting it acts to stabilise MTs independently of Taxol itself (red arrow).

be seen on the lattice of the MTs. As the concentration of MBP-Dgt4 increased, an increasing number of these MBP-Dgt4 could be seen associated with MTs (Fig. 5.4).

5.2.3. The Augmin subunits Dgt3, Dgt5, and Dgt6 interact with the gamma-TuRC subunit Dgp71WD

The comprehensive interactions between the Augmin subunits leave few interfaces available for interactions with MTs and γ-TuRC. Work done in human cells has demonstrated a direct interaction between the Augmin subunit Dgt6 and the γ-TuRC subunit Nedd1/GCP-WD (Uehara et al., 2009; Zhu et al., 2008). The homologue of this γ-TuRC subunit GCP-WD in *Drosophila* is Dgp71WD, also known as Grip71. Like its human homologue, the *Drosophila* Dgp71WD protein contains a WD40 repeat-containing domain, which generally form β-propeller structures (Stirnimann et al., 2010). Since β-propellers are often involved in protein-protein interactions (Fülöp and Jones, 1999; Stirnimann et al., 2010), and are able to form interactions with alpha helices (Fülöp and Jones, 1999), I hypothesised that Dgp71WD might, like its human homologue, provide the link between Augmin and γ-TuRC. The CLMS results (Section 5.2.1) suggest that the N-terminus of Dgt6 is occupied by interacting with other Augmin subunits, while the C-terminus of Dgt6 (Dgt6[C]) did not cross-link to other subunits and therefore is free for protein interaction outside of Augmin. Moreover, the Augmin CLMS results identified a series of parallel interactions between the N-termini of Dgt3 and Dgt5 (Fig. 5.2B) and structural prediction within the constraints of the CLMS data, carried out by Kacper Rogala (Charlotte Deane lab, Dept of Statistics, University of

Oxford), confirmed a high likelihood that the N-termini of Dgt3 (Dgt3^N) and Dgt5 (Dgt5^N) form a hetero-dimeric parallel coiled-coil, a structure often involved in protein-protein interactions. Furthermore, analysis done by Dr. Angel Chen (Juri Rappsilber lab, School of Biological Sciences, University of Edinburgh) using the COILS program has shown that the crosslinks between Dgt3^N and Dgt5^N coincide with regions with high probability of coiled coil formation (data not shown).

Since these data indicate that the C-terminus of Dgt6 (Dgt6^C) and the N-termini of Dgt3 (Dgt3^N) and Dgt5 (Dgt5^N) may be regions of interaction with proteins outside of the Augmin complex,   I decided to test whether Dgt3^N, Dgt5^N and/or Dgt6^C are able to interact with Dgp71WD. Constructs were generated by Life Technologies GeneArt® service for the bacterial expression of these three truncated Augmin proteins, fused to 6xHis tags. Another vector for bacterial expression of Dgp71WD fused to a GST tag was kindly provided by Professor Jordan Raff, University of Oxford. Protein purification conditions was optimised and each protein incubated with bacterially expressed and purified GST-Dgp71WD, both individually and in combination, Beads were then washed extensively and blotted with antibodies to detect either the 6xHis tag or the GST tag (Fig. 5.5). His-GFP was included as a control and did not bind to GST-Dgp71WD. GST alone was also included as a control and His-tagged Dgt3^N, Dgt5^N, and Dgt6^C minimally interact with this tag. However, all three Augmin subunits clearly interacted with GST-Dgp-WD (Fig. 5.5C). Some His-Dgt3^N was seen associated with GST-Dgp71WD when incubated alone, but much more was present when it was co-incubated with His-Dgt5^N. Whether this is due to these two regions forming a hetero-dimeric parallel coiled-coil or because His-Dgt3^N binds to His-Dgt5^N when incubated in combination is not
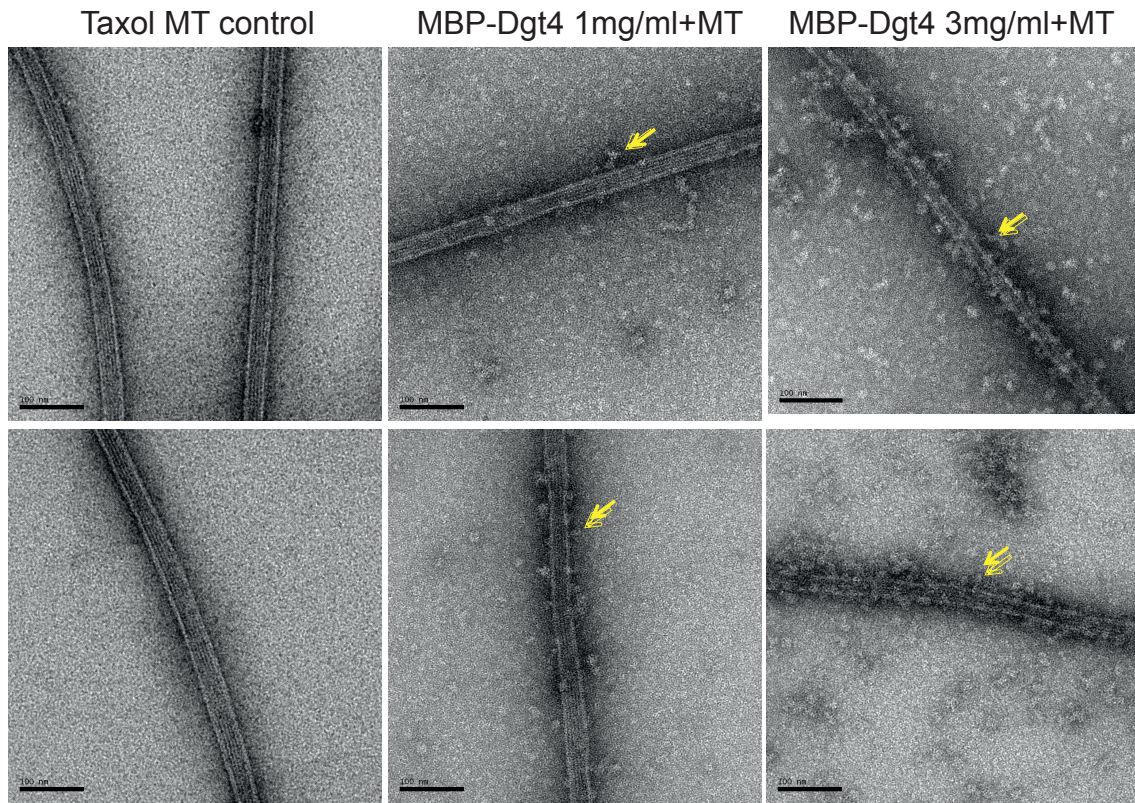
Figure 5.4- Dgt4 binds directly to MTs.

Transmission electron microscopy of negatively-stained MTs alone or pre-incubated with two concentrations of MBP-Dgt4. Dense masses could be seen binding to MTs in the presence of MBP-Dgt4 (yellow arrows). These dense masses on MTs increase in number at ioncrease concentrations of MBP-Dgt4. The data in this figure was generated by Dr Carolyn Moores (Birkbeck University).
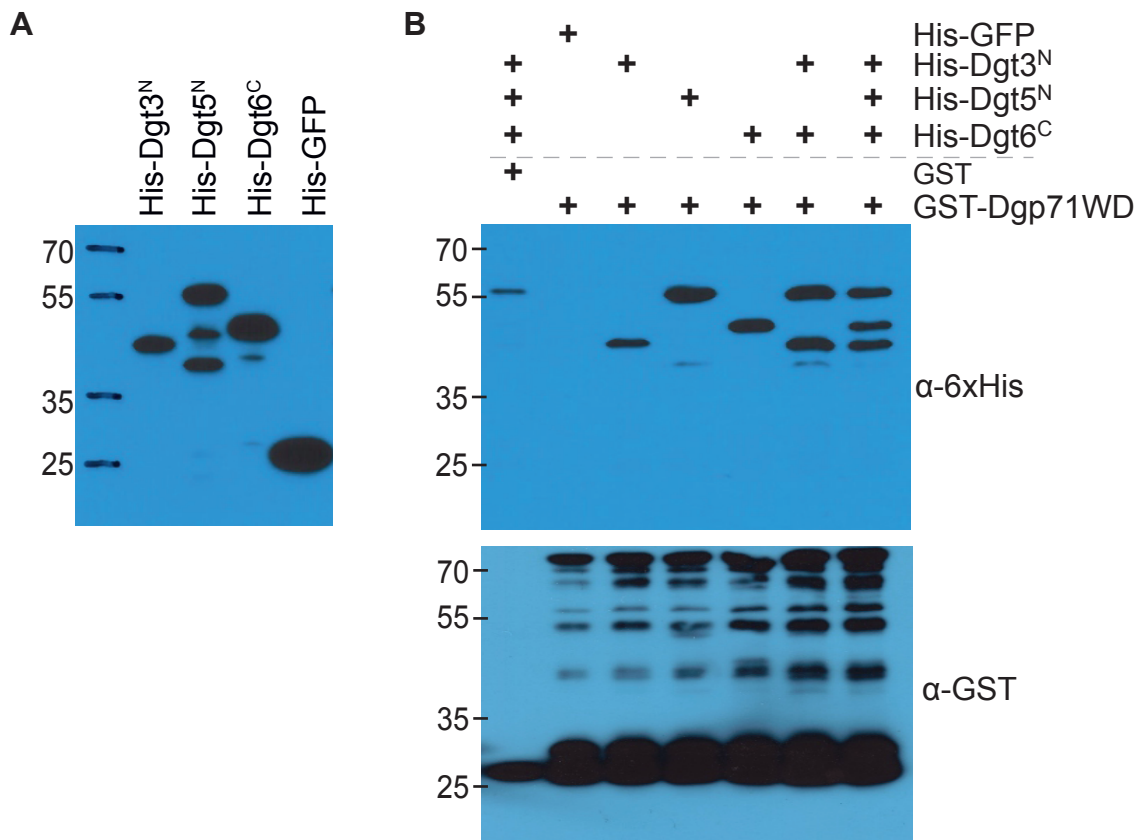
Figure 5.5- In vitro interactions between Augmin subunits and the γ-TuRC subunit Dgp71WD.

(A) Western blot with anti-6xHis showing the molecular weights of His-Dgt3^N, His-Dgt5^N, His-Dgt6^C and His-GFP. (B) GST pull-down of truncated Augmin subunits by Dgp71WD. Purified GST or GST-Dgp71WD covalently bound to glutathione beads were incubated with His-Dgt3^N, His-Dgt5^N, His-Dgt6^C and His-GFP, singly and in combination. Beads were washed extensively and subjected to Western blotting with either anti-His or anti-GST. His-Dgt6^C associates very weakly with GST alone. His-Dgt5^N and His-Dgt6^C associate strongly with GST-Dgp71WD. His-Dgt3^N associates weakly when alone, but increases its affinity in the presence of His-Dgt5^N. His-GFP provides a negative control and does not associate with either GST or GST-Dgp71WD.

clear. These combined results demonstrate an *in vitro* interaction between Dgp71WD and the Dgt3, Dgt5, and Dgt6 subunits of Augmin.

5.2.4. MBP-Dgt4 causes γ-Tubulin and Augmin mislocalisation.

Having shown that MBP-Dgt4 binds to MTs *in vitro*, it is important to confirm whether this occurs in vivo. To test this, I examined whether MBP-Dgt4 would be able to compete endogenous Augmin off the mitotic spindle *in vivo*. Since Augmin has been shown to recruit γ-TuRC to the spindle (Lawo et al., 2009; Meireles et al., 2009; Uehara et al., 2009; Wainman et al., 2009), this should also result in the inability of γ-TuRC to localise to the spindle. Due to their large size and syncytial nature, pre-cellularised *Drosophila* embryos are an excellent model system in which to inject proteins and monitor their response via time-lapse fluorescence microscopy (Hayward et al., 2014). I therefore injected either MBP or MBP-Dgt4 into early *Drosophila* embryos expressing either γ-Tubulin-GFP (to visualise γ-TuRC localisation) or Msd1-GFP (to visualise Augmin), and monitored their localisation over time.

Injection of MBP had no effect on localisation of either γ-Tubulin-GFP (n=3 embryos) or Msd1-GFP (n=3 embryos) and did not affect mitosis (not shown). Injection of MBP-Dgt4 had no effect on either γ-Tubulin-GFP (n=2 embryos) or Msd1-GFP (n=2 embryos) localisation during the first round of mitosis post-injection, indicating that the injection process itself did not impair natural embryo function. However, during the second round of mitosis after injection, initial spindle localisation of γ-Tubulin-GFP was only detected in areas distant to the injection site (Fig 5.6, red arrow), and gradually decreased in intensity (Fig 5.6, yellow arrow)

(n=25 spindles). The centrosomal localisation of γ-Tubulin-GFP was unaffected, which matches published data showing that Augmin disruption does not affect γ-Tubulin population at the centrosome (Lawo et al., 2009; Meireles et al., 2009; Uehara et al., 2009; Wainman et al., 2009) (Movie 5.1 found in electronic appendix folder Chapter 5). Similarly, although the localisation of Msd1-GFP (Fig. 5.7) was unaffected in the first round of mitosis post injection, its prevalence on the mitotic spindle localisation in the second round of mitosis was affected (Fig. 5.7, red arrow) (n=52 spindles). The localisation of Msd1 after injection of MBP-Dgt4 recapitulates that seen in an Augmin null mutant, which have long weak spindles constituted primarily of MTs restricted to the spindle equator (Fig. 5.7, yellow arrow), and which arrest prior to anaphase. Interestingly, however, injection of MBP-Dgt4 had no effect on centrosomal Msd1-GFP accumulation (movie 5.2 found in electronic appendix folder Chapter 5).
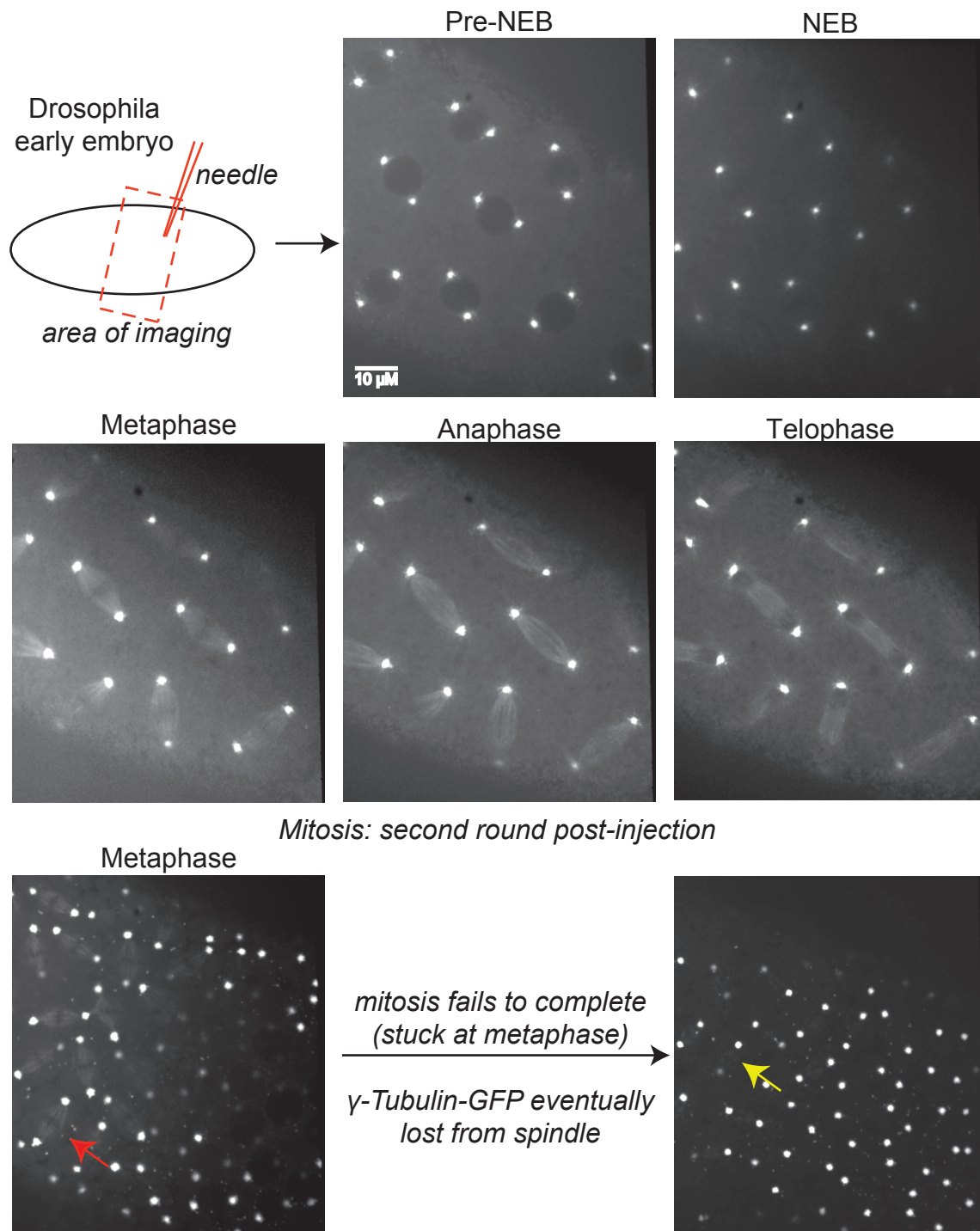
Figure 5.6- MBP-Dgt4 microinjection into γ-Tubulin-GFP embryos.
Purified MBP-Dgt4 was injected into Drosophila early embryos expressing γ-Tubulin-GFP to visualise the mitotic spindle. After injection, rounds of mitosis were observed, with each round beginning with Nuclear Envelope Breakdown (NEB). During the first round of mitosis post injection, mitosis is normal. γ-Tubulin-GFP localises to the centrosome in all stages, but begins to localise to the mitotic spindle at the onset of Metaphase, where it can be seen until mitosis completes. During the second round of mitosis, however, the effects of MBP-Dgt4 injection can be observed. Localisation of γ-Tubulin-GFP to the spindle (red arrow) can only be detected in areas distant from the injection site. Mitosis never completes, and eventually the spindle localisation of γ-Tubulin-GFP disappears (yellow arrow marks the centre of a centrosome pair). Scale bar applies to all images.
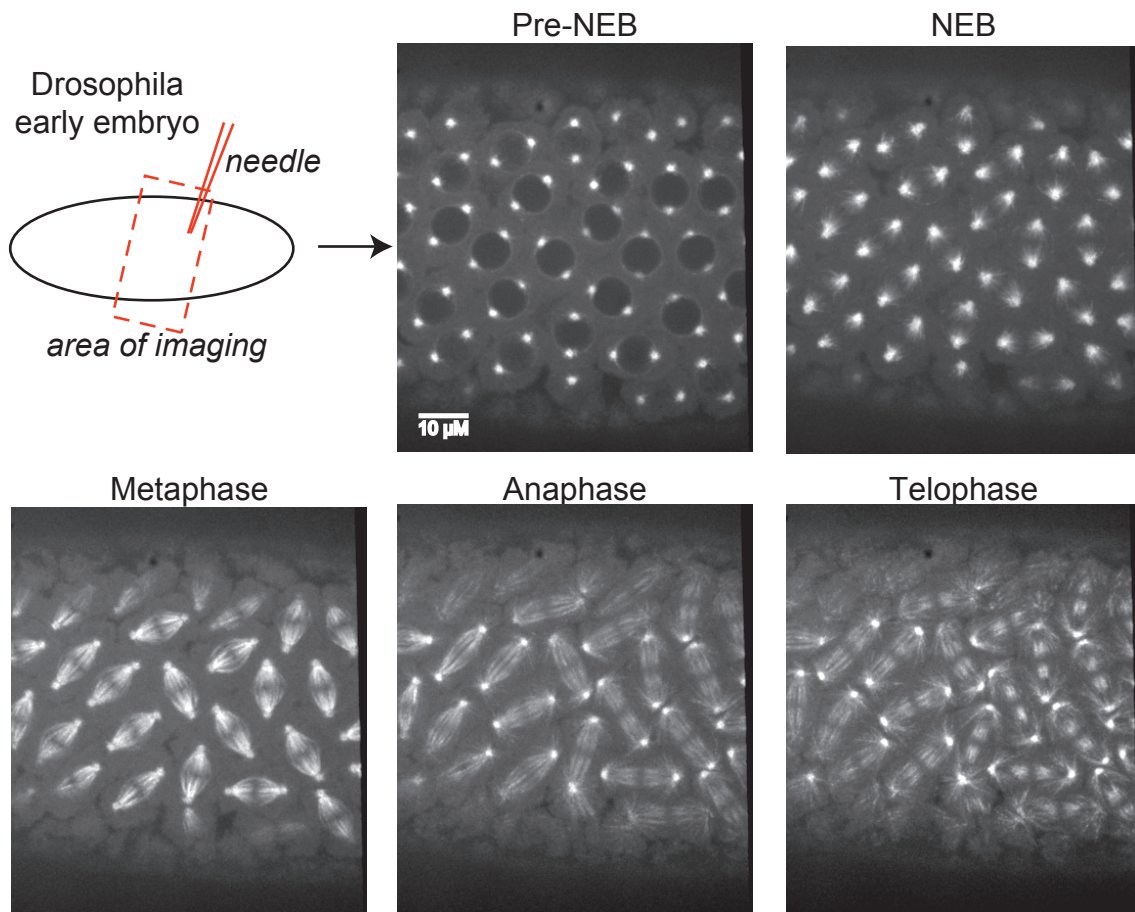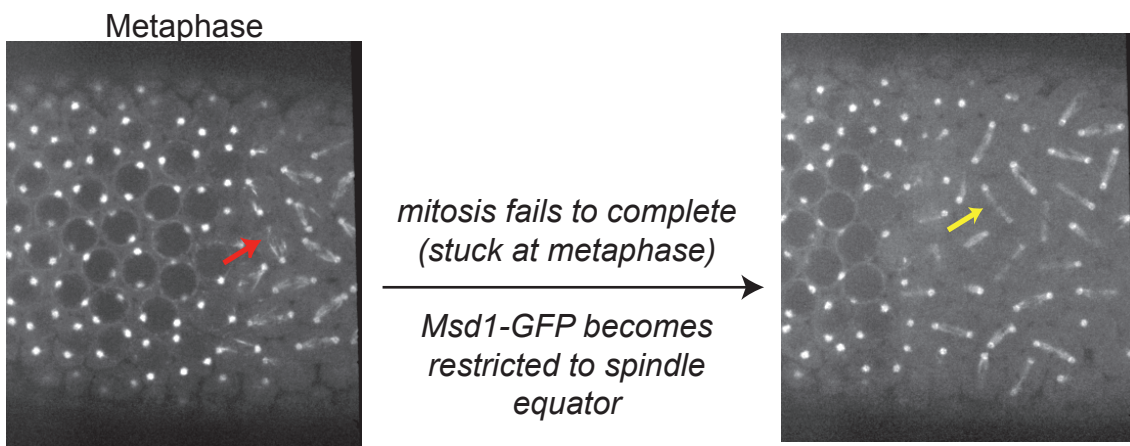
Figure 5.7- MBP-Dgt4 microinjection into Msd1-GFP embryos.
Purified MBP-Dgt4 was injected into Drosophila early embryos expressing Msd1-GFP to visualise Augmin. After injection, rounds of mitosis were observed, with each round beginning with Nuclear Envelope Breakdown (NEB). During the first round of mitosis post injection, mitosis is normal. Msd1-GFP localises to the centrosome in all stages, but begins to localise to the mitotic spindle at the onset of Metaphase, where it can be seen until mitosis completes. During the second round of mitosis, however, the effects of MBP-Dgt4 injection can be observed. Localisation of Msd1-GFP to the spindle (red arrow) is reduced. Mitosis never completes, and over time Msd1-GFP localisation becomes restricted to the spindle equator. Scale bar applies to all images.

5.3. Discussion

Augmin has been characterised as a template dependent MT nucleator through the recruitment of γ-TuRC to pre-existing MTs (Zhu et al., 2008). However, due to the difficulties of purifying the Augmin complex in sufficient quantity and purity, traditional means for discerning its structure, such as x-ray crystallography, are not feasible at the present time. Here, I took an alternative approach - Affinity Purification Crosslinking Mass Spectrometry (AP CLMS). CLMS has generally been used to verify structural information about protein complexes already characterised with crystal structures (Boal et al., 2006; Chen et al., 2010; Denison and Kodadek, 2004; Rappsilber, 2011). However, I have used the simplicity and the power of this approach to discern structural data of Augmin in the absence of any other information.

Prior to crosslinking, 2.5% of the sample was analysed by mass spectrometry. The protein abundance index for all Augmin subunits was approximately equal, aside from Msd1, which was present at approximately 3 times more than any other subunits. Although gel-filtration data (Chapter 3, Section 3.6) as well as sucrose gradient data (Goshima et al., 2008) suggests that the Augmin complex is be composed of subunits in a 1:1 ratio, to date, there is no direct evidence to confirm this. My data confirms that the 1:1 ratio is likely to be the case for all subunits except for Msd1. However, since the embryos used for the purification exogenously express Msd1, and Msd1 may oligomerise naturally (Chapter 5.2.3), the increased abundance of this protein detected in the GFP-IP by mass spectrometry may be an artefact of Msd1-GFP overexpression.

Crosslink mass spectrometry revealed insights into the topology of the Augmin complex, outlining the interacting subunits. It is important to note that since BS3 mostly crosslinks the primary amine group on lysine residues, and there are no lysine residues present in the region previously identified as required for the interaction of Wac and Dgt2 (Meireles et al., 2009), no crosslinks were detected within that region. However, the crosslinks identified between these two proteins are near to this region. Thus, crosslink residues do not equate to critical amino acids for interaction, but rather, give us hints as to approximate regions of protein-protein interaction. Encouragingly, despite the possible caveat of crosslinking reaction occurring between non-interacting proteins, it should be noted that although there were many additional, non-Augmin contaminating proteins identified from the GFP-IP, crosslinked peptides were only identified within Augmin subunits.

Most of the components of the Augmin complex are capable of being crosslinked with other subunits using BS3 (which has a theoretical crosslinking limit of 25Å), which leaves only limited interfaces available for interactions with non-Augmin proteins. As such, a few regions stood out as of potential interest. Using a 1% FDR on the CLMS data, the N terminal half of Dgt3 and Dgt5 and the C terminal half of Dgt6 failed to identify any other intra-Augmin crosslinks. Studies in human cell lines has demonstrated a direct interaction between the C-terminal half of hDgt6 and the the γ-TuRC subunit Nedd1/GCP-WD (Uehara et al., 2009), which contains a WD40-repeat-containg domain and therefore may form a β-propellor structure. In addition, it has been shown that coiled-coiled regions such as that found at the N-termini Dgt3 and Dgt5 can interact with β-propeller proteins (Wall et al., 1995). Together, this led me to hypothesise that one or more of these interfaces (Dgt3[N],

Dgt5[N] or Dgt6[c]) could act to link *Drosophila* Augmin to the *Drosophila* GCP-WD homologue, Dgp71WD.

Dgt3[N] and Dgt5[N] showed multiple parallel crosslinks, which also suggested they may form a heterodimeric coiled-coil in vivo. Although structural predictions by my collaborator Kacper Rogala (Charlotte Deane lab, Dept of Statistics, University of Oxford) indicated a strong likelihood that Dgt3 and Dgt5 would form parallel heterodimeric coiled-coils, they were statistically more likely to form homodimeric coiled-coils. In support of this, initial CLMS of a bacterially expressed and purified Dgt3/5/6/Dgp71WD complex failed to identify any Dgt3-Dgt5 cross linkages (data not shown). This could be due to the nature of the expression of each subunit in bacteria- i.e. that individual expression of Dgt3 or Dgt5 preferentially results in a strong homodimer formation that cannot be disrupted when the two purified proteins are added together. Clearly more work is required to fully understand the relationship between Dgt3 and Dgt5. Currently, attempt are being made at reconstituting a Dgt3/Dgt5 heterodimer through purifying the proteins in denaturing/ renaturing condition.

In contrast, there was a major discrepancy in inter-protein linkages for the C terminus of Dgt6 between using a 1% FDR, where no inter-protein linkages was identified, and the Target-Decoy method with a 5% FDR, where many inter-protein linkages were identified. *De novo* structural predictions carried out by Kacper Rogala (Charlotte Deane lab, Dept of Statistics, University of Oxford) suggested the C-terminus of Dgt6 to be without a distinct structure. Since the crosslinker BS3 reacts with lysines, it is possible the Dgt6[C], without a rigid structure, comes into contact with other parts of Augmin, albeit rarely, where crosslinks occur. The

difference between stringencies may therefore reflect more the flexibility of this region, rather than stable protein-protein interactions within Augmin *per se*. My hypothesis is consistent with the *in vitro* analysis; a GST-Dgp71WD pull-down assay demonstrated that Dgt3[N], Dgt5[N], and Dgt6[C] interact with Dgp71WD independently, and that all three Augmin subunits act together as an interface for Dgp71WD interaction. The interaction between Dgt6[C] ad Dgp71WD is consistent with interaction with human proteins, suggesting the functional groups identified with CLMS is conserved between humans and *Drosophila*.

As Augmin is proposed to function as a linker between the γ-TuRC and MTs, I also investigated potential subunits of the Augmin complex that might interface with MTs. Given the CLMS restrictions and the data above, two such MT-interacting regions seemed possible- Dgt4 and the N terminus of Wac. A role for Dgt4 is supported by a published study in human cell lines, where hDgt4 has been shown to directly bind to MTs (Wu et al., 2008). However, unlike the human protein, *Drosophila* Dgt4 does not have an identified MT binding domain. Interestingly, MT co-sedimentation assays revealed that bacterially expressed and purified Dgt4 and Wac both can bind MTs directly. Moreover, it is important to note that even in the absence of Taxol to stabilise MTs and prevent depolymerisation, both Tubulin and Wac are present in the pellet fraction, suggesting that Wac is able to stabilise MTs *in vitro*. This is in agreement with the results shown in Chapter 3 (Section 3.3.7), where the addition of purified Augmin complex to Tubulin resulted in the presence of long MTs (Fig. 3.7D,E). The ability of Dgt4 to bind to MTs is further supported by a preliminary EM study (Fig. 5.4), although the affinity between Dgt4 and MTs was concentration dependent.

If the *in vitro* binding capabilities of these Augmin domains are indicative of their *in vivo* functions, one might expect excess Dgt3[N], Dgt5[N] and Dgt6[C] to competitively inhibit the binding Augmin to the γ-TuRC, and excess Dgt4 and Wac[N] to inhibit the binding of Augmin (and therefore the γ-TuRC) to MTs. This was investigated by microinjection of Dgt4 into pre-cellularised *Drosophila* embryos. As might be expected, the consequences of injecting Dgt4 into embryos were not seen until after the first round of mitosis had been completed. This phenomenon has been reported for certain interfering antibodies (e.g. anti-Spd2;(Hayward et al., 2014)), and probably reflects a cell-cycle regulated interaction between Augmin and MTs such that the excess, free Dgt4 only has access to MTs following one mitosis. Upon entry into the second round of mitosis following injection, γ-Tubulin-GFP no longer localises to the spindle, while Msd1-GFP only localises to the centrosomes and to a region of the spindle at the equator. Whether the results from the Dgt4 injection actually reflects an inability of Msd1-GFP/Augmin to bind to a population of MTs in the presence of excess Dgt4, or whether this reflects a change in the shape of the mitotic spindle would need to be addressed by injecting Dgt4 into tubulin-GFP embryos, since it is possible injection of MBP-Dgt4 disrupted endogenous Augmin as a whole, instead of MBP-Dgt4 competing with Augmin for the MT binding sites.

In summary, the work presented in this Chapter provides novel insights into the structural relationship between the various Augmin subunits and their relationship to function. In doing so, it demonstrates the power of CLMS as a tool with which to provide testable hypotheses regarding the cellular function of protein complexes, expanding the base of CLMS from being a member of integrated structural biology

(Chen et al., 2010; Lasker et al., 2012) to a structure investigation method in its own right. The work suggests that a core of Augmin subunit interactions result in two major free interfaces. One, comprising Dgt4 and Wac, presents multiple MT-associating domains to pre-existing MTs, while the second, comprising Dgt3, Dgt5, and Dgt6, present multiple Dgp71WD-binding interfaces. The spatial distinction between the two, represented in cartoon form in Fig. 5.8, will ensure new MTs grow with a consistent polarity and branch angle from mother MTs and provide a molecular basis for the preservation of MT polarity that has been reported (Petry et al., 2013). Moreover, the multiplicity of interfaces serves to ensure a high likelihood of new MTs being generated.
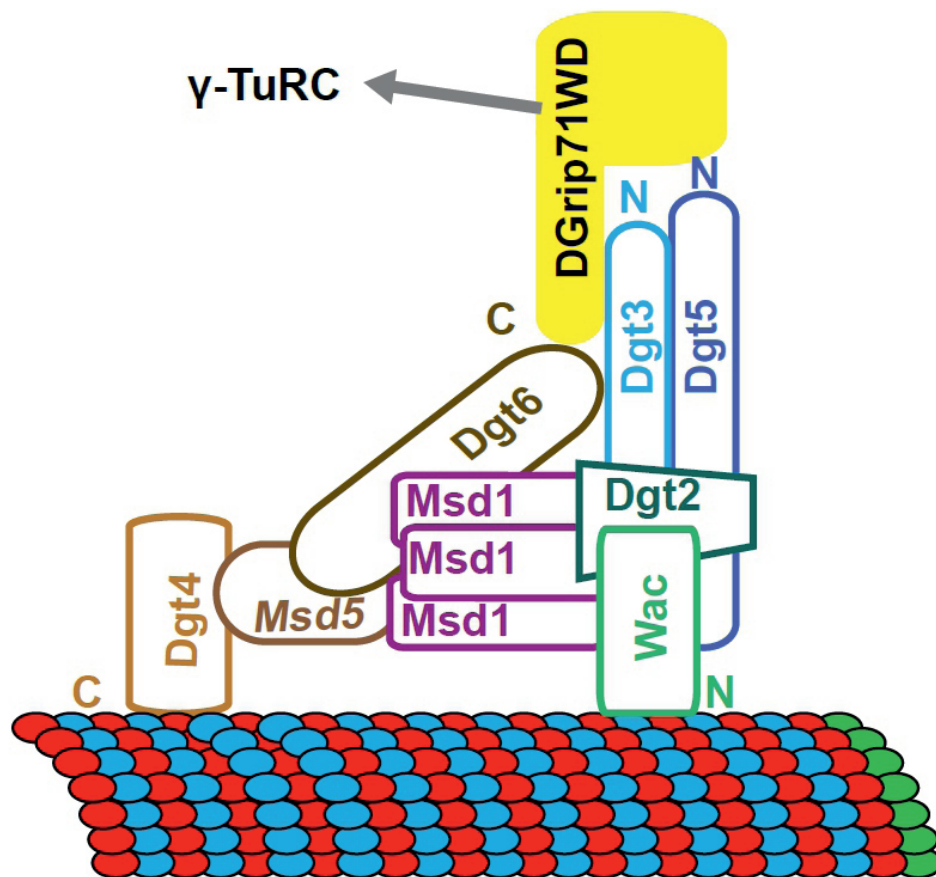
Figure 5.8- A model of the Augmin complex in relation to MTs and γ-TuRC

A cartoon of Augmin binding to MTs and to γ-TuRC, based on the results shown in this chapter. Dgt4 and Wac are the MT binding subunits, while Dgt3, Dgt5, and Dgt6 interact with the γ-TuRC subunit Dgp-WD. Augmin consists of 1 copy of each subunit with the exception of Msd1, which may be present in 3 copies. The spatial differntiation between the MT binding region and the γ-TuRC binding region accounts for the preservation of MT polarity previous reported (Petry et al 2013).

6. The role of Augmin in Oogenesis

6.1. Preface

A significant proportion of the work done in this chapter was done with the help of Dr. Tse-Bin Chou and his lab in National Taiwan University (Taipei, Taiwan). I thank Dr. Tse-Bin Chou and his staff for the many reagents, space, and expertise were also provided during of my visit to his laboratory.

6.2. Introduction

6.2.1. Developmental stages during oogenesis in Drosophila: oocyte specification and maturation

Oogenesis, the process by which a *Drosophila* female produces eggs, occurs in the ovary. *Drosophila* ovaries consists of approximately 16 elongated chambers called ovarioles, with the germarium at the anterior of the ovariole and the oviduct at the posterior (Cummings and King, 1969). To produce a mature egg, capable of being fertilised, a germline stem cell located at the anterior end of the germarium undergoes an asymmetric division to produce a cystoblast cell and a self-renewed germline stem cell (Lin and Spradling, 1993). The cystoblast then undergoes four rounds of cell division with incomplete cytokinesis to form 16 interconnected cells; the connections between these cells are called ring canals (Gabriel and Fogel, 1955; Robinson et al., 1994) and function to allow intercellular transport of materials between cells of the cyst (Ledbetter and Porter, 1964; Nicolas et al., 2009). Each cell varies in the number of ring canals it possesses; two cells contain 4 ring canals, while the others have less (Theurkauf, 1994). The centrioles of these 16 cells migrate towards one of the two cells which contain 4 ring canals, where

142

they generate a MT network extending through the ring canals and connecting the 16 cells (Megraw and Kaufman, 2000). This polarised cytoskeleton allows dynein, a minus-end directed MT motor (MacDougall et al., 2003) to transport maternal cues which trigger one cell to differentiate into an oocyte. Both cells with 4 ring canals enter meiosis I, but specification of oocyte cell fate is driven only in the cell containing the accumulated centrioles (Huynh and St Johnston, 2000). The other cell exits meiosis and, along with the remaining 14 cells, differentiates to become nurse cells (Deng and Lin, 2001). These continue DNA replication and manufacture almost all cell content for the oocyte, such as ribosomes, mRNAs, proteins, and cytoplasm (Cummings and King, 1969). In constrast, the oocyte remains arrested at prophase I (Mandelkow and Mandelkow, 1995).

The developing egg is then enveloped by follicle cells, a monolayer of mesoderm from the maternal germarium (Cummings and King, 1969). Two sets of uncommitted polar cells reside at each end of the egg chamber, which are later responsible for setting up the anterior-posterior axis. The polar cells and the oocyte express high levels of E-cadherin, a transmembrane protein involved in cell adhesion, allowing the oocyte to be positioned against one set of these polar cells (Vaughan et al., 2006). At this point, the developing egg is termed an egg chamber, and will undergo 14 distinct stages of development in order to reach maturity (Fig. 6.1). At stage 1, the egg chamber resides in the posterior end of the germarium. At stage 2 of development, the egg chamber is pinched off from the germarium, and begins to travel towards the oviduct. Between stage 1 and stage 6, the nurse cells undergo 4 rounds of DNA duplication, resulting in them having 64 chromosomes by stage 6. During these stages, the follicle cells undergo mitosis to
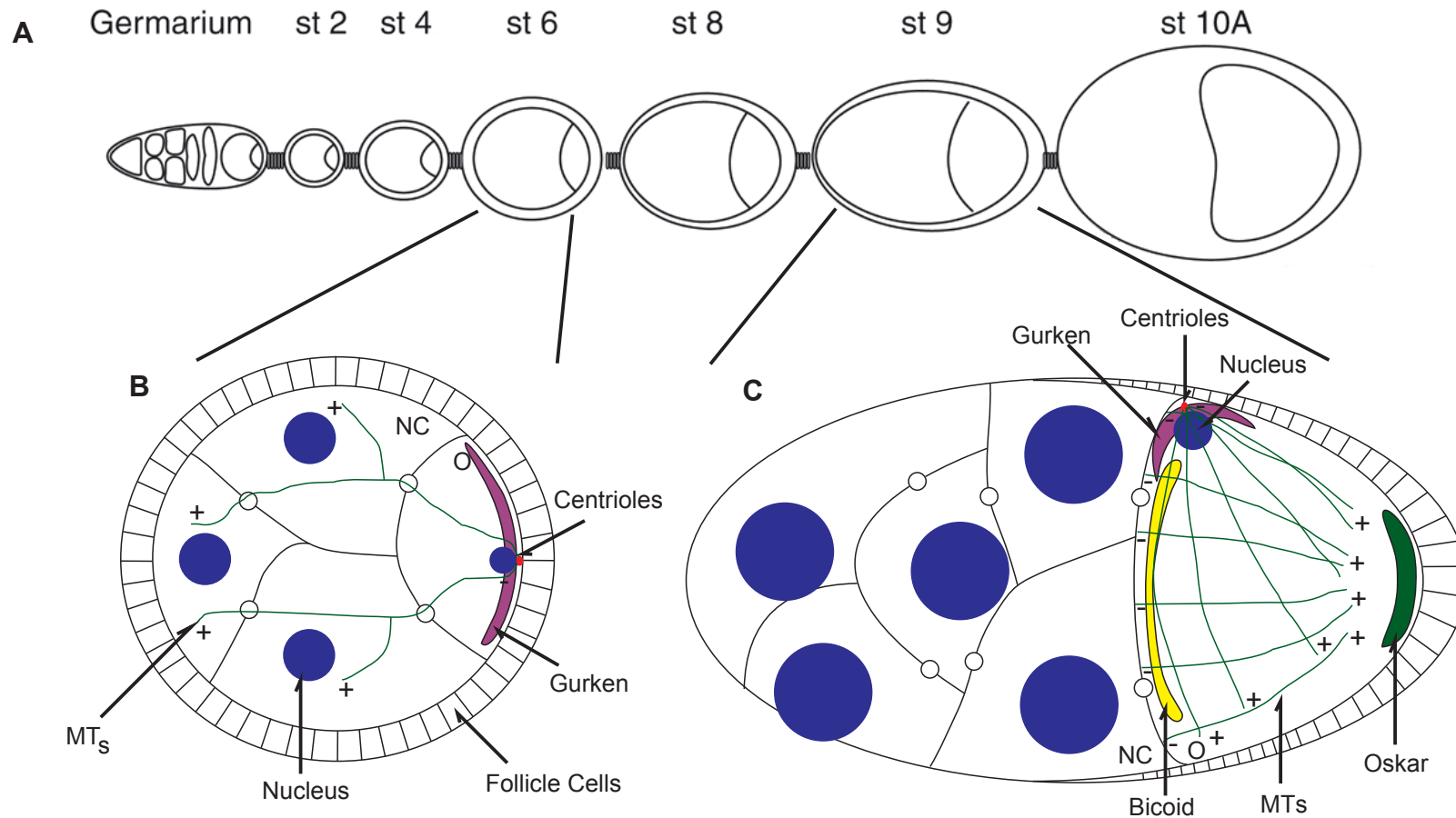
Figure 6.1- General description of Drosophila oogenesis.
Drosophila oogenesis begins in the germarium at the anterior of the ovary, and the oocyte migrates posteriorly along the ovariole as it matures, such that at maturation it reaches the uterus. (A) Schematic of a rough morphological appearanceof the oocyte at various stages of maturation. (B) At stage 6, the oocyte consists of 15 nurse cells and the oocyte, connected via cytoplasmic bridges called ring canals. MTs are nucleated from a number of centrioles, all which are located behind the oocyte nucleus. These MTs connect the 15 nurse cells and the oocyte via ring canals, allowing intercellular transport. At this stage, Gurken localises to the posterior cortex. (C) At stage 9, the nucleus and centrioles have migrated to the anterior dorsal corner. MTs are nucleated from these centrioles and from the anterior cortex, and serve to transport protein & RNA between cells and within the oocyte itself.. Maternal mRNA bicoid, oskar, and gurken can be observed at specific locations within the oocyte.
Figure 1a taken from Roth & Lynch (2009).

maintain coverage of the egg chamber (from 80 to 1200 cells). As development progresses, the egg chamber travels progressively toward the oviduct, entering the oviduct after stage 14 (Fig. 6.1).

6.2.2. Developmental stages during oogenesis in Drosophila: polarity specification

Polarisation of the egg chamber and the oocyte is essential for determining the overall polarity of the developing embryo, through the specification of the anterior:posterior and dorsal:ventral axes (Vaughan et al., 2006). This is achieved by localising three main mRNAs, *gurken*, *oskar* and *bicoid*, to specific locations within the oocyte at specific points of oogenesis; a process at least partly driven by the MT cytoskeleton (MacDougall et al., 2003; Mandelkow and Mandelkow, 1995; Robinson et al., 1994; Sung et al., 2008; Theurkauf et al., 1992).

During early to mid-oogenesis, *gurken* mRNA is transcribed in both the nurse cells and oocyte (Gabriel and Fogel, 1955), and is translated and secreted into the oocyte-follicle cell junction adjacent to the oocyte nucleus. From stages 2 to 6, the oocyte MT cytoskeleton drives the enrichment of *gurken* mRNA at the posterior cortex where the oocyte nucleus resides. The MTs are polarised, with their minus ends at the centriole-enriched oocyte posterior. Since *gurken* mRNA associates with the minus-end directed MT motor protein, dynein, it is thus transported to the posterior pole. Gurken is a Transforming Growth Factor-α-like protein that binds to the transmembrane protein Torpedo, the *Drosophila* homologue of the Epidermal Growth Factor Receptor (González-Reyes et al., 1995). Upon binding, Gurken signals the follicle cells to adopt a posterior cell fate (González-Reyes et al., 1995).

At stage 6, the follicle cells send an unknown signal back to the oocyte, triggering egg chamber elongation and MT reorganization. This reorganisation event triggers the onset of nuclear migration (Ledbetter and Porter, 1964). At the same time, the oocyte nucleus migrates from the posterior pole to the anterior dorsal corner. Centrioles have been implicated in the nuclear migration process, as centrioles have been shown to push the nucleus with growing MTs (Vaughan et al., 2006). However, other unknown redundant machineries are involved, since egg chambers lacking centrioles do not fail to position the nucleus correctly (Vaughan et al., 2006).

By stage 8, the MTs have fully re-organised, being nucleated from both the centrioles and the anterior cortex, creating an anterior to posterior MT density gradient. Again, the mechanisms generating the MTs from the cortex are unclear, as oocytes without centrioles build a robust MT network with an anterior-posterior gradient (Stevens et al., 2007).

During stages 8 to 10b, Gurken once again activates Torpedo, but this time at the anterior-dorsal corner. This triggers the repression of Pipe protein, causing these follicle cells to adopt a different cell fate, setting up the dorsal-ventral axis (Maccioni and Cambiazo, 1995; Zhu et al., 2005). At the same time, *oskar* mRNA is transported along the polarised MT bundles that develop at stage 10a via the plus-end directed motor kinesin-1 to the posterior of the oocyte. In contrast, *bicoid* mRNA is transported via dynein to the anterior cortex.

At stage 10a, the MT cytoskeleton undergoes its second re-organisation, and bundles of MTs form around the oocyte cortex. This process is not well understood but appears to be related to centriole independent mechanisms (Murphy and Borisy, 1975; Theurkauf, 1994). At stage 10b, these MT bundles begin to facilitate

ooplasmic streaming (Cooley and Theurkauf, 1994), the dynamic process by which the cytoplasm of the oocyte and the nurse cells is rapidly mixed (Cooley and Theurkauf, 1994). By stage 11, nurse cells began rapidly expelling their cell content (RNA, ribosomes, proteins, cytoplasms, etc.) into the oocyte, assisted by the ooplasmic streaming (Cooley and Theurkauf, 1994). The result is a shrinkage of the nurse cells and a concomitant increase in oocyte volume.

From stage 12-13, the oocyte continues to mature. The nurse cells undergo apoptosis, and are sloughed off. The oocyte reaches maturity at stage 14, when the oocyte nucleus exits prophase I and enters metaphase. It arrests at metaphase I, however, until it reaches the uterus in preparation for fertilisation. At stage 14, *bicoid* and *nanos* mRNA are translated at the anterior and posterior pole respectively. The diffusion gradient of these two proteins then sets up the signals required for the early developmental patterning of the *Drosophila* embryo.

6.2.3. Microtubule nucleation in the Drosophila egg chamber

Although centrioles are implicated in MT generation throughout oogenesis as described above, they are dispensable (Stevens et al., 2007). Stage 9 oocytes without centrioles build a robust MT network with an anterior-posterior gradient and transport of *gurken, oskar,* and *bicoid* mRNA is unaffected (Stevens et al., 2007). Centrioles have been implicated in the nuclear movement that occurs at stage 7 (Vaughan et al., 2006), but oocytes lacking centrioles migrate to the anterior-dorsal corner by stage 8 (Stevens et al., 2007; Vaughan et al., 2006). Therefore, currently, very little is known about the origin of the MTs that are nucleated during mid-oogenesis.

γ-TuRC has been implicated in MT nucleation (Moritz et al., 2000; Moritz et al., 1995; Oegema et al., 1999; Zheng et al., 1995). During mid-oogenesis, γ-Tubulin localises to the oocyte cortex (Maccioni and Cambiazo, 1995; Murphy and Borisy, 1975), where MTs are seen to originate from (Maccioni and Cambiazo, 1995; Parton et al., 2011), and thus, γ-TuRC is presumed to play an important role in MT assembly during mid-oogenesis. However, it has not been possible to tease out the specific roles γ-TuRC plays in oogenesis MT organisation, since flies lacking γ-Tubulin develop agametic ovaries, and fail to produce egg chambers (Tavosanis and Gonzalez, 2003). This is presumably due to the essential nature of γ-Tubulin during female meiosis I (Hughes et al., 2011).

Since γ-Tubulin recruitment to the centrosomes and mitotic spindle depends on Cnn and Augmin during mitosis (Megraw and Kaufman, 2000), it is possible that Cnn and Augmin may have functional relationships with γ-TuRC during oogenesis for MT organisation. Indeed, Cnn also localises to the oocyte cortex during mid-oogenesis (Megraw and Kaufman, 2000). However, the relationships between γ-Tubulin, Augmin and Cnn in the *Drosophila* oocyte have not been systematically addressed.

In this chapter, I show the importance of Augmin and Cnn in MT generation and maintenance during *Drosophila* oogenesis. I also provide evidence which suggests that Augmin localises to the anterior cortex during mid-oogenesis, similar to Cnn. Using both *wacΔ12* (shown to be *augmin*-null) (Meireles et al., 2009) and a severely hypomorphic *cnn* mutant, I show that, while Oskar protein localization is unaffected, the localisation of Gurken protein is mildly perturbed. In addition, I demonstrate Cnn localization is disrupted in *augmin* mutant oocytes. Together, this

work suggests a role for both Cnn and Augmin in regulating MT generation outside of mitosis.

6.3. Results

6.3.1. Augmin subunits are present in the egg chamber

To investigate if members of the Augmin complex were present in *Drosophila* egg chambers, and if so, where they localised, WT ovaries were fixed with formaldehyde, and stained with antibodies to the Augmin subunit Dgt6. At the anterior end of the germarium, fluorescence could be detected in a bipolar spindle pattern (Fig. 6.2A). Judging from the position of the staining, this signal is likely to be from the mitotic divisions of the cystoblast as it forms the 16 cell cystocyst. Since Augmin is known to localise to the spindle during mitosis (Meireles et al., 2009; Wainman et al., 2009), this indicates that the antibody does indeed detect Dgt6. However, Dgt6 staining in stage 1-10b egg chambers showed strong localisation to the oocyte nucleus, with some low-level fluorescence throughout the cytoplasm (Fig. 6.2B). Unexpectedly, Dgt6 localisation to the oocyte nucleus was also present in Augmin-null (*wacΔ12*) mutant egg chambers (Fig. 6.2C). A stage 9 egg chamber for WT and *wacΔ12* has been selected as representation.

To determine if this general diffuse staining and nuclear localisation was due to the Dgt6 antibodies binding non-specifically, or truly reflective of Dgt6 localisation, live egg chambers from flies carrying a Dgt6-GFP transgene were examined. Similarly to the localisation in fixed and stained egg chambers, Dgt6-GFP was found throughout the nurse cell cytoplasm and localised, albeit weakly, to the oocyte

nucleus (Fig 6.2G). In addition, Dgt6-GFP localised to the anterior cortex in the oocyte. To determine whether the localisation was reflective of Augmin in general or specific to Dgt6-GFP, egg chambers expressing either Msd1-GFP or Msd2-GFP were also examined. Msd2-GFP also localised to the anterior cortex of the oocyte but, in contrast to Dgt6, was excluded from the nuclei of nurse cells and the oocyte. Msd1-GFP showed a general cytoplasmic localization in both nurse cells and the oocyte (Fig. 6.2D) and was also observed within ring canals (Fig. 6.2E). Since all 3 subunits have slightly different localisations, this may indicate that each subunit is present in both an unbound form as well as within the Augmin complex, or that the Augmin complex in the egg chamber does not contain all 8 subunits.

6.3.2. Augmin is involved in MT nucleation and maintenance

Augmin has been shown to localize to MTs during mitosis (Meireles et al., 2009; Wainman et al., 2009). Since Msd1-GFP, Msd2-GFP, and Dgt6-GFP did not exhibit MT-like fluorescence within the oocyte, nor did immunofluorescence with anti-Dgt6, I presumed that Augmin either does not associate with MTs during oogenesis or that the levels of association fall below detection limits. However, given that Augmin appears to be present in the oocyte, and the previously demonstrated role for the Augmin complex in generating MTs, I sought to determine whether Augmin is involved in MT nucleation and maintenance during oogenesis. The *wacΔ12* mutant *Drosophila* line possesses a mutation in *wac* in which the start codon, along with the first 12 amino acids of the coding sequence, is removed resulting in a null mutation (Meireles et al., 2009). Previous work in Drosophila S2 cells has demonstrated that removal of one subunit of the complex results in reduced levels
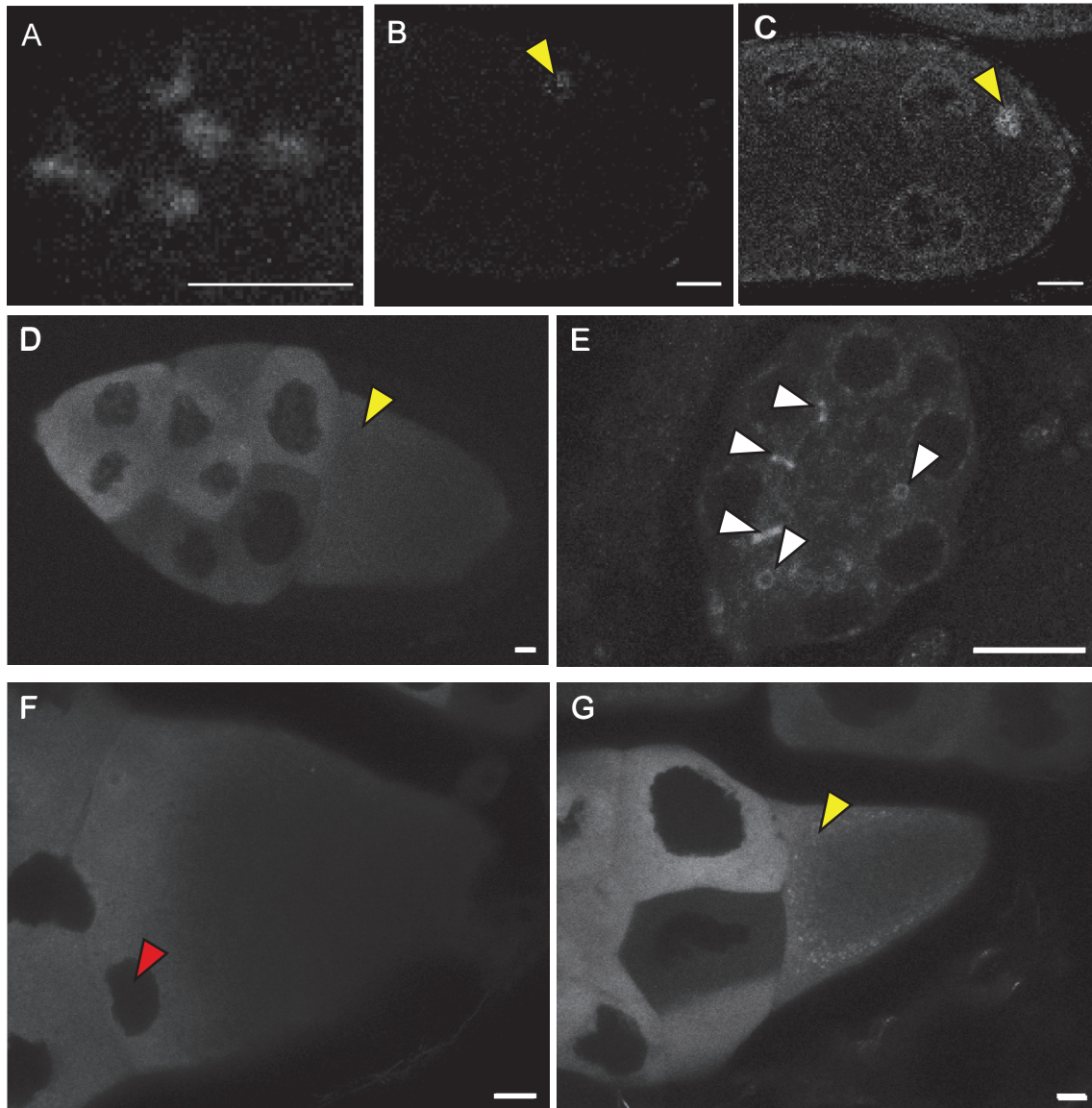
Figure 6.2. Members of the Augmin complex are present in egg chambers.
A-C. Immunofluorescence of Dgt6 localisation. In mitotic cells of the germarium, Dgt6 localizes to the bipolar spindle (A). In the stage 9 egg chamber, Dgt6 localises to the nucleus in the oocyte only (yellow arrow) as well as faintly throughout the cytoplasm (B, C). There was no difference in Dgt6 localization between WT (B) and wacΔ12 (C) egg chambers at stage 9.

D-G. Live imaging of Augmin subunits tagged with GFP. Msd1-GFP is found throughout the cytoplasm of the nurse cells and oocyte, and also localises to the nucleus in the oocyte only (D, yellow arrow). Msd1-GFP was additionally observed in the ring canals (E, white arrows). Msd2-GFP (F), and Dgt6-GFP (G) also localize throughout the cytoplasm of the nurse cells, but appear to form an anterior-to-posterior gradient in the oocyte. Msd2-GFP is excluded from the oocyte nucleus (F, red arrow) while Dgt6 appears to be present in the oocyte nucleus (G, yellow arrow)

Scale bars represent 10μm, except for A (5μm).

of other subunits, presumably through complex instability (Goshima et al., 2008; Meireles et al., 2009). Since Wac is an Augmin subunit, it is presumed the *wacΔ12* mutation is null for Augmin function. Ovaries from WT and *wacΔ12* flies were fixed with formaldehyde, and stained with anti-Tubulin to examine the MT networks at different stages of oogenesis. A robust MT anterior-posterior gradient could be seen in stage 8-9 WT oocytes (Fig. 6.3). By stage 10a, MT bundles could be detected (Fig. 6.3). MT networks were also present in follicle cells. In contrast, MT networks could not be detected in *wacΔ12* stage 8-9 oocytes. However, by stage 10a, *wacΔ12* oocytes had observable MT bundles, indicating recovery of MT networks. *wacΔ12* follicle cells showed no observable MT defects.

To determine whether this apparent difference in MT organisation in *wacΔ12* was dependent upon fixation conditions, I also examined oocytes from flies expressing Tubulin-GFP with or without the *wacΔ12* mutation. In control oocytes, MT networks could be observed in nurse cells, follicle cells, and oocytes. Similar to the fixed and stained egg chambers, WT stage 9 oocytes had a robust MT anterior-posterior gradient (Fig. 6.4). In partial agreement with previous immunofluorescence results, changes in the MT network were observed in *wacΔ12* flies expressing Tubulin-GFP. 66% of *wacΔ12* stage 8 oocytes (n=14) and 46% of stage 9 oocytes (n=28) had a clear anterior-posterior MT gradient. The remaining oocytes had either short MTs, or no observable MTs (Fig. 6.4). Similar observations were made with RFP-Tubulin, suggesting the observed effect was not due to a GFP or C-terminal tagging effect (not shown). Observations could not be done for stage 10a oocytes and beyond, due to the limitations of imaging deep into tissues. In agreement with immunofluorescence results, no obvious MT defects could be seen in follicle cells

or nurse cells. However, mitotic follicle cells in *wacΔ12* possessed bipolar spindles with low MT density as is expected from an Augmin null mutant (Meireles et al., 2009) (Fig. 6.4), indicating that the *wacΔ12* Tubulin-GFP egg chambers do indeed lack Augmin.

Since a proportion of stage 8-9 *wacΔ12* oocytes had no observable MTs, I next examined the dynamics of MT generation using oocytes expressing EB1-GFP. EB1 is a protein that binds to the growing plus-end of MTs and has been successfully used in *Drosophila* oocyte as a marker for MT growth (Parton et al., 2011). EB1-GFP comets were observed in stage 8-9 control (Movie 6.1 found in electronic appendix folder Chapter 6) and *wacΔ12* oocytes (Movie 6.2 found in electronic appendix folder chapter 6). No discernible difference could be observed compared to WT, suggesting that MTs in *wacΔ12* oocytes are being generated, but not maintained.

6.3.3. Gurken protein is mislocalized in wacΔ12 mutants

The consistent MT phenotype observed in *wacΔ12* oocytes during stages 8 and 9 (i.e. oocytes with reduced or no observable MT networks) might be expected to alter the localisation of polarity determinants positioned during these stages. I therefore examined the effect of Augmin loss on Gurken protein localization. WT and *wacΔ12* ovaries were fixed with formaldehyde, and stained with anti-Gurken antibodies. Strong or weak fluorescence intensity was judged by eye. In stage 6 oocytes, Gurken localised to the posterior cortex in 82.4% of WT oocytes (n=34), but only 7.5% of *wacΔ12* oocytes (n=40) (Fig. 6.5). In stage 8-10b, strong fluorescence intensity was observed at the anterior-dorsal corner in WT oocytes
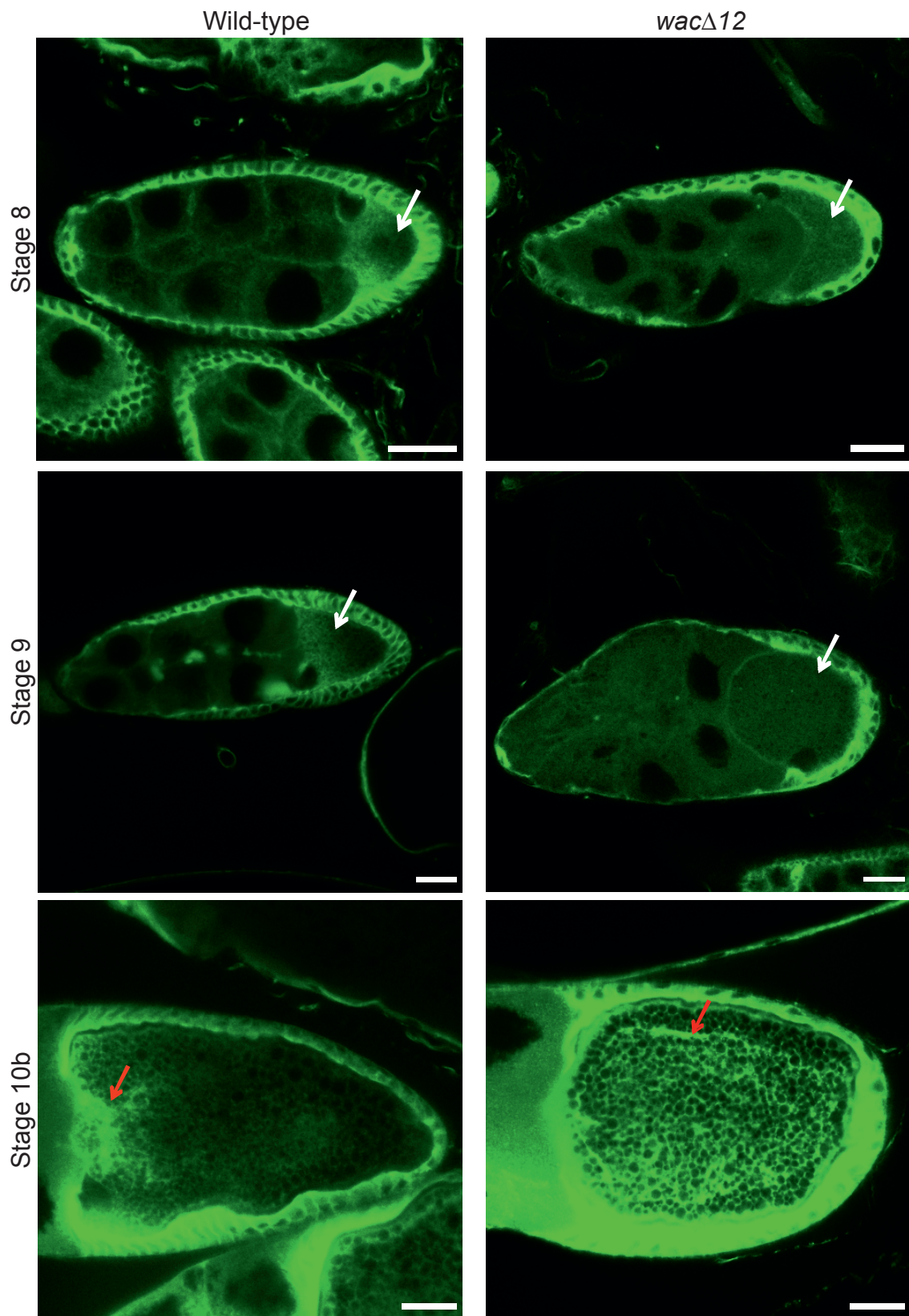
Figure 6.3- Wac△12 oocytes have perturbations in MT organisation.
Immunofluoresence of *Drosophila* egg chambers with anti-tubulin. White arrows indicate the oocyte. In wild-type oocytes, an anterior to posterior gradient of MTs can be seen which is maintained at stages 9 & 10. This MT gradient was lost in wac△12 oocytes. In wild-type oocytes, MT bundles begin to appear at stage 10b, and these are still observed in wac△12 (yellow arrows). Scale bar, 25µm.
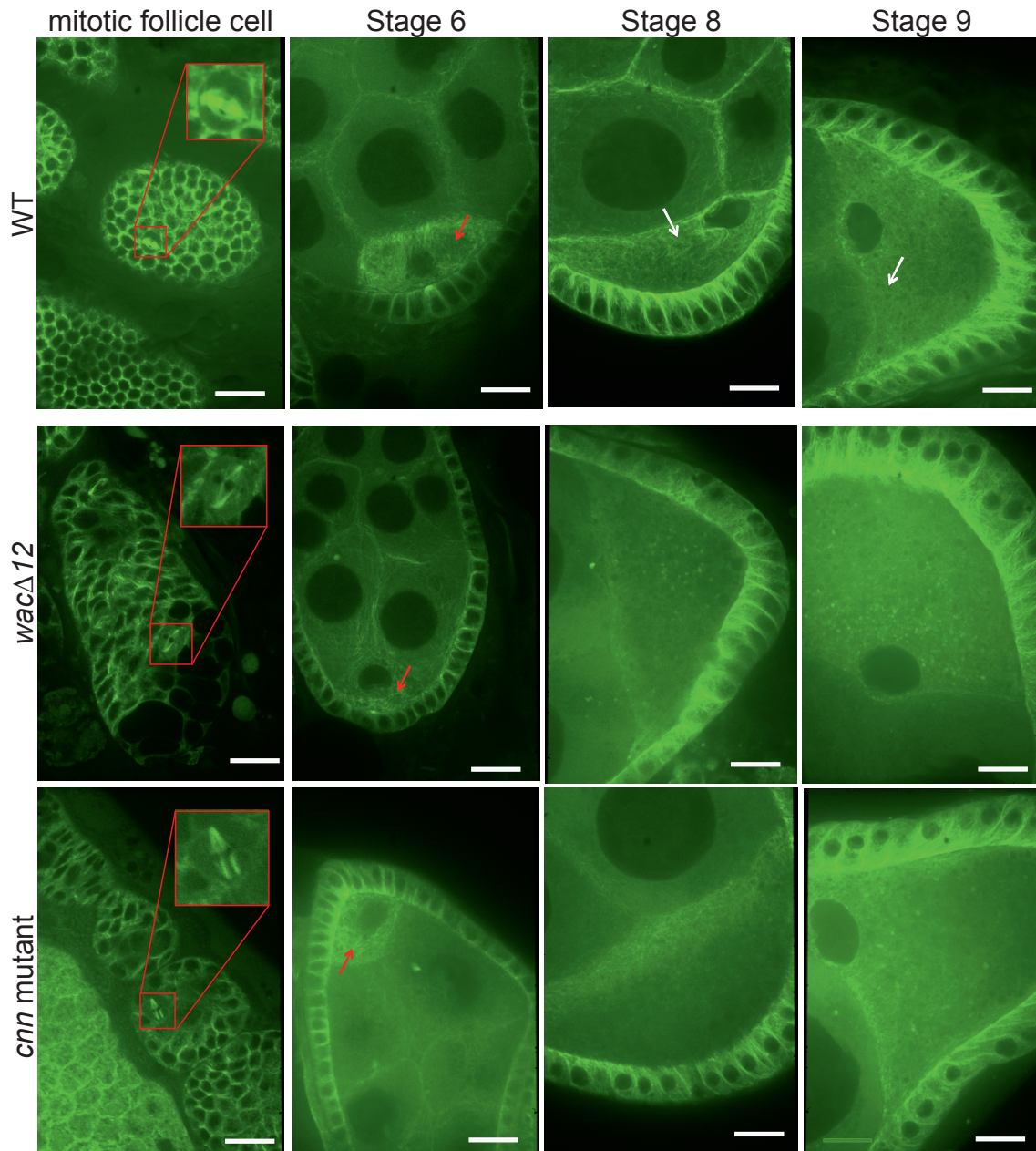
Figure 6.4- MT networks in wacΔ12 and Cnn mutant oocytes.
Live microscopy of wild-type (WT), wacΔ12 and Cnn mutant egg chambers. A robust bipolar spindle with high MT density and focused poles could be seen in WT mitotic follicle cells. wacΔ12 mitotic follicle cells exhibit a classical Augmin phenotype of reduced spindle density, while CnnHK21/Cnn-mfs7 mitotic follicle cells exhibits a classical centrosome mutant phenotype with unfocused poles. At stage 6, oocytes (indicated by red arrows) have a higher density of MTs than the nurse cells. In both wacΔ12 and Cnn mutant oocytes, MT density appears to be comparable to WT. At stages 8 & 9, robust MT networks can be visualised in WT oocytes (white arrows). These MT networks are arranged in an anterior to posterior gradient. However, in both wacΔ12 and Cnn mutant oocytes MTs are shorter and appear less robust. Scale bars, 15μm.

WT   wacΔ12   WT   wacΔ12   WT   wacΔ12
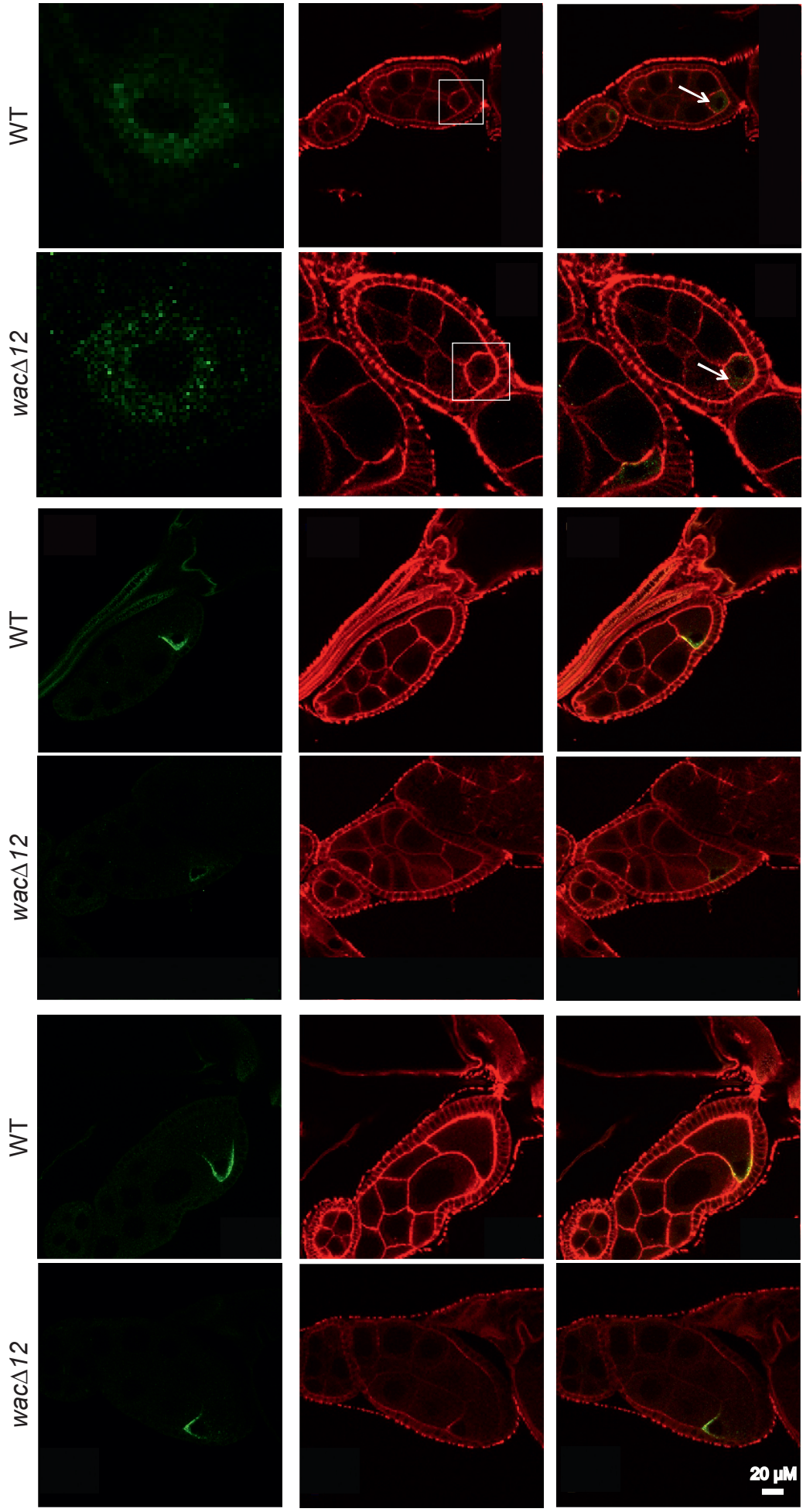
Stage 6   Stage 8   Stage 9

20 µM

Figure 6.5- Gurken protein localization is affected in wacΔ12 oocytes.
Immunofluoresence of *Drosophila* egg chambers with anti-Gurken antibodies (green) and phalloidin (red). At stage 6, the image showing Gurken signal (green) is magnified from the egg chamber as the stage 6 oocyte is small; the region used for magnification is indicated by the white box on the phalloidin image (red). Gurken localises to the posterior cortex of the oocyte in WT egg chambers at stage 6 of development. In wacΔ12 stage 6 oocytes, however, Gurken localisation is not concentrated at the posterior. White arrows indicate the position of the oocyte in the merged panel. During stages 8 to 10b of oocyte development in WT oocytes, Gurken localizes to the anterior dorsal corner where the nucleus resides. Although localization was not affected in wacΔ12 oocytes at stage 8 to 10b, staining was weaker. Scale bar of 20 µM applies to all panels, except for the zoomed images of WT and *wacΔ12* stage 6 oocyte (green).

89.5% of the time (n=57). In *wacΔ12* stage 8-10b oocytes, although Gurken localization itself was not affected, strong fluorescence was detected in only 21% (n=57) of the oocytes (Fig. 6.5). Although Gurken is implicated in nuclear migration at stage 7, there were no incidences of nuclear mislocalisation in *wacΔ12* stage 8-10b oocytes.

6.3.4. Augmin is dispensable for Oskar protein localization

Since the disruption of MT networks in *wacΔ12* oocytes leads to reduced Gurken localization in stage 7, I theorised that other polarity determinants might be affected. A second polarity determinant which relies on MTs for mRNA transport and therefore protein localisation is *oskar*. Therefore, WT and *wacΔ12* ovaries were fixed with formaldehyde, and stained with anti-Oskar antibody. Oskar protein localised tightly against the posterior cortex from stage 9 to stage 10b in WT oocytes. There was no observable difference in Oskar localisation in *wacΔ12* oocytes in comparison to WT between stages 9 to 10b (Fig 6.6). Therefore, Augmin appears to be dispensable for Oskar protein localization.

6.3.5. Transgenic oskar mRNA expression has a deleterious maternal effect on Augmin mutant egg chambers

oskar mRNA translation is spatially controlled. Only when it reaches the posterior cortex does translation initiate (Murphy and Borisy, 1975). It is possible that although the protein localization was not affected, Augmin might still be involved in *oskar* mRNA transport. To investigate this, the ms2-MCP system for mRNA

localization, was used (Becalska and Gavis, 2009). MS2 is a single-stranded RNA bacteriophage in which certain regions form stem-loop structures. The RNA sequence is recognised by the MS2 RNA major coat protein (MCP), which when tagged with GFP, can be used to track mRNA movement (Becalska and Gavis, 2009). A line co-expressing *oskar*-MS2 and MCP-GFP was a kind gift from Dr. Tse-bin Chou (National Taiwan University) and these flies were crossed with *wacΔ12* mutant flies to eventually produce homozygous *wacΔ12* mutant flies in which *oskar*-mRNA could be visualised (Fig. 6.7A). Egg chambers from these flies were examined to determine the localisation of *oskar* mRNA.

However, *wacΔ12* egg chambers of these flies, which were derived from both parents carrying the *oskar* mRNA transgenes (Fig. 6.7A), had severe phenotypic defects. The ovaries were atrophic, and the females laid no embryos. Very rarely was there an egg chamber that could be staged. The majority of egg chambers often had multiple oocytes, and/ or multiple nuclei (Fig. 6.7B). Although *oskar*-mRNA did not localize to the posterior pole in most oocytes (Fig. 6.7B), the mislocalisation was most likely due to the gross morphological defects. Since flies expressing both *wacΔ12* and labelled oskar mRNA which laid normal embryos inherited the oskar transgene from the father, it is likely that this effect is due to inheriting the transgene from the mother. It is thus not possible to fully tease out the role of Augmin on mRNA transport in these flies due to a combined maternal effect of *wacΔ12* and *oskar* mRNA.

Oskar | Phalloidin | Oskar
Phalloidin

WT | wacΔ12 | cnn mutant

Stage 9

WT | wacΔ12 | cnn mutant

Stage 10a

20 μM
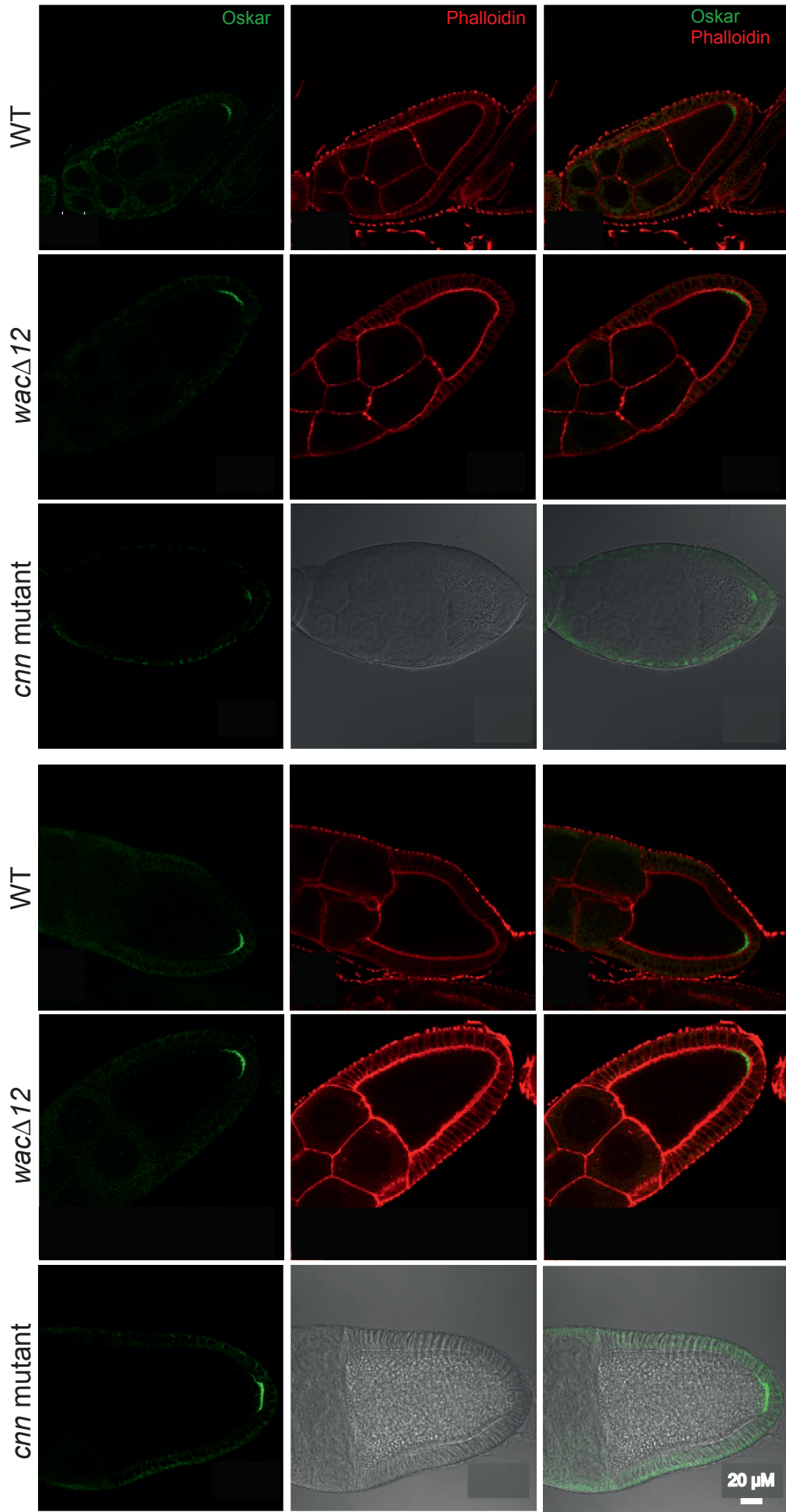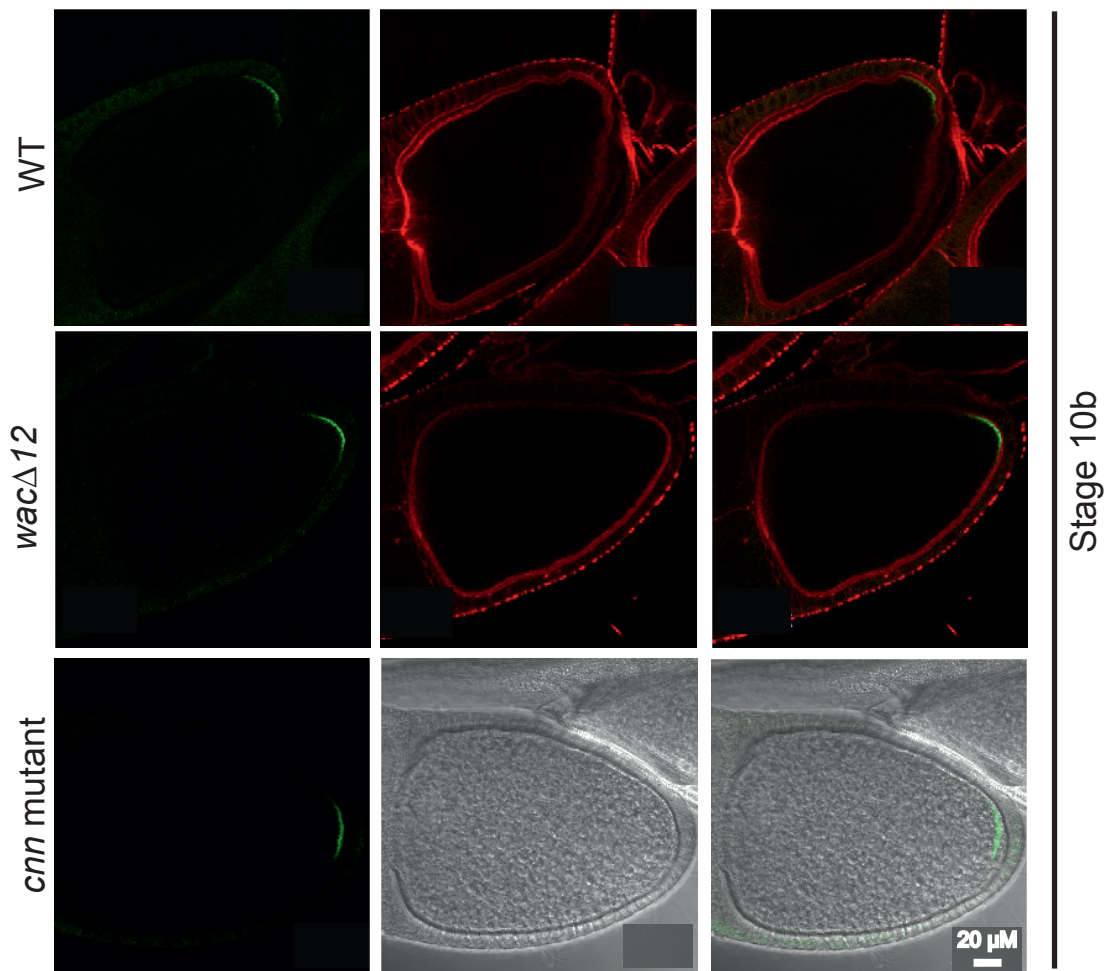
Figure 6.6- Augmin is dispensable for Oskar protein localisation in the oocyte.

Drosophila egg chambers were stained with anti-Oskar (green) and Phalloidin (red). Oskar localized to the posterior pole of the oocyte in WT egg chambers from stage 9 of oocyte development, and persists to stage 10b. There was no difference in Oskar localization in *wacΔ12* or *cnn* mutant oocytes. Scale bar of 20 µM applies to all panels.
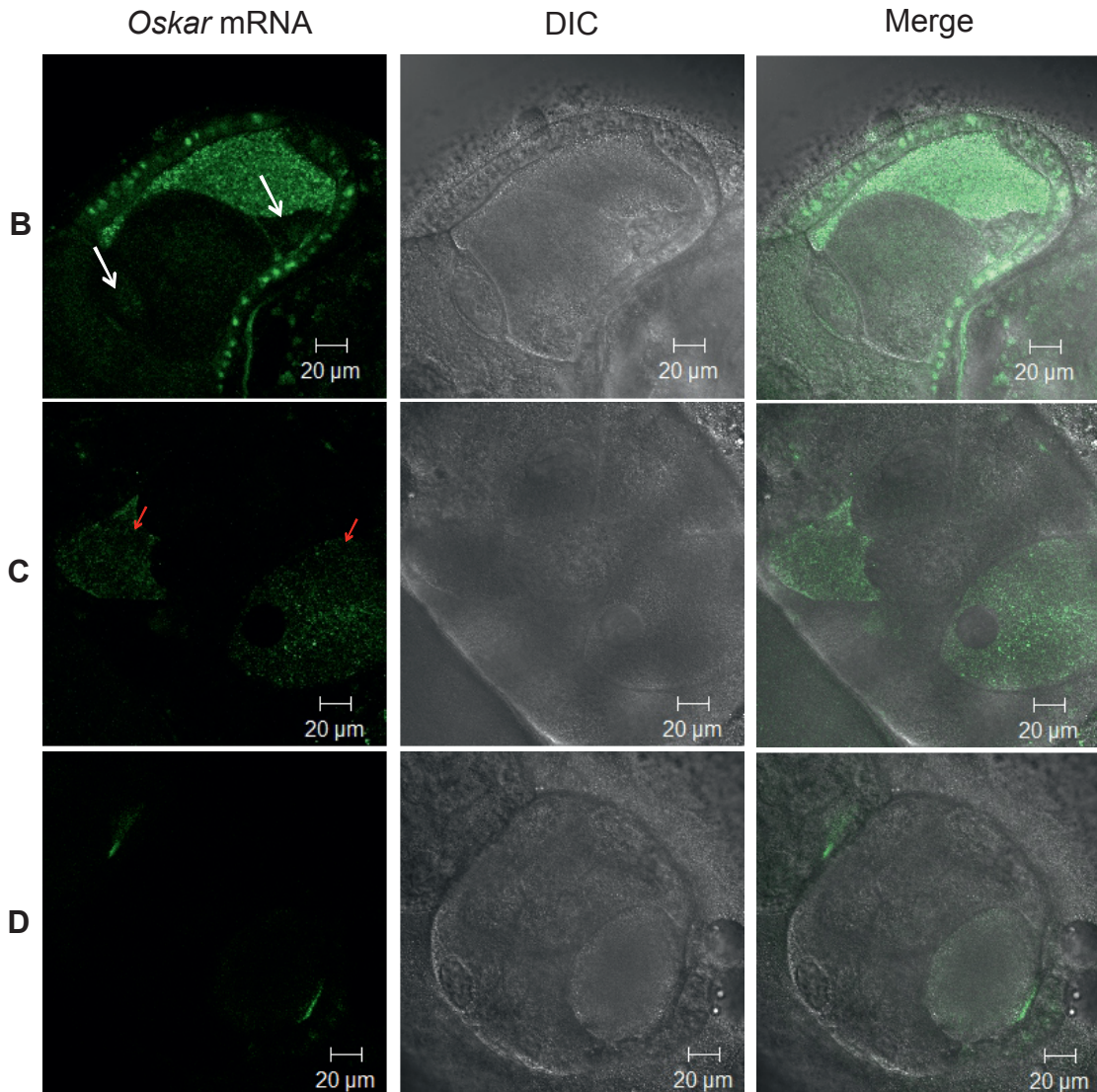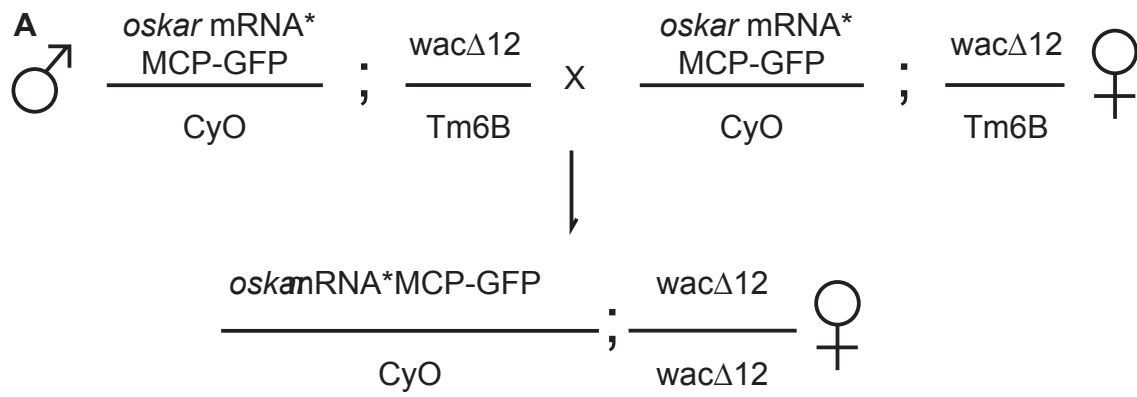
Figure 6.7- *oskar* mRNA and wacΔ12 have a combined maternal effect on oocyte development.
(A) Genetic cross showing generation of female oskar mRNA *wacΔ12* homozygous flies, where both parents carried the labelled *oskar* mRNA transgene. (B-D) Egg chambers from these flies were visualised using the ms2-MCP-GFP system. These female flies rarely produced egg chambers and those that were produced phenotypic defects. Examples of such defects include multiple nuclei as indicated by white arrows (B), multiple oocytes as indicated by red arrows (C), or generally misshapen cells (D).

6.3.6. Augmin is dispensable for oskar mRNA transport

It was clear that the *oskar* mRNA transgene and *wacΔ12* allele had a combined maternal effect, since ovaries of *oskar* mRNA transgenic fly or ovaries of homozygous *wacΔ12* are phenotypically normal. To reduce the maternal effect, I mated male *wacΔ12* flies carrying the *oskar* mRNA transgene, with female *wacΔ12* flies without the *oskar* mRNA transgene (Fig. 8). The resulting ovaries and egg chambers had normal morphology under light and fluorescence microscopy (Fig. 9). In WT oocytes, o*skar* mRNA primarily localized to the anterior cortex at stage 8. By stage 9, *oskar* mRNA had both an anterior and a posterior cortex localization. At stages 10a and 10b, *oskar* mRNA only localized to the anterior cortex in WT oocytes (Fig. 6.8B). This is in agreement with previously published studies (Keates and Hall, 1975). Since *oskar* mRNA is translationally controlled, and only arrives at the posterior pole by stage 9, this is in agreement with the Oskar immunofluorescence described in Section 5.2.4. No differences in *oskar* localisation were observed in egg chambers from *wacΔ12* flies (Fig. 6.8B). The results imply Augmin is dispensable for *oskar* mRNA transport.

6.3.7. A *cnn* mutant recapitulates the Augmin mutant phenotype

Cnn is a *Drosophila* centrosomal protein that is responsible for recruiting γ-TuRC to the pericentriolar material, facilitating mitotic MT nucleation (Megraw et al., 1999). During oogenesis Cnn and γ-TuRC have been reported to have similar localization profiles (Megraw and Kaufman, 2000). Thus, I decided to explore the potential role of Cnn in MT reorganization during mid-oogenesis, in relation to Augmin. To investigate if Cnn is involved in generating MTs in *Drosophila* egg chambers, flies

expressing a severe hypomorphic mutant of Cnn and co-expressing Tubulin-GFP were dissected, and egg chambers observed live using fluorescence microscopy. Similar to the *wacΔ12*/Augmin-null mutant, *cnn* mutant egg chambers had normal MT networks in the nurse cells and follicle cells. However, at stage 8-9 *cnn* mutant oocytes had either short or no MTs (Fig. 6.4).

To determine if MTs are generated at all, egg chambers of Cnn mutant flies expressing EB1-GFP were observed with live microscopy. Again, similarly to Augmin mutant oocytes, EB1 comets could be observed in stage 9 *cnn* mutant oocytes (Movie 6.3).

To investigate if Cnn, like Wac*/*Augmin, is involved in Gurken localization, egg chambers were stained with anti-Gurken antibody. Again, similarly to *wacΔ12*/Augmin egg chambers, Gurken was not localised to the posterior cortex in stage 6 oocytes from *cnn* mutants, but was instead present throughout the oocyte (Fig. 6.9). Interestingly, by stage 8-9, although Gurken localized to the anterior-dorsal corner, punctate foci could also be observed within the cytoplasm of the oocyte (Fig. 6.9) which were not seen in the *wacΔ12* mutant.

Lastly, to investigate whether Cnn has a role in Oskar localizationegg chambers were stained with anti-Oskar antibody. Oskar could be detected at the posterior cortex in the *cnn* mutant oocyte throughout stages 9-10b, with no difference in intensity or localization compared to WT (Fig 6.6).

Thus, the observed phenotypes of *cnn* mutant egg chambers are similar to those found in *wacΔ12*/Augmin mutant egg chambers, with the exception that *cnn* oocytes have punctate foci of Gurken within the cytoplasm at stages 8-10b. Since
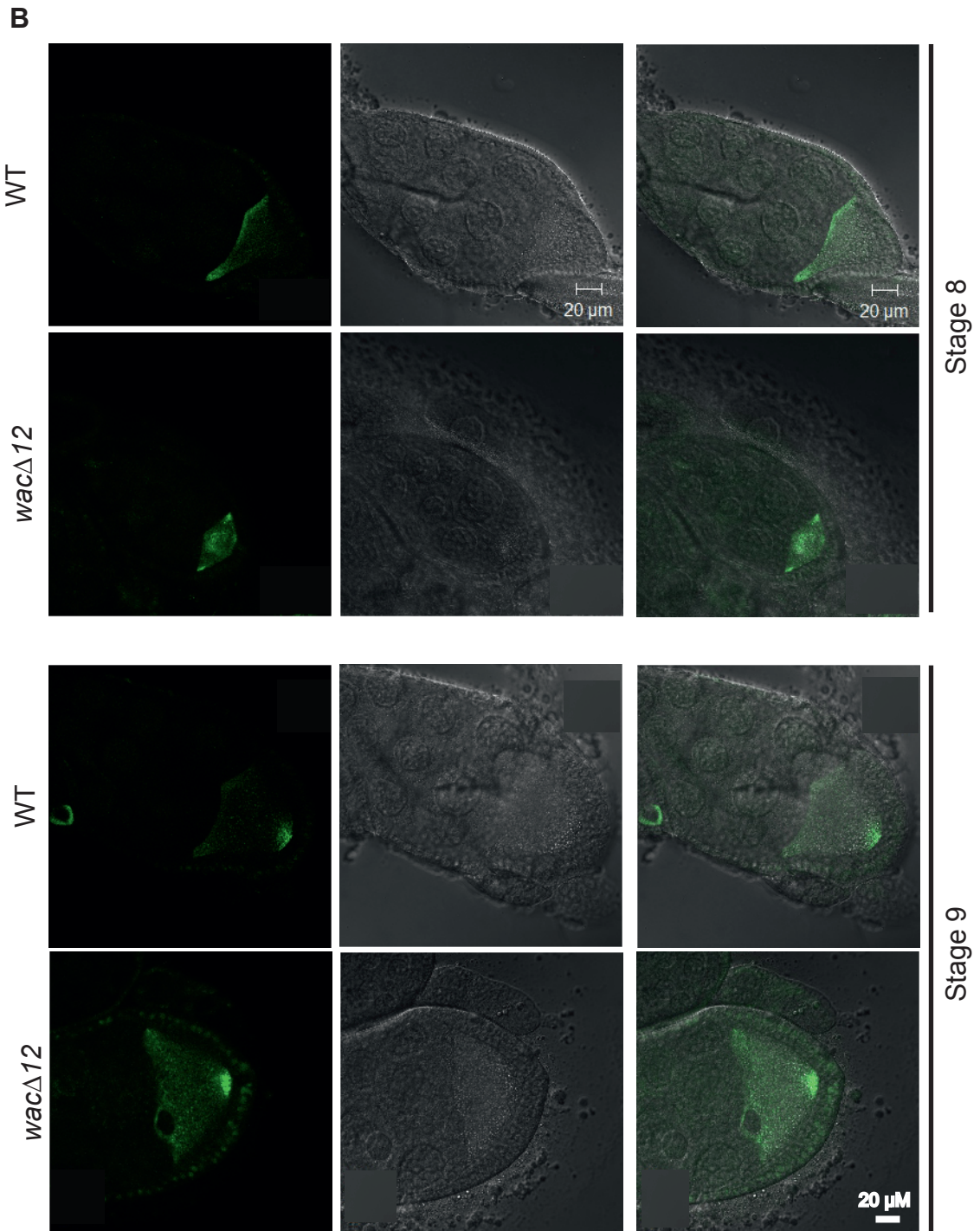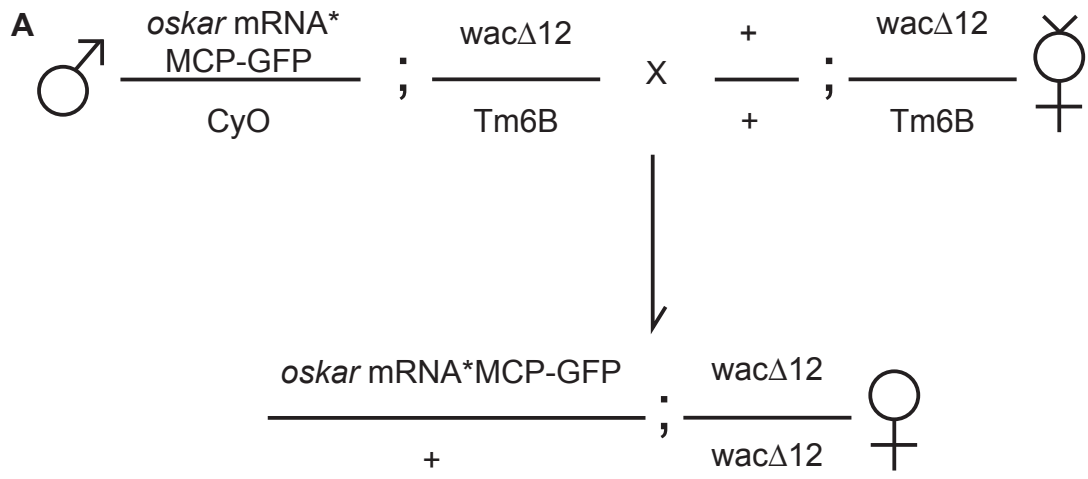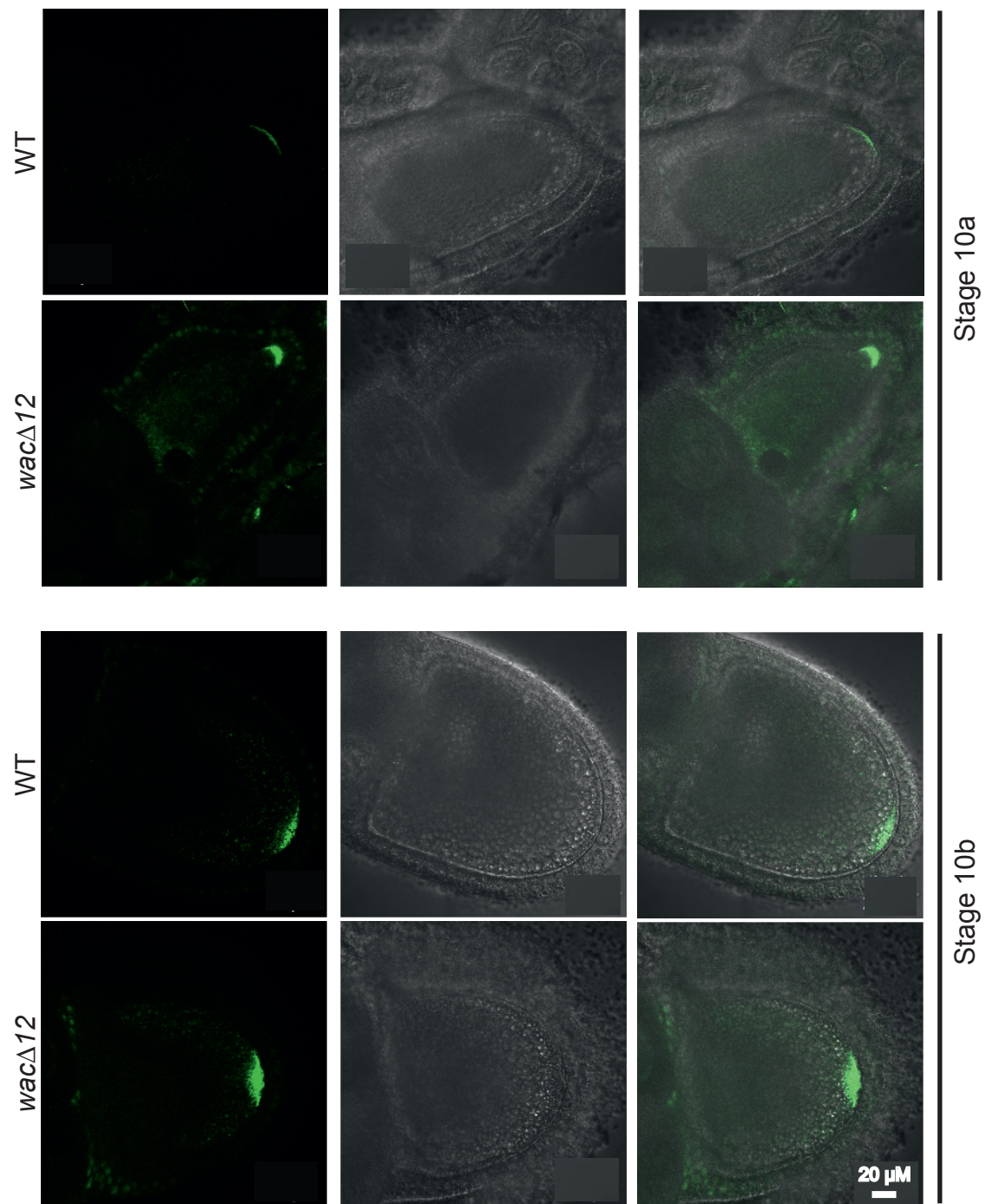
Figure 6.8- Augmin is dispensable for *oskar* mRNA transport
(A) (A) Genetic cross showing generation of female oskar mRNA wacΔ12 homozygous flies, where only one parent carried the labelled *oskar* mRNA transgene. (B-D) Live cell imaging of *oskar* mRNA visualised using the ms2-MCP-GFP system. Unlike the homozygous wacΔ12 flies from parents both carrying the labelled *oskar* transgene, egg chambers from these flies rarely had morphological defects. At stage 8 of development, *oskar*-mRNA localised to the anterior cortex in both WT and wacΔ12 oocytes. During stages 9 to 10b, oskar-mRNA localized to the posterior cortex and there was no obvious effect of Augmin loss. Scale bar of 20 µM applies to all panels.

WT

cnn

WT

cnn

WT

cnn

Stage 6

Stage 8

Stage 9

20 μM
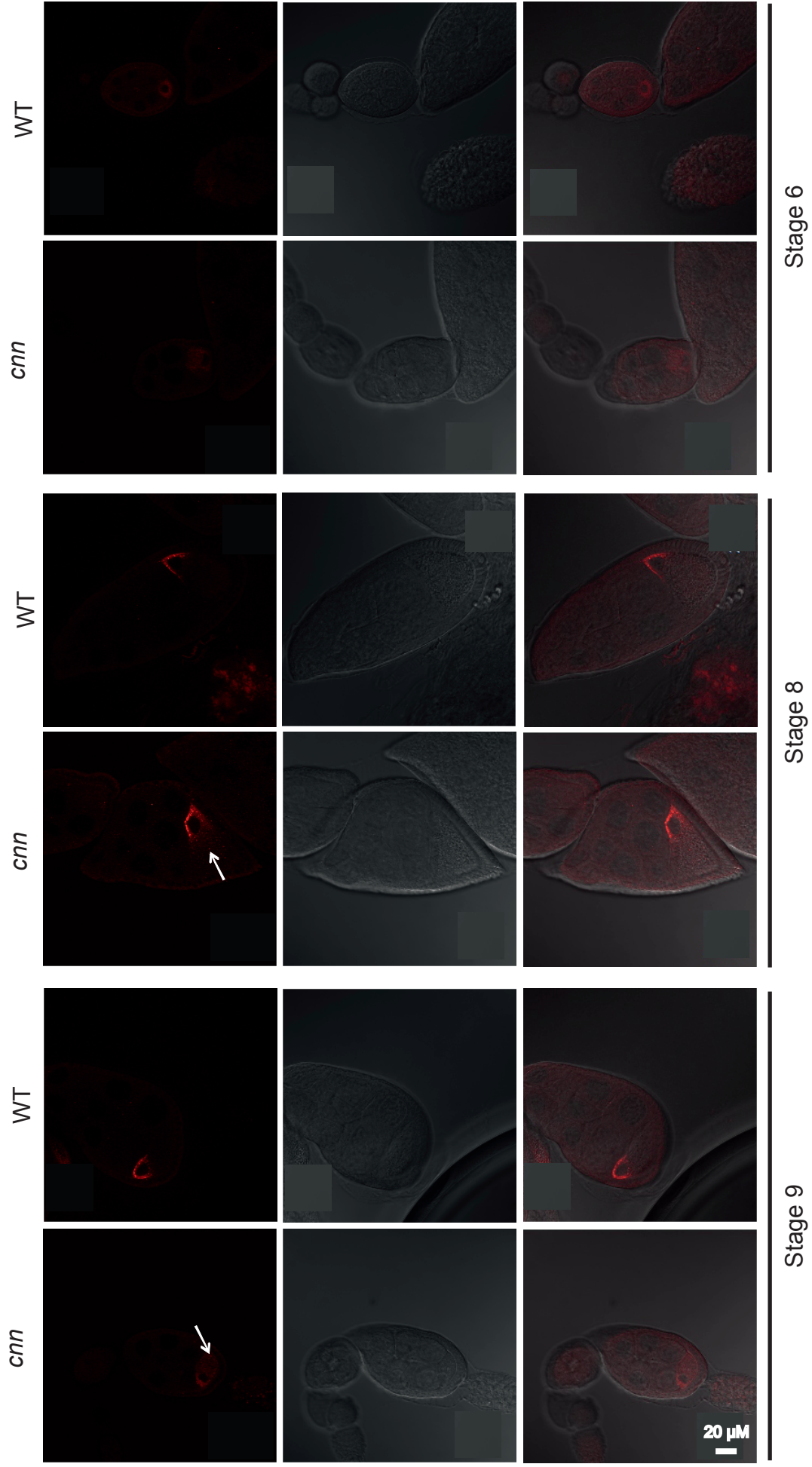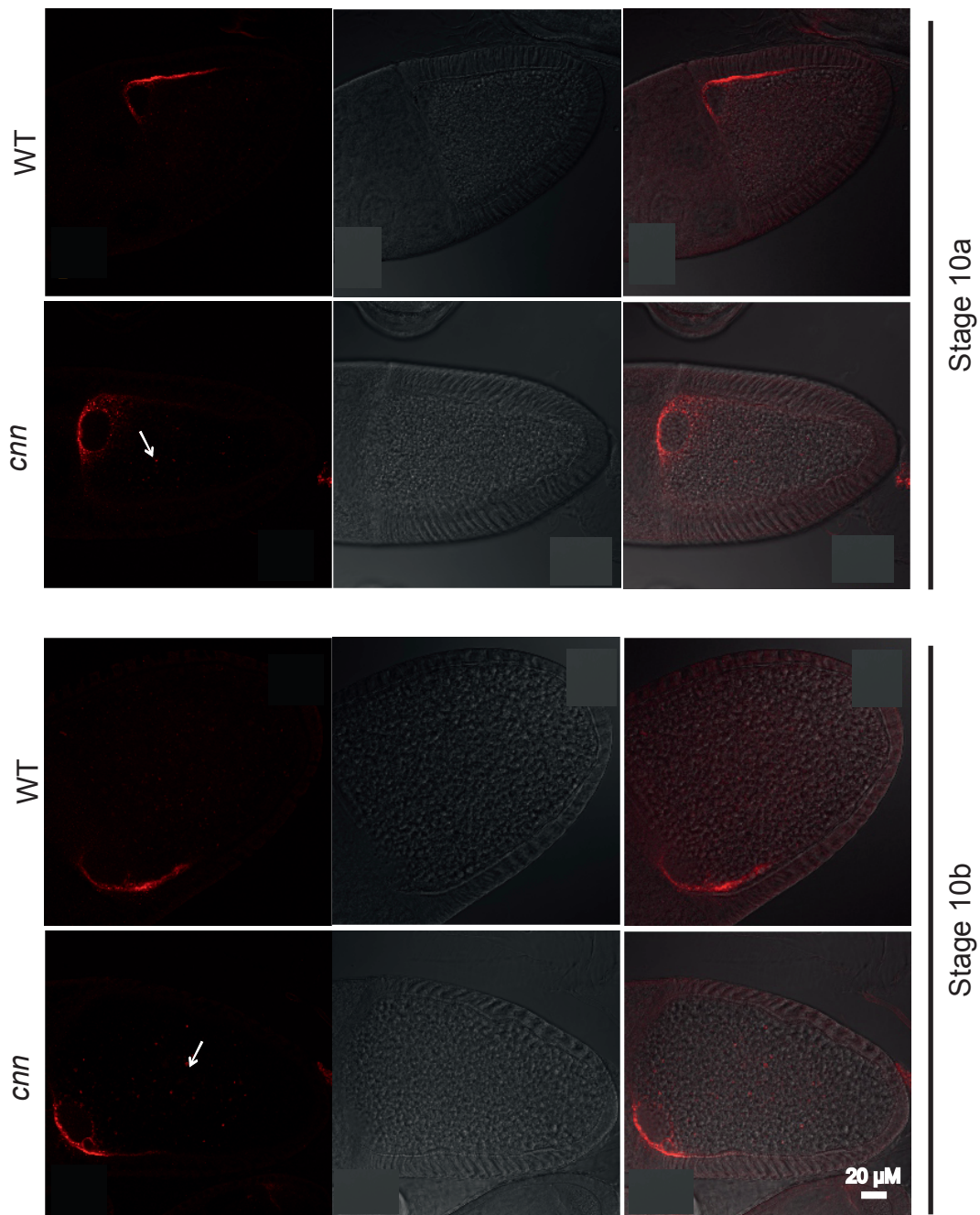
Figure 6.9- Cnn is involved in Gurken localisation in the oocyte.
Cnn mutant ovaries were stained with anti-Gurken antibodies (red). Gurken localises to the posterior cortex of the oocyte in WT egg chambers at stage 6 of development. In the Cnn mutant at stage 6, however, this localisation is rarely present. At stages 8 to 10b, in WT egg chambers Gurken localizes to the anterior dorsal corner where the nucleus resides. Although localisation of Gurken was not affected in Cnn mutant oocytes during stages 8 to 10b, Gurken staining was more diffuse than in WT, with additional punctate foci found within the middle of the oocytes(white arrows). Scale bar of 20 µM applies to all panels.

WT

wacΔ12

WT

wacΔ12

Stage 8

Stage 9

Cnn
Phalloidin

20 μM
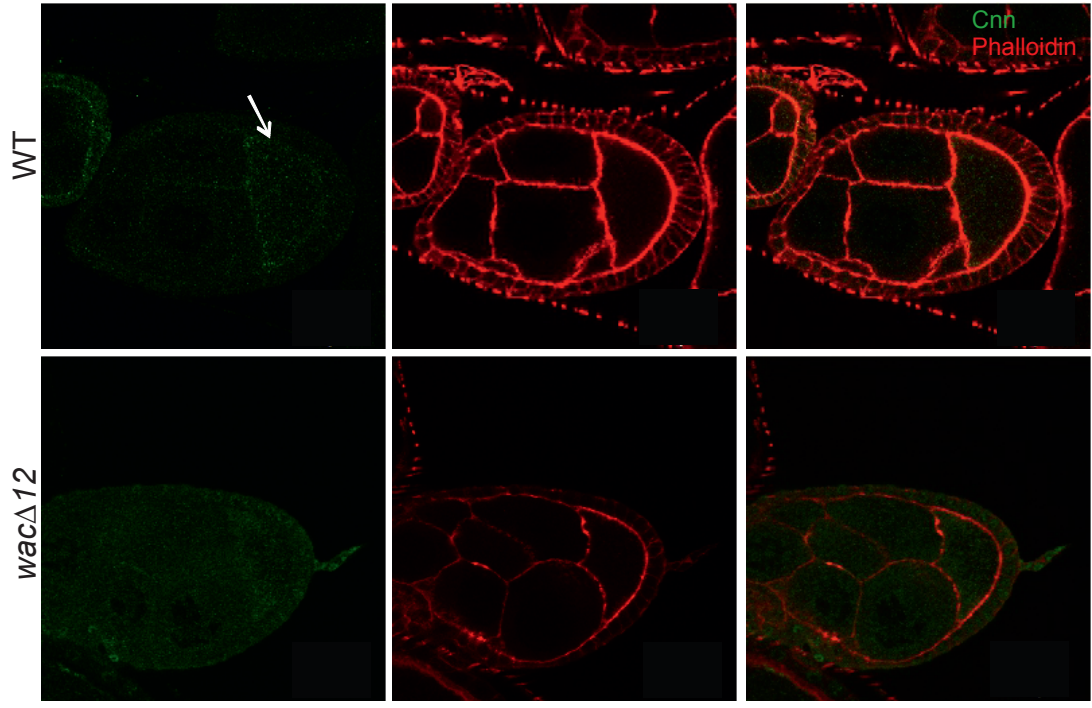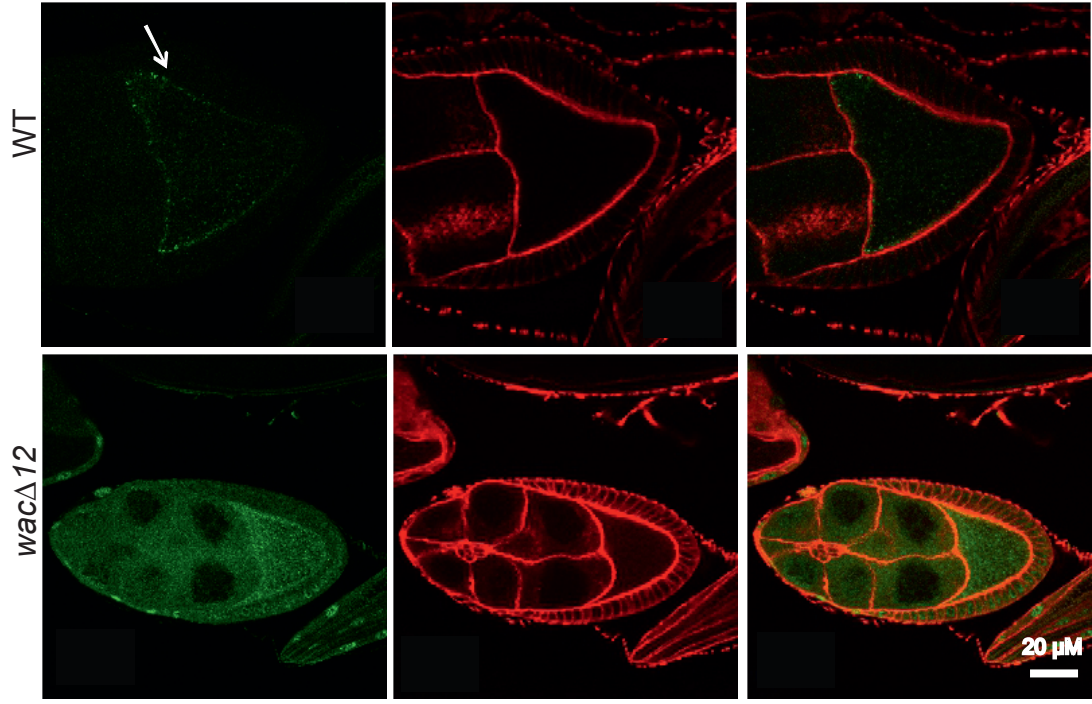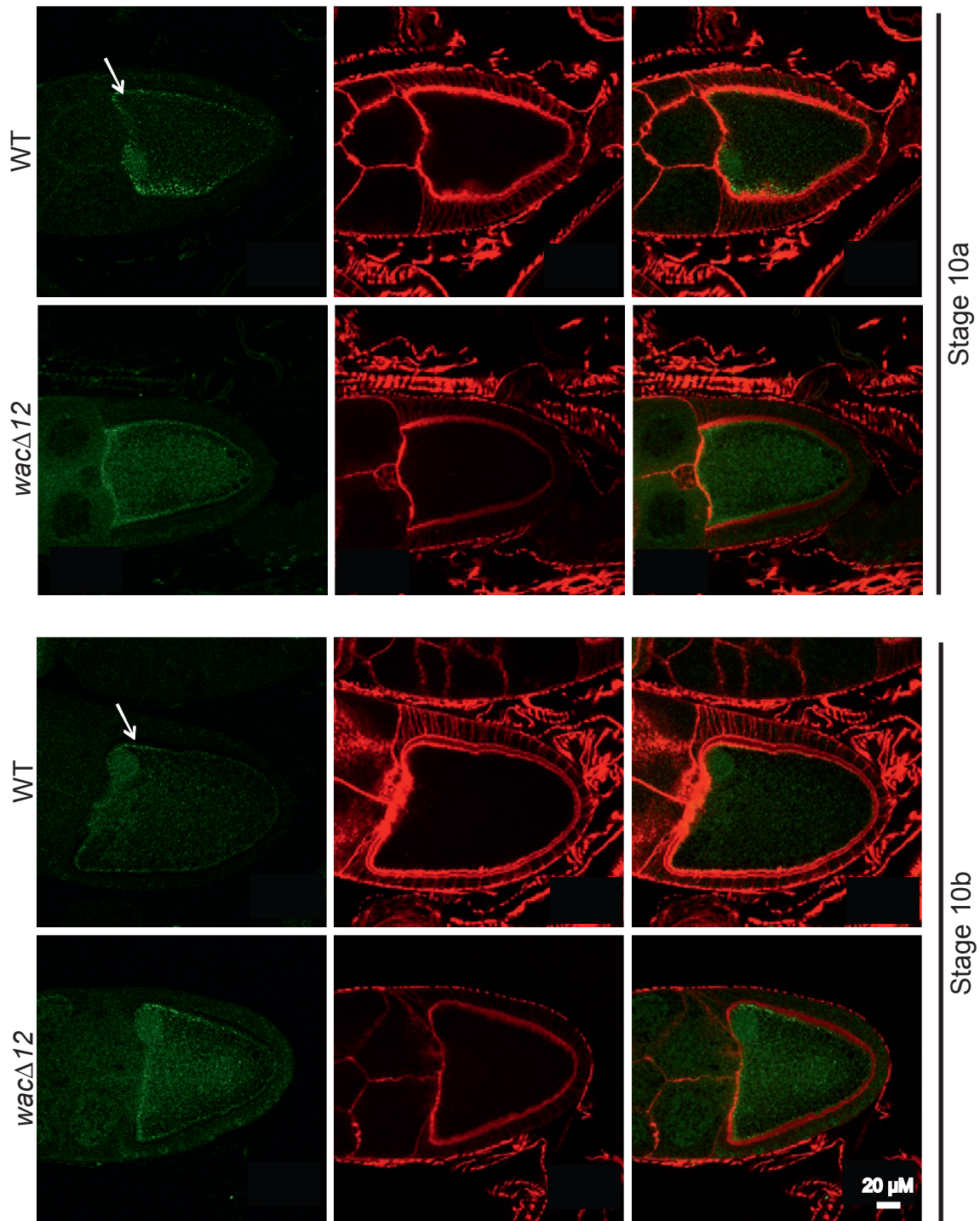
Figure 6.10- Augmin is involved in Cnn localization in the oocyte
Drosophila ovaries were stained with anti-Cnn (green) and phalloidin (red).
Beginning at stage 8 of oocyte development, Cnn localises to the oocyte cortex
in WT egg chambers (white arrows). *wacΔ12* oocytes show a similar localisation
of Cnn, but the localisation appears more diffuse. Scale bar of 20 μM applies to
all panels.

the phenotypes of these two mutants are so similar, it may be that Augmin and Cnn interact.

6.3.8. *wacΔ12*/Augmin is involved in Cnn localization during oogenesis

Since the *cnn* mutant recapitulates the *wacΔ12* null mutant phenotype during oogenesis, I decided to determine the relationship between the two. WT and *wacΔ12* ovaries were fixed with formaldehyde and stained with antibodies specific for Cnn. WT egg chambers displayed a generalised cytoplasmic localisation of Cnn, throughout all stages of development, with stronger staining around the oocyte cortex. This cortical localization was qualitatively at its most pronounced at the anterior from stages 8-10a, becoming more uniform by stage 10b (Fig. 6.10). Although Cnn was still localised to the oocyte cortex in *wacΔ12* egg chambers (similar to WT), this localisation was more diffuse in stages 8-10b (Fig. 6.10). Thus, functional Augmin complex appears to be important for Cnn localization in oogenesis.

6.4. Discussion

Drosophila oogenesis is a complicated process involving the correct setup of axis and morphogen determinants both during oogenesis and to provide cues for the embryo post-fertilisation. During early oogenesis, MTs are nucleated at the posterior cortex of the oocyte, and expand to become a MT network connecting the 15 nurse cells and the oocyte (Theurkauf, 1994). During mid-oogenesis, the oocyte undergoes a drastic MT reorganization event. Starting from stage 8 of oocyte development, MTs become nucleated from the oocyte anterior cortex and grow towards the posterior pole. It is believed that this MT reorganization is essential for correct localisation of maternal mRNAs responsible for morphogen determinantion (MacDougall et al., 2003; Mandelkow and Mandelkow, 1995; Robinson et al., 1994; Sung et al., 2008; Theurkauf et al., 1992). However, this process of MT reorganization is poorly understood. In this Chapter, I have provided evidence that the Augmin complex, the template-dependent MT nucleator responsible for increasing MT density during mitosis, is involved in generating MTs during mid-oogenesis. I also show that Cnn, which localizes to the anterior cortex at mid-oogenesis and has been implicated in γ-TuRC recruitment, is involved in this process.

6.4.1. The Augmin complex is likely to exist in Drosophila ovaries

I have shown that components of the Augmin complex are present within the germarium, as well as in egg chambers at stages 1-10b. Although fixed ovaries were positive for Dgt6 by immunofluoresence, one of the Augmin subunits, there were discrepancies in its localisation compared to that of Dgt6-GFP in live egg

chambers. Egg chambers stained with anti-Dgt6 showed not a faint cytoplasmic localisation but localised mainly to the oocyte nucleus, while Dgt6-GFP had a stronger cytoplasmic localisation and very weak nuclear localisation. Also, Dgt6-GFP was excluded from the nuclei of nurse cells, whereas anti-Dgt6 staining was not. Given that the expected pre-meiotic mitotic spindle staining was found in the germarium using the anti-Dgt6 antibody, and that anti-Dgt6 antibody has been shown to be specific in syncytial embryos (Hayward et al., 2014), we can conclude that the antibody recognises Dgt6. However, this does not rule out the possibility that additional epitopes are recognised in the developing oocyte. Indeed, the simplest explanations are that the nuclear staining reflects either an artefact of staining or recognition of cross-reacting proteins, or that fusion of Dgt6 with GFP results in some mislocalisation.

Augmin is likely required for the initial cell divisions during development of the 16-cell egg chamber, since it is required for syncytial division in the early embryo (Meireles et al., 2009; Wainman et al., 2009). Since all proteins required during syncytial divisions are produced by the mother and must be present in the egg chamber, Augmin must be present in these egg chambers, but the dynamics of its production and function during oocyte will need to be further investigated. Therefore, I examined the localisation of 3 Augmin subunits in the egg chamber by live-cell fluorescence microscopy. While Msd2-GFP and Dgt6-GFP both showed localization to the anterior cortex of the oocyte, Msd1-GFP localised additionally to ring canals. The three subunits also show differences in localisation to the oocyte nucleus. This difference in localisation may reflect overexpression artefacts or those due to GFP tagging. However, since Augmin has been shown to be

important in mitosis which is not occurring at these stages of oocyte development, it may be that Augmin is present as a reduced complex or that proteins are present individually outside the complex. I have used many of the existing tools available to probe localisation of Augmin subunits, but this has not been exhaustive. The main rationale was to determine whether Augmin localises to distinct MT populations within the developing oocyte. From the work presented here, encompassing both antibody localisation and the localisation of Augmin subunit GFP-fusions known to localise to MTs in Drosophila embryos (Hayward et al., 2014; Wainman et al., 2009), the diffuse cytoplasmic localisation of Augmin subunits would suggest that Augmin, in this case, does not bind MTs in the egg chamber.

It would nonetheless be prudent to confirm the relationship between Augmin subunits expressed in the developing oocyte. To confirm whether the full hetero-octomeric complex is present, or if subcomplexes exist, oocyte extracts could be subjected to gel-filtration and/or sucrose gradient sedimentation. These techniques have previously been used to assess the size of Augmin (Goshima et al., 2008; Wainman et al., 2009), (Section 3.3.6), showing that subunits are present in a common fraction of ~340kD. I could also apply the purification techniques which I used in Chapter 3 to immobilise or purify any Augmin complex in egg chambers and examine whether a complex of the correct size is present.

In addition, in *Drosophila* S2 cells, RNAi of any single Augmin subunit results in the reduction in the protein level of all other subunits, and thus, it has been generally accepted that Augmin destabilizes when any subunits is removed (Goshima et al., 2008). This has been the rationale behind the use of the *wacΔ12* mutant in the work presented in this chapter. Since very few studies have been done on the

biochemical properties of Augmin, gel-filtration/sucrose gradient-based analyses from WT and *wacΔ12* oocyte extracts would help to define whether this is indeed the case.

6.4.2. Augmin and Cnn are required during mid-oogenesis for a robust MT network.

My experiments have suggested that the Augmin complex and Cnn are both involved in generating and/or maintaining MT networks during *Drosophila* mid-oogenesis. In both *wacΔ12*/Augmin-null and hypomorphic Cnn mutants, no discernible MT defects could be observed either prior to stage 6 egg chambers or from stage 10 onwards. However, I found reproducible defects in MT network generation in egg chambers from these mutants between stages 8 and 9, as the oocyte undergoes MT reorganization. However, I have also shown that EB1 comets are present in the oocytes of these mutants at stages 8-9 at a similar density to control. This suggests that, in mutant oocytes, MTs are being generated by Wac or Cnn independent processes such as centrosomes (Vaughan et al., 2006), nucleus (Januschke et al., 2006), or oocyte cortical membrane, but that they are short-lived and that the role of Augmin and Cnn is likely to be MT stabilisation. This would agree with the results in Section 5.2.2, which suggests that the role of Augmin is in MT stabilisation rather than generation.

One caveat in interpreting the MT phenotype seen in stages 8-9 oocytes of the *wacΔ12* mutant is that this may not reflect an Augmin-specific function of Wac. In Chapter 5, I demonstrated that Wac has the ability to stabilise MTs and prevent them being depolymerised by cold treatment *in vitro* (Chapter 5, Section 5.2.2 &

Fig. 5.3). It is therefore possible that Wac serves to protect MTs from catastrophe in the oocyte during at stages 8 and 9, and the observed phenotype is Wac specific.

My data has also implicated a possible interaction between Augmin and Cnn, since Cnn localization to the oocyte cortex is more diffuse in Augmin mutants. Although, to date, no studies have implicated a direct relationship between Augmin and Cnn, reduction in Augmin levels results in centrosome fragmentation (Lawo et al., 2009). It is therefore possible that during oogenesis, Cnn localisation is dependent on Augmin. Further experiments will be required to investigate oocyte MT generation in the absence of both Augmin/Wac and Cnn. However, since investigations in fly tissues carrying null mutations in both Augmin and *cnn* are unable to complete mitosis (Hayward et al., 2014; Wainman et al., 2009), it is highly probable that the pre-meiotic mitoses would not complete and that an egg chamber would never be formed. It might be possible to use RNAi against both Augmin and Cnn since the RNAi can be expressed after initial 4 rounds of mitosis has completed. Expressing RNAi this way could thus separate the effect of removing Augmin and Cnn during mitosis, from oogenesis.

6.4.3. Augmin and Cnn generate the population of MTs involved in transient Gurken localization

Consistent with the observations that Augmin and Cnn both have a role in MT generation and/or maintenance during stage 8-9, I have shown that Gurken localization, which relies on MT networks for transport, is transiently affected in both *wac* and *cnn* mutants. This mis-localisation is apparent at Stage 6, prior to nuclear migration and continues through stages 8-10b, where *wacΔ12* mutant

oocytes accumulated less Gurken around the nucleus, while *cnn* mutants exhibited Gurken punctae in the cytoplasm. These observations pose two questions: (i) why, if Gurken fails to localise correctly in Stage 6, and Gurken functions to destabilise MTs to trigger nuclear migration (Koch and Spitzer, 1983), is nuclear migration in stage 7-8 not affected? (ii) why, when both *wac* and *cnn* mutants have similar MT phenotypes at Stages 8-10b, does the localistion of Gurken differ between them?

In the *wacΔ12* oocytes, the centriolar-derived population of MTs would be around the nucleus, anchoring the translated Gurken protein. The general destabilization of MTs in wac mutants would cause mRNA localisation to occur much less efficiently than in control oocytes. However, it would be expected that some *gurken* mRNA would be captured, localised and translated, leading to a reduced Gurken anterior signal.

In the *cnn* mutant however, the centrosome-organised population of MTs would not be present. Since *gurken* mRNA is translated in the endoplasmic reticulum, then processed in the Golgi, and the Golgi is transported via Dynein (Nicolas et al., 2009), the lack of a focused MT minus end at the centrioles would be expected to cause defects in Golgi localization. Gurken protein would therefore traffic through the Golgi after translation but, due to a lack of a focused MT minus end, would diffuse into the cytoplasm instead of trafficking correctly post-Golgi.

In addition, since transport of protein between the endoplasmic reticulum and the Golgi is MT dependent, an alternate possibility is that Cnn is involved in generating the MTs involved in this transport. In fact, the punctate Gurken foci seen in the Cnn mutant looked very similar to Gurken localization when the oocyte has been

treated with Brefeldin A that blocks transport from the endoplasmic reticulum to the Golgi (McKean et al., 2001).

6.4.4. Augmin and Cnn are dispensable for oskar mRNA and Oskar protein localization

Previous studies have implicated MTs to be essential for Oskar localization (Brendza, 2000; Doerflinger et al., 2010; Murphy and Borisy, 1975; Steinhauer and Kalderon, 2006). It was therefore surprising that *wacΔ12* and *cnn* mutant egg chambers, having MT network defects during mid-oogenesis, had no defects in Oskar localisation. WT, *wacΔ12*, and *cnn* mutant egg chambers had the same Oskar protein localization between stage 9 and 10b. Since *oskar* mRNA is translationally repressed until it reaches the posterior pole, a fluorescent transgenic *oskar* mRNA line was used to examine the possible defect in mRNA transport. When a heterozygous *wacΔ12* mother without the *oskar* mRNA transgene was used, the resulting homozygous *wacΔ12* egg chambers localised *oskar* mRNA normally.

My findings seem to suggest that an organised MT array at Stages 8-9 is largely dispensable for *oskar* mRNA transport and Oskar protein localization. Previous studies on MT defects have shown that Kinesin I mutants (Murphy and Borisy, 1975), or mutants that affect MT reorganization (Doerflinger et al., 2010; Dutcher and Trabuco, 1998) all affected *oskar* mRNA transport. However, these studies each have caveats. In the Kinesin I mutant study (Murphy and Borisy, 1975), it was found that the lack of Kinesin I removed the ability of the oocyte to transport *oskar* mRNA away from the cortex. Since MTs are still being made in the *wacΔ12* and

cnn mutant oocytes (see EB1 movies 6.1, 6.2 & 6.3), it is likely that Kinesin I is still able to perform its role in my mutants. Finally, in Maelstrom and Bazooka mutants (Doerflinger et al., 2010; Dutcher and Trabuco, 1998), MT reorganization is affected and thus the whole oocyte cortex contained an even distribution of MT plus-ends. The observed *oskar* mRNA transport defect was therefore due to motors unable to determine where the oocyte posterior was located. In *wacΔ12* and *cnn* mutant oocytes however, MT reorganization still occurred, and thus, the MT plus-ends were properly distributed around the cortex. Therefore the MT-dependent motors remain unaffected.

How then could *oskar* mRNA localise to the posterior in the absence of an organised MT array? One possibility is that actin networks play a role. Didum, which has been implicated in MT polarity, is the *Drosophila* homologue of the human protein Myosin V, an actin motor, and has also been implicated in *oskar* mRNA transport (Krauss et al., 2009). To date, there is no direct evidence for a MT-independent transport pathway for *oskar* mRNA. However, it is possible that Didum might transport *oskar* mRNA on actin networks in the absence of a robust MT network. An alternative is that in the absence of a robust MT network, *oskar* mRNA merely uses diffusion for transport. Since *oskar* mRNA is constantly being transported out of the nurse cells, the highest concentration of *oskar* mRNA would be at the anterior cortex and simple diffusion would result in some oskar reaching the posterior pole. Here, it would become anchored by actin (Tanaka, 2013; Tanaka and Nakamura, 2008), mopping up diffusible *oskar* mRNA, resulting in a gradual accumulation. One way to test this hypothesis is to treat *wacΔ12* and *cnn* mutant egg chambers with cytochalasin to destabilize actin networks. If *oskar*

mRNA uses passive diffusion transport, one would expect to see an exclusively cytoplasmic localization.

Interestingly, when females heterozygous for labelled *oskar* mRNA transgene and *wacΔ12* were crossed to males of the same genotype, the resulting homozygous *wacΔ12* flies had serious oogenesis defects. In contrast, females mutant for *wacΔ12*, but not carrying labelled *oskar* mRNA transgene produced developmentally normal egg chambers when crossed to male *wacΔ12* flies carrying labelled *oskar* mRNA transgene. This shows that expression of high levels of labelled *oskar* mRNA in a *wacΔ12* mutant background greatly affects oogenesis. It is not clear why this should be the case. However, one possibility is that, although no defects in the *wacΔ12* mutant MT network are visible prior to Stage 8-9, Augmin/Wac does contribute to MT function earlier in oogenesis. High-level expression of labelled *oskar* mRNA in the absence of Augmin at these early stages may be sufficient to compromise the development of the oocyte, perhaps by placing additional strain on MT networks, resulting in general defects in cell morphology.

6.4.5. A robust MT network is not required for Gurken signal, and Oskar localization

The work in this Chapter strongly suggests that Wac (and therefore Augmin) and Cnn are required transiently for the generation of an anterior-posterior MT gradient at stage 8-9 of Drosophila oogenesis. It also demonstrates, for the first time, that a robust MT network does not appear to be necessary for overall Oskar and Gurken localization. The oocyte is able to use alternative methods of transporting *oskar*

mRNA, and Oskar protein is correctly localised. It is possible that *gurken* mRNA transport is affected, but Gurken protein localisation and signalling remained unaffected. My data demonstrates the robustness of the oogenesis process, suggesting redundant processes exist to ensure generation of functional egg chambers for reproduction.

The data also suggests that Cnn may rely on Augmin for localisation, since Cnn staining is more diffuse in *wacΔ12* oocytes. It is possible that in the absence of Augmin, Cnn is upregulated in a compensatory manner, causing the more diffuse staining. A quantitative Western blot for Cnn in lysates of *wacΔ12* ovaries might indicate whether this is the case. It is also possible that the roles of the Augmin complex differ in oogenesis to those observed in early embryos, and the phenotype that I have observed is Wac specific. To test this hypothesis, mutants of other Augmin subunits will need to be examined. If these additional mutants recapitulate the *wacΔ12* phenotype, then I can be confident the observed phenotype is a result of disruption of Augmin.

7. General Discussion

7.1. Summary of findings

Augmin has been characterised as a hetero-octomeric complex responsible for template-dependent MT nucleation. At the onset of my research, it was known that human Augmin recruits γ-TuRC to pre-existing MTs through the MT interacting subunit HAUS8 (*Drosophila* Dgt4 homologue), and the C-terminus of HAUS6 (*Drosophila* Dgt6 homologue) (Johmura et al., 2011; Tsai et al., 2011; Uehara et al., 2009; Wu et al., 2008; Zhu et al., 2008). Without Augmin, cells cannot efficiently generate MTs during mitosis, resulting in the spindle having low MT density (Goshima et al., 2007; Hughes et al., 2008; Meireles et al., 2009; Wainman et al., 2009). Augmin has also been implicated in generating a specific population of MTs from the kinetochore, as cells lacking Augmin cannot generate kinetochore-mediated MTs (Bucciarelli et al., 2009).

However, many outstanding questions still remained. It was not known whether Augmin preferentially binds to the MT ends, or if Augmin binds to the MT lattice. Although Augmin has been characterised to recruit γ-TuRC to pre-existing MTs, Dgt4 has been shown to interact with NDC80 and Didum (Bucciarelli et al., 2009; Giot et al., 2003; Wu et al., 2009), and thus it was possible that Augmin might recruit other components to MTs. Although there was some data regarding the relationships between the different Augmin subunits (Meireles et al., 2009; Uehara et al., 2009), it was very limited. Lastly, it was not known if Augmin played a role in regulating MTs during interphase, but some evidence suggested it may, since

knockdown of several of the Augmin subunits had phenotypes during interphase (Hughes et al., 2008).

To address these questions, a combined biochemical and cell-based approach was used. To determine the effect of Augmin on MT growth and dynamics, I have attempted to purify Augmin from syncytial embryos. To determine if Augmin recruited other MAPs to MTs, I have used quantitative mass spectrometry to determine whether certain proteins are significantly reduced after Augmin depletion. To determine the protein relations between Augmin subunits, I opted to use cross-linking mass spectrometry (CLMS). Finally, to determine the functions of Augmin outside of mitosis, I have examined the organisation of the MT cytoskeleton at different stages of *Drosophila* egg chamber and oocyte development.

Recently, a study was published which suggested that Augmin generates branched MTs from the MT lattice, which infers that Augmin does not preferentially bind to the MT ends (Kamasaki et al., 2013; Petry et al., 2013). Human Augmin was also shown to be phosphorylated by both Plk1, and Aurora-A, which alters its ability to bind MTs (Tsai et al., 2011; Uehara et al., 2009). Although the question of whether Augmin has a preferential MT binding end was partially answered, I have nonetheless made progress in the other questions. My *in vitro* characterisation of particular domains of Augmin subunits, which was part of a wider CLMS approach, has shown that Augmin can directly stabilise MTs *in vitro*, most likely through the subunit Wac. I have also shown that although *Drosophila* Dgt6 lacks the MT binding domain of human Dgt6, it still bind to MTs *in vitro*. I have identified Mud as a potential protein recruited by Augmin to MTs. I have also teased out the inter-protein relationships between Augmin subunits, as well as implicated Dgt3 and

Dgt5 as subunits that recruit γ-TuRC, in addition to Dgt6. Finally, I have shown that the Augmin subunit Wac, at least, has a role outside of mitosis in the organisation of the polarised oocyte cytoskeleton.

7.2. Augmin stabilises MTs through the Wac subunit, which may contribute to building a robust bipolar spindle

Cells lacking functional Augmin complex through gene knockout or RNAi knockdown of any single subunit have low spindle density and are unable to recruit γ-TuRC to the spindle (Goshima et al., 2007; Hughes et al., 2008). The Augmin complex has also been shown to be important for kinetochore-mediated MT nucleation (Bucciarelli et al., 2009). Thus, it is generally thought that Augmin augments spindles through template-dependent MT nucleation, generating kinetochore-mediated MTs by first binding the short MTs generated by the kinetochore and subsequently recruiting γ-TuRC to the region.

Other very recent work in the our lab has shown that Augmin which is purified using a novel photocleavable affinity purification approach yielded an intact complex of 95% purity, without any γ-TuRC components. When Tubulin was incubated with this pure, soluble Augmin, long MTs were generated, in comparison to a GFP control. No branched MTs were detected, suggesting the presence of γ-TuRC was unlikely, and that the Augmin complex alone promotes MT growth through stabilisation. My work has shown that, in MT cosedimentation assays, Wac appears to stabilise MTs. Thus, it is possible that the Augmin complex, through the Wac subunit, may promote the robustness of the spindle simply by its MT stabilising property.

7.3. Augmin may play a role in MT maintenance outside mitosis

The role of Augmin has yet to be studied in detail outside of mitosis. The only published evidence to date which suggests that Augmin may have an effect on interphase MTs is from the original MAP proteomics study done in the Wakefield lab, where knockdown of Dgt2 and Wac resulted in a compacted MT phenotype in interphase S2 cells (Hughes et al., 2008). This is in contrast to mitotic Augmin, where removal of any single Augmin subunits results in the destabilisation of the whole complex (Goshima et al., 2008; Meireles et al., 2009; Wainman et al., 2009), resulting in the same phenotype of low spindle density and inability of the cell to recruit γ-TuRC to the spindle. It is therefore likely the biochemical properties of interphase Augmin are different than mitotic Augmin.

Although the wacΔ12 allele is null for Wac, and is therefore accepted as Augmin-null (Meireles et al., 2009), the state of the Augmin complex has not been fully tested in various interphase cell types. It is therefore unclear whether the shown in Chapter 6 are due to an effect of the wacΔ12 allele, or due to lack of functional Augmin complex. Regardless, since Wac is one of two Augmin subunits that have an interphase phenotype after RNAi knockdown, if there is an interphase process that involves Augmin, it is likely to involve Wac.

The *Drosophila* follicle cells which surrounds the egg chamber differentiate into cuboidal epithelium and require a robust MT network for this differentiation process (Theurkauf et al., 1993). Since removal of centrosomes has no effect on these follicle cells (Stevens et al., 2007), I postulated that alternative MTOCs might play a role in nucleating follicle cell MTs. In contrast to the interphase MT phenotype in S2

cells, it was therefore quite surprising that the follicle cells of the *wacΔ12* egg chambers had no discernable MT phenotype. It is possible that both centrosomes and Augmin contribute to the follicle cell differentiation process but, upon removal of one MT-generating pathway, the other is up-regulated. Such compensatory mechanisms are present in the Drosophila syncytial mitotic blastorderm (Hayward et al., 2014). This hypothesis is difficult to test, since cells lacking both centrosomes and Augmin never complete mitosis, and thus, no follicle cells would ever arise.

Another possibility is that centrosomes and Augmin are not major MTOCs responsible for cell differentiation, and other MTOCs such as the Golgi and the nuclear envelope are responsible for most of the MT nucleation. A third further possibility is that MTOCs are not necessary at all, and that MTs spontaneously generated within the cytoplasm are sufficient. Since interphase MTs are more stable, it is possible that differentiating cells rely mostly on MT-stabilising MAPs for the process. Evidence supporting the third possibility lies in the relatively few EB1 tracks within the follicle cells compared to mitotic cells and the oocyte, yet follicle cells maintain a dense MT network.

The *wacΔ12* allele however, does have an effect on the oocyte, a specialised interphase cell that uses MT reorganisation to affect inter- and intracellular transport. At stage 7, the oocyte destabilises its MT network, rearranging the MTOCs so that MTs are nucleated at the anterior cortex, as opposed to the posterior pole. This reorganisation event allows proper transport of maternal determinants such as *oskar*, *bicoid*, and *gurken* mRNA (discussed in Chapter 6). The *wacΔ12* oocytes have defects in re-establishing the MT network after

reorganisation, with MT phenotypes ranging from appearing flimsy and short to non-existent. These phenotypes can be explained by the dual functions of Augmin in nucleating MTs from templates, where the reduced number of MTs results in the oocyte being unable to build a robust network, as well as the ability of Augmin to promote MT growth through stabilisation in a similar manner to Doublecortin, where reduced stability of MTs in the oocyte causes more MT catastrophe events resulting in MT network destabilisation (Moores et al., 2004). Unexpectedly however, oocytes had no difficulties localising *oskar* mRNA, and have only minor difficulties with Gurken protein localisation. This again could reflect compensatory processes which ultimately demonstrate the dispensibility of a robust MT network for MT mediated transport.

7.4. Cell cycle regulation

The Augmin subunit Msd1-GFP localises to the spindle throughout mitosis. However, post cellularisation, Msd1-GFP localises to centrosomes and to MTs only when cells enter mitosis (data not shown). It is therefore clear that the localisation of Augmin is controlled in a cell-cycle dependent manner. The regulation of Augmin from interphase to mitosis is elusive, but evidence points towards phosphorylation. It has been shown that Aurora A and Plk1 phosphorylate human Augmin, resulting in alterations in the ability of Augmin to associate with MTs (Johmura et al., 2011; Tsai et al., 2011). It has also been demonstrated that the ability of *Xenopus* Augmin to generate branched MTs is facilitated by TPX2 (Petry et al., 2013). Since TPX2 is an effector of Aurora A (Dodson and Bayliss, 2012), it is possible TPX2 may increase the efficiency of Augmin function through Aurora A activity. There

has been no data as yet on whether Aurora B may phosphorylate Augmin and affect its activity. Aurora B is a related kinase to Aurora A, and localises strongly to kinetochores by metaphase. There is, however, an additional weak population on the spindle itself (Simon Li, unpublished observations). It is therefore tempting to speculate that since Aurora B is in the same spatial and temporal region where Augmin-specified MT generation is taking place, *Drosophila* Augmin activity may be controlled by Aurora B.

The Wakefield lab has also attempted to explore cell-cycle control mechanisms for *Drosophila* Augmin by using commercially available Aurora A, Aurora B, Plk1, and CDK1 kinases (Pete Jones, unpublished work). However, in contrast to the published results in humans, none of the kinases phosphorylated Augmin *in vitro*. One possible explanation is that since the commercially-available kinases are human proteins, they are unable to recognise *Drosophila* Augmin. To date, the cell-cycle kinase mediated control of Augmin therefore continues to be poorly understood.

7.5. The wider implications of understanding Augmin function: a role in Cancer?

There are many genes that regulate proliferation and senescence of cells. Disregulation of these pathways may result in duplication of oncogenes such as Ras (Malumbres and Barbacid, 2003) and Myc (Meyer and Penn, 2008) and/ or loss of tumour suppressor genes such as p53 (Noon et al., 2010) and Bax (Hassan et al., 2014) resulting in cancer. In fact, aneuploidy is often a hallmark of cancer (Davoli et al., 2013; Gordon et al., 2012). Cells with reduced or mutated Augmin

subunits often have chromosome misalignments and monopolar spindles (Hughes et al., 2008), which may cause chromosome missegregation and lead to aneuploidy. In fact, since its discovery, Augmin has been implicated in many cancers (Sarhadi et al., 2013; Shah et al., 2009). It is therefore reasonable to assume Augmin may be important in initial cancer progression by increasing the number of copies of oncogenes, or by decreasing the number of copies of tumour suppressor genes, through errors in chromosome segregation.

In cancer cells, centrosome supernumeracy is a common occurrence (Leber et al., 2010). Yet these cancer cells are able to build a functional bipolar spindle and successfully complete mitosis. This is due to the ability of the cancer cells to cluster these multiple centrosomes (Leber et al., 2010), and Augmin has been implicated in centrosome clustering (Leber et al., 2010). It is thus not surprising that many cancers have elevated levels of Augmin (Uhlén et al., 2005), since higher levels of Augmin might help cancer cells cluster these extra centrosomes.

Traditional cancer therapies, such as targeting the MT cytoskeleton and cell division machinery (e.g. through use of Taxol) lack specificity, as they often target healthy cells as well as malignant cells. Since the function of the Augmin complex during cell division is controlled by mitotic kinases (Johmura et al., 2011; Tsai et al., 2011), small molecule kinase inhibitors against Aurora-A and Plk1 present a possible target for cancers with elevated levels of Augmin with centrosome numeracy. However, the current knowledge of cell cycle control of Augmin remains severely limited. The work presented in this thesis demonstrates the use of new tools such as CLMS and Quantitative comparative MAP (QC-MAP) proteomics, to begin to dissect the roles of individual Augmin subunits in relation to the properties

of the complex. It is with such detailed knowledge that the precise mode of action of Augmin should be elucidated. Once we understand the molecular details on how Augmin clusters centrosomes and how it focus spindle poles, in relation to molecular detail, we will have a much clearer path to how small molecule inhibitors, both existing and new, might be used to inhibit these functions.

8. References

Adams, M.D., S.E. Celniker, R.A. Holt, C.A. Evans, J.D. Gocayne, P.G. Amanatides, S.E. Scherer, P.W. Li, R.A. Hoskins, R.F. Galle, R.A. George, S.E. Lewis, S. Richards, M. Ashburner, S.N. Henderson, G.G. Sutton, J.R. Wortman, M.D. Yandell, Q. Zhang, L.X. Chen, R.C. Brandon, Y.H. Rogers, R.G. Blazej, M. Champe, B.D. Pfeiffer, K.H. Wan, C. Doyle, E.G. Baxter, G. Helt, C.R. Nelson, G.L. Gabor, J.F. Abril, A. Agbayani, H.J. An, C. Andrews-Pfannkoch, D. Baldwin, R.M. Ballew, A. Basu, J. Baxendale, L. Bayraktaroglu, E.M. Beasley, K.Y. Beeson, P.V. Benos, B.P. Berman, D. Bhandari, S. Bolshakov, D. Borkova, M.R. Botchan, J. Bouck, P. Brokstein, P. Brottier, K.C. Burtis, D.A. Busam, H. Butler, E. Cadieu, A. Center, I. Chandra, J.M. Cherry, S. Cawley, C. Dahlke, L.B. Davenport, P. Davies, B. de Pablos, A. Delcher, Z. Deng, A.D. Mays, I. Dew, S.M. Dietz, K. Dodson, L.E. Doup, M. Downes, S. Dugan-Rocha, B.C. Dunkov, P. Dunn, K.J. Durbin, C.C. Evangelista, C. Ferraz, S. Ferriera, W. Fleischmann, C. Fosler, A.E. Gabrielian, N.S. Garg, W.M. Gelbart, K. Glasser, A. Glodek, F. Gong, J.H. Gorrell, Z. Gu, P. Guan, M. Harris, N.L. Harris, D. Harvey, T.J. Heiman, J.R. Hernandez, J. Houck, D. Hostin, K.A. Houston, T.J. Howland, M.H. Wei, C. Ibegwam, et al. 2000. The genome sequence of Drosophila melanogaster. *Science (New York, N.Y.)*. 287:2185-2195.

Al-Bassam, J., H. Kim, G. Brouhard, A. van Oijen, S.C. Harrison, and F. Chang. 2010. CLASP promotes microtubule rescue by recruiting tubulin dimers to the microtubule. *Developmental cell*. 19:245-258.

Amos, L., and A. Klug. 1974. Arrangement of subunits in flagellar microtubules. *Journal of cell science*. 14:523-549.

Azimzadeh, J., and W.F. Marshall. 2010. Building the centriole. *Current biology : CB*. 20:R816-825.

Back, J.W., L. de Jong, A.O. Muijsers, and C.G. de Koster. 2003. Chemical cross-linking and mass spectrometry for protein structural modeling. *Journal of molecular biology*. 331:303-313.

Bajer, A.S., and J. Molè-Bajer. 1986. Reorganization of microtubules in endosperm cells and cell fragments of the higher plant Haemanthus in vivo. *The Journal of cell biology*. 102:263-281.

Baker, J.R. 1955. The Cell-theory: a Restatement, History, and Critique: Part V. The Multiplication of Nuclei. *Quarterly Journal of Microscopical Science*. s3-96:449-481.

Basto, R., J. Lau, T. Vinogradova, A. Gardiol, C.G. Woods, A. Khodjakov, and J.W. Raff. 2006. Flies without centrioles. *Cell*. 125:1375-1386.

Becalska, A.N., and E.R. Gavis. 2009. Lighting up mRNA localization in Drosophila oogenesis. *Development (Cambridge, England)*. 136:2493-2503.

Boal, A.K., H. Tellez, S.B. Rivera, N.E. Miller, G.D. Bachand, and B.C. Bunker. 2006. The stability and functionality of chemically crosslinked microtubules. *Small (Weinheim an der Bergstrasse, Germany)*. 2:793-803.

Borisy, G.G., J.M. Marcum, J.B. Olmsted, D.B. Murphy, and K.A. Johnson. 1975. Purification of tubulin and associated high molecular weight proteins from porcine brain and characterization of microtubule assembly in vitro. *Annals of the New York Academy of Sciences*. 253:107-132.

Borisy, G.G., and E.W. Taylor. 1967. The mechanism of action of colchicine. Binding of colchincine-3H to cellular protein. *The Journal of cell biology*. 34:525-533.

Brendza, R.P. 2000. A Function for Kinesin I in the Posterior Transport of oskar mRNA and Staufen Protein. *Science*. 289:2120-2122.

Brunet, S., Z. Polanski, M.H. Verlhac, J.Z. Kubiak, and B. Maro. 1998. Bipolar meiotic spindle formation without chromatin. *Current biology : CB*. 8:1231-1234.

Bryan, J., and L. Wilson. 1971. Are cytoplasmic microtubules heteropolymers? *Proceedings of the National Academy of Sciences of the United States of America*. 68:1762-1766.

Bucciarelli, E., C. Pellacani, V. Naim, A. Palena, M. Gatti, and M.P. Somma. 2009. Drosophila Dgt6 interacts with Ndc80, Msps/XMAP215, and gamma-tubulin to promote kinetochore-driven MT formation. *Current Biology*. 19:1839-1845.

Cao, J., J. Crest, B. Fasulo, and W. Sullivan. 2010. Cortical actin dynamics facilitate early-stage centrosome separation. *Current biology : CB*. 20:770-776.

Capalbo, L., P.P. D'Avino, V. Archambault, and D.M. Glover. 2011. Rab5 GTPase controls chromosome alignment through Lamin disassembly and relocation of the NuMA-like protein Mud to the poles during mitosis. *Proceedings of the National Academy of Sciences of the United States of America*. 108:17343-17348.

Caplow, M., R. Ruhlen, J. Shanks, R.A. Walker, and E.D. Salmon. 1989. Stabilization of microtubules by tubulin-GDP-Pi subunits. *Biochemistry*. 28:8136-8141.

Caplow, M., and J. Shanks. 1996. Evidence that a single monolayer tubulin-GTP cap is both necessary and sufficient to stabilize microtubules. *Molecular biology of the cell*. 7:663-675.

Caplow, M., J. Shanks, and R. Ruhlen. 1994. How taxol modulates microtubule disassembly. *The Journal of biological chemistry*. 269:23399-23402.

Carazo-Salas, R.E., G. Guarguaglini, O.J. Gruss, A. Segref, E. Karsenti, and I.W. Mattaj. 1999. Generation of GTP-bound Ran by RCC1 is required for chromatin-induced mitotic spindle formation. *Nature*. 400:178-181.

Carlier, M.F., and D. Pantaloni. 1981. Kinetic analysis of guanosine 5'-triphosphate hydrolysis associated with tubulin polymerization. *Biochemistry*. 20:1918-1924.

Cassimeris, L., D. Gard, P.T. Tran, and H.P. Erickson. 2001. XMAP215 is a long thin molecule that does not increase microtubule stiffness. *J Cell Sci*. 114:3025-3033.

Chabin-Brion, K., J. Marceiller, F. Perez, C. Settegrana, A. Drechou, G. Durand, and C. Pous. 2001. The Golgi Complex Is a Microtubule-organizing Organelle. *Molecular Biology of the Cell*. 12:2047-2060.

Chen, Z.A., A. Jawhari, L. Fischer, C. Buchen, S. Tahir, T. Kamenski, M. Rasmussen, L. Lariviere, J.-C. Bukowski-Wills, M. Nilges, P. Cramer, and J. Rappsilber. 2010. Architecture of the RNA polymerase II-TFIIF complex revealed by cross-linking and mass spectrometry. *The EMBO journal*. 29:717-726.

Cheng, Y., Y. Chen, X. Sun, Y. Li, C. Huang, H. Deng, and Z. Li. 2014. Identification of Potential Serum Biomarkers for Rheumatoid Arthritis by High-Resolution Quantitative Proteomic Analysis. *Inflammation*.

Chou, T.B., and N. Perrimon. 1996. The autosomal FLP-DFS technique for generating germline mosaics in Drosophila melanogaster. *Genetics*. 144:1673-1679.

Clarke, P.R., and C. Zhang. 2008. Spatial and temporal coordination of mitosis by Ran GTPase. *Nature reviews. Molecular cell biology*. 9:464-477.

Clegg, C., and D. Hayes. 1974. Identification of Neighbouring Proteins in the Ribosomes of Escherichia coli. A Topographical Study with the Cross-Linking Reagent Dimethyl Suberimidate. *European Journal of Biochemistry*. 42:21-28.

Collins, C.A., and R.B. Vallee. 1989. Preparation of microtubules from rat liver and testis: cytoplasmic dynein is a major microtubule associated protein. *Cell motility and the cytoskeleton*. 14:491-500.

Colombié, N., A.A. Głuszek, A.M. Meireles, and H. Ohkura. 2013. Meiosis-specific stable binding of augmin to acentrosomal spindle poles promotes biased microtubule assembly in oocytes. *PLoS genetics*. 9:e1003562-e1003562.

Cooley, L., and W.E. Theurkauf. 1994. Cytoskeletal functions during Drosophila oogenesis. *Science (New York, N.Y.)*. 266:590-596.

Crane, R., B. Gadea, L. Littlepage, H. Wu, and J.V. Ruderman. 2004. Aurora A, meiosis and mitosis. *Biology of the cell / under the auspices of the European Cell Biology Organization*. 96:215-229.

Cummings, M.R., and R.C. King. 1969. The cytology of the vitellogenic stages of oogenesis inDrosophila melanogaster. I. General staging characteristics. *Journal of Morphology*. 128:427-441.

Davoli, T., A.W. Xu, K.E. Mengwasser, L.M. Sack, J.C. Yoon, P.J. Park, and S.J. Elledge. 2013. Cumulative haploinsufficiency and triplosensitivity drive aneuploidy patterns and shape the cancer genome. *Cell*. 155:948-962.

Debec, A., and C. Abbadie. 1989. The acentriolar state of the Drosophila cell lines 1182. *Biology of the cell / under the auspices of the European Cell Biology Organization*. 67:307-311.

Deng, W., and H. Lin. 2001. Asymmetric germ cell division and oocyte determination during Drosophila oogenesis. *International review of cytology*. 203:93-138.

Denison, C., and T. Kodadek. 2004. Toward a general chemical method for rapidly mapping multi-protein complexes. *Journal of proteome research*. 3:417-425.

Desai, A., and T.J. Mitchison. 1997. Microtubule polymerization dynamics. *Annual review of cell and developmental biology*. 13:83-117.

Desai, A., S. Verma, T.J. Mitchison, and C.E. Walczak. 1999. Kin I Kinesins Are Microtubule-Destabilizing Enzymes. *Cell*. 96:69-78.

Dimitrov, A., M. Quesnoit, S. Moutel, I. Cantaloube, C. Poüs, and F. Perez. 2008. Detection of GTP-tubulin conformation in vivo reveals a role for GTP remnants in microtubule rescues. *Science (New York, N.Y.)*. 322:1353-1356.

Dix, C.I., and J.W. Raff. 2007. Drosophila Spd-2 recruits PCM to the sperm centriole, but is dispensable for centriole duplication. *Current biology : CB*. 17:1759-1764.

Dodson, C.A., and R. Bayliss. 2012. Activation of Aurora-A kinase by protein partner binding and phosphorylation are independent and synergistic. *The Journal of biological chemistry*. 287:1150-1157.

Doerflinger, H., N. Vogt, I.L. Torres, V. Mirouse, I. Koch, C. Nüsslein-Volhard, and D. St Johnston. 2010. Bazooka is required for polarisation of the Drosophila anterior-posterior axis. *Development (Cambridge, England)*. 137:1765-1773.

Douglas, M.E., and M. Mishima. 2010. Still entangled: assembly of the central spindle by multiple microtubule modulators. *Seminars in cell & developmental biology*. 21:899-908.

Drechsel, D.N., and M.W. Kirschner. 1994. The minimum GTP cap required to stabilize microtubules. *Current biology : CB*. 4:1053-1061.

Du, L., J. Xu, X. Li, N. Ma, Y. Liu, J. Peng, M. Osato, W. Zhang, and Z. Wen. 2011. Rumba and Haus3 are essential factors for the maintenance of hematopoietic stem/progenitor cells during zebrafish hematopoiesis. *Development (Cambridge, England)*. 138:619-629.

Duncan, T., and J.G. Wakefield. 2011. 50 Ways To Build a Spindle: the Complexity of Microtubule Generation During Mitosis. *Chromosome research an international journal on the molecular supramolecular and evolutionary aspects of chromosome biology*:321-333.

Dutcher, S.K., N.S. Morrissette, A.M. Preble, C. Rackley, and J. Stanga. 2002. Epsilon-tubulin is an essential component of the centriole. *Mol Biol Cell*. 13:3859-3869.

Dutcher, S.K., and E.C. Trabuco. 1998. The UNI3 gene is required for assembly of basal bodies of Chlamydomonas and encodes delta-tubulin, a new member of the tubulin superfamily. *Mol Biol Cell*. 9:1293-1308.

Erickson, H.P. 1974. Assembly of microtubules from preformed, ring-shaped protofilaments and 6-S tubulin. *Journal of supramolecular structure*. 2:393-411.

Erickson, H.P., and D. Stoffler. 1996. Protofilaments and rings, two conformations of the tubulin family conserved from bacterial FtsZ to alpha/beta and gamma tubulin. *The Journal of cell biology*. 135:5-8.

Espreafico, E.M., D.E. Coling, V. Tsakraklides, K. Krogh, J.S. Wolenski, G. Kalinec, and B. Kachar. 1998. Localization of myosin-V in the centrosome. *Proceedings of the National Academy of Sciences of the United States of America*. 95:8636-8641.

Evans, L., T. Mitchison, and M. Kirschner. 1985. Influence of the centrosome on the structure of nucleated microtubules. *The Journal of cell biology*. 100:1185-1191.

Fava, F., B. Raynaud-Messina, J. Leung-Tack, L. Mazzolini, M. Li, J.C. Guillemot, D. Cachot, Y. Tollon, P. Ferrara, and M. Wright. 1999. Human 76p: A new member of the gamma-tubulin-associated protein family. *The Journal of cell biology*. 147:857-868.

Ferretti, R., V. Palumbo, A. Di Savino, S. Velasco, M. Sbroggiò, P. Sportoletti, L. Micale, E. Turco, L. Silengo, G. Palumbo, E. Hirsch, J. Teruya-Feldstein, S. Bonaccorsi, P.P. Pandolfi, M. Gatti, G. Tarone, and M. Brancaccio. 2010. Morgana/chp-1, a ROCK inhibitor involved in centrosome duplication and tumorigenesis. *Developmental cell*. 18:486-495.

Fisher, D., L. Krasinska, D. Coudreuse, and B. Novák. 2012. Phosphorylation network dynamics in the control of cell cycle transitions. *Journal of cell science*. 125:4703-4711.

Foe, V.E., and B.M. Alberts. 1983. Studies of nuclear and cytoplasmic behaviour during the five mitotic cycles that precede gastrulation in Drosophila embryogenesis. *Journal of cell science*. 61:31-70.

Forler, D., T. Köcher, M. Rode, M. Gentzel, E. Izaurralde, and M. Wilm. 2003. An efficient protein complex purification method for functional proteomics in higher eukaryotes. *Nature biotechnology*. 21:89-92.

Fourniol, F.J., C.V. Sindelar, B. Amigues, D.K. Clare, G. Thomas, M. Perderiset, F. Francis, A. Houdusse, and C.A. Moores. 2010. Template-free 13-protofilament microtubule-MAP assembly visualized at 8 A resolution. *The Journal of cell biology*. 191:463-470.

Fu, J., M. Bian, Q. Jiang, and C. Zhang. 2007. Roles of Aurora kinases in mitosis and tumorigenesis. *Molecular cancer research : MCR*. 5:1-10.

Fülöp, V., and D.T. Jones. 1999. Beta propellers: structural rigidity and functional diversity. *Current opinion in structural biology*. 9:715-721.

Gabriel, M.L., and S. Fogel. 1955. Great Experiments in Biology. Prentice-Hall, Inc., Englewood Cliffs, N. J.

Gardner, M.K., M. Zanic, C. Gell, V. Bormuth, and J. Howard. 2011. Depolymerizing kinesins Kip3 and MCAK shape cellular microtubule architecture by differential control of catastrophe. *Cell*. 147:1092-1103.

Gatlin, J.C., and K. Bloom. 2010. Microtubule motors in eukaryotic spindle assembly and maintenance. *Seminars in cell & developmental biology*. 21:248-254.

Giansanti, M.G., E. Bucciarelli, S. Bonaccorsi, and M. Gatti. 2008. Drosophila SPD-2 is an essential centriole component required for PCM recruitment and astral-microtubule nucleation. *Current biology : CB*. 18:303-309.

Gibbons, I.R. 1963. Studies on the protein components of cilia from Tetrahymena pyriformis. *Proceedings of the National Academy of Sciences of the United States of America*. 50:1002-1010.

Gibbons, I.R., and A.J. Rowe. 1965. Dynein: A Protein with Adenosine Triphosphatase Activity from Cilia. *Science (New York, N.Y.)*. 149:424-426.

Giot, L., J.S. Bader, C. Brouwer, A. Chaudhuri, B. Kuang, Y. Li, Y.L. Hao, C.E. Ooi, B. Godwin, E. Vitols, G. Vijayadamodar, P. Pochart, H. Machineni, M. Welsh, Y. Kong, B. Zerhusen, R. Malcolm, Z. Varrone, A. Collis, M. Minto, S. Burgess, L. McDaniel, E. Stimpson, F. Spriggs, J. Williams, K. Neurath, N. Ioime, M. Agee, E. Voss, K. Furtak, R. Renzulli, N. Aanensen, S. Carrolla, E. Bickelhaupt, Y. Lazovatsky, A. DaSilva, J. Zhong, C.A. Stanyon, R.L. Finley, K.P. White, M. Braverman, T. Jarvie, S. Gold, M. Leach, J. Knight, R.A. Shimkets, M.P. McKenna, J. Chant, and J.M. Rothberg. 2003. A protein interaction map of Drosophila melanogaster. *Science (New York, N.Y.)*. 302:1727-1736.

González-Reyes, A., H. Elliott, and D. St Johnston. 1995. Polarization of both major body axes in Drosophila by gurken-torpedo signalling. *Nature*. 375:654-658.

Goodenough, U.W., and H.S. StClair. 1975. BALD-2: a mutation affecting the formation of doublet and triplet sets of microtubules in Chlamydomonas reinhardtii. *J Cell Biol*. 66:480-491.

Goodwin, S.S., and R.D. Vale. 2010. Patronin regulates the microtubule network by protecting microtubule minus ends. *Cell*. 143:263-274.

Gordon, D.J., B. Resio, and D. Pellman. 2012. Causes and consequences of aneuploidy in cancer. *Nature reviews. Genetics*. 13:189-203.

Goshima, G., S.S. Goodwin, N. Zhang, J.M. Scholey, R.D. Vale, and N. Stuurman. 2007. Genes Required for Mitotic Spindle Assembly in Drosophila S2 Cells. *Science*. 316:417-421.

Goshima, G., M. Mayer, N. Zhang, N. Stuurman, and R.D. Vale. 2008. Augmin: a protein complex required for centrosome-independent microtubule generation within the spindle. *The Journal of cell biology*. 181:421-429.

Green, N.M. 1975. Advances in Protein Chemistry Volume 29. Elsevier. 85-133 pp.

Gunawardane, R.N. 2000. Characterization and Reconstitution of Drosophila gamma-Tubulin Ring Complex Subunits. *The Journal of Cell Biology*. 151:1513-1524.

Gunawardane, R.N., O.C. Martin, and Y. Zheng. 2003. Characterization of a New γTuRC Subunit with WD Repeats. *Molecular Biology of the Cell*. 14:1017-1026.

Gupta, K.K., M.V. Joyce, A.R. Slabbekoorn, Z.C. Zhu, B.A. Paulson, B. Boggess, and H.V. Goodson. 2010. Probing interactions between CLIP-170, EB1, and microtubules. *Journal of molecular biology*. 395:1049-1062.

Güttinger, S., E. Laurell, and U. Kutay. 2009. Orchestrating nuclear envelope disassembly and reassembly during mitosis. *Nature reviews. Molecular cell biology*. 10:178-191.

Hallen, M.A., J. Ho, C.D. Yankel, and S.A. Endow. 2008. Fluorescence recovery kinetic analysis of gamma-tubulin binding to the mitotic spindle. *Biophysical journal*. 95:3048-3058.

Hamel, E., and C.M. Lin. 1990. Reexamination of the role of nonhydrolyzable guanosine 5'-triphosphate analogues in tubulin polymerization: reaction conditions are a critical factor for effective interactions at the exchangeable nucleotide site. *Biochemistry*. 29:2720-2729.

Hassan, M., H. Watari, A. AbuAlmaaty, Y. Ohba, and N. Sakuragi. 2014. Apoptosis and Molecular Targeting Therapy in Cancer. *BioMed research international*. 2014:150845-150845.

Hauf, S., I.C. Waizenegger, and J.M. Peters. 2001. Cohesin cleavage by separase required for anaphase and cytokinesis in human cells. *Science (New York, N.Y.)*. 293:1320-1323.

Hayward, D., J. Metz, C. Pellacani, and J.G. Wakefield. 2014. Synergy between multiple microtubule-generating pathways confers robustness to centrosome-driven mitotic spindle formation. *Developmental cell*. 28:81-93.

Heald, R., R. Tournebize, T. Blank, R. Sandaltzopoulos, P. Becker, A. Hyman, and E. Karsenti. 1996. Self-organization of microtubules into bipolar spindles around artificial chromosomes in Xenopus egg extracts. *Nature*. 382:420-425.

Heinrichs, A. 2006. The spindle matrix revisited. *Nature Reviews Molecular Cell Biology*. 7:307-307.

Ho, C.-M.K., T. Hotta, Z. Kong, C.J.T. Zeng, J. Sun, Y.-R.J. Lee, and B. Liu. 2011. Augmin plays a critical role in organizing the spindle and phragmoplast microtubule arrays in Arabidopsis. *The Plant cell*. 23:2606-2618.

Homer, H. 2013. The APC/C in female mammalian meiosis I. *Reproduction (Cambridge, England)*. 146:R61-71.

Hoog, J.L., S.M. Huisman, Z. Sebo-Lemke, L. Sandblad, J.R. McIntosh, C. Antony, and D. Brunner. 2011. Electron tomography reveals a flared morphology on growing microtubule ends. *J Cell Sci*. 124:693-698.

Hotta, T., Z. Kong, C.-M.K. Ho, C.J.T. Zeng, T. Horio, S. Fong, T. Vuong, Y.-R.J. Lee, and B. Liu. 2012. Characterization of the Arabidopsis augmin complex

uncovers its critical function in the assembly of the acentrosomal spindle and phragmoplast microtubule arrays. *The Plant cell*. 24:1494-1509.

Huang, B., M.J. Troese, S. Ye, J.T. Sims, N.L. Galloway, D.L. Borjesson, and J.A. Carlyon. 2010. Anaplasma phagocytophilum APH_1387 is expressed throughout bacterial intracellular development and localizes to the pathogen-occupied vacuolar membrane. *Infection and immunity*. 78:1864-1873.

Hughes, J.R., A.M. Meireles, K.H. Fisher, A. Garcia, P.R. Antrobus, A. Wainman, N. Zitzmann, C. Deane, H. Ohkura, and J.G. Wakefield. 2008. A microtubule interactome: complexes with roles in cell cycle and mitosis. *PLoS Biology*. 6:e98-e98.

Hughes, S.E., J.S. Beeler, A. Seat, B.D. Slaughter, J.R. Unruh, E. Bauerly, H.J.G. Matthies, and R.S. Hawley. 2011. Gamma-tubulin is required for bipolar spindle assembly and for proper kinetochore microtubule attachments during prometaphase I in Drosophila oocytes. *PLoS genetics*. 7:e1002209-e1002209.

Hunter, A.W., M. Caplow, D.L. Coy, W.O. Hancock, S. Diez, L. Wordeman, and J. Howard. 2003. The kinesin-related protein MCAK is a microtubule depolymerase that forms an ATP-hydrolyzing complex at microtubule ends. *Molecular cell*. 11:445-457.

Huynh, J.R., and D. St Johnston. 2000. The role of BicD, Egl, Orb and the microtubules in the restriction of meiosis to the Drosophila oocyte. *Development (Cambridge, England)*. 127:2785-2794.

Hwang, L.H., L.F. Lau, D.L. Smith, C.A. Mistrot, K.G. Hardwick, E.S. Hwang, A. Amon, and A.W. Murray. 1998. Budding yeast Cdc20: a target of the spindle checkpoint. *Science (New York, N.Y.).* 279:1041-1044.

Hyman, A.A., S. Salser, D.N. Drechsel, N. Unwin, and T.J. Mitchison. 1992. Role of GTP hydrolysis in microtubule dynamics: information from a slowly hydrolyzable analogue, GMPCPP. *Molecular biology of the cell.* 3:1155-1167.

Inoué, S. 1952. THE EFFECT OF COLCHICINE ON THE MICROSCOPIC AND SUBMICROSCOPIC STRUCTURE OF THE MITOTIC SPINDLE. *Expl Cell Res.* Suppl. 2:305-312.

Inoué, S. 1953. Polarization optical studies of the mitotic spindle. *Chromosoma.* 5:487-500.

Inoué, S., and H. Sato. 1967. Cell motility by labile association of molecules. The nature of mitotic spindle fibers and their role in chromosome movement. *The Journal of general physiology.* 50:Suppl:259-292.

Januschke, J., L. Gervais, L. Gillet, G. Keryer, M. Bornens, and A. Guichet. 2006. The centrosome-nucleus complex and microtubule organization in the Drosophila oocyte. *Development Cambridge England.* 133:129-139.

Jeong, A.L., and Y. Yang. 2013. PP2A function toward mitotic kinases and substrates during the cell cycle. *BMB reports.* 46:289-294.

Joglekar, A.P., K.S. Bloom, and E.D. Salmon. 2010. Mechanisms of force generation by end-on kinetochore-microtubule attachments. *Current opinion in cell biology.* 22:57-67.

Johmura, Y., N.-K. Soung, J.-E. Park, L.-R. Yu, M. Zhou, J.K. Bang, B.-Y. Kim, T.D. Veenstra, R.L. Erikson, and K.S. Lee. 2011. Regulation of microtubule-

based microtubule nucleation by mammalian polo-like kinase 1. *Proceedings of the National Academy of Sciences of the United States of America*. 108:11446-11451.

Joshi, H.C. 1993. Gamma-tubulin: the hub of cellular microtubule assemblies. *BioEssays : news and reviews in molecular, cellular and developmental biology*. 15:637-643.

Kalab, P., R.T. Pu, and M. Dasso. 1999. The ran GTPase regulates mitotic spindle assembly. *Current biology : CB*. 9:481-484.

Kamasaki, T., E. O'Toole, S. Kita, M. Osumi, J. Usukura, J.R. McIntosh, and G. Goshima. 2013. Augmin-dependent microtubule nucleation at microtubule walls in the spindle. *The Journal of cell biology*. 202:25-33.

Karsenti, E., and I. Vernos. 2001. The mitotic spindle: a self-made machine. *Science (New York, N.Y.)*. 294:543-547.

Keates, R.A., and R.H. Hall. 1975. Tubulin requires an accessory protein for self assembly in microtubules. *Nature*. 257:418-421.

Keating, T.J., and G.G. Borisy. 2000. Immunostructural evidence for the template mechanism of microtubule nucleation. *Nature cell biology*. 2:352-357.

Kellogg, D.R., and B.M. Alberts. 1992. Purification of a multiprotein complex containing centrosomal proteins from the Drosophila embryo by chromatography with low-affinity polyclonal antibodies. *Molecular biology of the cell*. 3:1-11.

Kellogg, D.R., C.M. Field, and B.M. Alberts. 1989. Identification of microtubule-associated proteins in the centrosome, spindle, and kinetochore of the early Drosophila embryo. *The Journal of cell biology*. 109:2977-2991.

Khodjakov, A., R.W. Cole, B.R. Oakley, and C.L. Rieder. 2000. Centrosome-independent mitotic spindle formation in vertebrates. *Current Biology*. 10:59-67.

Khodjakov, A., and C.L. Rieder. 1999. The sudden recruitment of gamma-tubulin to the centrosome at the onset of mitosis and its dynamic exchange throughout the cell cycle, do not require microtubules. *The Journal of cell biology*. 146:585-596.

Kiseleva, E., S. Rutherford, L.M. Cotter, T.D. Allen, and M.W. Goldberg. 2001. Steps of nuclear pore complex disassembly and reassembly during mitosis in early Drosophila embryos. *J. Cell Sci.* 114:3607-3618.

Kline-Smith, S.L., and C.E. Walczak. 2004. Mitotic spindle assembly and chromosome segregation: refocusing on microtubule dynamics. *Molecular cell*. 15:317-327.

Koch, E.A., and R.H. Spitzer. 1983. Multiple effects of colchicine on oogenesis in Drosophila: induced sterility and switch of potential oocyte to nurse-cell developmental pathway. *Cell and tissue research*. 228:21-32.

Kollman, J.M., A. Merdes, L. Mourey, and D.A. Agard. 2011. Microtubule nucleation by γ-tubulin complexes. *Nature reviews. Molecular cell biology*. 12:709-721.

Krauss, J., S. López de Quinto, C. Nüsslein-Volhard, and A. Ephrussi. 2009. Myosin-V regulates oskar mRNA localization in the Drosophila oocyte. *Current biology : CB*. 19:1058-1063.

Lajoie-Mazenc, I., Y. Tollon, C. Detraves, M. Julian, A. Moisand, C. Gueth-Hallonet, A. Debec, I. Salles-Passador, A. Puget, and H. Mazarguil. 1994. Recruitment of antigenic gamma-tubulin during mitosis in animal cells:

presence of gamma-tubulin in the mitotic spindle. *Journal of cell science*.
107 (Pt 1:2825-2837.

Lasker, K., F. Förster, S. Bohn, T. Walzthoeni, E. Villa, P. Unverdorben, F. Beck, R.
Aebersold, A. Sali, and W. Baumeister. 2012. Molecular architecture of the
26S proteasome holocomplex determined by an integrative approach.
*Proceedings of the National Academy of Sciences of the United States of
America*. 109:1380-1387.

Lawo, S. 2013. Centrosome and Mitotic Spindle Organization in Human Cells.

Lawo, S., M. Bashkurov, M. Mullin, M.G. Ferreria, R. Kittler, B. Habermann, A.
Tagliaferro, I. Poser, J.R.A. Hutchins, B. Hegemann, D. Pinchev, F.
Buchholz, J.-M. Peters, A.A. Hyman, A.-C. Gingras, and L. Pelletier. 2009.
HAUS, the 8-subunit human Augmin complex, regulates centrosome and
spindle integrity. *Current Biology*. 19:816-826.

Leber, B., B. Maier, F. Fuchs, J. Chi, P. Riffel, S. Anderhub, L. Wagner, A.D. Ho,
J.L. Salisbury, M. Boutros, and A. Krämer. 2010. Proteins required for
centrosome clustering in cancer cells. *Science translational medicine*.
2:33ra38-33ra38.

Ledbetter, M.C. 1963. A "MICROTUBULE" IN PLANT CELL FINE STRUCTURE.
The Journal of Cell Biology. 19:239-250.

Ledbetter, M.C., and K.R. Porter. 1964. Morphology of Microtubules of Plant Cell.
Science. 144:872-874.

Leguy, R., R. Melki, D. Pantaloni, and M.F. Carlier. 2000. Monomeric gamma -
tubulin nucleates microtubules. *The Journal of biological chemistry*.
275:21975-21980.

Liang, Z.-Y., M.A. Hallen, and S.A. Endow. 2009. Mature Drosophila meiosis I spindles comprise microtubules of mixed polarity. *Current biology : CB*. 19:163-168.

Lin, H., and A.C. Spradling. 1993. Germline stem cell division and egg chamber development in transplanted Drosophila germaria. *Developmental biology*. 159:140-152.

Loughlin, R., R. Heald, and F. Nédélec. 2010. A computational model predicts Xenopus meiotic spindle organization. *The Journal of cell biology*. 191:1239-1249.

Ludueña, R.F. 2013. A hypothesis on the origin and evolution of tubulin. *International review of cell and molecular biology*. 302:41-185.

Ma, N., U.S. Tulu, N.P. Ferenz, C. Fagerstrom, A. Wilde, and P. Wadsworth. 2010. Poleward transport of TPX2 in the mammalian mitotic spindle requires dynein, Eg5, and microtubule flux. *Molecular biology of the cell*. 21:979-988.

Ma, X., D.W. Ehrhardt, and W. Margolin. 1996. Colocalization of cell division proteins FtsZ and FtsA to cytoskeletal structures in living Escherichia coli cells by using green fluorescent protein. *Proceedings of the National Academy of Sciences of the United States of America*. 93:12998-13003.

Maccioni, R.B., and V. Cambiazo. 1995. Role of microtubule-associated proteins in the control of microtubule assembly. *Physiological reviews*. 75:835-864.

MacDougall, N., A. Clark, E. MacDougall, and I. Davis. 2003. Drosophila gurken (TGFalpha) mRNA localizes as particles that move within the oocyte in two dynein-dependent steps. *Developmental cell*. 4:307-319.

Mahoney, N.M., G. Goshima, A.D. Douglass, and R.D. Vale. 2006. Making microtubules and mitotic spindles in cells without functional centrosomes. *Current biology : CB*. 16:564-569.

Maia, A.R.R., X. Zhu, P. Miller, G. Gu, H. Maiato, and I. Kaverina. 2013. Modulation of Golgi-associated microtubule nucleation throughout the cell cycle. *Cytoskeleton (Hoboken, N.J.)*. 70:32-43.

Malumbres, M., and M. Barbacid. 2003. RAS oncogenes: the first 30 years. *Nature reviews. Cancer*. 3:459-465.

Mandelkow, E., and E.M. Mandelkow. 1995. Microtubules and microtubule-associated proteins. *Curr Opin Cell Biol*. 7:72-81.

Mandelkow, E.M., E. Mandelkow, and R.A. Milligan. 1991. Microtubule dynamics and microtubule caps: a time-resolved cryo-electron microscopy study. *The Journal of cell biology*. 114:977-991.

Masoud, K., E. Herzog, M.-E. Chabouté, and A.-C. Schmit. 2013. Microtubule nucleation and establishment of the mitotic spindle in vascular plant cells. *The Plant journal : for cell and molecular biology*. 75:245-257.

Matos, I., A.J. Pereira, M. Lince-Faria, L.A. Cameron, E.D. Salmon, and H. Maiato. 2009. Synchronizing chromosome segregation by flux-dependent force equalization at kinetochores. *The Journal of cell biology*. 186:11-26.

Maurer, S.P., F.J. Fourniol, G. Bohner, C.A. Moores, and T. Surrey. 2012. EBs recognize a nucleotide-dependent structural cap at growing microtubule ends. *Cell*. 149:371-382.

McKean, P.G., S. Vaughan, and K. Gull. 2001. The extended tubulin superfamily. *J Cell Sci*. 114:2723-2733.

McNally, F.J., K. Okawa, A. Iwamatsu, and R.D. Vale. 1996. Katanin, the microtubule-severing ATPase, is concentrated at centrosomes. *J Cell Sci*. 109 (Pt 3):561-567.

McNally, F.J., and R.D. Vale. 1993. Identification of katanin, an ATPase that severs and disassembles stable microtubules. *Cell*. 75:419-429.

Megraw, T.L., and T.C. Kaufman. 2000. The centrosome in Drosophila oocyte development. *Current topics in developmental biology*. 49:385-407.

Megraw, T.L., K. Li, L.R. Kao, and T.C. Kaufman. 1999. The centrosomin protein is required for centrosome assembly and function during cleavage in Drosophila. *Development (Cambridge, England)*. 126:2829-2839.

Mehta, A.D., R.S. Rock, M. Rief, J.A. Spudich, M.S. Mooseker, and R.E. Cheney. 1999. Myosin-V is a processive actin-based motor. *Nature*. 400:590-593.

Meireles, A.M., K.H. Fisher, N. Colombié, J.G. Wakefield, and H. Ohkura. 2009. Wac: a new Augmin subunit required for chromosome alignment but not for acentrosomal microtubule assembly in female meiosis. *The Journal of cell biology*. 184:777-784.

Mejillano, M.R., J.S. Barton, J.P. Nath, and R.H. Himes. 1990. GTP analogues interact with the tubulin exchangeable site during assembly and upon binding. *Biochemistry*. 29:1208-1216.

Melki, R., M.F. Carlier, and D. Pantaloni. 1990. Direct evidence for GTP and GDP-Pi intermediates in microtubule assembly. *Biochemistry*. 29:8921-8932.

Meunier, S., and I. Vernos. 2012. Microtubule assembly during mitosis - from distinct origins to distinct functions? *Journal of cell science*. 125:2805-2814.

Meyer, N., and L.Z. Penn. 2008. Reflecting on 25 years with MYC. *Nature reviews. Cancer*. 8:976-990.

Mitchison, T., and M. Kirschner. 1984. Dynamic instability of microtubule growth. *Nature*. 312:237-242.

Mitchison, T.J. 1986. The role of microtubule polarity in the movement of kinesin and kinetochores. *Journal of cell science. Supplement*. 5:121-128.

Mitchison, T.J., and M.W. Kirschner. 1985. Properties of the kinetochore in vitro. I. Microtubule nucleation and tubulin binding. *The Journal of cell biology*. 101:755-765.

Mitchison, T.J., and E.D. Salmon. 2001. Mitosis: a history of division. *Nature cell biology*. 3:E17-21.

Mohri, H. 1968. Amino-acid Composition of "Tubulin" constituting Microtubules of Sperm Flagella. *Nature*. 217:1053-1054.

Moores, C.A., M. Perderiset, F. Francis, J. Chelly, A. Houdusse, and R.A. Milligan. 2004. Mechanism of microtubule stabilization by doublecortin. *Molecular cell*. 14:833-839.

Morgan, T.H. 1910. Sex limited inheritance in Drosophila. *Science (New York, N.Y.)*. 32:120-122.

Moritz, M., M.B. Braunfeld, V. Guénebaut, J. Heuser, and D.A. Agard. 2000. Structure of the gamma-tubulin ring complex: a template for microtubule nucleation. *Nature cell biology*. 2:365-370.

Moritz, M., M.B. Braunfeld, J.W. Sedat, B. Alberts, and D.A. Agard. 1995. Microtubule nucleation by gamma-tubulin-containing rings in the centrosome. *Nature*. 378:638-640.

Muller, H.J. 1927. Artificial transmutation of the gene. *Science (New York, N.Y.)*. 66:84-87.

Murata, T., S. Sonobe, T.I. Baskin, S. Hyodo, S. Hasezawa, T. Nagata, T. Horio, and M. Hasebe. 2005. Microtubule-dependent microtubule nucleation based on recruitment of gamma-tubulin in higher plants. *Nature cell biology*. 7:961-968.

Murphy, D.B., and G.G. Borisy. 1975. Association of high-molecular-weight proteins with microtubules and their role in microtubule assembly in vitro. *Proc Natl Acad Sci U S A*. 72:2696-2700.

Murphy, D.B., K.A. Johnson, and G.G. Borisy. 1977. Role of tubulin-associated proteins in microtubule nucleation and elongation. *Journal of molecular biology*. 117:33-52.

Musacchio, A. 2011. Spindle assembly checkpoint: the third decade. *Philos Trans R Soc Lond B Biol Sci*. 366:3595-3604.

Musacchio, A., and E.D. Salmon. 2007. The spindle-assembly checkpoint in space and time. *Nature reviews. Molecular cell biology*. 8:379-393.

Nakaoka, Y., T. Miki, R. Fujioka, R. Uehara, A. Tomioka, C. Obuse, M. Kubo, Y. Hiwatashi, and G. Goshima. 2012. An inducible RNA interference system in Physcomitrella patens reveals a dominant role of augmin in phragmoplast microtubule generation. *The Plant cell*. 24:1478-1493.

Nicklas, R.B., and C.A. Koch. 1969. Chromosome micromanipulation. 3. Spindle fiber tension and the reorientation of mal-oriented chromosomes. *J Cell Biol*. 43:40-50.

Nicolas, E., N. Chenouard, J.-C. Olivo-Marin, and A. Guichet. 2009. A dual role for actin and microtubule cytoskeleton in the transport of Golgi units from the nurse cells to the oocyte across ring canals. *Molecular biology of the cell*. 20:556-568.

Nilsson, C.L., R. Dillon, A. Devakumar, S.D.H. Shi, M. Greig, J.C. Rogers, B. Krastins, M. Rosenblatt, G. Kilmer, M. Major, B.J. Kaboord, D. Sarracino, T. Rezai, A. Prakash, M. Lopez, Y. Ji, W. Priebe, F.F. Lang, H. Colman, and C.A. Conrad. 2010. Quantitative phosphoproteomic analysis of the STAT3/IL-6/HIF1alpha signaling network: an initial study in GSC11 glioblastoma stem cells. *Journal of proteome research*. 9:430-443.

Nogales, E., K.H. Downing, L.A. Amos, and J. Löwe. 1998. Tubulin and FtsZ form a distinct family of GTPases. *Nature structural biology*. 5:451-458.

Nogales, E., M. Whittaker, R.A. Milligan, and K.H. Downing. 1999. High-resolution model of the microtubule. *Cell*. 96:79-88.

Noon, A.P., N. Vlatković, R. Polański, M. Maguire, H. Shawki, K. Parsons, and M.T. Boyd. 2010. p53 and MDM2 in renal cell carcinoma: biomarkers for disease progression and future therapeutic targets? *Cancer*. 116:780-790.

O'Brien, E.T., and H.P. Erickson. 1989. Assembly of pure tubulin in the absence of free GTP: effect of magnesium, glycerol, ATP, and the nonhydrolyzable GTP analogues. *Biochemistry*. 28:1413-1422.

Oakley, C.E., and B.R. Oakley. 1989. Identification of gamma-tubulin, a new member of the tubulin superfamily encoded by mipA gene of Aspergillus nidulans. *Nature*. 338:662-664.

Oegema, K., C. Wiese, O.C. Martin, R.A. Milligan, A. Iwamatsu, T.J. Mitchison, and Y. Zheng. 1999. Characterization of two related Drosophila gamma-tubulin complexes that differ in their ability to nucleate microtubules. *The Journal of Cell Biology*. 144:721-733.

Oguchi, Y., S. Uchimura, T. Ohki, S.V. Mikhailenko, and S. Ishiwata. 2011. The
bidirectional depolymerizer MCAK generates force by disassembling both
microtubule ends. *Nat Cell Biol*. 13:846-852.

Ohba, T., M. Nakamura, H. Nishitani, and T. Nishimoto. 1999. Self-organization of
microtubule asters induced in Xenopus egg extracts by GTP-bound Ran.
Science (New York, N.Y.). 284:1356-1358.

Olmsted, J.B., J.M. Marcum, K.A. Johnson, C. Allen, and G.G. Borisy. 1974.
Microtuble assembly: some possible regulatory mechanisms. *Journal of
supramolecular structure*. 2:429-450.

Ozon, S., A. Guichet, O. Gavet, S. Roth, and A. Sobel. 2002. Drosophila stathmin:
a microtubule-destabilizing factor involved in nervous system formation.
Molecular biology of the cell. 13:698-710.

Paintrand, M., M. Moudjou, H. Delacroix, and M. Bornens. 1992. Centrosome
organization and centriole architecture: their sensitivity to divalent cations.
Journal of structural biology. 108:107-128.

Parton, R.M., R.S. Hamilton, G. Ball, L. Yang, C.F. Cullen, W. Lu, H. Ohkura, and I.
Davis. 2011. A PAR-1-dependent orientation gradient of dynamic
microtubules directs posterior cargo transport in the Drosophila oocyte. *The
Journal of cell biology*. 194:121-135.

Peters, J.-M. 2006. The anaphase promoting complex/cyclosome: a machine
designed to destroy. *Nature reviews. Molecular cell biology*. 7:644-656.

Petry, S., A.C. Groen, K. Ishihara, T.J. Mitchison, and R.D. Vale. 2013. Branching
microtubule nucleation in Xenopus egg extracts mediated by augmin and
TPX2. *Cell*. 152:768-777.

Petry, S., C. Pugieux, F.J. Nédélec, and R.D. Vale. 2011. Augmin promotes meiotic spindle formation and bipolarity in Xenopus egg extracts. *Proceedings of the National Academy of Sciences of the United States of America*. 108:14473-14478.

Piehl, M., U.S. Tulu, P. Wadsworth, and L. Cassimeris. 2004. Centrosome maturation: measurement of microtubule nucleation throughout the cell cycle by using GFP-tagged EB1. *Proceedings of the National Academy of Sciences of the United States of America*. 101:1584-1588.

Pryer, N.K., R.A. Walker, V.P. Skeen, B.D. Bourns, M.F. Soboeiro, and E.D. Salmon. 1992. Brain microtubule-associated proteins modulate microtubule dynamic instability in vitro. Real-time observations using video microscopy. *Journal of cell science*. 103 (Pt 4:965-976.

Qi, H., U. Rath, Y. Ding, Y. Ji, M.J. Blacketer, J. Girton, J. Johansen, and K.M. Johansen. 2005. EAST interacts with Megator and localizes to the putative spindle matrix during mitosis in Drosophila. *Journal of cellular biochemistry*. 95:1284-1291.

Qi, H., U. Rath, D. Wang, Y.-Z. Xu, Y. Ding, W. Zhang, M.J. Blacketer, M.R. Paddy, J. Girton, J. Johansen, and K.M. Johansen. 2004. Megator, an essential coiled-coil protein that localizes to the putative spindle matrix during mitosis in Drosophila. *Molecular biology of the cell*. 15:4854-4865.

Queenan, A.M., G. Barcelo, C. Van Buskirk, and T. Schupbach. 1999. The transmembrane region of Gurken is not required for biological activity, but is necessary for transport to the oocyte membrane in Drosophila. *Mechanisms of development*. 89:35-42.

Raaijmakers, J.A., and R.H. Medema. 2014. Function and regulation of dynein in mitotic chromosome segregation. *Chromosoma*. 123:407-422.

Rappsilber, J. 2011. The beginning of a beautiful friendship: cross-linking/mass spectrometry and modelling of proteins and multi-protein complexes. *Journal of structural biology*. 173:530-540.

Rath, U., D. Wang, Y. Ding, Y.-Z. Xu, H. Qi, M.J. Blacketer, J. Girton, J. Johansen, and K.M. Johansen. 2004. Chromator, a novel and essential chromodomain protein interacts directly with the putative spindle matrix protein skeletor. *Journal of cellular biochemistry*. 93:1033-1047.

Raynaud-Messina, B., and A. Merdes. 2007. Gamma-tubulin complexes and microtubule organization. *Current Opinion in Cell Biology*. 19:24-30.

Reschen, R.F., N. Colombie, L. Wheatley, J. Dobbelaere, D. St Johnston, H. Ohkura, and J.W. Raff. 2012. Dgp71WD is required for the assembly of the acentrosomal Meiosis I spindle, and is not a general targeting factor for the γ-TuRC. *Biology open*. 1:422-429.

Rivero, S., J. Cardenas, M. Bornens, and R.M. Rios. 2009. Microtubule nucleation at the cis-side of the Golgi apparatus requires AKAP450 and GM130. *The EMBO journal*. 28:1016-1028.

Robinson, D.N., K. Cant, and L. Cooley. 1994. Morphogenesis of Drosophila ovarian ring canals. *Development*. 120:2015-2025.

Roostalu, J., and T. Surrey. 2013. The multiple talents of kinesin-8. *Nat Cell Biol*. 15:889-891.

Rösli, C., J.-N. Rybak, D. Neri, and G. Elia. 2008. Quantitative recovery of biotinylated proteins from streptavidin-based affinity chromatography resins. *Methods in molecular biology (Clifton, N.J.)*. 418:89-100.

Rothbauer, U., K. Zolghadr, S. Muyldermans, A. Schepers, M.C. Cardoso, and H. Leonhardt. 2008. A versatile nanotrap for biochemical and functional studies with fluorescent fusion proteins. *Molecular & cellular proteomics : MCP*. 7:282-289.

Ruiz, F., N. Garreau de Loubresse, and J. Beisson. 1987. A mutation affecting basal body duplication and cell shape in Paramecium. *J Cell Biol*. 104:417-430.

Ruiz, F., A. Krzywicka, C. Klotz, A. Keller, J. Cohen, F. Koll, G. Balavoine, and J. Beisson. 2000. The SM19 gene, required for duplication of basal bodies in Paramecium, encodes a novel tubulin, eta-tubulin. *Curr Biol*. 10:1451-1454.

Rybak, J.-N., S.B. Scheurer, D. Neri, and G. Elia. 2004. Purification of biotinylated proteins on streptavidin resin: a protocol for quantitative elution. *Proteomics*. 4:2296-2299.

Salmon, E.D. 2005. Microtubules: a ring for the depolymerization motor. *Current biology : CB*. 15:R299-302.

Sapp, J. 1994. Evolution by Association : A History of Symbiosis. Oxford University Press. 272 pp.

Sarhadi, V.K., L. Lahti, I. Scheinin, A. Tyybäkinoja, S. Savola, A. Usvasalo, R. Räty, E. Elonen, P. Ellonen, U.M. Saarinen-Pihkala, and S. Knuutila. 2013. Targeted resequencing of 9p in acute lymphoblastic leukemia yields concordant results with array CGH and reveals novel genomic alterations. *Genomics*. 102:182-188.

Schöckel, L., M. Möckel, B. Mayer, D. Boos, and O. Stemmann. 2011. Cleavage of cohesin rings coordinates the separation of centrioles and chromatids. *Nature cell biology*. 13:966-972.

Shah, S.P., R.D. Morin, J. Khattra, L. Prentice, T. Pugh, A. Burleigh, A. Delaney, K. Gelmon, R. Guliany, J. Senz, C. Steidl, R.A. Holt, S. Jones, M. Sun, G. Leung, R. Moore, T. Severson, G.A. Taylor, A.E. Teschendorff, K. Tse, G. Turashvili, R. Varhol, R.L. Warren, P. Watson, Y. Zhao, C. Caldas, D. Huntsman, M. Hirst, M.A. Marra, and S. Aparicio. 2009. Mutational evolution in a lobular breast tumour profiled at single nucleotide resolution. *Nature*. 461:809-813.

Sharp, D.J., and G.C. Rogers. 2004. A Kin I-dependent Pacman-flux mechanism for anaphase A. *Cell cycle (Georgetown, Tex.)*. 3:707-710.

Shelanski, M.L. 1968. Properties of the rotein subunit of central-pair and outer-doublet microtubules of sea urchin flagella. *The Journal of Cell Biology*. 38:304-315.

Stearns, T., L. Evans, and M. Kirschner. 1991. Gamma-tubulin is a highly conserved component of the centrosome. *Cell*. 65:825-836.

Steinhauer, J., and D. Kalderon. 2006. Microtubule polarity and axis formation in the Drosophila oocyte. *Developmental dynamics : an official publication of the American Association of Anatomists*. 235:1455-1468.

Stephens, R.E. 1970. Thermal fractionation of outer fiber doublet microtubules into A- and B-subfiber components: A- and B-tubulin. *Journal of Molecular Biology*. 47:353-363.

Stephenson, R., and N.H. Metcalfe. 2013. Drosophila melanogaster: a fly through its history and current use. *The journal of the Royal College of Physicians of Edinburgh*. 43:70-75.

Stevens, N.R., A.A.S.F. Raposo, R. Basto, D. St Johnston, and J.W. Raff. 2007. From stem cell to embryo without centrioles. *Current biology : CB*. 17:1498-1503.

Stevenson, V., A. Hudson, L. Cooley, and W.E. Theurkauf. 2002. Arp2/3-dependent pseudocleavage [correction of psuedocleavage] furrow assembly in syncytial Drosophila embryos. *Current biology : CB*. 12:705-711.

Stewart, R.J., K.W. Farrell, and L. Wilson. 1990. Role of GTP hydrolysis in microtubule polymerization: evidence for a coupled hydrolysis mechanism. *Biochemistry*. 29:6489-6498.

Stirnimann, C.U., E. Petsalaki, R.B. Russell, and C.W. Müller. 2010. WD40 proteins propel cellular networks. *Trends in biochemical sciences*. 35:565-574.

Sung, H.-H., I.A. Telley, P. Papadaki, A. Ephrussi, T. Surrey, and P. Rørth. 2008. Drosophila ensconsin promotes productive recruitment of Kinesin-1 to microtubules. *Developmental cell*. 15:866-876.

Syred, H.M., J. Welburn, J. Rappsilber, and H. Ohkura. 2013. Cell cycle regulation of microtubule interactomes: multi-layered regulation is critical for the interphase/mitosis transition. *Molecular & cellular proteomics : MCP*. 12:3135-3147.

Tadros, W., and H.D. Lipshitz. 2009. The maternal-to-zygotic transition: a play in two acts. *Development (Cambridge, England)*. 136:3033-3042.

Tanaka, K. 2013. Regulatory mechanisms of kinetochore-microtubule interaction in mitosis. *Cellular and molecular life sciences : CMLS*. 70:559-579.

Tanaka, T., and A. Nakamura. 2008. The endocytic pathway acts downstream of Oskar in Drosophila germ plasm assembly. *Development (Cambridge, England)*. 135:1107-1117.

Tanenbaum, M.E., and R.H. Medema. 2010. Mechanisms of centrosome separation and bipolar spindle assembly. *Dev Cell*. 19:797-806.

Tavosanis, G., and C. Gonzalez. 2003. gamma-Tubulin function during female germ-cell development and oogenesis in Drosophila. *Proceedings of the National Academy of Sciences of the United States of America*. 100:10263-10268.

Taylor, E.W. 1965. The mechanism of colchicine inhibition of mitosis. I. Kinetics of inhibition and the binding of H3-colchcine. *The Journal of cell biology*. 25:SUPPL:145-160.

Teixidó-Travesa, N., J. Villén, C. Lacasa, M.T. Bertran, M. Archinti, S.P. Gygi, C. Caelles, J. Roig, and J. Lüders. 2010. The γTuRC Revisited: A Comparative Analysis of Interphase and Mitotic Human γTuRC Redefines the Set of Core Components and Identifies the Novel Subunit GCP8. *Molecular Biology of the Cell*. 21:3963-3972.

Theurkauf, W.E. 1994. Microtubules and cytoplasm organization during Drosophila oogenesis. *Developmental biology*. 165:352-360.

Theurkauf, W.E., B.M. Alberts, Y.N. Jan, and T.A. Jongens. 1993. A central role for microtubules in the differentiation of Drosophila oocytes. *Development Cambridge England*. 118:1169-1180.

Theurkauf, W.E., S. Smiley, M.L. Wong, and B.M. Alberts. 1992. Reorganization of the cytoskeleton during Drosophila oogenesis: implications for axis

specification and intercellular transport. *Development (Cambridge, England)*. 115:923-936.

Thompson, A., J. Schäfer, K. Kuhn, S. Kienle, J. Schwarz, G. Schmidt, T. Neumann, and C. Hamon. 2003. Tandem Mass Tags: A Novel Quantification Strategy for Comparative Analysis of Complex Protein Mixtures by MS/MS. *Analytical Chemistry*. 75:1895-1904.

Tooley, J., and P.T. Stukenberg. 2011. The Ndc80 complex: integrating the kinetochore's many movements. *Chromosome research : an international journal on the molecular, supramolecular and evolutionary aspects of chromosome biology*. 19:377-391.

Tournebize, R., A. Popov, K. Kinoshita, A.J. Ashford, S. Rybina, A. Pozniakovsky, T.U. Mayer, C.E. Walczak, E. Karsenti, and A.A. Hyman. 2000. Control of microtubule dynamics by the antagonistic activities of XMAP215 and XKCM1 in Xenopus egg extracts. *Nature cell biology*. 2:13-19.

Tran, P.T., P. Joshi, and E.D. Salmon. 1997. How tubulin subunits are lost from the shortening ends of microtubules. *Journal of structural biology*. 118:107-118.

Tsai, C.Y., B. Ngo, A. Tapadia, P.-H. Hsu, G. Wu, and W.-H. Lee. 2011. Aurora-A phosphorylates Augmin complex component Hice1 protein at an N-terminal serine/threonine cluster to modulate its microtubule binding activity during spindle assembly. *The Journal of biological chemistry*. 286:30097-30106.

Uehara, R., R.-s. Nozawa, A. Tomioka, S. Petry, R.D. Vale, C. Obuse, and G. Goshima. 2009. The augmin complex plays a critical role in spindle microtubule generation for mitotic progression and cytokinesis in human cells. *Proceedings of the National Academy of Sciences of the United States of America*. 106:6998-7003.

Uhlén, M., E. Björling, C. Agaton, C.A.-K. Szigyarto, B. Amini, E. Andersen, A.-C. Andersson, P. Angelidou, A. Asplund, C. Asplund, L. Berglund, K. Bergström, H. Brumer, D. Cerjan, M. Ekström, A. Elobeid, C. Eriksson, L. Fagerberg, R. Falk, J. Fall, M. Forsberg, M.G. Björklund, K. Gumbel, A. Halimi, I. Hallin, C. Hamsten, M. Hansson, M. Hedhammar, G. Hercules, C. Kampf, K. Larsson, M. Lindskog, W. Lodewyckx, J. Lund, J. Lundeberg, K. Magnusson, E. Malm, P. Nilsson, J. Odling, P. Oksvold, I. Olsson, E. Oster, J. Ottosson, L. Paavilainen, A. Persson, R. Rimini, J. Rockberg, M. Runeson, A. Sivertsson, A. Sköllermo, J. Steen, M. Stenvall, F. Sterky, S. Strömberg, M. Sundberg, H. Tegel, S. Tourle, E. Wahlund, A. Waldén, J. Wan, H. Wernérus, J. Westberg, K. Wester, U. Wrethagen, L.L. Xu, S. Hober, and F. Pontén. 2005. A human protein atlas for normal and cancer tissues based on antibody proteomics. *Molecular & cellular proteomics : MCP*. 4:1920-1932.

Uhlmann, F., F. Lottspeich, and K. Nasmyth. 1999. Sister-chromatid separation at anaphase onset is promoted by cleavage of the cohesin subunit Scc1. *Nature*. 400:37-42.

Uhlmann, F., D. Wernic, M.A. Poupart, E.V. Koonin, and K. Nasmyth. 2000. Cleavage of cohesin by the CD clan protease separin triggers anaphase in yeast. *Cell*. 103:375-386.

Vale, R.D. 1991. Severing of stable microtubules by a mitotically activated protein in Xenopus egg extracts. *Cell*. 64:827-839.

Vale, R.D., T.S. Reese, and M.P. Sheetz. 1985. Identification of a novel force-generating protein, kinesin, involved in microtubule-based motility. *Cell*. 42:39-50.

Vaughan, S., M. Shaw, and K. Gull. 2006. A post-assembly structural modification to the lumen of flagellar microtubule doublets. *Curr Biol*. 16:R449-450.

Venken, K.J.T., and H.J. Bellen. 2014. Chemical mutagens, transposons, and transgenes to interrogate gene function in Drosophila melanogaster. *Methods (San Diego, Calif.)*. 68:15-28.

Vernos, I., and E. Karsenti. 1996. Motors involved in spindle assembly and chromosome segregation. *Current Opinion in Cell Biology*. 8:4-9.

Vérollet, C., N. Colombié, T. Daubon, H.-M. Bourbon, M. Wright, and B. Raynaud-Messina. 2006. Drosophila melanogaster gamma-TuRC is dispensable for targeting gamma-tubulin to the centrosome and microtubule nucleation. *The Journal of cell biology*. 172:517-528.

Vogt, N., I. Koch, H. Schwarz, F. Schnorrer, and C. Nüsslein-Volhard. 2006. The gammaTuRC components Grip75 and Grip128 have an essential microtubule-anchoring function in the Drosophila germline. *Development (Cambridge, England)*. 133:3963-3972.

Voter, W.A., E.T. O'Brien, and H.P. Erickson. 1991. Dilution-induced disassembly of microtubules: relation to dynamic instability and the GTP cap. *Cell motility and the cytoskeleton*. 18:55-62.

Wagner, R.P. 1999. Rudolph Virchow and the Genetic Basis of Somatic Ecology. *Genetics*. 151:917-920.

Wainman, A., D.W. Buster, T. Duncan, J. Metz, A. Ma, D. Sharp, and J.G. Wakefield. 2009. A new Augmin subunit, Msd1, demonstrates the importance of mitotic spindle-templated microtubule nucleation in the absence of functioning centrosomes. *Genes & development*. 23:1876-1881.

Walczak, C.E. 2006. Kinesin-8s: motoring and depolymerizing. *Nat Cell Biol.* 8:903-905.

Walker, D.L., D. Wang, Y. Jin, U. Rath, Y. Wang, J. Johansen, and K.M. Johansen. 2000. Skeletor, a novel chromosomal protein that redistributes during mitosis provides evidence for the formation of a spindle matrix. *The Journal of cell biology.* 151:1401-1412.

Walker, R.A., N.K. Pryer, and E.D. Salmon. 1991. Dilution of individual microtubules observed in real time in vitro: evidence that cap size is small and independent of elongation rate. *The Journal of cell biology.* 114:73-81.

Wall, M.A., D.E. Coleman, E. Lee, J.A. Iñiguez-Lluhi, B.A. Posner, A.G. Gilman, and S.R. Sprang. 1995. The structure of the G protein heterotrimer Gi alpha 1 beta 1 gamma 2. *Cell.* 83:1047-1058.

Weisenberg, R.C. 1972. Microtubule formation in vitro in solutions containing low calcium concentrations. *Science.* 177:1104-1105.

Weisenberg, R.C., G.G. Borisy, and E.W. Taylor. 1968a. The colchicine-binding protein of mammalian brain and its relation to microtubules. *Biochemistry.* 7:4466-4479.

Weisenberg, R.C., G.G. Broisy, and E.W. Taylor. 1968b. Colchicine-binding protein of mammalian brain and its relation to microtubules. *Biochemistry.* 7:4466-4479.

Weiss, E.L. 2012. Mitotic exit and separation of mother and daughter cells. *Genetics.* 192:1165-1202.

Westermann, S., H.-W. Wang, A. Avila-Sakar, D.G. Drubin, E. Nogales, and G. Barnes. 2006. The Dam1 kinetochore ring complex moves processively on depolymerizing microtubule ends. *Nature.* 440:565-569.

White, E.A., and M. Glotzer. 2012. Centralspindlin: at the heart of cytokinesis. *Cytoskeleton (Hoboken, N.J.)*. 69:882-892.

Wiese, C., and Y. Zheng. 2000. A new function for the gamma-tubulin ring complex as a microtubule minus-end cap. *Nature cell biology*. 2:358-364.

Wilde, A., and Y. Zheng. 1999. Stimulation of microtubule aster formation and spindle assembly by the small GTPase Ran. *Science (New York, N.Y.)*. 284:1359-1362.

Wilson, E.B. 1911. The Cell in Development and Inheritance.

Woodruff, J.B., O. Wueseke, and A.A. Hyman. 2014. Pericentriolar material structure and dynamics. *Philosophical transactions of the Royal Society of London. Series B, Biological sciences*. 369.

Wu, G., Y.-T. Lin, R. Wei, Y. Chen, Z. Shan, and W.-H. Lee. 2008. Hice1, a novel microtubule-associated protein required for maintenance of spindle integrity and chromosomal stability in human cells. *Molecular and cellular biology*. 28:3652-3662.

Wu, G., R. Wei, E. Cheng, B. Ngo, and W.-H. Lee. 2009. Hec1 contributes to mitotic centrosomal microtubule growth for proper spindle assembly through interaction with Hice1. *Molecular biology of the cell*. 20:4686-4695.

Wu, X., B. Kocher, Q. Wei, and J.A. Hammer. 1998. Myosin Va associates with microtubule-rich domains in both interphase and dividing cells. *Cell motility and the cytoskeleton*. 40:286-303.

Zhang, D., G.C. Rogers, D.W. Buster, and D.J. Sharp. 2007. Three microtubule severing enzymes contribute to the "Pacman-flux" machinery that moves chromosomes. *The Journal of cell biology*. 177:231-242.

Zhang, J., and T.L. Megraw. 2007. Proper recruitment of gamma-tubulin and D-TACC/Msps to embryonic Drosophila centrosomes requires Centrosomin Motif 1. *Molecular biology of the cell*. 18:4037-4049.

Zheng, Y., M.K. Jung, and B.R. Oakley. 1991. Gamma-tubulin is present in Drosophila melanogaster and Homo sapiens and is associated with the centrosome. *Cell*. 65:817-823.

Zheng, Y., M.L. Wong, B. Alberts, and T. Mitchison. 1995. Nucleation of microtubule assembly by a gamma-tubulin-containing ring complex. *Nature*. 378:578-583.

Zhu, H., J.A. Coppinger, C.-Y. Jang, J.R. Yates, and G. Fang. 2008. FAM29A promotes microtubule amplification via recruitment of the NEDD1-gamma-tubulin complex to the mitotic spindle. *The Journal of cell biology*. 183:835-848.

Zhu, H., K. Fang, and G. Fang. 2009. FAM29A, a target of Plk1 regulation, controls the partitioning of NEDD1 between the mitotic spindle and the centrosomes. *Journal of Cell Science*. 122:2750-2759.

Zhu, X., J. Sen, L. Stevens, J.S. Goltz, and D. Stein. 2005. Drosophila pipe protein activity in the ovary and the embryonic salivary gland does not require heparan sulfate glycosaminoglycans. *Development (Cambridge, England)*. 132:3813-3822.

Appendix

Control 1 / Augmin 1	Control 1/ Augmin 2	Control 1/ Augmin 3
Ccs	VGAT	CG11619
dgt4	Nrg	didum
dgt6	CG31357	bt
wac	ball	dgt4
dgt5	Bsg	msd1
msd5	CG32506	dgt6
dgt2	Hira	CG5355
msd1	RpS12	CG3262
dgt3	CG3262	wac
ome	CG5359	BigH1
CG9603	Brd8	dgt5
CG13449	Orc2	Trxr-1
Vha100-1	puf	msd5
CG14476	Prpk	Dcp-1
lqfR	cathD	dgt2
Xe7	CG11577	lqfR
GCC185	Pgam5	His1:CG33858
CG11619	CG12592	CG17896
RpS30	didum	Xe7
didum	Rpb7	kz
CG10237	RagC-D	Mhc
CG9795	for	dor
mRpS31	Ranbp16	GCC185
Rif1	CG14516	CG43208

CG5525	Rpt4R	mld
Dcp-1	CHIP	mud
Trxr-1	mop	EfTuM
Rab14	mRpL52	CG17493
kz	CG1598	PyK
CG17202	Sh3beta	CG10465
mud	CG1970	dgt3
Sym	Dlc90F	Aats-ala
Tcp-1eta	mRpS11	CG5664
Rab10	MED6	Ack-like
CG5664	BRWD3	CG12170
ArfGAP1	skpA	for
G9a	mRpS35	ome
CG7246	thoc6	CG4968
vir	CG4164	CG9125
jar	CG17150	CG6937
Dbp80	Nup44A	CG14215
gw	Ack-like	fab1
DNA-ligI	MED23	Mtpalpha
CG11779	CG1316	nuf
CG14651	msd1	CG17078
fs(1)Ya	Cul5	CG5592
cnn	ash2	Prpk
Cct1	CG9125	Klp98A
CG16734	CG33233	tud
ro	CG9547	Sam-S

Control 2 / Augmin 1	Control 2 / Augmin 2	Control 2 / Augmin 3
Ccs	VGAT	Ccs
CG11449	Nrg	CG11449
Vha100-1	dgt6	Hsc70-1
CG13449	CG9547	Vha100-1
Hsc70-1	msd5	ome
ome	CG10418	CG13449
ro	CG1399	ro
ric8a	dgt4	CG13217
CG9603	wac	r-l
CG10748	PlexA	ric8a
lilli	CG31357	lilli
CG13217	CG13217	lqfR
CG6118	msd1	mRpS31
mRpS31	ms(3)72Dt	kz
CG10418	Nrk	CG6118
dgt4	dgt2	CG9394
r-l	Hsc70-1	CG10418
lqfR	MSBP	Atg16
CG9394	CG4586	CG5355
Cht11	l(1)10Bb	DppIII
kz	Nopp140	ms(3)72Dt
dgt6	Mhc	CG10748
CoVa	Csp	CG9603
Atg16	CG4164	Aats-val
Sep2	Brd8	CG17202
Sry-beta	ric8a	Cht11

Clect27	CG7139	CG6654
CG17202	CG17202	CG5613
ms(3)72Dt	Acn	Sep2
RpS30	ball	Sod
CG6654	CG1309	CG16734
CG16734	CG8783	CoVa
enc	CG42497	Pglym78
Aats-val	Psn	dgt6
CG16985	HDAC6	Xe7
wac	mRpS35	TfIIEbeta
ssp2	IntS3	beta4GalNAcTA
Nrk	dgt5	bt
Aatf	CG13457	dgt4
CG4586	S-Lap5	GCC185
Xe7	capu	Argk
CG5613	CG8892	CG4586
Nmd3	Sem1	nuf
ari-1	Pten	mwh
Gapdh1	ash1	Aatf
CG7971	d4	CG16985
cana	ari-1	Yp2
GCC185	lap	Sry-beta
mwh	CG9246	CG1532
128up	Drep-2	dsx

Control 3 / Augmin 1	Control 3 / Augmin 2	Control 3 / Augmin 3

CG14476	Nrg	dgt4
dgt4	VGAT	DNA-ligI
Ccs	CG31357	dgt6
CG6453	Bsg	CG11779
dgt6	ball	CG11619
ArfGAP1	Brd8	CG8108
DNA-ligI	RpS12	Vps13
Cam	Hira	l(1)G0289
wac	Pgam5	eIF5B
pelo	CG32506	msd1
CG3800	Orc2	CG10237
TppII	CG3800	Tcp-1eta
CG5168	CG14516	dgt5
CG8108	puf	Mtpalpha
dgt5	CG1598	wac
CG12288	CG12592	Lpin
pcm	Sh3beta	Rpn13
CG10237	Rpt4R	Lsd-2
ArfGAP3	CG5359	CG3800
Tcp-1eta	CG9922	dgt2
l(1)G0289	mRpS11	Sh3beta
CstF-64	l(1)G0289	Prosalpha7
Map205	Ranbp16	Prosbeta6
dgt3	CG9547	TppII
RanGAP	mRpL52	CG7461
Bre1	CstF-64	Prosbeta1
Ripalpha	CHIP	Prosbeta7

Sym	MED6	Prosalpha3
Bsg	Prpk	Prosbeta4
ash1	CG11577	Prosalpha5
CG3689	Rpb7	msd5
RpS30	CG33233	Bsg
Prosalpha5	mop	CG5384
Prosbeta4	cathD	l(3)76BDr
CG14712	ste24a	Rab14
CaMKII	tomb	dgt3
Vps13	Ca-P60A	CG9323
ste24a	wls	Sym
l(1)G0320	fax	CG9796
CG11779	ash1	Hrb98DE
Prosalpha2	Prosbeta1	Drp1
Cdk12	MED23	Prosbeta3
CG10748	CG4281	Psn
dgt2	RagC-D	CG12159
l(3)76BDr	Uch-L5	CG17202
Prosbeta1	Dlc90F	Prosalpha6
l(2)not	Sec61alpha	asparagine-synthetase
fon	blp	qkr58E-1
rump	CG34132	SmB
mRpS21	CG8108	Rpn9

Appendix Table 1- List of top 50 proteins based on TMT ratios after normalising to Tubulin, with Augmin subunits highlighted in yellow, and Didum highlighted in red.

Protein 1	Linkage 1	Protein 2	Linkage 2	notes
Dgt2	209	Dgt2	217	between proteins
Dgt5	116	Dgt5	123	between proteins
Dgt5	92	Dgt5	102	between proteins
Dgt5	97	Dgt5	100	between proteins
Dgt6	23	Dgt6	143	between proteins
Dgt6	23	Dgt6	71	between proteins
Dgt6	352	Dgt6	359	between proteins
Dgt6	362	Dgt6	390	between proteins
Dgt6	390	Dgt6	462	between proteins
Dgt6	462	Dgt6	475	between proteins
Msd1	240	Msd1	305	between proteins
Msd1	25	Msd1	110	between proteins
Msd1	25	Msd1	113	between proteins
Msd1	25	Msd1	33	between proteins
Msd1	25	Msd1	45	between proteins
Msd1	25	Msd1	48	between proteins
Msd1	25	Msd1	78	between proteins
Msd1	33	Msd1	100	between proteins
Msd1	33	Msd1	110	between proteins
Msd1	33	Msd1	45	between proteins
Msd1	33	Msd1	78	between proteins
Msd1	44	Msd1	113	between proteins
Msd1	45	Msd1	113	between proteins
Msd1	83	Msd1	113	between proteins

Msd5	26	Msd5	135	between proteins
Wac	123	Wac	140	between proteins
Wac	123	Wac	143	between proteins
Msd1	25	Msd1	25	within protein
Msd1	113	Msd1	113	within protein
Dgt3	508	Dgt2	193	within protein
Dgt3	72	Dgt5	71	within protein
Dgt3	72	Dgt5	73	within protein
Dgt3	119	Dgt5	116	within protein
Dgt3	119	Dgt5	124	within protein
Dgt3	249	Dgt5	297	within protein
Dgt3	322	Dgt5	378	within protein
Dgt3	508	Wac	132	within protein
Dgt2	55	Dgt5	154	within protein
Dgt2	193	Msd1	25	within protein
Dgt2	193	Msd1	113	within protein
Dgt2	193	Wac	132	within protein
Dgt2	193	Wac	143	within protein
Dgt2	214	Wac	143	within protein
Dgt2	214	Wac	146	within protein
Dgt2	217	Wac	143	within protein
Dgt5	625	Wac	132	within protein
Dgt5	632	Wac	140	within protein
Dgt6	237	Msd1	25	within protein
Dgt6	270	Msd1	33	within protein
Dgt6	270	Msd1	78	within protein

Dgt6	190	Msd5	17	within protein
Dgt6	190	Msd5	26	within protein
Msd1	113	Msd5	226	within protein
Dgt4	44	Msd5	86	within protein

Appendix Table 2- List of crosslinked peptides within and between Augmin subunits with 1% FDR search restriction. 29 intra-protein crosslinks, and 25 inter-protein crosslinks were identified.

Protein 1	Linkage 1	Protein 2	Linkage 2	notes
Dgt2	193	Dgt3	508	between proteins
Dgt2	55	Dgt5	154	between proteins
Dgt2	214	Dgt5	653	between proteins
Dgt2	160	Dgt5	124	between proteins
Dgt2	193	Dgt6	545	between proteins
Dgt2	193	Msd1	113	between proteins
Dgt2	193	Msd1	25	between proteins
Dgt2	193	Wac	132	between proteins
Dgt2	214	Wac	146	between proteins
Dgt2	214	Wac	143	between proteins
Dgt2	193	Wac	140	between proteins
Dgt2	217	Wac	143	between proteins
Dgt2	193	Wac	143	between proteins
Dgt2	217	Wac	146	between proteins
Dgt3	72	Dgt5	73	between proteins
Dgt3	72	Dgt5	71	between proteins
Dgt3	119	Dgt5	124	between proteins
Dgt3	119	Dgt5	116	between proteins
Dgt3	249	Dgt5	286	between proteins
Dgt3	249	Dgt5	297	between proteins
Dgt3	230	Dgt5	277	between proteins
Dgt3	324	Dgt5	383	between proteins
Dgt3	322	Dgt5	378	between proteins
Dgt3	336	Dgt5	378	between proteins
Dgt3	508	Dgt5	154	between proteins
Dgt3	318	Dgt5	378	between proteins
Dgt3	324	Dgt6	561	between proteins

Dgt3	324	Dgt6	390	between proteins
Dgt3	324	Dgt6	555	between proteins
Dgt3	165	Msd1	113	between proteins
Dgt3	334	Msd1	137	between proteins
Dgt3	508	Wac	132	between proteins
Dgt4	97	Msd5	174	between proteins
Dgt5	315	Dgt6	352	between proteins
Dgt5	98	Dgt6	353	between proteins
Dgt5	98	Dgt6	143	between proteins
Dgt5	98	Dgt6	360	between proteins
Dgt5	100	Dgt6	353	between proteins
Dgt5	413	Msd1	113	between proteins
Dgt5	625	Wac	132	between proteins
Dgt5	632	Wac	140	between proteins
Dgt5	632	Wac	146	between proteins
Dgt5	606	Wac	132	between proteins
Dgt6	71	Dgt6	71	between proteins
Dgt6	270	Msd1	78	between proteins
Dgt6	82	Msd1	113	between proteins
Dgt6	237	Msd1	25	between proteins
Dgt6	270	Msd1	33	between proteins
Dgt6	285	Msd1	78	between proteins
Dgt6	265	Msd1	45	between proteins
Dgt6	190	Msd5	17	between proteins
Dgt6	190	Msd5	26	between proteins
Dgt6	462	Msd5	18	between proteins
Dgt6	71	Msd5	87	between proteins
Dgt6	143	Msd5	87	between proteins

Dgt6	71	Msd5	86	between proteins
Msd1	113	Msd1	113	between proteins
Msd1	25	Msd1	25	between proteins
Msd1	113	Msd5	226	between proteins
Dgt2	209	Dgt2	217	within protein
Dgt2	212	Dgt2	217	within protein
Dgt2	51	Dgt2	55	within protein
Dgt2	101	Dgt2	192	within protein
Dgt3	230	Dgt3	324	within protein
Dgt3	508	Dgt3	522	within protein
Dgt3	210	Dgt3	324	within protein
Dgt3	118	Dgt3	336	within protein
Dgt3	271	Dgt3	273	within protein
Dgt4	97	Dgt4	105	within protein
Dgt5	97	Dgt5	100	within protein
Dgt5	116	Dgt5	124	within protein
Dgt5	98	Dgt5	102	within protein
Dgt5	430	Dgt5	441	within protein
Dgt5	305	Dgt5	315	within protein
Dgt5	97	Dgt5	102	within protein
Dgt5	73	Dgt5	81	within protein
Dgt5	71	Dgt5	97	within protein
Dgt5	71	Dgt5	102	within protein
Dgt5	1	Dgt5	475	within protein
Dgt5	1	Dgt5	15	within protein
Dgt6	390	Dgt6	462	within protein
Dgt6	19	Dgt6	23	within protein
Dgt6	362	Dgt6	390	within protein

238

Dgt6	475	Dgt6	481	within protein
Dgt6	390	Dgt6	481	within protein
Dgt6	573	Dgt6	589	within protein
Dgt6	462	Dgt6	475	within protein
Dgt6	353	Dgt6	362	within protein
Dgt6	23	Dgt6	143	within protein
Dgt6	23	Dgt6	71	within protein
Dgt6	444	Dgt6	462	within protein
Dgt6	555	Dgt6	589	within protein
Dgt6	574	Dgt6	589	within protein
Dgt6	444	Dgt6	475	within protein
Dgt6	71	Dgt6	82	within protein
Dgt6	352	Dgt6	390	within protein
Dgt6	71	Dgt6	143	within protein
Dgt6	422	Dgt6	462	within protein
Dgt6	389	Dgt6	442	within protein
Dgt6	390	Dgt6	442	within protein
Dgt6	362	Dgt6	364	within protein
Msd1	44	Msd1	113	within protein
Msd1	33	Msd1	45	within protein
Msd1	83	Msd1	113	within protein
Msd1	33	Msd1	113	within protein
Msd1	84	Msd1	113	within protein
Msd1	45	Msd1	113	within protein
Msd1	25	Msd1	113	within protein
Msd1	33	Msd1	110	within protein
Msd1	25	Msd1	33	within protein
Msd1	25	Msd1	44	within protein

Msd1	109	Msd1	113	within protein
Msd1	33	Msd1	78	within protein
Msd1	110	Msd1	113	within protein
Msd1	25	Msd1	110	within protein
Msd1	44	Msd1	48	within protein
Msd1	25	Msd1	78	within protein
Msd1	25	Msd1	45	within protein
Msd1	33	Msd1	100	within protein
Msd1	42	Msd1	48	within protein
Msd1	45	Msd1	83	within protein
Msd1	25	Msd1	100	within protein
Msd1	25	Msd1	42	within protein
Msd1	42	Msd1	113	within protein
Msd1	100	Msd1	110	within protein
Msd1	33	Msd1	48	within protein
Msd5	26	Msd5	135	within protein
Msd5	72	Msd5	86	within protein
Msd5	135	Msd5	143	within protein
Msd5	163	Msd5	178	within protein
Wac	132	Wac	143	within protein
Wac	132	Wac	140	within protein
Wac	140	Wac	146	within protein
Wac	132	Wac	146	within protein
Wac	143	Wac	156	within protein
Wac	131	Wac	143	within protein

Appendix Table 3- List of crosslinked peptides within and between Augmin subunits with Target Decoy database method, with a 5% FDR constraint. The search method revealed 77 intra-protein linkages, and 59 inter-protein linkages.